Many-body channels in baryon-antibaryon annihilation in relativistic heavy-ion collisions

Dissertation zur Erlangung
des Doktorgrades der Naturwissenschaften

vorgelegt beim
Fachbereich 07 - Mathematik und Informatik, Physik, Geographie
der Justus-Liebig-Universität Gießen

JUSTUS-LIEBIG-
UNIVERSITÄT
GIESSEN

von
Eduard Seifert

März 2018
Gießen

Gutachter: Prof. Dr. Dr. Wolfgang Cassing
Prof. Dr. Claudia Höhne

Zusammenfassung

Aktuelles Forschungsgebiet der Hochenergiephysik ist die Untersuchung der Eigenschaften des Quark-Gluon-Plasmas (QGP) durch Schwerionenkollisionen (SIKs). Die Interpretation experimenteller Messdaten in Hinblick auf Eigenschaften des QGP setzt jedoch ein genaues Verständnis aller hadronischer Reaktionen voraus. Die hadronischen Reaktionen müssen in transporttheoretischen Modellen implementiert und durch Vergleich mit experimentellen Daten auf ihren Einfluss überprüft werden. Ungeklärt ist bis dato die Bedeutsamkeit der Baryon-Antibaryon Annihilation und Reproduktion im Strangeness-Sektor für Teilchenspektren aus SIKs. Vor allem die Reproduktion durch mehr als zwei Mesonen wird in den meisten transporttheoretischen Modellen unberücksichtigt gelassen, obwohl hier die Produktionsschwelle durch die Reaktion mehrerer Teilchen herabgesetzt ist und somit einen nicht zu vernachlässigenden Beitrag liefern sollte. Diese Arbeit widmet sich dieser Fragestellung und untersucht die Baryon-Antibaryon Annihilation und Reproduktion in relativistischen SIKs.

Die Baryon-Antibaryon Annihilation und Reproduktion wird in der Parton-Hadron-String Dynamics (PHSD) Transporttheorie zunächst um den Strangeness-Sektor erweitert. In Ergänzung zu den Baryon-Antibaryon $\leftrightarrow$ 3 Mesonen Reaktionen ($B\bar{B} \leftrightarrow 3M$) im leichten Quark-Sektor sind die Matrixelemente für Kanäle mit einfacher und mehrfacher Strangeness zu spezifizieren. In dieser Arbeit wird ein Reduktionsparameter λ eingeführt, der durch die größere Masse des "strange" Quarks relativ zu den leichten (u, d) Quarks motiviert wird. Die finalen Resultate werden explizit als Funktion von λ vorgestellt und diskutiert. Die Zuverlässigkeit der numerischen Implementierung wird durch Tests der Detailed-Balance Relation in Boxsimulationen mit periodischen Randbedingungen überprüft. Anschließend wird der Einfluss der $B\bar{B} \leftrightarrow 3M$ Reaktionen auf Teilchenspektren in PHSD Simulationen von SIKs in dem Energiebereich von FAIR/NICA bis LHC untersucht, d.h. von invarianten Energien $\sqrt{s_{NN}} = 7\,\mathrm{GeV}$ bis 2.76 TeV. Die Untersuchungen ergeben, dass die $B\bar{B} \leftrightarrow 3M$ Kanäle unterhalb von $\sqrt{s_{NN}} = 130\,\mathrm{GeV}$ nahezu keinen Einfluss auf Meson- und Baryonspektren haben; nur die Antibaryonen sind betroffen. Die $2 \leftrightarrow 3$ Kanäle — mit dem Strangeness-Sektor — beeinflussen die Antibaryon-Rapiditätsspektren im unteren SPS Energiebereich $\sqrt{s_{NN}} < 7\,\mathrm{GeV}$ stärker als im oberen SPS Energiebereich von $\sqrt{s_{NN}} \approx 17\,\mathrm{GeV}$ und ergeben eine bessere Übereinstimmung der PHSD Resultate mit den experimentellen Messdaten. Der Baryonsektor wird bei ultrarelativistischen Energien von RHIC und LHC ($\sqrt{s_{NN}} > 20\,\mathrm{GeV}$) von den $B\bar{B} \leftrightarrow 3M$ Kanälen ebenfalls beeinflusst und die

Beschreibung der Messdaten mit PHSD wird generell verbessert. Wir untersuchen weiterhin den Unterschied zwischen Berechnungen mit den vollen $B\bar{B} \leftrightarrow 3M$ Reaktionen zu Berechnungen, die nur die Annihilation berücksichtigen, entsprechend der Vorgehensweise anderer aktueller Transportansätze. Im Antibaryonensektor finden wir Abweichungen von bis zu einem Faktor 2.5, mit den größten Abweichungen bei den unteren SPS oder FAIR/NICA Energien.

Summary

The current focus in high-energy physics is the study of the properties of the Quark Gluon Plasma (QGP) in Heavy-Ion Collisions (HICs). The interpretation of experimental data with respect to the properties of the QGP requires precise a understanding of all hadronic interactions, which have to be implemented in transport theoretical models and their influence has to be tested in comparison with experimental data. The significance of the baryon-antibaryon annihilation and reproduction in the strangeness sector for particle spectra from HICs has not yet been clarified. Particularly the reproduction by more than two mesons is not taken into account in most of the transport theoretical models, although the production threshold is reduced by the reaction of several particles and thus should have a significant contribution. This work is devoted to this question and examines the baryon-antibaryon annihilation and reproduction in relativistic HICs.

As a first step the baryon-antibaryon annihilation and reproduction is extended to the strangeness sector in the Parton-Hadron-String Dynamics (PHSD) transport approach. In addition to the baryon-antibaryon $\leftrightarrow$ 3 mesons reactions ($B\bar{B} \leftrightarrow 3M$), matrix elements for channels with single and multiple strangeness have to be specified. In this thesis, a suppression parameter λ is introduced, which is motivated by the larger mass of the strange quarks relative to the light (u, d) quarks. The final results are presented and discussed as an explicit function of λ. The reliability of the numerical implementation is confirmed by tests of the detailed-balance relations in box simulations with periodic boundary conditions. Subsequently, the influence of the $B\bar{B} \leftrightarrow 3M$ reactions on particle spectra in PHSD simulations of HICs in the energy range from FAIR/NICA to LHC will be investigated, i.e. $\sqrt{s_{NN}} = 7\,\text{GeV}$ to $2.76\,\text{TeV}$. The investigations show that below $\sqrt{s_{NN}} = 130\,\text{GeV}$ the $B\bar{B} \leftrightarrow 3M$ channels have almost no influence on meson and baryon spectra; only the antibaryons are affected. The $B\bar{B} \leftrightarrow 3M$ channels — including the strangeness sector — influence the antibaryon rapidity spectra in the lower SPS energy range $\sqrt{s_{NN}} < 7\,\text{GeV}$ more strongly than in the upper SPS energy range of $\sqrt{s_{NN}} \approx 17\,\text{GeV}$ and result in a better agreement of the PHSD results with experimental data. At ultra-relativistic energies of RHIC and LHC ($\sqrt{s_{NN}} > 20\,\text{GeV}$) the baryon sector is affected by the $B\bar{B} \leftrightarrow 3M$ channels as well and the description of experimental data is generally improved. We, additionally, examine the difference between calculations with the full $B\bar{B} \leftrightarrow 3M$ reactions to calculations that only consider annihilation, corresponding to the procedure of other current transport approaches. In the antibaryon sector we find deviations of up to a factor of 2.5, with the largest deviations at the lower SPS or FAIR/NICA energies.

Contents

Chapter 1

Introduction

Before the 1950s the physics community had knowledge of electrodynamics and gravity as well as some attracting force that kept the nucleons bound to a nucleus. In the beginning of the 1950s particle accelerators had reached energies of hundreds of MeV and together with observations of cosmic rays lead to the discovery of a lot of "elementary particles" — which also nucleons were assumed to be. This bunch of "elementary particles" was known as the **particle zoo** and irritated the physics community because it was generally assumed that nature would be made up of only a few building blocks.

In the late 1960s at the Stanford Linear Accelerator Center (SLAC) the evidence for a substructure of the nucleons was observed when a linear electron accelerator with a maximum energy of 25 GeV started operation. By colliding electrons with an energy of $E_{\text{lab}} = 4.9\,\text{GeV}$ with nucleons in a ^{12}C target and extracting the structure function from the differential cross section it was found that the nucleons have three point-like constituents that were later identified with quarks. The idea of a substructure of the particle zoo circulated in the community already since the beginning of the 1960s originating from three independent researchers, Petermann, Gell-Mann and Zweig, who grouped the particle zoo into multiplets according to current algebra. With the experimental evidence of the inner structure of the nucleons the **quark model** from the mid-1960s was established.

In the quark model the **valence quarks** define the quantum numbers of the hadron and the **sea quarks** (virtual quark-antiquark pairs) together with gluons make up most of its mass and influence the deep-inelastic scattering spectra due to their charge. The valence quarks in the nucleon and its resonances are called **up** (u) and **down** (d) quarks. As the accelerator techniques evolved and even higher energies were reached, one found a second generation of quarks that are in the order of emergence the **strange** (s) and **charm** (c) quarks. Their names are of historical nature: Initially, the Σ baryons/hyperons could not be described with the u and d quarks such that Gell-Mann introduced a "strange" quark. The charm quark got its name because in $e^+ + e^-$ collisions at an invariant mass of around 3 GeV the long-living/sharply peaked J/ψ meson emerges that surprised the community since (due to its large mass) it should decay almost instantly in case of only

Tab. 1.1 – Properties of the different quark species taken from Ref. [1].

Generation	Name	Symbol	Charge [e]	Flavor quantum number	Mass [MeV]
1	Up	u	+2/3	$I_z = +1/2$	$2.2^{+0.6}_{-0.4}$
	Down	d	-1/3	$I_z = -1/2$	$4.7^{+0.5}_{-0.4}$
2	Charm	c	+2/3	$C = +1$	1280 ± 30
	Strange	s	-1/3	$S = -1$	96^{+8}_{-4}
3	Top	t	+2/3	$T = +1$	173100 ± 600
	Bottom	b	-1/3	$B' = -1$	4180^{+40}_{-30}

u, d or s quark content, but because of its "charming" quark it can only decay through the weak interaction, extending its lifetime substantially. Then, there is the last generation of bottom (b) and top (t) quarks, whereof the top quark is too heavy for bound states and directly decays after production. In Table 1.1 the quarks and their electric charges, flavor quantum numbers and masses are listed. Besides the electric charge the quarks hold one of three color charges (red, green, blue) whereby they interact with gluons. This color interaction is described by **Quantum ChromoDynamics** (QCD) which is the theory of the strong interaction, and builds with the electroweak interaction the **standard model** of particle physics. QCD is a non-abelian gauge theory with symmetry SU(3) where "3" stands for the number of color charges. The gluon in QCD is the equivalent of the photon in electrodynamics: the interaction mediator, but with the difference that the gluon itself carries color charge — unlike the photon that does not carry electric charge. The gluons interact with each other through the color charge already in first order of the coupling. An important feature of QCD is that the quarks are confined in hadrons since the running coupling of QCD becomes large for low energies or large distances. Only in the asymptotic limit of high energies the quarks become asymptotically free. This limits perturbative methods to high energies/temperatures, where the coupling becomes small. Thus, non-perturbative theoretical methods are needed to investigate QCD at lower energies or temperatures.

In the QCD phase diagram we know reasonably well the properties of matter at almost zero temperature and a density of normal nuclear matter $n \approx 0.16\,\mathrm{fm}^{-3}$ (or the corresponding baryon chemical potential μ_B), which represents only a small region of the phase diagram. The experimental exploration of the phase diagram started with the European Organization for Nuclear Research (CERN) Proton Synchrotron (PS) and the Brookhaven National Laboratory (BNL) Alternating Gradient Synchrotron (AGS) around 1960 which were able to accelerate Au nuclei up to an energy of $E_{\mathrm{lab}} = 11A\,\mathrm{GeV}$ [2]. The PS became a pre-accelerator for the Super PS (SPS) in 1976 at CERN and investigated Pb+Pb collisions in the energy range $E_{\mathrm{lab}} = 20 - 158A\,\mathrm{GeV}$ but was still unable to clearly discover the **Quark Gluon Plasma** (QGP) phase in which the quarks

move freely inside a sea of gluons marking the confinement/deconfinement transition. The QGP phase was experimentally first validated at the Relativistic Heavy-Ion Collider (RHIC) at BNL and seems to be an almost perfect fluid with the smallest ever observed shear viscosity [3]. The last missing piece of the standard model was the experimental discovery of the **Higgs boson** that is responsible for the mass generation in the standard model. At the Large Hadron Collider (LHC) at CERN in July 2012 this major puzzle piece was discovered in p+p collisions at the collision energies of $\sqrt{s} = 7$ and 8 TeV [4]. The LHC marks the largest collider that is capable of producing the highest man-made collision energies. By the end of 2018 one expects a proposal for an extension of the LHC called the Future Circular Collider (FCC) that would cap the terrestrial reachable energy up to 100 TeV for p+p collisions [5].

Since no other facility on earth could compete any longer with the mammoth accelerators at CERN in the race to higher energies, in the hopes of finding exciting new physics beyond the standard model and maybe glimpse into some supersymmetric nature, other facilities focused on lower energies in higher detail to explore the QCD phase diagram and possibly hidden physics from rare processes. At the top RHIC and LHC energies only the high temperature and low density/baryon chemical potential part of the phase diagram can be explored. With lower collision energy one explores the higher density part of the phase diagram where a **Critical EndPoint** (CEP) is expected [6]. The CEP marks the point in the phase diagram in which the confinement-deconfinement transition turns from a first order into a crossover phase transition when going from higher to lower densities. The CEP is expected to be approximately in the same region for the confinement-deconfinement transition as for the chirally broken-chirally restored phase transition accessible from theory. The QCD phase diagram is sketched in Figure 1.1 where additionally to the expected phases from different models also the approximate paths of HICs at the different facilities are indicated. The information on the phases and transitions come from different models, e.g. at low densities lattice QCD (lQCD) finds a crossover phase transition and is the only *ab initio* approach that numerically solves QCD on a discretized space-time lattice [7–12]. Due to the so-called sign problem, where in the probability measure the fermion mass determinant becomes complex as soon as finite chemical potentials are considered, calculations far from vanishing chemical potential are quite involved and with the current technology and approaches not possible.

Other methods capable of accessing the phase diagram are effective models and functional approaches, however, they require certain approximations. Effective models do not use the original degrees of freedom from the QCD lagrangian — the quarks and gluons — but introduce effective degrees of freedom that are essentially compound structures of the quarks or gluons. E.g. in the Nambu-Jona-Lasinio (NJL) model one integrates out the gluons which leads to a local four-fermion interaction similar to the formation of cooper pairs in superconductors from solid state physics. The NJL or the Polyakov loop extended version (PNJL) works in the low energy regime and does not include a confinement-deconfinement phase transition but is capable of calculating the chiral phase transition — with the scalar quark condensate $\langle \bar{q}q \rangle$ as the order parameter [13]. In the chirally restored phase the chiral partners, e.g. ρ and a_1, obtain the same spectral

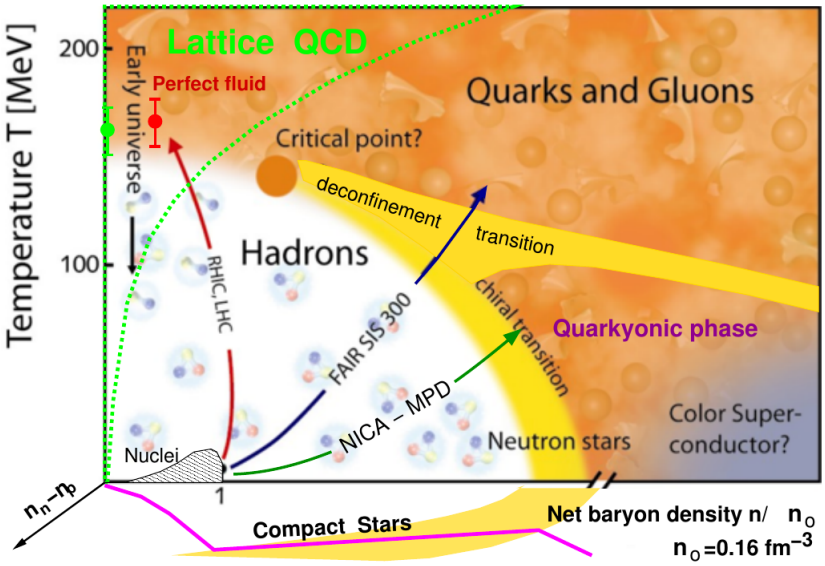

Fig. 1.1 – Sketch of the QCD phase diagram. Depicted are the different phases of the phase diagram according to theory and the approximate domains for different heavy-ion facilities and lattice calculations. Besides the temperature and density axes also the isospin asymmetry axis is depicted that is relevant for astrophysics. The figure is taken from Ref. [14].

functions and the masses will merge. On the other hand the quark masses will drop in the chirally restored phase, which is important for HICs at lower energies and even explains the long-standing puzzle of the "horn" in the K^+/π^+ excitation function [15].

The functional methods have to introduce a truncation scheme to close their tower of coupled equations. The most prominent functional methods in the field are the Functional Renormalization Group (FRG) and Dyson-Schwinger Equations (DSE). FRG solves the truncated Wetterich flow equation of the scale-dependent effective action from the macroscopic to the microscopic scale where the fixed points give information on the physical system [16]. DSEs are infinitely coupled equations that connect the free Green function with the self-energy to the full Green function whose solution needs a closed truncation scheme. Besides the calculation of the QCD phase diagram the DSE are capable of calculating particle spectra (even of exotic states like tetra-quarks) [17–21]. Additionally, the DSE give rise to the Kadanoff-Baym equations that are the foundation of the Parton-Hadron-String Dynamics (PHSD) transport approach, see Sec. 2.1. Altogether the FRG and DSE provide information on the approximate location of the CEP of the chiral phase transition.

For the search of the CEP and general mapping of the QCD phase diagram the Beam Energy Scan (BES) program was started in 2010 at RHIC and focuses on the energies $\sqrt{s_{NN}} = 5.5, 7.7, 11.5, 19.6, 27, 39$ and 62.4 GeV using Au+Au collisions. As already mentioned, interesting processes are rare such that for lower energies high luminosities are needed to find signals that contain hints towards interesting physics. For this pur-

pose the high luminosity Facility for Antiprotons and Ion Research (FAIR) at the GSI Helmholtzzentrum für Schwerionenforschung in Germany and the Nuclotron-based Ion Collider fAcility (NICA) at the Joint Institute for Nuclear Research (JINR) in Russia are currently under construction after decades of planning. Their respective energy ranges are $\sqrt{s_{NN}} = 4 - 9\,\mathrm{GeV}$ and $\sqrt{s_{NN}} = 4 - 11\,\mathrm{GeV}$. First beams are expected in 2019 for NICA and around 2025 for FAIR.

The extraction of information from the QGP phase is a very complicated matter since it only exists for a short time after the collision of the nuclei in the fireball spanning only a few fm/c. After the partonic phase of the collision the particles still interact with each other inelastically, changing their particle species (excluding decays). As the system expands, the chemical freeze-out occurs after which the particles no longer interact via inelastic collisions and keep their particle species. At even later times the kinetic freeze-out happens when the particle density is too low for even elastic collisions to occur. The only thing the detectors see are these particles (and their decay products) with the momentum configuration from the kinetic freeze-out. A successful extrapolation to the QGP phase from the final particle spectra requires probes that are either created inside the QGP and travel ideally unperturbed to the detectors or probes that are influenced by the QGP in a specific manner that allows to draw conclusions about the properties of the QGP. To name a few probes:

Jet quenching

Jets are formed in the hard scattering of a quark of a nucleon with a quark in another nucleon and signify the high transverse momentum p_t hadronic showers that are induced from each scattered quark. Jet quenching is the momentum suppression of a jet due to the dense matter of the surrounding QGP and as such gives information about matter properties of the QGP. If the origin of the jets lies in the outer perimeter of the fireball one jet might directly exit the fireball unhindered while the other (in the rest frame back-to-back) produced jet traverses through the fireball and loses momentum on its way. This momentum loss can be extracted when the jets are measured in coincidence by taking into account the restframe motion and assuming that no gluon is involved (this would make it a three-jet event, where the angle between the jets is not fixed anymore). By comparing data from nucleus+nucleus collisions to p+p data one can quantify the jet quenching [22, 23].

Low p_t-hadrons

The low p_t-hadrons form the major part in a heavy-ion collision and from these collective properties about the initial conditions (partonic densities of the colliding nuclei) as well as the final state (hydrodynamic flows) can be studied [24].

Quarkonia

Quarkonia states are mesons with the same type of quark and antiquark and their formation probability is supposed to be modified in the presence of a QGP (because of the free quark-antiquark pairs therein). The same holds true in general for the

occurrence of quarks other than u and d that are already present in the initial nuclei [25].

Electromagnetic probes

Photons are in theory excellent probes of the QGP phase because they exit the QGP — formed in a HIC — with almost no interaction with the surrounding matter, carrying the ideally unperturbed energy from its production. However, the problem is the disentanglement of the photons coming from decay processes, the initial hard scatterings of the impinging nuclei, hadronic bremsstrahlung and other hadronic interactions involving the emittance of a photon. Additionally, Compton scattering as well as a Doppler shift might change the original energy of the photon. Other than the photon, also dileptons (lepton-antilepton pairs, e.g. e^-e^+) are excellent electromagnetic probes, because they are scattered back-to-back in their rest frame and as long as the lepton and its respective antilepton are measured in coincidence in a detector with equivalent rest frame momenta one can be sure that they have the same origin [26].

The investigations of the QGP are not only important for the understanding of the standard model but also for astrophysics since the fireball, created in HICs, is equivalent to the state of the early universe — a few microseconds after the big bang — so that the expansion of the fireball should show similar features to the expansion of the early universe only on a much smaller scale.

For the extraction of the baryon chemical potential μ_B and the temperature T (or equivalently baryon density n and temperature T) at the chemical freeze-out — at which the final particle abundances are fixed — statistical models are employed [3] that give for each collision system (projectile, target and energy) a point in the phase diagram. The statistical models assume that the particles after the chemical freeze-out are a gas of non-interacting resonances and are referred to as Hadron Resonance Gas (HRG) models. Each particle species has the contribution of

$$\ln Z_i(T,V,\mu) = \pm\frac{V\,g_i}{2\pi^2}\int_0^\infty \mathrm{d}p\,p^2 \ln[1 \pm \lambda_i \mathrm{e}^{-\frac{1}{T}\sqrt{p^2+m_i^2}}], \tag{1.1}$$

to the total partition function Z, with the +(-) signs for fermions (bosons), g_i as the degeneracy factor and λ_i the fugacity of the particle species i:

$$\lambda_i(T,\mu_B,\mu_S,\mu_Q) = \exp\left(\frac{B_i\mu_B + S_i\mu_S + Q_i\mu_Q}{T}\right). \tag{1.2}$$

In the fugacity each conserved quantity obtains a chemical potential. From simple thermodynamic relations every other thermodynamic quantity can be derived from the partition function including the net particle density, that can also take into account the branching ratios from resonance decays. To extract the baryon chemical potential μ_B and temperature T of a HIC the free parameters are varied until the total particle densities of the statistical model fit the experiment. Although the assumptions of the

statistical models are rather simple, they give a good idea about the position in the QCD phase diagram that is probed in the collision system.

To get a deeper understanding of the dynamics of a HIC hydrodynamical, transport and a mixture of both models are used. In these approaches different concepts for the evolution of a HIC can be tested and hence verified or falsified to some extent. The different approaches have their strengths and weaknesses, e.g. the hydrodynamical models assume that the system is locally equilibrated after about 1 fm/c, which is fulfilled at high energies (RHIC and LHC), where the hydrodynamical approaches suggest the QGP to be an almost perfect liquid. For top RHIC and LHC energies the hydrodynamical models provide very good results [27–30]. Yet, the constraint of local equilibration is under no circumstances fulfilled at low-energy HICs and, thus, results from hydrodynamical calculations at low energies should be taken critically. Another weak point of hydrodynamical models is the strong dependence on the initial conditions and to some extent the Equation of State (EoS) used in the calculations [27, 31].

Transport approaches based on the Boltzmann or the quantum-statistically extended Vlasov-Uehling-Uhlenbeck (VUU) transport equations can by definition only be used in dilute systems or — translated into HIC terms — low collision energies where this constraint is approximately fulfilled due to Pauli-blocking for the nucleons. The advantage of transport simulations is that no equilibrium is required and that a system, that starts far-off equilibrium, will after some time equilibrate. Transport models basically consider $1 \rightarrow n, 2 \leftrightarrow 2, 2 \leftrightarrow 1$ and $2 \rightarrow 3$ types of reactions where a cross-section or transition matrix element is available either from experimental data or effective models. A prominent transport model, that works well at low energies, is the Ultra-relativistic Quantum Molecular Dynamics model (UrQMD) [32–34] or the Isospin Quantum Molecular Dynamics model (IQMD) [35, 36]. An exceptional transport approach is PHSD that takes root in the Kadanoff-Baym equations and by definition can be used for dense and strongly interacting systems [37, 38] which makes it well suited for the description of HICs. Additionally, PHSD incorporates a hadronic as well as a QGP phase and is capable to describe a huge number of experimental observables in a wide range of energies (from FAIR/NICA up to LHC energies) [15, 26, 39, 40]. Hybrid models use for the initial collisions a transport model and switch — for space-time cells above some energy density — to a hydro-phase and after the system expanded back to the transport model. Such work was done with the UrQMD-hydro, see Ref. [41]

Most models neglect interactions of three or even more particles, which might have a significant influence on the results since it is easier to overcome production thresholds for heavy particles like hyperons or multi-strange baryons. One such process, that might have an important role on the HIC dynamics, is the baryon-antibaryon ($B\bar{B}$) annihilation and recreation through three or more mesons. Most models (like UrQMD or IQMD) consider the annihilation but neglect the inverse recreation of $B\bar{B}$. The first modelling of the backwards channels has been carried out in Ref. [42] for the light quark sector, where the transition matrix element was extracted from the total inelastic cross-section of $p\bar{p}$ collisions and the reaction probabilities were calculated on the basis of detailed balance.

The annihilation process was described by the quark rearrangement model (QRM) in which the valence quarks of the $B\bar{B}$ pair are regrouped into three mesons and vice-versa ($2 \leftrightarrow 3$). It was found that in central collisions of heavy nuclei the annihilation is almost compensated by the inverse recreation channels [42]. As pointed out in Refs. [43, 44] all strangeness exchange channels in the hadronic phase have to be taken into account. For this we extend in this thesis the $2 \leftrightarrow 3$ channels from the light to the strange quark sector and investigate the impact of three-body channels on HICs in the energy range spanning FAIR to LHC.

This work is structured as follows: We start in Chapter 2 with an introduction to the PHSD transport approach with all its components. Then, in Chapter 3 the Quark Rearrangement Model (QRM) for the baryon-antibaryon annihilation into three mesons and vice versa (with the shorthands $B\bar{B} \leftrightarrow 3M$ and $2 \leftrightarrow 3$) and its extension to the strange quark sector is presented. The numerical implementation of the QRM is tested in box simulations with periodic boundary conditions in Chapter 4. Afterwards, in Chapter 5 we implement the $2 \leftrightarrow 3$ reactions — including the strangeness sector — into PHSD and investigate the influence of the $2 \leftrightarrow 3$ channels as well as the strange quark sector on rapidity spectra, transverse mass spectra and midrapidity yields as a function of centrality for collisions of Pb+Pb (or Au+Au) at energies $\sqrt{s_{NN}} = 4.7 - 2760\,\mathrm{GeV}$[1]. We continue with detailed predictions at FAIR and NICA energies for the antibaryon spectra using different matrix elements for the $2 \leftrightarrow 3$ channels in the strangeness sector in Chapter 6 and close with our conclusions in Chapter 7.

The appendices contain an introduction to on-shell phase spaces in Appendix A, while Appendix B contains information on the numerical implementation of the $2 \leftrightarrow 3$ reactions. In Appendix C we study the numerical dependence on the cell volume as well as the impact for different collision criteria and strangeness suppressions in the transition matrix element. A table of all possible $B\bar{B} \leftrightarrow 3M$ channels in the light and strangeness sector is given in Appendix D.

[1] A conversion table between the bombarding energies E_{lab} and the invariant energies per nucleon $\sqrt{s_{NN}}$ for the respective facilities is given in Table 1.2.

Tab. 1.2 – Conversion table of the center-of-mass energy $\sqrt{s_{NN}}$ to the corresponding bombarding energy E_{lab} for the facilities addressed in this thesis.

$\sqrt{s_{NN}}$ [GeV]	E_{lab} [GeV]	Facilities
3.6	6	
4.1	8	AGS,FAIR,NICA
4.7	10.7	
6.3	20	
7.6	30	FAIR,NICA,
8.8	40	RHIC,SPS
10.7	60	
12.3	80	RHIC,SPS
17.3	158	
19.6	200	
27	390	
39	810	RHIC
130	9000	
200	21300	
2760	4060000	LHC

Chapter 2

Parton-Hadron-String Dynamics (PHSD)

The PHSD is a microscopic, covariant transport approach for strongly interacting systems. Due to its basis on the Kadanoff-Baym equations [45–48] — which are discussed in the following subsection — it describes correctly the equilibration process of systems that are far out-of equilibrium [49] and goes beyond the quasiparticle approximation by incorporating dynamical spectral functions for the partons. The PHSD incorporates a partonic as well as a hadronic phase to describe all stages of a heavy-ion collision with transitions from strings to dynamical partons as well as dynamical hadronization. PHSD is capable of simulating the full time evolution of a relativistic heavy-ion collision — from impinging nuclei in their "groundstates" to the final hadronic particles — ranging from SchwerIonen-Synchrotron (SIS), Alternating Gradient Synchrotron (AGS) over Facility for Antiproton and Ion Research (FAIR)/ Nuclotron-based Ion Collider fAcility (NICA) up to Relativistic Heavy-Ion Collider (RHIC) and Large Hadron Collider (LHC) energies and is able to reproduce a large number of observables in these energy regimes for p+p, p+A and A+A reactions [15, 26].

In this chapter, we present the ingredients of the PHSD approach that is used in this work. We start with an introduction to the Kadanoff-Baym equations for the Green functions and a derivation of the equations of motion of PHSD. Furthermore, we present the Dynamical QuasiParticle Model (DQPM), which is relevant for the dynamics in the partonic phase, and close with exemplary heavy-ion collisions at intermediate energies ($\sqrt{s_{NN}} = 3 - 17\,\mathrm{GeV}$) where we highlight the main features of PHSD simulations.

2.1 Kadanoff-Baym equations

The Kadanoff-Baym equations are equations of motion for two-point Green functions G. In quantum field theory the Green functions are calculated as vacuum expectation values of products of field operators and are identified with the propagators of the system. For

the derivation of the equations of motion of the Green functions one defines a closed time path (CTP) [50] on which the two time variables of the Green function are located and that also defines the contour for the time integration. The CTP is illustrated in Fig. 2.1. Focusing on scalar fields ϕ we can define four different Green functions, with

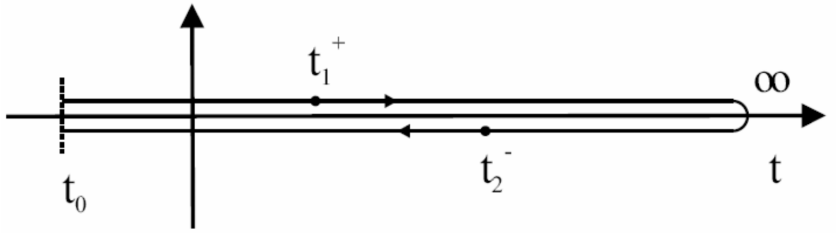

Fig. 2.1 – Illustration of the CTP. The time t_1 lies on the chronological (+) branch and the time t_2 lies on the antichronological (-) branch. The figure is taken from [51].

+ and — indicating the chronologic and antichronologic branch location of the indices, respectively, as follows:

$$iG^c(x,y) = iG^{++}(x,y) = \langle\, \hat{T}^c(\phi(x)\phi(y))\, \rangle \tag{2.1}$$
$$iG^<(x,y) = iG^{+-}(x,y) = \langle \phi(y)\phi(x) \rangle \tag{2.2}$$
$$iG^>(x,y) = iG^{-+}(x,y) = \langle \phi(x)\phi(y) \rangle \tag{2.3}$$
$$iG^a(x,y) = iG^{--}(x,y) = \langle\, \hat{T}^a(\phi(x)\phi(y))\, \rangle\,, \tag{2.4}$$

with x and y being 4-vectors ($x = (x^0, \mathbf{x})$), while x^0 stands for the time coordinate. Time ordering has only to be taken into account when both variables lie on the same branch. The causal time-ordering operator T^c orders fields of later time to the left and the anti-causal time operator T^a orders fields of later time to the right — corresponding to the order on the CTP. The Green functions $G^{\gtrless}$ are called **Wightman functions**. The Green functions (2.1-2.4) can also be written in matrix form according to the location of the time variable as [37, 52]

$$G(x,y) = \begin{array}{c} \\ + \\ - \end{array} \begin{array}{c} \begin{array}{cc} + & - \end{array} \\ \begin{pmatrix} G^c(x,y) & G^<(x,y) \\ G^>(x,y) & G^a(x,y) \end{pmatrix} \end{array}. \tag{2.5}$$

Additionally, the retarded Green function G^R and the advanced Green function G^A are given as

$$\begin{aligned} G^R(x,y) =& \theta(t_1 - t_2)[G^>(x,y) - G^<(x,y)] \\ &= G^c(x,y) - G^<(x,y) = G^>(x,y) - G^a(x,y) \end{aligned} \tag{2.6}$$

$$\begin{aligned} G^A(x,y) =& -\theta(t_2 - t_1)[G^>(x,y) - G^<(x,y)] \\ &= G^c(x,y) - G^>(x,y) = G^<(x,y) - G^a(x,y). \end{aligned} \tag{2.7}$$

The starting point for the derivation of the Kadanoff-Baym equations is the **Dyson-Schwinger equation**, which relates the full Green function G (meaning fully interacting) to the free Green function G_0 via the self-energy Σ:

$$G(x,y) = G_0(x,y) + G_0(x,x') \odot \Sigma(x',y') \odot G(y',y). \tag{2.8}$$

In Eq. (2.8) $\odot$ symbolizes an integration over the intermediate space-time points x' and y', with the time integration following the CTP. The self-energy Σ incorporates the interaction into the free propagator, "dressing" the bare/free propagator with a cloud of self-interaction. Using the matrix notation Eq. (2.8) takes the form

$$\begin{aligned}\begin{pmatrix} G^c(x,y) & G^<(x,y) \\ G^>(x,y) & G^a(x,y) \end{pmatrix} &= \begin{pmatrix} G_0^c(x,y) & G_0^<(x,y) \\ G_0^>(x,y) & G_0^a(x,y) \end{pmatrix} \\ + \begin{pmatrix} G_0^c(x,x') & G_0^<(x,x') \\ G_0^>(x,x') & G_0^a(x,x') \end{pmatrix} &\odot \begin{pmatrix} \Sigma^c(x',y') & -\Sigma^<(x',y') \\ -\Sigma^>(x',y') & \Sigma^a(x',y') \end{pmatrix} \odot \begin{pmatrix} G^c(y',y) & G^<(y',y) \\ G^>(y',y) & G^a(y',y) \end{pmatrix}.\end{aligned} \tag{2.9}$$

The scalar, inverse, free one-particle propagator is defined via the negative differential operator of the Klein-Gordon equation $G_{0x}^{-1} = -(\partial_\mu^x \partial_x^\mu + m^2)$, with the bare mass of the particle m. Applying G_{0x}^{-1} on the free propagator G_0 one ends up with the path-ordered δ-function

$$G_{0x}^{-1} \begin{pmatrix} G_0^c(x,y) & G_0^<(x,y) \\ G_0^>(x,y) & G_0^a(x,y) \end{pmatrix} = \delta(\mathbf{x}-\mathbf{y}) \begin{pmatrix} \delta(x_0-y_0) & 0 \\ 0 & -\delta(x_0-y_0) \end{pmatrix} \tag{2.10}$$

$$G_{0x}^{-1} G_0^{\mathrm{R/A}}(x,y) = \delta(x-y). \tag{2.11}$$

In order to obtain the **Kadanoff-Baym equations** Eq. (2.9) is convoluted with G_{0x}^{-1} from the left; this leads to

$$-(\partial_\mu^x \partial_x^\mu + m^2) G^{\mathrm{R/A}}(x,y) = \delta(x-y) + \Sigma^{\mathrm{R/A}}(x,x') \odot G^{\mathrm{R/A}}(x',y) \quad , \tag{2.12}$$

$$-(\partial_\mu^x \partial_x^\mu + m^2) G^{\gtrless}(x,y) = \Sigma^{\mathrm{R}}(x,x') \odot G^{\gtrless}(x',y) + \Sigma^{\gtrless}(x,x') \odot G^{\mathrm{A}}(x',y). \tag{2.13}$$

Note that the Kadanoff-Baym equations for the retarded and advanced Green functions only depend on retarded and advanced quantities, respectively.

What we are still lacking is an expression for the self-energy Σ. In order to obtain self-consistently derived self-energies that conserve all important quantities such as energy, momentum and causality, we vary the effective action $\Gamma[G]$ with respect to the full propagator G [53]:

$$\Sigma = 2i \frac{\partial \Phi}{\partial G}, \tag{2.14}$$

where Φ is the sum of all irreducible diagrams to infinite order. For the derivation of the two-point self-energy it is sufficient to consider only two-particle-irreducible (2PI) diagrams, that are up to the second order in the coupling constant. Here, 2PI means that we cannot create two disjunct diagrams by cutting a propagator line.

For the further derivation of the equations of motion we perform a **Wigner-transformation** into phase space. The Wigner-transformation is basically a Fourier-transformation over the relative coordinate $r = x - y$ at the center coordinate $R = (x + y)/2$ and is defined for a function $f(x, y)$ as follows

$$\tilde{f}(R,p) = \int_{-\infty}^{\infty} \mathrm{d}^4 r \; f(R + r/2, R - r/2)\, \mathrm{e}^{i\, p^\mu r_\mu}, \tag{2.15}$$

with $p = (p^0, \mathbf{p})$ the energy-momentum 4-vector and where we identify functions with a "˜" as Wigner-transformed.

Following Ref. [51], Wigner-transforming a convolution integral

$$H(x,y) = F(x,y') \odot G(y',y) \tag{2.16}$$

gives

$$\tilde{H}(p,x) = e^{i\frac{1}{2}(\partial_p^\mu \cdot \partial_\mu^{x'} - \partial_x^\mu \partial_\mu^{p'})} [\tilde{F}(p,x)\tilde{G}(p',x')]\Big|_{x'=x,p'=p}, \tag{2.17}$$

where we now have to restrict ourselves to a specific order in the momentum and coordinate space derivatives to cope with the exponential function. Assuming smooth functions $\tilde{F}$ and $\tilde{G}$ as a function of x, it is sufficient to take only terms up to first order in the gradients — known as the **first-order gradient expansion** —

$$\tilde{H}(p,x) = \tilde{F}(p,x)\tilde{G}(p,x) + i\frac{1}{2}\{\tilde{F}(p,x), \tilde{G}(p,x)\}, \tag{2.18}$$

with the relativistic generalization of the Poisson bracket,

$$\{\tilde{F}(p,x), \tilde{G}(p,x)\} = \partial_\mu^p \tilde{F}(p,x) \cdot \partial_x^\mu \tilde{G}(p,x) - \partial_x^\mu \tilde{F}(p,x) \cdot \partial_\mu^p \tilde{G}(p,x). \tag{2.19}$$

To get the properties of the spectral function we Wigner-transform the Kadanoff-Baym equations for the retarded and advanced Green functions (2.12) and find that the real part of the retarded and advanced Green function (self-energy) are equal as well as that the imaginary parts differ only by a minus sign. With this we can decompose the retarded and advanced Green functions as well as self-energies in the following way,

$$\tilde{G}^{R/A} = \mathrm{Re}\, \tilde{G}^R \mp i\tilde{A}/2, \tag{2.20}$$

$$\tilde{\Sigma}^{R/A} = \mathrm{Re}\, \tilde{\Sigma}^R \mp i\tilde{\Gamma}/2, \tag{2.21}$$

with $\tilde{A}$ denoting the spectral function and $\tilde{\Gamma}$ the particle width. Solving the system of the four real valued coupled equations (the real and imaginary equations have to be satisfied independently) one ends up with the spectral function, which is of relativistic Breit-Wigner shape,

$$\tilde{A} = \frac{\tilde{\Gamma}}{[\underbrace{p_0^2 - \mathbf{p}^2 - m^2 - \mathrm{Re}\, \tilde{\Sigma}^R}_{:=\tilde{M}(p,x)}]^2 + \tilde{\Gamma}^2/4} = \frac{\tilde{\Gamma}}{\tilde{M}^2 + \tilde{\Gamma}^2/4}, \tag{2.22}$$

and of dimension [energy^{-2}]. For the dynamics of the system we will now focus on the Wightman-transformed Wigner-functions $G^{\gtrless}$, that are purely imaginary (making $i\tilde{G}^{\gtrless}$ real valued). Following a similar scheme as for $G^{R/A}$ and introducing distribution functions for the Green function and self-energy as

$$i\tilde{G}^{<} = \tilde{N}\tilde{A}, \qquad i\tilde{G}^{>} = [1+\tilde{N}]\tilde{A}, \tag{2.23}$$

$$i\tilde{\Sigma}^{<} = \tilde{N}^{\Sigma}\tilde{\Gamma}, \qquad i\tilde{\Sigma}^{>} = [1+\tilde{N}^{\Sigma}]\tilde{\Gamma}, \tag{2.24}$$

one finds the generalized transport equations [37, 38, 45, 48, 54–57] in **Botermans-Malfliet** form

$$\frac{1}{2}\tilde{A}\tilde{\Gamma}\left[\{\tilde{M}, i\tilde{G}^{<}\} - \frac{1}{\tilde{\Gamma}}\{\tilde{\Gamma}, \tilde{M}\cdot i\tilde{G}^{<}\}\right] = i\tilde{\Sigma}^{<}i\tilde{G}^{>} - i\tilde{\Sigma}^{>}i\tilde{G}^{<}. \tag{2.25}$$

Eq. (2.25) retains the characteristics of the full Kadanoff-Baym equations for the quantum equilibration process and allows for a transport theoretical implementation. Hence, it is used for the derivation of the PHSD equations of motion.

Solving Eq. (2.25) requires an ansatz for $\tilde{G}^{<}$, which can be identified with the generalized phase space distribution function $F(x,p)$ used in transport (except for a factor i). Here, an extended testparticle ansatz is chosen consisting additionally to the standard degrees of freedom (space coordinate $\mathbf{x}$, time t and momentum $\mathbf{p}$) of the energy ϵ since we are dealing with off-mass-shell particles (short off-shell). The ansatz takes the form

$$F(x,p) = i\tilde{G}^{<}(x,p) \sim \sum_{i=1}^{N} \delta^{(3)}(\mathbf{x}-\mathbf{x}_i(t))\,\delta^{(3)}(\mathbf{p}-\mathbf{p}_i(t))\,\delta(p_0-\epsilon_i(t)), \tag{2.26}$$

which in the limit of $N\to\infty$ converges to the correct distribution function. The equations of motion for the testparticles are [38]

$$\frac{\mathrm{d}\mathbf{x}_i}{\mathrm{d}t} = \frac{1}{1-C_{(i)}}\frac{1}{2\epsilon_i}\left[2\,\mathbf{p}_i + \nabla_{p_i}\mathrm{Re}\,\tilde{\Sigma}^R_{(i)} + \frac{\epsilon_i^2 - \mathbf{p}_i^2 - M_0^2 - \mathrm{Re}\,\tilde{\Sigma}^R_{(i)}}{\tilde{\Gamma}_{(i)}}\nabla_{p_i}\tilde{\Gamma}_{(i)}\right], \tag{2.27}$$

$$\frac{\mathrm{d}\mathbf{p}_i}{\mathrm{d}t} = \frac{1}{1-C_{(i)}}\frac{1}{2\epsilon_i}\left[\nabla_{x_i}\mathrm{Re}\,\tilde{\Sigma}^R_{(i)} + \frac{\epsilon_i^2 - \mathbf{p}_i^2 - M_0^2 - \mathrm{Re}\,\tilde{\Sigma}^R_{(i)}}{\tilde{\Gamma}_{(i)}}\nabla_{x_i}\tilde{\Gamma}_{(i)}\right], \tag{2.28}$$

$$\frac{\mathrm{d}\epsilon_i}{\mathrm{d}t} = \frac{1}{1-C_{(i)}}\frac{1}{2\epsilon_i}\left[\frac{\partial\mathrm{Re}\,\tilde{\Sigma}^R_{(i)}}{\partial t} + \frac{\epsilon_i^2 - \mathbf{p}_i^2 - M_0^2 - \mathrm{Re}\,\tilde{\Sigma}^R_{(i)}}{\tilde{\Gamma}_{(i)}}\frac{\partial\tilde{\Gamma}_{(i)}}{\partial t}\right], \tag{2.29}$$

with the notation $f_{(i)} \equiv f(t, \mathbf{x}_i(t), p_i(t), \epsilon_i(t)$. $C_{(i)}$ has the function of a Lorentz-factor and transforms the system time t to the eigentime of the particle i and is given by the energy derivatives

$$C_{(i)} = \frac{1}{2\epsilon_i}\left[\frac{\partial\mathrm{Re}\,\tilde{\Sigma}^R_{(i)}}{\partial\epsilon_i} + \frac{\epsilon_i^2 - \mathbf{p}_i^2 - M_0^2 - \mathrm{Re}\,\tilde{\Sigma}^R_{(i)}}{\tilde{\Gamma}_{(i)}}\frac{\partial\tilde{\Gamma}_{(i)}}{\partial\epsilon_i}\right]. \tag{2.30}$$

Equations (2.27-2.29) are the equations of motion employed in the PHSD transport approach. Due to their basis on the Kadanoff-Baym equations PHSD is capable of describing the equilibration of systems far out-of equilibrium and thus is used for the simulation of heavy-ion collisions with strongly interacting degrees of freedom, i.e. dynamical spectral functions of finite width.

2.2 The Dynamical Quasiparticle Model

The Dynamical Quasiparticle Model (DQPM) is employed to describe the properties of the quarks q, antiquarks $\bar{q}$ and gluons g in the Quark Gluon Plasma (QGP) phase in the PHSD framework. In the DQPM these partonic degrees of freedom have effective masses M and spectral widths γ — stemming from their complex self-energies — characterizing their Lorentzian spectral functions A as

$$A(p) = \frac{2\gamma p_0}{(p^\mu p_\mu - M^2)^2 + 4\gamma^2 p_0^2}. \tag{2.31}$$

Comparing Eq. (2.31) with (2.22) we identify:

$$\tilde{\Gamma} = 2\gamma p_0, \qquad\qquad M^2 = m^2 + \mathrm{Re}\,\tilde{\Sigma}^R. \tag{2.32}$$

Here, the masses and spectral widths depend on the temperature T and the masses additionally on the quark chemical potential μ_q in line with hard thermal loop (HTL) calculations in the asymptotic high-momentum regime:

$$M_g^2(T) = \frac{g^2}{6}\left((N_c + \frac{1}{2}N_f)T^2 + \frac{N_c}{2}\sum_g \frac{\mu_q^2}{\pi^2}\right), \tag{2.33}$$

$$M_{q/\bar{q}}^2(T) = \frac{N_c^2 - 1}{8N_c} g^2 \left(T^2 + \frac{\mu_{q/\bar{q}}^2}{\pi^2}\right), \tag{2.34}$$

$$\gamma_g(T) = N_c \frac{g^2 T}{8\pi} \ln\frac{2c}{g^2}, \tag{2.35}$$

$$\gamma_{q/\bar{q}}(T) = \frac{N_c^2 - 1}{2N_c} \frac{g^2 T}{8\pi} \ln\frac{2c}{g^2}. \tag{2.36}$$

In equation (2.34) the constituent quark masses m_q are assumed to be negligible and thus the effective masses (squared) may be identified with $\mathrm{Re}\,\tilde{\Sigma}^R$. The factor c in Eqs. (2.35) and (2.36) is related to a magnetic cut-off, while N_f and N_c are the number of flavors and colors, respectively, and are both equal to 3 while the critical temperature $T_c \approx 158\,\mathrm{MeV}$ is taken from lattice QCD (lQCD). The running coupling squared in (2.33)-(2.36) takes the functional form,

$$g^2(T/T_c) = \frac{48\pi^2}{(11N_c - 2N_f)\ln(\lambda^2(T/T_c - T_s/T_c)^2)}, \tag{2.37}$$

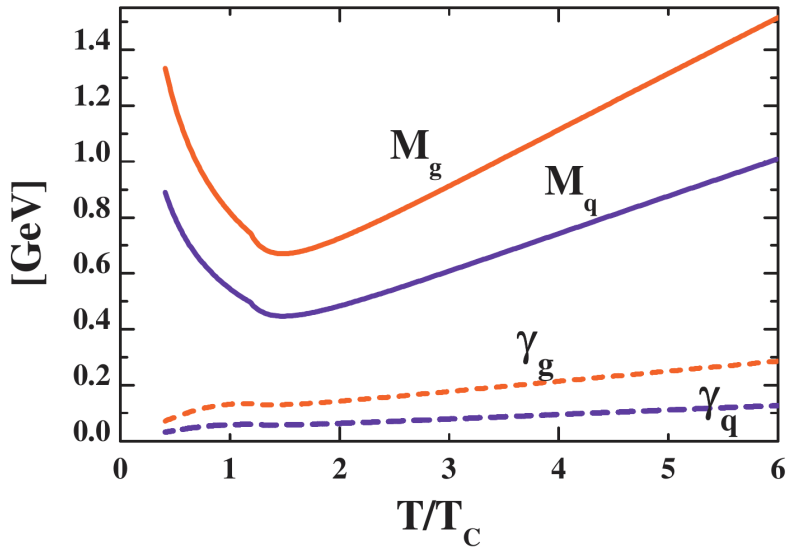

Fig. 2.2 – DQPM masses M and widths γ of the quarks/antiquarks q and gluons g as a function of temperature T (from Ref. [58]).

with the parameters T_s and λ. The spectral widths (2.35,2.36) are generated by the following hard two-body scattering processes:

$$gg \leftrightarrow gg, \qquad gg \leftrightarrow g, \qquad g \leftrightarrow q\bar{q}, \tag{2.38}$$

$$gp \leftrightarrow gp, \qquad pp \leftrightarrow pp, \tag{2.39}$$

where we abbreviate either quarks q or antiquarks $\bar{q}$ with p. Using dynamic simulations it was shown in Ref. [59] that the contribution of the inelastic collisions are negligible compared to the elastic 2↔2 ones. Furthermore, processes with higher numbers of gluons are suppressed due to their large effective masses and, hence, can be neglected.

Looking at Eqs. (2.33-2.37) we see that the DQPM has only three free parameters λ, T_s and c. These parameters are fixed by fitting the equation of state calculated in lQCD [7–12]. The resulting temperature dependence of the masses and widths generated with this parameter set is shown in Fig. 2.2.

The entropy density in the quasiparticle limit is the grandcanonical quantity from which other thermodynamic quantities in the DQPM framework can be derived. The entropy density in propagator form reads [60–64]

$$\begin{aligned} s^{dqp} = &- d_g \int \frac{\mathrm{d}^4p}{(2\pi)^4} \frac{\partial n_B(p_0/T}{\partial T} \left(\mathrm{Im}\ln(-\Delta^{-1}) + \mathrm{Im}\,\Pi\,\mathrm{Re}\,\Delta\right) \\ &- d_q \int \frac{\mathrm{d}^4p}{(2\pi)^4} \frac{\partial n_F((p_0-\mu_q)/T)}{\partial T} \left(\mathrm{Im}\ln(-S_q^{-1}) + \mathrm{Im}\,\Sigma_q\,\mathrm{Re}\,S_q\right) \\ &- d_{\bar{q}} \int \frac{\mathrm{d}^4p}{(2\pi)^4} \frac{\partial n_F((p_0+\mu_q)/T)}{\partial T} \left(\mathrm{Im}\ln(-S_{\bar{q}}^{-1}) + \mathrm{Im}\,\Sigma_{\bar{q}}\,\mathrm{Re}\,S_{\bar{q}}\right), \end{aligned} \tag{2.40}$$

with the Bose and Fermi distribution functions $n_B(p_0/T) = (\exp(p_0/T) - 1)^{-1}$ and $n_F((p_0 - \mu_q)/T) = (\exp((p_0 - \mu_q)/T) + 1)^{-1}$, respectively, as well as the quasiparticle propagators of gluons, quarks and antiquarks

$$\Delta^{-1} = p^\mu p_\mu - \Pi, \qquad S_q^{-1} = p^\mu p_\mu - \Sigma_q, \qquad S_{\bar{q}} = p^\mu p_\mu - \Sigma_{\bar{q}}, \tag{2.41}$$

where the quasiparticle self-energies Π and Σ are given from the ansatz with the Lorentzian spectral functions as

$$\Pi = M_g^2 - 2i\gamma_g p_0, \qquad \Sigma_q = M_q^2 - 2i\gamma_q p_0. \tag{2.42}$$

The degeneracy factor for the quarks q and antiquarks $\bar{q}$ has (for three flavors N_f) the value $d_q = d_{\bar{q}} = 2N_c N_f = 18$ while for the gluons it is $d_g = 2(N_c^2 - 1) = 16$.

An excellent agreement to the lQCD entropy density s, energy density ε and the interaction measure $\varepsilon - 3P$ from the BMW group [65] is found with the parameter set $\lambda = 2.42$, $T_s/T_c = 0.46$ and $c = 14.4$, see Fig. 2.3. The pressure P and energy density ε

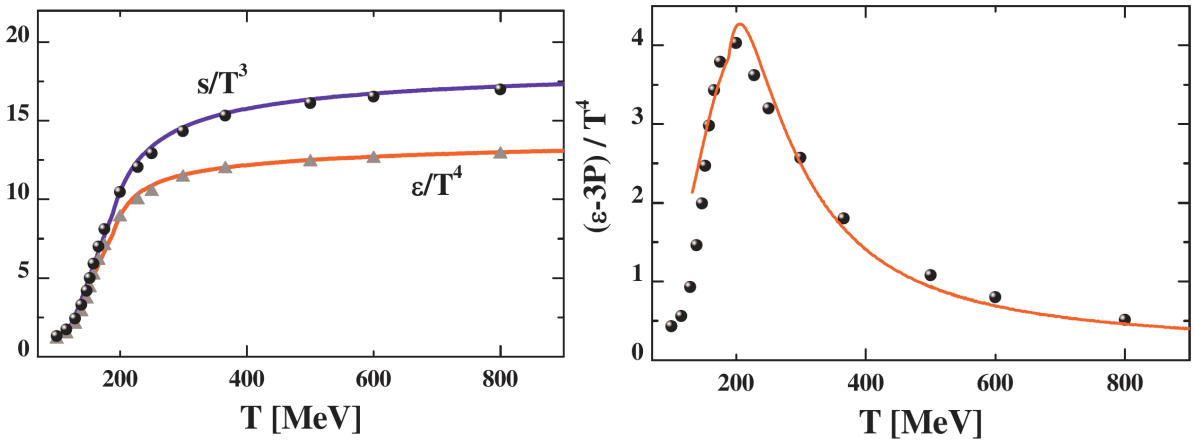

Fig. 2.3 – Comparison between the entropy density s, energy density ε (left) and interaction measure $\varepsilon - 3P$ (right) from DQPM calculations to lQCD results of the BMW group [65]. The figures are taken from Ref. [58].

are derived from the entropy density,

$$s = \frac{\mathrm{d}P}{\mathrm{d}T}, \qquad \varepsilon = Ts - P, \tag{2.43}$$

where the pressure is obtained by integrating the entropy density over the temperature.

Furthermore, in DQPM the partons generate a selfconsistent scalar mean-field $U_s(x)$ in which they propagate, the gradient of which produces a scalar force on the quarks and antiquarks. The scalar mean-field $U_s(x)$ acting on quarks and antiquarks is calculated by the derivative

$$U_s(\rho_s) = \frac{\mathrm{d}V_p(\rho_s)}{\mathrm{d}\rho_s}, \tag{2.44}$$

where the potential energy density V_p is defined by,

$$V_p(T,\mu_q) = T^{00}_{g-}(T,\mu_q) + T^{00}_{q-}(T,\mu_q) + T^{00}_{\bar{q}-}(T,\mu_q), \tag{2.45}$$

with

$$T^{00}_{i-}(T) = d_i \int \frac{\mathrm{d}^4p}{(2\pi)^4} 2p_0^2 A_i(p_0)\theta(p_0) n_i(p_0,T)\theta(-P^2), \tag{2.46}$$

as the space-like part of the energy-momentum tensor component T^{00} of the parton i with respective distribution n_i, degeneracy d_i and spectral function A_i defined above. The scalar mean field U_s (as a function of the scalar density ρ_s) is displayed in Fig. 2.4, with ρ_s in logarithmic scale. We see that U_s does not change significantly for low scalar densities ($\rho_s < 10\,\mathrm{fm}^{-3}$) and is in the order of a few GeV at scalar densities relevant for HICs up to RHIC and LHC energies. In actual PHSD transport simulations the scalar density of the quasiparticles is calculated on a space-time grid and the resulting force on the quasiparticle i is then proportional to $M_i/E_i\ \mathrm{d}U_s/\mathrm{d}\rho_s\ \nabla\rho_s(x_i)$.

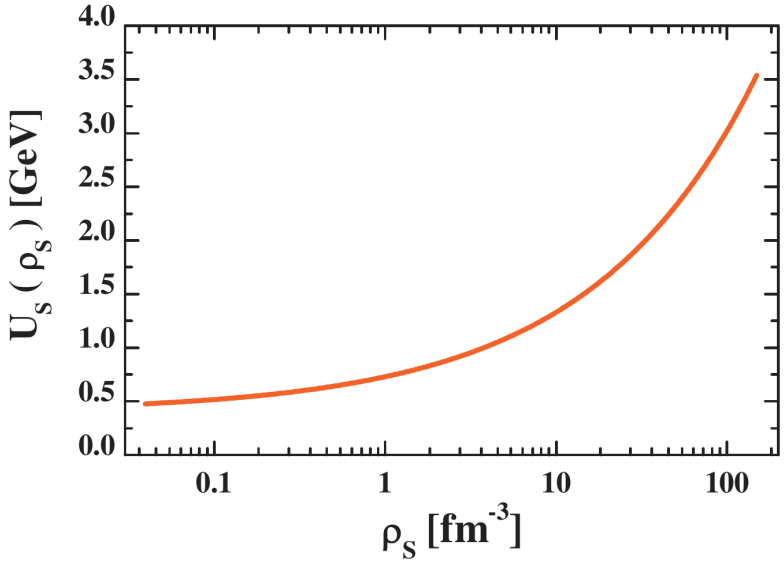

Fig. 2.4 – The DQPM scalar mean field U_s for quarks and antiquarks as a function of the scalar density ρ_s (taken from Ref. [58]).

2.3 Heavy-ion collisons

The theoretical foundation of PHSD — consisting of the DQPM for the partonic degrees of freedom and the equations of motion from the Kadanoff-Baym equations — was discussed in the previous sections and we will now look in detail at further aspects of PHSD. To this aim the hadronic degrees of freedom will be specified as well as the initial conditions for a heavy-ion reaction. Furthermore, the particle production by the LUND string model is introduced, the dynamics in the QGP phase is described and the hadronization is discussed. This section will close with a look at the final hadronic interactions and the impact of the different stages on the final particle numbers.

2.3.1 General aspects

PHSD uses the generalized testparticle ansatz (defined by Eq. (2.26)) for the description of the particles while physical observables are calculated by taking the average over an ensemble of N systems simulated in parallel. For the formation of the QGP phase, the hadronization and the baryon-antibaryon annihilation and recreation (that will be introduced in chapter 3) the calculation is performed partly on a space-time grid. The lattice is Lorentz-contracted in the direction of the colliding nuclei, identified with the z-axis. The velocity of the nuclei will change during the collision making the Lorentz-contraction time dependent. The timestep $\mathrm{d}t$ is also directly coupled to the gamma factor γ_{cm} and will be — depending on the laboratory energy E_{lab} — initially rather small $\mathrm{d}t \approx 0.5/\gamma_{cm}$ [fm/c]. As the system expands the gamma factor drops and the space-time lattice becomes more coarse.

Table 2.1 contains a summary of the mesons and baryons considered in PHSD. The light and strange quark sector is the standard for PHSD calculations and will only be considered in this work. If one is interested in the charm quark sector, one has to explicitly activate the corresponding routines (described in Refs. [66–68]) at the beginning of the calculation. In general, every particle is treated as being off-shell with Lorenzian spectral functions with specific widths and pole masses. The testparticles are assigned energies according to the respective spectral function of the particle species. Invoking the on-mass-shell constraint back we can translate the energy p_0 and momentum $\mathbf{p}$ of

Tab. 2.1 – Mesons and baryons in PHSD.

Quark sector	Mesons	Baryons
light	$\pi, \rho, a_1, \eta, \eta', \omega, \phi$	$p, n, \Delta(1232), N(1440), N(1535)$
strange	$K^{\pm}, K^0, \bar{K}^0, K^{*\pm}, K^{*0}, \bar{K}^{*0}$	$\Lambda, \Sigma, \Sigma^*, \Xi, \Xi^*, \Omega^-$
charm	$J/\Psi, \Psi', \eta_c, D^{\pm}, D^0, \bar{D}^0,$ $D^{*\pm}, D^{*0}, \bar{D}^{*0}, D_s^{\pm}, D_s^{*\pm}$	$\Lambda_c, \Sigma_c, \Sigma_c^*, \Xi_c, \Xi_c', \Xi_c^*, \Omega_c^0, \Omega_c^{*0}$

testparticle i to a mass by $m_i^2 = p_{i0}^2 - \mathbf{p}_i^2$. To achieve reliable spectral functions a large number of ensembles N is crucial.

2.3.2 Initialization

In a HIC we start with two nuclei flying towards each other at given energies and impact parameters. The momentum and coordinate space distributions of the impinging nuclei have to be close to reality if we want to describe actual experimental observables in an unbiased way. For the nuclear density profile $\rho(r)$ as a function of the radius of the nucleus with a mass number A a Woods-Saxon distribution is employed in PHSD:

$$\rho(r) = \rho_0 \frac{1 + \omega(r/R)^2}{1 + \exp(\frac{r-R}{a})}, \tag{2.47}$$

with ρ_0 as the density in the center of the nucleus, ω the deviation from a spherical shape, R as the nucleus radius and a as the skin depth. In (2.47) R and a are both functions of the mass number A,

$$R = R_0 A^{1/3}, \qquad a\,[\mathrm{fm}] = 0.02444\, A^{1/3} + 0.2864, \tag{2.48}$$

with $R_0 = 1.096\,\mathrm{fm}$. In this work we will look at spherical nuclei and thus have $\omega = 0$. The resulting density profile for a ^{64}Cu,^{197}Au and ^{208}Pb nucleus is presented in Fig. 2.5. The Pb nucleus is slightly larger than the Au nucleus and the skin depth is somewhat

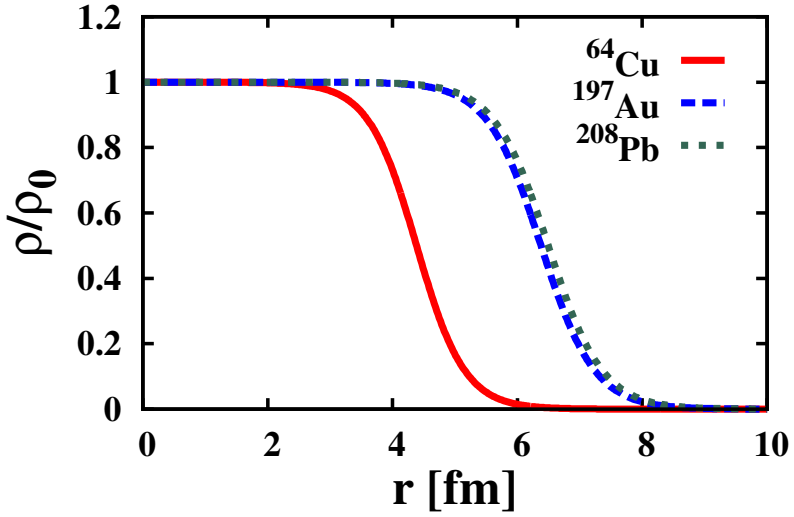

Fig. 2.5 – Woods-Saxon distribution of a ^{64}Cu,^{197}Au and ^{208}Pb nucleus.

different, but these small differences propagate in a HIC to apparent differences in the final particle spectra, making the correct initial conditions crucial.

In PHSD the nuclei are taken to be in the semi-classical groundstate, i.e. the nucleons are assigned a momentum $0 < |\mathbf{p}| < p_F$ with p_F denoting the Fermi momentum according

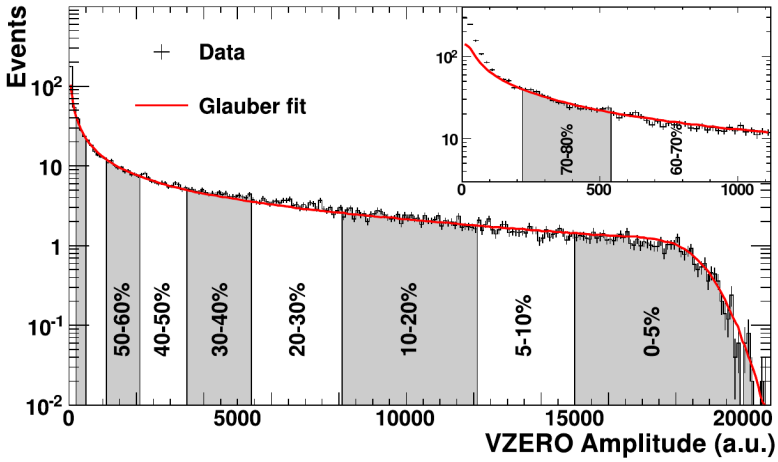

Fig. 2.6 – Example for the centrality class section used in experiments. The figure is taken from the ALICE collaboration for Pb+Pb collisions at $\sqrt{s_{NN}} = 2.76\,\text{TeV}$ [69].

to the local density of the nucleus:

$$p_F(r) = \sqrt[3]{\frac{3}{2}\pi^2\rho(r)}. \tag{2.49}$$

This momentum-space distribution is known as the Thomas-Fermi approximation. After the distribution of momenta to the nucleons by Monte Carlo the nucleus is boosted to its (numerical) rest frame since the Monte Carlo selection leads to a small but non-zero value for the total momentum of the nucleus.

The two nuclei are located at some distance from each other in the z-direction which they have to pass before the first collisions happen. In a HIC most of the time the nuclei do not fly centrally towards each other but are displaced by the impact parameter — denoted by b — in x-direction. This determines in PHSD the centrality class of interest.

Since the impact parameter b cannot be measured directly in experiment, the evaluation of the number of participants N_{part} or wounded nucleons N_w in PHSD defines the experimental centrality class. The selection of the centrality classes used in the evaluation of the experimental data follows the scheme shown in Fig. 2.6 (taken from [69]). The total cross section is divided into slices of certain percentages that the experimentalists choose by convention and then either N_{part} or N_w is extracted from the data sets using a fit by the Glauber model. The impact parameter for a e.g. 0-5% central Pb+Pb collision at $20A\,\text{GeV}$ can differ to a collision at $158A\,\text{GeV}$ as the total cross section varies for different energies. 0% centrality means that we have an impact parameter of $b = 0\,\text{fm}$ — a perfectly central collision — and 100% centrality is equivalent to the sum of the two nuclear radii.

Finally, after specifying the nuclei in their "groundstate" the spatially (in x- and z-direction displaced) nuclei are boosted in z-direction towards each other according to the investigated energy, e.g. with boost momenta $P_{\text{boost}} = 8.6\,\text{GeV}$ ($\widehat{=}\sqrt{s_{NN}} = 17.3\,\text{GeV}$).

2.3.3 Strings

In the initial hard scatterings strings are formed according to the LUND string model [70–72]. Strings are color-neutral objects where a color electric field is stretched between the drifting colored string ends, that can either be quarks/antiquarks or di(anti)quarks. A baryon string consists of a diquark and quark string end and a meson of a quark and antiquark string end.

We now introduce the concept of "leading" and "secondary" (pre-)hadrons. The string ends stemming from the initial hard scatterings are called "leading". They pick up almost instantly a quark/antiquark from the vauum and form a color-neutral leading pre-hadron. The number of leading quarks/antiquarks from the inital hard scattering is two (three) for mesons (baryons) but in practice it is commonly only one leading quark/antiquark, because the leading quarks/antiquarks are chosen by the highest momenta in the center-of-mass of the string.

As the string ends drift apart, the color electric field energy between the strings builds up linearly with the string tension $\kappa \approx 0.176\,\mathrm{GeV}^2 \approx 0.9\,\mathrm{GeV/fm}$, in line with lQCD calculations, until the energy is high enough to create a real $q\bar{q}$ pair from the vacuum. The secondary pre-hadrons interact with the surrounding matter only after the formation time $\tau_f \approx 0.5 - 0.8\,\mathrm{fm/c}$ after the initial collision. The formation time has to be taken in the eigentime t_f of the secondaries. This process is sketched in Fig. 2.7, where the pink shaded area indicates the hadronization of the pre-hadrons. The leading pre-

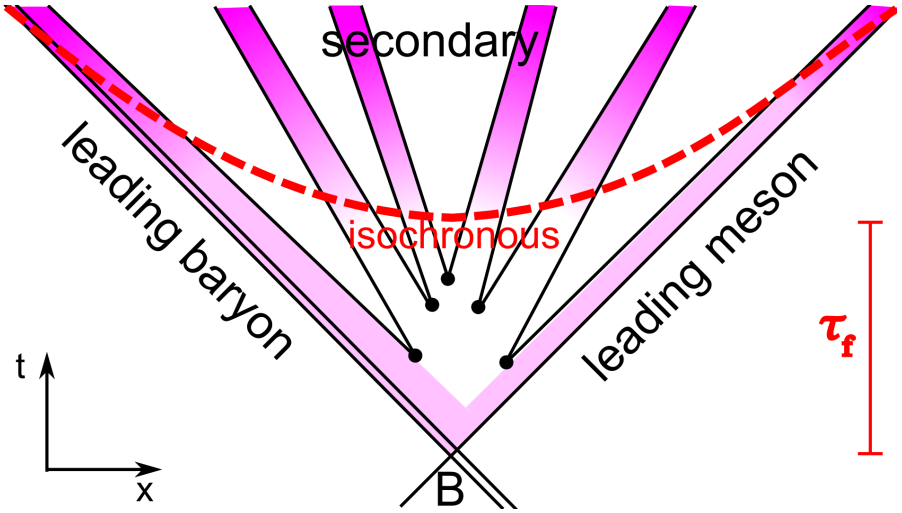

Fig. 2.7 – Illustration of the string formation and decay in the center-of-mass frame of the initial baryon, whose string ends (diquark and quark) are drifting apart. The leading pre-hadrons are formed almost instantly (pink area) whereas the secondary prehadrons are only formed after the formation time τ_f, illustrated by the isochronous time hyperbola.

hadrons may interact instantly with reduced cross sections, according to the constituent quark model, e.g. for quarks the cross section is $\sigma_{\mathrm{lead}} = 1/3\sigma_{NN}$. The masses of the pre-hadrons are given by the invariant mass of the fusing string ends. Neglecting the

constituent quark masses we have particles moving along the light cone, held together to a pre-hadron by the string tension κ. This is displayed in Fig. 2.8 where the initial quark and antiquark separate by the transverse momentum q_0 and $\bar{q}_0$, respectively, and the enclosed areas are equal to the transverse energy/mass of the pre-hadrons, denoted by m^2.

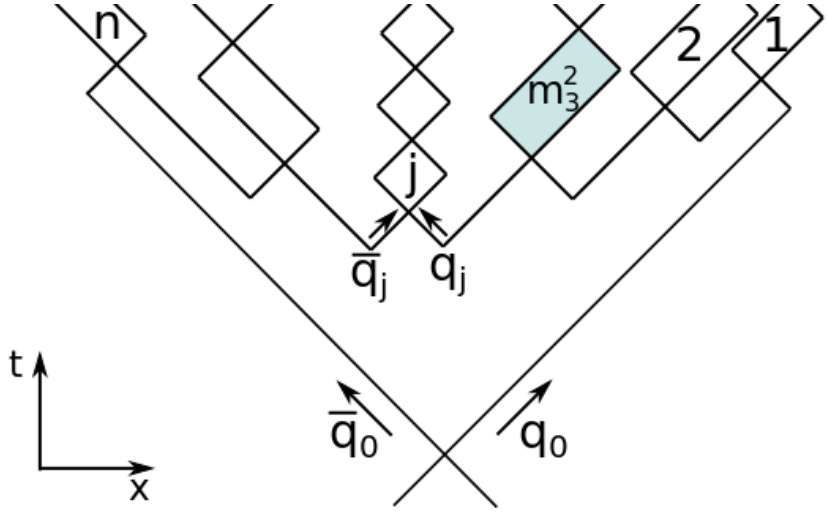

Fig. 2.8 – Illustration of the mass formation of a string for the case of massless quarks drifting apart from each other with the transverse momenta q_0 and $\bar{q}_0$, respectively. The enclosed area of the prehadrons is equal to their transverse masses squared m_i^2.

The actual chemistry of the string decay is given by the **Schwinger formula**. For a shorthand derivation we look at a produced $q\bar{q}$ pair produced at time $t = 0$ and distance $r = 0$. If we separate the $q\bar{q}$ pair to a distance r from the origin we raise the string potential by $2\kappa r$. The transverse energy squared of the quark/antiquark is given by $m_t^2 = p_t^2 + m^2$ so that each virtual parton has to have a longitudinal momentum of

$$p_L^2 + m_t^2 = (\kappa r)^2 \qquad \Rightarrow \qquad p_l = i\sqrt{m_t^2 - (\kappa r)^2}. \tag{2.50}$$

The $q\bar{q}$ pair becomes real for $r \geq m_t/\kappa$, forming a constraint on the distance integration for the action of this process,

$$S = 2\int_0^{m_t/\kappa} \mathrm{d}r \sqrt{m_t^2 - (\kappa r)^2} \tag{2.51}$$

$$= 2\frac{m_t^2}{\kappa}\int_0^1 \mathrm{d}x\sqrt{1-x^2} \tag{2.52}$$

$$= \pi\frac{m_t^2}{2\kappa}. \tag{2.53}$$

Finally, the Schwinger formula is given by the tunnelling amplitude

$$J = \exp(-S) = \exp\left(-\frac{\pi m_t^2}{2\kappa}\right). \tag{2.54}$$

Important for the chemistry of the string decay are only the relative probabilities of forming either a $u\bar{u}$,$d\bar{d}$,$s\bar{s}$ or any of the possible diquark-antidiquark pairs. The relative factors used in PHSD — without Chiral Symmetry Restoration (CSR) — are

$$u : d : s : diquark = \begin{cases} 1:1:0.3:0.07 & \text{for } \sqrt{s_{NN}} \geq 37\,\text{GeV}, \\ 1:1:0.4:0.07 & \text{for } \sqrt{s_{NN}} \leq 8\,\text{GeV}. \end{cases} \tag{2.55}$$

In between $\sqrt{s_{NN}} = 8$ and 37 GeV the relative factor for s is linearly approximated between 0.3 and 0.4 . When the CSR is taken into account the masses of quarks change with the scalar quark condensate and with this also the ratios of the different abundances. The derivation of the relevant formulae in the non-linear $\sigma - \omega$ model and the implementation into PHSD of the CSR is described in the work of Alessia Palmese [15]. Fig. 2.9 a) is taken from the same publication and shows the different ratios in case of CSR.

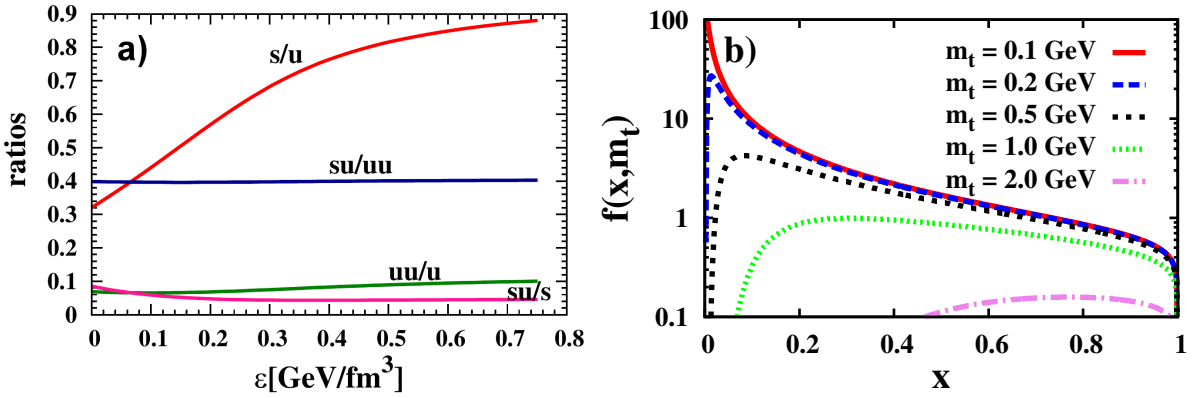

Fig. 2.9 – a) The quark and diquark ratios in the string decay (hadronic environment) as a function of the energy density ε for $T = 0$. The figure is taken from [15]. b) The LUND fragmentation function as a function of the energy fraction x for transverse masses $0.1\,\text{GeV} \leq m_t \leq 2\,\text{GeV}$.

The masses of the pre-hadrons are chosen according to the LUND fragmentation function $f(x, m_t)$, giving the probability for a hadron with transverse mass m_t to acquire the energy fraction x,

$$f(x, m_t) \approx \frac{1}{x}(1-x)^a \exp\left(\frac{-b\, m_t^2}{x}\right), \tag{2.56}$$

with $a = 0.23$ and $b = 0.34\,\text{GeV}^{-2}$. This fragmentation function is shown in Fig. 2.9 b) for transverse masses $0.1\,\text{GeV} \leq m_t \leq 2\,\text{GeV}$.

2.3.4 Quark gluon plasma

When the local energy density ε of a cell in its rest frame is larger than the critical energy density of $\varepsilon_c \approx 0.5\,\text{GeV/fm}^3$ the newly produced hadrons (formed from the

strings) are dissolved into their respective quarks, antiquarks and mean-field energy. In Fig. 2.10 the energy-density profile of a central Pb+Pb collision at 40A GeV bombarding energy for different time slices is shown. In panel (a) we see the in z-direction Lorentz-

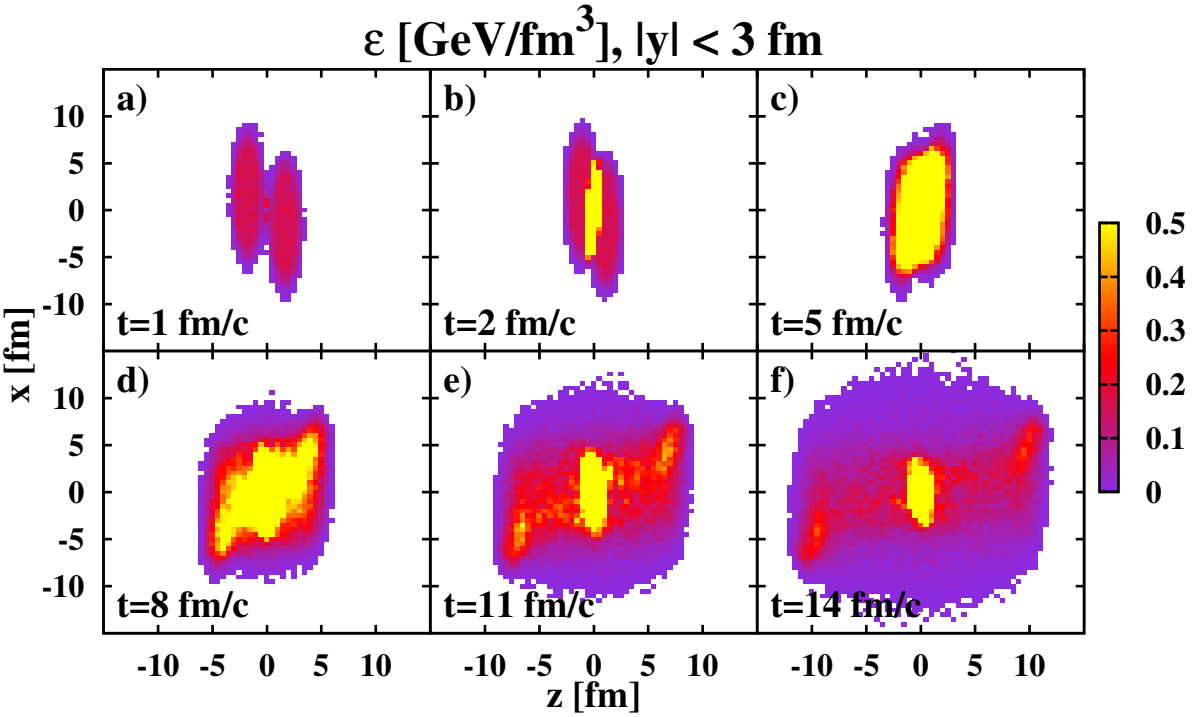

Fig. 2.10 – Profile of the central local energy density for a Pb+Pb collision at 40A GeV and an impact parameter of 3 fm for the times t =1,2,5,8,11 and 14 fm/c.

contracted nuclei just touching each other; the energy density is distributed according to the abundance of protons and neutrons and is $\approx 0.15\,\mathrm{GeV/fm^3}$. In (b) the energy density of the center is already higher than the critical energy density ε_c for the QGP phase transition (yellow area). As the system expands the energy density drops until a QGP can no longer be formed and hadronizes. In the periphery this process ends at 11 fm/c whereas in the center of the collision a QGP can still be found for times $t \geq 14\,\mathrm{fm/c}$.

To illustrate the extension of the QGP phase and its duration for different systems we show in Fig. 2.11 the energy fraction of the QGP as a function of time for different bombarding energies and impact parameters. We see that the QGP formation starts already at rather small energies ($\sqrt{s_{NN}} = 6.3\,\mathrm{GeV}$) with small QGP droplets. At $\sqrt{s_{NN}} = 17.3\,\mathrm{GeV}$ already a third of the energy is contained in the QGP at time $t \approx 2\,\mathrm{fm/c}$. The maximum of the energy density fraction shifts to smaller times when going up in energy due to the higher velocities of the nuclei, whereas the peak shifts to later times when the impact parameter is increased because of the later overlap of the nuclei. The QGP dies out around 10 fm/c for energies lower than $\sqrt{s_{NN}} = 39\,\mathrm{GeV}$ and has a substantial life time of about 40 fm/c at the top RHIC energy ($\sqrt{s_{NN}} = 200\,\mathrm{GeV}$).

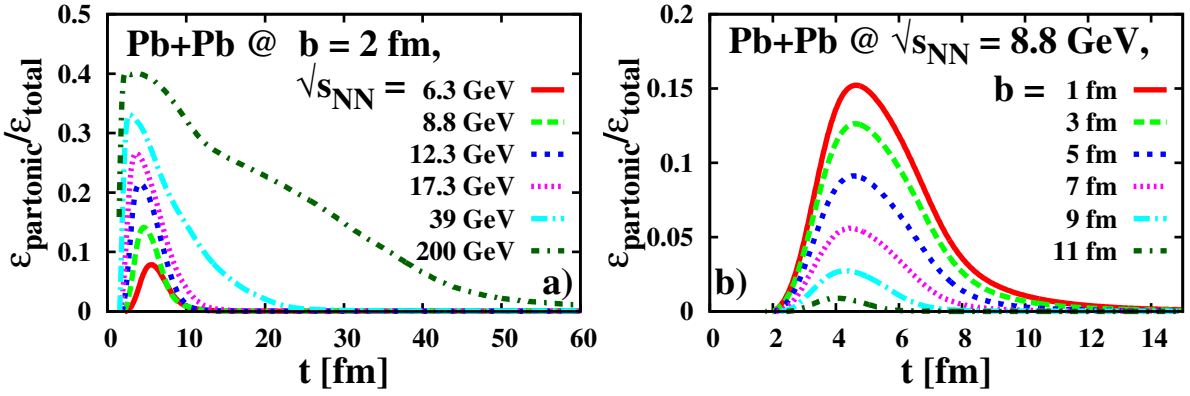

Fig. 2.11 – The energy fraction of the QGP as a function of time t in Pb+Pb collisions for different collision energies $\sqrt{s_{NN}}$ at an impact parameter of $b = 2\,\mathrm{fm}$ (a) and a variety of impact parameters for $40A\,\mathrm{GeV}$ ($\sqrt{s_{NN}} = 8.8\,\mathrm{GeV}$) (b).

In the dissolution of the pre-hadrons the spectral properties of the partons are defined by the DQPM, where they are treated as off-shell quasiparticles (see Sec. 2.2). Inside the QGP the partons interact with each other via cross sections calculated in the DQPM. The following (quasi-)elastic,

$$q + q \to q + q, \qquad q + \bar{q} \to q + \bar{q}, \qquad \bar{q} + \bar{q} \to \bar{q} + \bar{q}, \tag{2.57}$$

$$g + g \to g + g, \qquad g + q \to g + q, \qquad g + \bar{q} \to g + \bar{q}, \tag{2.58}$$

and inelastic,

$$q + \bar{q} \leftrightarrow g, \tag{2.59}$$

interactions are considered in PHSD. The probability for a gluon to decay into a $s\bar{s}$ quark pair is slightly suppressed due to the higher mass of the s quark in comparison to u and d quarks.

As the system expands the local energy densities will drop close to the critical energy density ε_c and the quarks start to hadronize into off-shell mesons and baryons. The hadronization process is driven (for example) for the fusion of a quark-antiquark pair with the energy-momentum vectors q and $\bar{q}$ into a meson with the energy-momentum vector p by the Lorentz-invariant transition rate

$$\frac{\mathrm{d}N_m(x,p)}{\mathrm{d}^4x\,\mathrm{d}^4p} = \mathrm{Tr}_q\mathrm{Tr}_{\bar{q}}\,\delta^4(p - p_q - p_{\bar{q}})\delta^4\left(\frac{x_q + x_{\bar{q}}}{2} - x\right) p_q^0 A_q(p_q) p_{\bar{q}}^0 A_{\bar{q}}(p_{\bar{q}})|v^2_{q\bar{q}}| \times W_m\,(x_q - x_{\bar{q}}, p_q - p_{\bar{q}})\, f_q(x_q,p_q) f_{\bar{q}}(x_{\bar{q}},p_{\bar{q}})\delta(\mathrm{flavor}), \tag{2.60}$$

with f_i and A_i as the phase-space distribution and the spectral functions of the quarks and antiquarks, respectively, as well as $|v_{q\bar{q}}|^2$ the transition matrix element squared obtained within the DQPM. In Eq. (2.60) Tr_i is a short-hand notation for

$$Tr_i = \sum_i \int \mathrm{d}^4x_i \int \frac{\mathrm{d}^4p_i}{(2\pi)^4}, \tag{2.61}$$

and W_m is the dimensionless phase-space distribution for the meson:

$$W_m(x,p) = \exp\left(-\frac{x^2}{b^2}\right)\exp\left(-b^2p^2\right). \tag{2.62}$$

The parameter $b^2 = \langle r^2\rangle = 0.64\,\mathrm{fm}^2$ corresponds to the average radius squared of a meson in its rest frame. Additionally, in Eq. (2.60) we have energy, momentum and flavor conserving delta functions which assure that all quantum numbers are conserved during hadronization. Furthermore, the hadronization rate can be directly translated into the fusion of three (anti)quarks into a(n) (anti)baryon. The transition matrix element $|v_{q\bar{q}}|^2$ depends on the local energy density and has a higher value for lower energy densities, forcing the system into a hadronic phase since the dissolution of the hadrons into partons is suppressed by the large parton masses at lower energy densities (or temperature T; cf. Fig. 2.2).

2.3.5 Hadronic scattering

In the hadronic phase, that is dominant at low bombarding energies or can be found in the corona and late times of a relativistic HIC, the particles interact elastically and inelastically with cross sections measured either in experiment or calculated in effective theories when experimental data are not available. Cross sections σ of two particles are taken to be geometrical in PHSD, meaning that the cross section defines a real area, which the colliding particles have to reach for the interaction to happen. With this geometrical interpretation of the cross section we define a maximum impact parameter b_{max} between two testparticles as

$$b \leq b_{max} = \sqrt{\frac{\sigma}{\pi}}. \tag{2.63}$$

Strings are formed in baryon-baryon collisions above $\sqrt{s} = 2.6\,\mathrm{GeV}$ and $\sqrt{s} = 2.2\,\mathrm{GeV}$ in meson-baryon reactions. For all reactions with lower invariant energy $\sqrt{s}$ detailed balance is used for the backward channel. In PHSD currently 2-particle interactions ($2 \leftrightarrow 2$), formation of resonances and their decay ($1 \leftrightarrow 2$) and the annihilation of antibaryons in baryonic matter via the formation of three mesons ($2 \leftrightarrow 3$) are incorporated. In this work we will have a special emphasis on the last type of interactions as we will extend them to the strange quark sector and inspect how the final baryon and antibaryon spectra are modified.

2.3.6 Overview

In this subsection we investigate the relative importance of the different production channels. We here focus on particles stemming from the partonic phase, particles produced from a string and particles from $B\bar{B} \leftrightarrow 3M$ (short for baryon-antibaryon annihilation

into three mesons and reproduction through the inverse channel) without strange quark suppression — the meaning of this will be discussed in Chapter 4.1. For this we show in Fig. 2.12 a compilation of the reaction rates in the forward and backward direction (when applicable) as a function of time for central Pb+Pb collisions at $\sqrt{s_{NN}} = 4.7, 8.8$ and 200 GeV. For the lower energies the QGP phase has a significant rate only in the

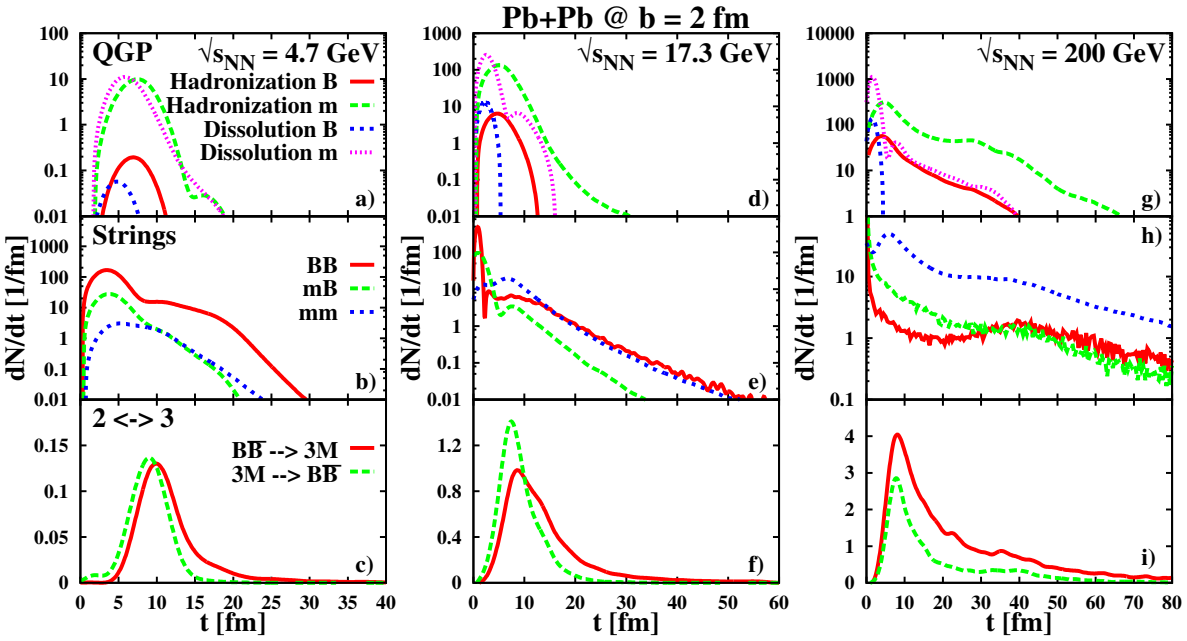

Fig. 2.12 – Compilation of the QGP dissolution and hadronization rates (upper panels), the inelastic string formation rates (middle panels) and the baryon-antibaryon annihilation and reproduction rates (lower panel) from PHSD as a function of time for central Pb+Pb collisions at $\sqrt{s_{NN}} = 4.7, 8.8$ and 200 GeV. The meson (m) and baryon (B) interactions are presented separately.

first 20 fm/c where the energy densities are high enough to sustain the QGP whereas at $\sqrt{s_{NN}} = 200$ GeV mesons hadronize even beyond 70 fm/c at high rapidities. The string formation rate from baryon-baryon scattering rises sharply in the first fm/c after the nuclei collide, then proceeds almost on a plateau until it finally drops exponentially. The meson-meson and meson-baryon rates show a similar behavior, only the order of the process with the highest reaction rate changes with energy. At 4.7 GeV the string formation from baryon-baryon scatterings dominates throughout the collision whereas at $\sqrt{s_{NN}} = 17.3$ GeV the baryon-baryon and meson-baryon string formations lie on top of each other for times $t > 15$ fm/c and the meson-meson rates dominate at 200 GeV. The $B\bar{B} \leftrightarrow 3M$ reaction rates are peaked around 10 fm/c after which they also drop almost exponentially. Depending on the energy we find both a net annihilation and reproduction by $2 \leftrightarrow 3$ reactions — the net-annihilation as a function of energy will be discussed in more detail in Sec. 5.3. In general the QGP becomes more significant as we go up in energy and at the top RHIC energy of $\sqrt{s_{NN}} = 200$ GeV hadronization from the QGP is the main production channel.

To see what kind of processes the final antibaryons experienced during the collision we show in Fig. 2.13 the accumulated number of times a $\bar{p}, \bar{\Lambda} + \bar{\Sigma}^0$ and $\bar{\Xi}^+$ went through any of the three interesting processes in a Pb+Pb collision at impact parameter $b = 2\,\text{fm}$ and energies $\sqrt{s_{NN}} = 4.7, 8.8$ and $200\,\text{GeV}$. Depending on the particle and energy the

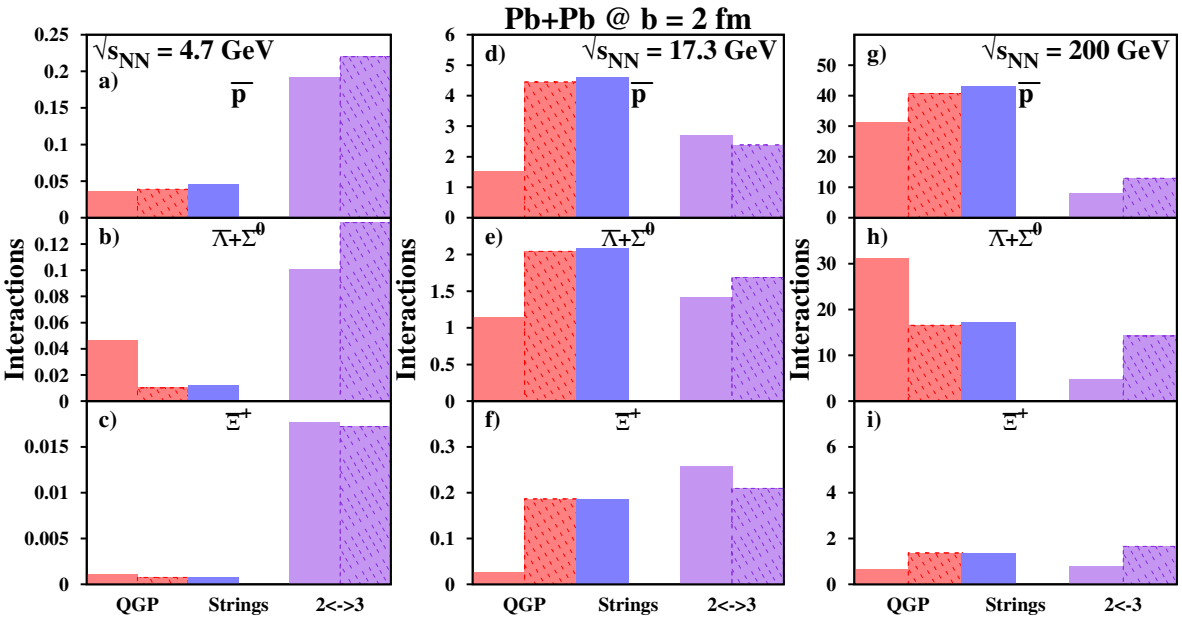

Fig. 2.13 – The accumulated number of dissolutions and hadronizations in the QGP phase (red), productions through strings (blue) and annihilations and recreations through $B\bar{B} \leftrightarrow 3M$ interactions (purple) of $\bar{p}, \bar{\Lambda} + \bar{\Sigma}^0$ and $\bar{\Xi}^+$ in Pb+Pb collisions at an impact parameter of b =2 fm and collision energies $\sqrt{s_{NN}} = 4.7, 8.8$ and $200\,\text{GeV}$. The full boxes indicate the gain and the dashed boxes the loss through the respective process.

different reaction types show a varying behaviour. In general the relative number of $2 \leftrightarrow 3$ processes drops as one goes up in energy but at the same time the differences between the annihilation and reproduction increase such that the final particle spectra are influenced by a larger amount. At the lowest energy $\sqrt{s_{NN}} = 4.7\,\text{GeV}$ the number of $2 \leftrightarrow 3$ reactions for the antibaryons is more than three times larger than any of the other interactions, whereas at the top RHIC energy of $\sqrt{s_{NN}} = 200\,\text{GeV}$ the $2 \leftrightarrow 3$ interactions are the lowest. In the antibaryon sector almost all of the particles produced in string decays get dissolved into the QGP phase throughout all energies. The antibaryon production from the QGP phase varies with energy and particle species, e.g. the hadronization of $\bar{\Lambda} + \bar{\Sigma}^0$ surpasses the string production at $\sqrt{s_{NN}} = 4.7\,\text{GeV}$ and $200\,\text{GeV}$ in contrast to $17.3\,\text{GeV}$ where the opposite is found, such that no clear trend with increasing energy is evident.

We learn from Figs. 2.12 and 2.13 that with rising energy the QGP phase becomes the main production process for hadrons in general and especially for the antibaryons. The interactions in the late stages of a collision happen mainly through strings because — due to the low particle density from the expansion — neither a QGP can be formed

nor a three meson fusion nor $2 \leftrightarrow 3$ occur too frequently. Depending on the particle species and collision energy a net annihilation or recreation can be found due to the $2 \leftrightarrow 3$ reactions, changing to a certain degree the abundance of antibaryons; a thorough analysis at different energies will be given in Chapter 5.

Chapter 3

The quark rearrangement model (QRM)

In this chapter we present the quark rearrangement model that is extended in this work to the strangeness sector. The quark rearrangement model is used for the description of baryon-antibaryon annihilation and recreation through three mesons ($B\bar{B} \leftrightarrow 3M$). In this model the backward reaction of three mesons fusing into a $B\bar{B}$ pair is easily realized through the constraint of detailed balance. Up to today other transport approaches like the Ultra-relativistic Quantum Molecular Dynamics model (UrQMD) [32,33] discard the backward channel and only consider the annihilation. The importance of $B\bar{B}$ recreation and of the strangeness sector in HICs is still an open issue that is addressed in chapter 5. We start with the motivation for the QRM from low-energy $p\bar{p}$ annihilation and then derive the reaction probabilities using detailed balance and the Lorentz-invariant transition rates for number changing processes. The model has originally been introduced in Ref. [42].

3.1 Concept

As discussed in Ref. [42] one experimentally finds a dominant annihilation of $p\bar{p}$ into five pions at invariant energies $2.3\,\mathrm{GeV} \leq \sqrt{s} \leq 4\,\mathrm{GeV}$, see Fig. 3.1. The final number of five pions may be interpreted as an initial annihilation into $\pi\rho\rho$ with the ρ mesons decaying subsequently into two pions each. The channel $\pi\pi\rho$ then leads to four final pions, the channel $\pi\omega\rho$ to six final pions, the channel $\rho\omega\rho$ to seven final pions, etc. Accordingly, the baryon-antibaryon annihilation in the first step is a two-to-three reaction with a conserved number of quarks and antiquarks. This is the basic assumption of the quark rearrangement model which is also illustrated in Fig. 3.2. The annihilation reaction $p\bar{p} \to \pi\rho\rho$ is the dominant process in $p\bar{p}$ annihilation for invariant masses below 4 GeV, typical for scatterings in the hadronic phase of a heavy-ion collision. By allowing the mesons M_i to be any member of the 0^- or 1^- nonets one can describe

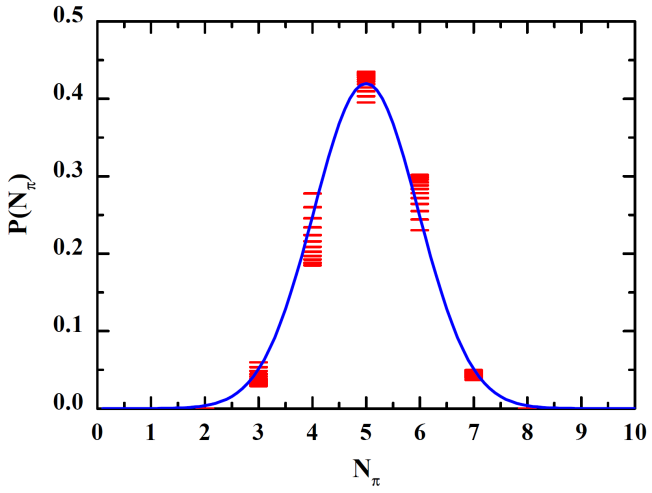

Fig. 3.1 – Distribution in the final number of pions $P(N_\pi)$ for $p\bar{p}$ annihilation at invariant energies $2.3\,\mathrm{GeV} \leq \sqrt{s} \leq 4\,\mathrm{GeV}$ (short lines). The solid line is a Gaussian parametrization fitted to the experimental data. The figure is taken from Ref. [42].

an arbitrary $B\bar{B}$ annihilation and recreation by rearranging the quark and antiquark content. An implementation of baryon-antibaryon annihilation in such a manner misses the annihilation into one or two mesons, however, higher numbers of final mesons are implemented through the subsequent decay channels one finds in transport approaches such as PHSD. This approach gives a realistic description for $p\bar{p}$ annihilation and we assume that for other baryon-antibaryon pairs than $p\bar{p}$ a similar annihilation pattern holds. Since there are no measurements of annihilation cross sections other than $n\bar{p}$ and $p\bar{p}$ this is our best guess which might be falsified by experiment.

3.2 Covariant transition rates

The quark rearrangement model only contains reactions of the kind $2 \leftrightarrow 3$. The detailed balance based Lorentz-invariant on-shell collision rate for the reaction $B\bar{B} \to 3M$ in a volume element of size $\mathrm{d}V$ and time-step size $\mathrm{d}t$ is written as [42]:

$$\frac{\mathrm{d}N_{\mathrm{coll}}[B\bar{B} \to 3 \text{ mesons}]}{\mathrm{d}t\,\mathrm{d}V} = \sum_c \sum_{c'} \frac{1}{(2\pi)^6} \int \frac{\mathrm{d}^3p_1}{2E_1} \frac{\mathrm{d}^3p_2}{2E_2}\, W_{2,3}(\sqrt{s}) \times R_3(p_1+p_2;c) N^c_{\mathrm{fin}} f_1(x,p_1) f_2(x,p_2). \quad (3.1)$$

In (3.1) c' denotes all $B\bar{B}$ pairs with the properties $c' = (m_1^{c'}, m_2^{c'}; \nu^{c'})$; c are all the possible meson channels with $c = (m_3^c, m_4^c, m_5^c; \lambda^c)$, with m being the masses of the respective particles, and ν and λ the quantum numbers signifying the channel (charge,

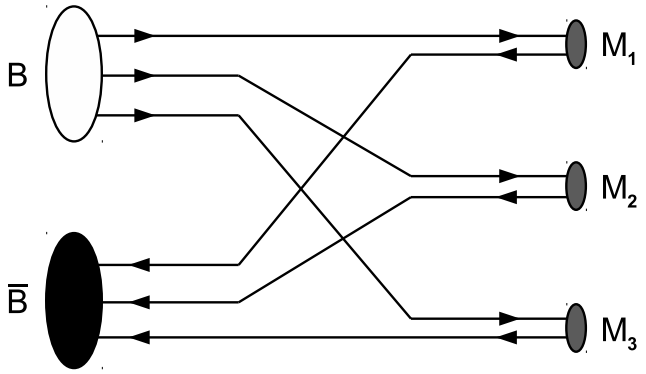

Fig. 3.2 – Illustration of the quark rearrangement model for a general baryon-antibaryon pair $B\bar{B}$ annihilating into three mesons M and vice versa. Here the meson M_i may be any of the 0^- or 1^- nonets.

parity, spin and strangeness). We assume that the transition matrix element squared $W_{2,3}$ does not significantly depend on the outgoing momenta and just on the invariant mass of the reaction, which holds approximately true for $p\bar{p}$ as we will see later, and allows the splitting of the phase-space integral. A formulation based on the matrix element will ensure detailed balance. The on-shell n-body phase-space integral is defined by

$$R_n(P; m_1, \ldots, m_n) = \left(\frac{1}{(2\pi)^3}\right)^n \int \prod_{k=1}^{n} \frac{\mathrm{d}^3 p_k}{2E_k} \, (2\pi)^4 \times \delta^4 \left(P - \sum_{j=1}^{n} p_j\right) \tag{3.2}$$

and in case of a constant transition matrix element dominates the interaction rate of the system. The factor N^c_{fin} is the multiplicity of the meson triple c and results from the summation over the spin s and possible isospin projections F_{iso} compatible with charge conservation of the meson channel c:

$$N^c_{\mathrm{fin}} = (2s_3 + 1)(2s_4 + 1)(2s_5 + 1)\frac{F_{\mathrm{iso}}}{N_{\mathrm{id}}!}. \tag{3.3}$$

The division by $N_{\mathrm{id}}!$, with N_{id} denoting the number of identical mesons, ensures that each charge configuration is only considered once for a given meson triple. The functions f are the distribution functions of the $B\bar{B}$ pair in momentum and coordinate space. When looking at a specific $B\bar{B}$ pair one has to make sure that only meson channels are considered which conserve charge, energy and parity. The probability of this specific $B\bar{B}$ pair c' to annihilate into any of these possible meson channels c is related to the

total annihilation cross section of the $B\bar{B}$-pair $\sigma_{\text{ann}}^{c'}$ [73]:

$$\begin{aligned}\frac{P_{\text{tot}}^{c'}\mathrm{d}V}{\mathrm{d}t} =& \frac{1}{4E_1E_2}\sum_c W_{2,3}(\sqrt{s})R_3(p_1+p_2;c)N_{\text{fin}}^c \\ =& v_{\text{rel}}\sigma_{\text{ann}}^{c'}(\sqrt{s}),\end{aligned} \tag{3.4}$$

$$v_{\text{rel}} = \frac{\sqrt{\lambda(s,m_1^2,m_2^2)}}{2E_1E_2}\ ;\ \lambda(a,b,c) = (a-b-c)^2 - 4bc, \tag{3.5}$$

where dV and dt are taken finite. The probability for a specific final state $\tilde{P}^{c'\to c}$ in case of an annihilation is then given by the available phase space and the multiplicity of all possible meson channels c:

$$\tilde{P}^{c'\to c} = N_3(c',\sqrt{s})R_3(p_1+p_2;c)N_{\text{fin}}^c, \tag{3.6}$$

$$\text{with}\quad N_3^{-1}(c',\sqrt{s}) = \sum_c R_3(p_1+p_2;c)N_{\text{fin}}^c, \tag{3.7}$$

where the sum runs only over those meson channels c that conserve the quantum numbers of c'.

In order to determine the probability for the three-meson fusion rate we start with the Lorentz-invariant reaction rate for this process [42],

$$\begin{aligned}&\frac{\mathrm{d}N_{\text{coll}}[3\text{ mesons}\to B\bar{B}]}{\mathrm{d}t\,\mathrm{d}V} = \\ &\sum_c\sum_{c'}\frac{1}{(2\pi)^9}\int\frac{\mathrm{d}^3p_3}{2E_3}\frac{\mathrm{d}^3p_4}{2E_4}\frac{\mathrm{d}^3p_5}{2E_5}\ W_{2,3}(\sqrt{s}) \\ &\times R_2(p_3+p_4+p_5;c')N_B^{c'}f_3(x,p_3)f_4(x,p_4)f_5(x,p_5),\end{aligned} \tag{3.8}$$

where $N_B^{c'}$ denotes the multiplicity of the final state and the two-body phase-space integral R_2 is given by

$$R_2(\sqrt{s};m_1,m_2) = \frac{\sqrt{\lambda(s,m_1^2,m_2^2)}}{8\pi s} \tag{3.9}$$

with λ defined in Eq. (3.5). The transition matrix element squared $W_{2,3}$ is not known but using Eq. (3.10) [73]

$$\begin{aligned}&\sum_m\sum_{\lambda_m}W_{2,m}(P^\mu = p_1^\mu + p_2^\mu;i,j;\lambda_m)R_m(P^\mu;M_3,\ldots,M_{m+1}) = \\ &\qquad 2\sqrt{\lambda(s,M_1^2,M_2^2)}\sigma_{i,j}(\sqrt{s}) = 4E_1E_2v_{\text{rel}}\sigma_{i,j}(\sqrt{s})\end{aligned} \tag{3.10}$$

for our special problem of $2\leftrightarrow 3$ processes one gets,

$$\begin{aligned}\sum_c P_{c\to c'}(\sqrt{s}) =& \sum_c W_{2,3}(\sqrt{s})R_3(\sqrt{s},c)N_{\text{fin}}^c \\ =& W_{2,3}N_3^{-1}(\sqrt{s},c') \stackrel{!}{=} 4E_1E_2v_{\text{rel}}\sigma_{\text{ann}}^{c'}(\sqrt{s}),\end{aligned} \tag{3.11}$$

where we have taken $W_{2,3}$ out of the sum over the baryon-antibaryon pairs and end up with the expression for the normalisation constant for the invariant energy $\sqrt{s}$ from Eq. (3.7). Inserting Eq. (3.11) for the transition matrix element squared into (3.8) gives the result for the transition probability for a specific meson channel c fusing together and forming a specific $B\bar{B}$ pair c',

$$\frac{P^{c\to c'}\mathrm{d}V^2}{\mathrm{d}t} = \frac{1}{4E_3E_4E_5}\sigma^{c'}_{\mathrm{ann}}(\sqrt{s})N_3(c',\sqrt{s}) \times \frac{\lambda(s,m_1^2,m_2^2)}{8\pi s}N_B^{c'}. \tag{3.12}$$

Note that all energies and momenta in the calculations of the transition probabilities are in the laboratory frame.

3.3 Annihilation cross sections

For the calculation of actual collision probabilities, Eq. (3.4) and (3.12), we are still missing the cross sections. As already mentioned above we assume the cross sections to depend only on the invariant energy, not the outgoing momenta. This assumption is approximately fulfilled for $p\bar{p}$ and $n\bar{p}$ annihilation, see Fig. 3.3 where the cross section can be fitted by $\sigma^{p\bar{p}}_{\mathrm{ann}}(\sqrt{s}) = 50\,\mathrm{mb}/v_{\mathrm{rel}}$, with v_{rel} denoting the relative velocity. Other channels have not been measured so far. Since there are no experimental data available we assume a similar behavior for different spin combinations like $p\bar{\Delta}$. Furthermore,

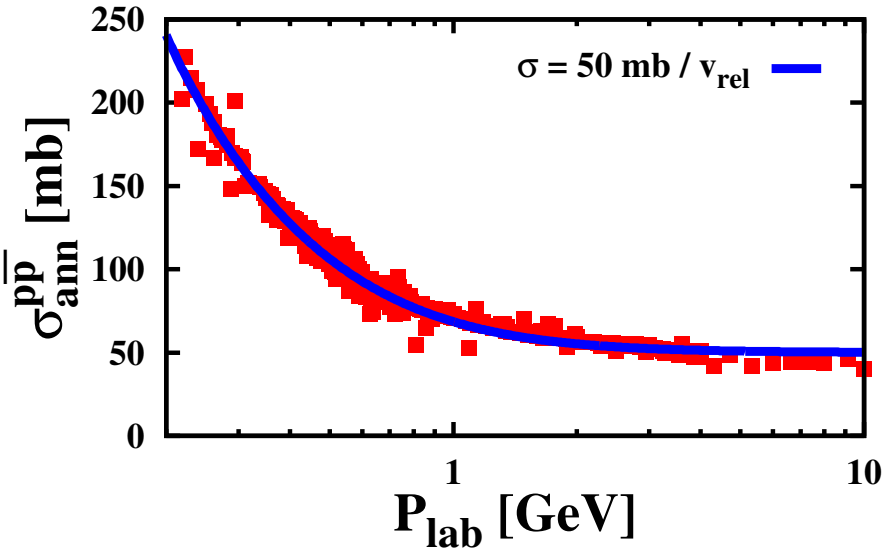

Fig. 3.3 – $p\bar{p}$ annihilation cross section as a function of momentum in the laboratory P_{lab}. The data points are taken from [1] and the solid line is a fit by the function 50 mb/v_{rel} with v_{rel} denoting the relative velocity in the laboratory system (3.5).

the cross section was measured experimentally in the vacuum where the cross section diverges for small relative momenta. In the calculations for HICs we take into account

only next-neighbour interactions due to the medium and thus cut the cross section at 80 mb resulting in an effective maximum interaction range of about 1.6 fm.

In this work we investigate in particular the strangeness sector. We model the cross sections of particles with strangeness by

$$\sigma_{\text{ann}}^{c'}(\sqrt{s}) = \sigma_{\text{ann}}^{p\bar{p}} \lambda^{\varsigma+\bar{\varsigma}}, \tag{3.13}$$

where ς and $\bar{\varsigma}$ are the number of strange and antistrange quarks in the $B\bar{B}$ pair c' and $\lambda \in [0, 1]$ is a factor suppressing the transition matrix element for particles taking part in the quark rearrangement model and effectively suppressing the cross section. This parametrization is motivated by PYTHIA [74] simulations where one sees a similar suppression for particles with strangeness compared to non-strange particles at the same energy above threshold. In the first investigations of the QRM in PHSD at SPS energies in Sec. 5.1 the suppression factor has the value λ=0.5 which is in rough agreement with the PYTHIA simulations embedded in PHSD. We choose a dependence on not just the net strangeness S but the sum of strange and antistrange quarks $\bar{\varsigma} + \varsigma$ due to their higher mass and a subsequent suppression of the rearrangement. The implementation with the strangeness $|S| = |\bar{\varsigma} - \varsigma|$ instead of $\bar{\varsigma} + \varsigma$ has no practical influence on the final results in case of relativistic heavy-ion collisions (cf. Appendix C.3). For nucleus-nucleus collisions at RHIC and LHC energies, discussed in Secs. 5.2 and 5.3, no suppression of the strangeness sector is taken into account.

Chapter 4

Box simulations

In this chapter we present the numerical realization of the QRM including the strangeness sector in a classical transport simulation in a box with periodic boundary conditions before incorporating the QRM in PHSD. By using box simulations we can check the physical correctness of our implementation and test the fulfillment of detailed balance in equilibrium. Additionally, the feasibility of the extended QRM in production runs of PHSD for relativistic heavy-ion collisions is tested.

4.1 Numerical method

In the extended QRM the particles listed in Table 2.1 in the light and strange quark sector are taken into account. Since the QRM is based on the valence quark picture we consider the hidden strangeness of the η — amounting to 50% light quark content and 50% $s\bar{s}$ content — and take ϕ to contain 83.1% $s\bar{s}$ according to the experimentally measured branching ratio into particles with strangeness. Looking only at the different mass channels — that are possible under these assumptions and the conservation of the quark content and parity — we end up with more than 2000 channels for the $2 \leftrightarrow 3$ reactions that are given explicitly in Appendix D.

In order to save computational time the possible combinations of $B\bar{B}/3M$ and final state particles with their charge constellation and multiplicity have to be calculated beforehand. All of this information needs to be stored to allow for a fast access. More details on the numerics are given in Appendix B.

In Eqs. (3.4) and (3.12), furthermore, the three-body phase-space R_3 is needed which is evaluated by

$$R_3(\sqrt{s}; m_1, m_2, m_3) = \int_{(m_1+m_2)^2}^{(\sqrt{s}-m_3)^2} \frac{\mathrm{d}M_2^2}{2\pi} R_2(\sqrt{s}; m_3, M_2) R_2(M_2; m_1, m_2), \tag{4.1}$$

with R_2 defined in Eq. (A.10) and given analytically. To make the computation feasible R_3 needs to be fitted. An almost perfect fitting function, that reproduces the phase-space close to threshold and up to more than 10 GeV above threshold, is given by

$$R_3(t, m_1, m_2, m_3) = a_1 t^{a_2} \left(1 - \frac{1}{a_3 t + 1 + a_4}\right), \tag{4.2}$$

with $t = \sqrt{s} - m_1 - m_2 - m_3$ and $a_i > 0$. The fit parameters a_i have been evaluated for each combination of meson masses m_1, m_2, m_3 and stored on file. For further details on the phase-space integrals we refer the reader to appendix A.

To check the consistency of our numerical implementation of the $2 \leftrightarrow 3$ reactions and their rates in equilibrium we use transport simulations in a box with periodic boundary conditions. We recall that in equilibrium — according to detailed balance — the reaction rate for $B\bar{B} \to 3M$ should be the same as for $3M \to B\bar{B}$. Furthermore, for a consistent implementation detailed balance should not only be fulfilled for the sum of all reaction channels but on a channel-by-channel basis. In the box simulations discussed below only the $B\bar{B} \leftrightarrow 3M$ reactions are considered and all particles are taken as stable such that no decays occur. Due to the large number of mass channels, an initialization with every possible channel is not feasible. Therefore, we look at systems which are initialized by a single type of baryon and antibaryon adding up to 100 systems for the consistency check (when leaving out the conservation of parity — in general the difference between calculations with and without parity conservation is negligible). The box simulations have the following initial conditions:

- The box volume is about 18000 fm^3 with periodic boundary conditions.
- All simulations have the same energy density $\varepsilon = 0.4\,\mathrm{GeV/fm}^3$ with 10% of the energy distributed to kinetic energy.
- The ratio between baryons and antibaryons is set to 2:1 and the net baryon density amounts to $\rho_B \approx 0.2\,\mathrm{fm}^{-3}$.
- The initial momentum distribution is of Boltzmann-shape.
- For the box simulations a suppression of channels including strangeness is neglected, i.e. $\lambda = 1$.

A representation of a typical initial condition in coordinate space is shown in Fig. 4.1. We recall that the fusion of three mesons can not be described in a Lorentz-invariant way by geometrical collision criteria between the particles due to the three inertial systems. To find a solution we employ the in-cell method introduced by Lang *et al.* [75] and adopted also in Ref. [42]. We mention that this method is also employed for $2 \leftrightarrow 3$ reactions in partonic cascade calculations by Xu *et al.* [76]. The in-cell method can be used for any number of colliding particles since there is no problem with time ordering due to the locality of the formulation. In the in-cell method space-time is divided into

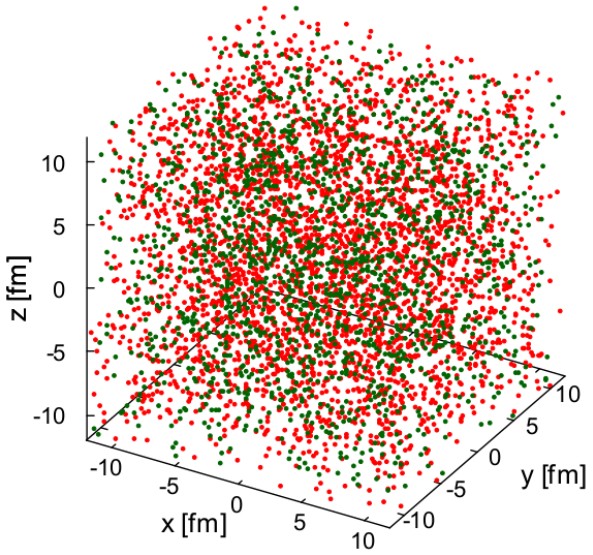

Fig. 4.1 – Coordinate space initialization of a box simulation. The red and green dots stand for baryons and antibaryons, respectively.

four dimensional cells with widths $\mathrm{d}x, \mathrm{d}y, \mathrm{d}z, \mathrm{d}t$ and only particles inside the same cell may interact with each other. One calculates the reaction probabilities of each particle with every other one inside the same cell and the actual collision and the final state is chosen by Monte Carlo. The possible final states and multiplicities in Eqs. (3.4) and (3.12) are precalculated to save computational time during the transport simulation. The cell size and the time step $\mathrm{d}t$ are optimized for the problem under investigation such that the total probability of a transition in a local cell does not exceed unity but is also not too small. For the actual calculations shown below we use $\mathrm{d}t = 4$ fm/c and $\mathrm{d}V$=40 fm^3 which ensures that the transition probabilities are always below unity.

4.2 Box simulations of the QRM

We now discuss results for a few selected systems. We present randomly picked ensembles that cover the qualitative range of possible systems, i.e. systems consisting of only initial light quarks, only initial strange/antistrange quarks as well as a variety of combinations of light and strange quarks/antiquarks. In Fig. 4.2 the time evolution of the particle densities for a system initialized only with protons and antiprotons is shown to demonstrate the production and annihilation of different particle species in a system consisting initially only of protons and antiprotons. After the first timestep of the simulation a lot of new mesons like pions, ρ and ω mesons are formed. At later times also strange mesons and baryons are formed because of the partial $s\bar{s}$ content of ϕ and η. In equilibrium the system has a significant amount of mesons and baryons with strange and antistrange quarks. However, the generation of strange quarks — even for the meson sector — takes a long time ($\approx 60\,\mathrm{fm/c}$) to produce significantly high strange

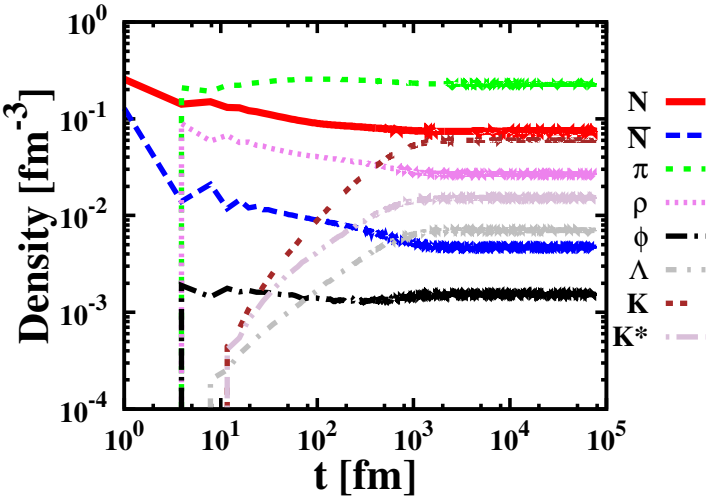

Fig. 4.2 – Particle densities of a $p\bar{p}$ initialized system as a function of time. The particle species correspond to the following lines: the red solid line corresponds to nucleons, the blue dashed line to antinucleons, the green short-dashed line to pions, the violet dotted line to ρ mesons, the black dashed-dotted line to ϕ mesons, the grey dashed-doubly-dotted line to Λ's, the brown doubly-dashed line to kaons and the beige short-dashed-dotted line to the vector kaons K^*. The different charge states of the particles have been summed over and K denotes the sum of K^+, K^-, K^0 and $\bar{K}^0$.

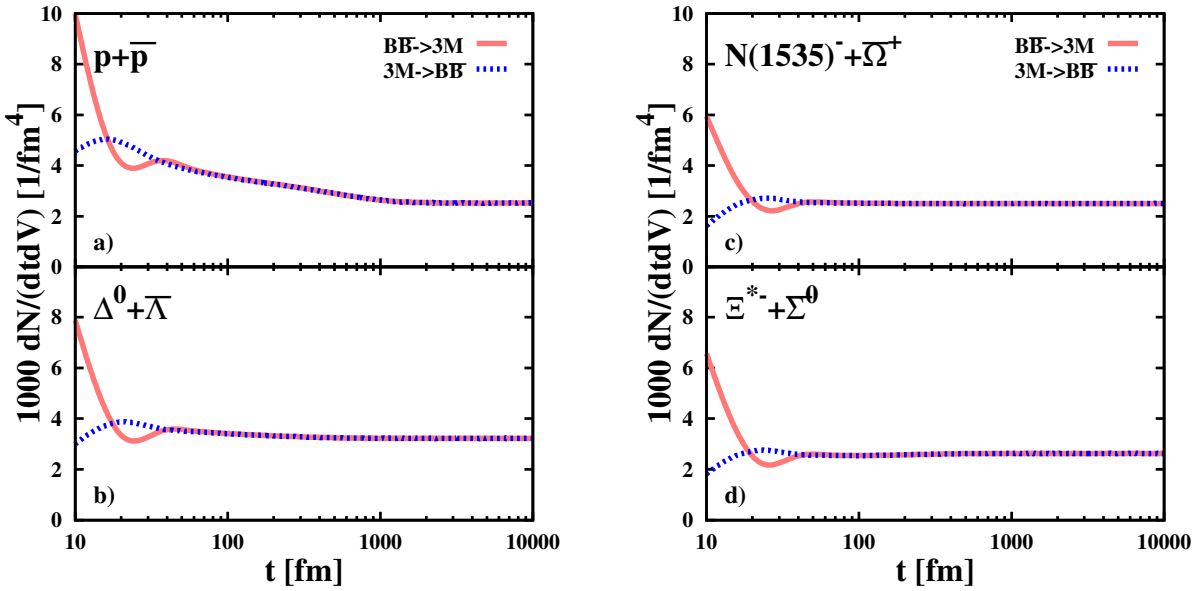

Fig. 4.3 – Total reaction rate (per volume dV) as a function of time for two different initializations. The solid (slightly transparent) red lines correspond to the baryon-antibaryon annihilation and the red dotted lines to the formation. The systems are initialized with only $p + \bar{p}$ (a), $\Delta^0 + \bar{\Lambda}$ (b), $\mathrm{N}(1535)^- + \bar{\Omega}^+$ (c) and $\Xi^{*-} + \bar{\Sigma}^0$ (d).

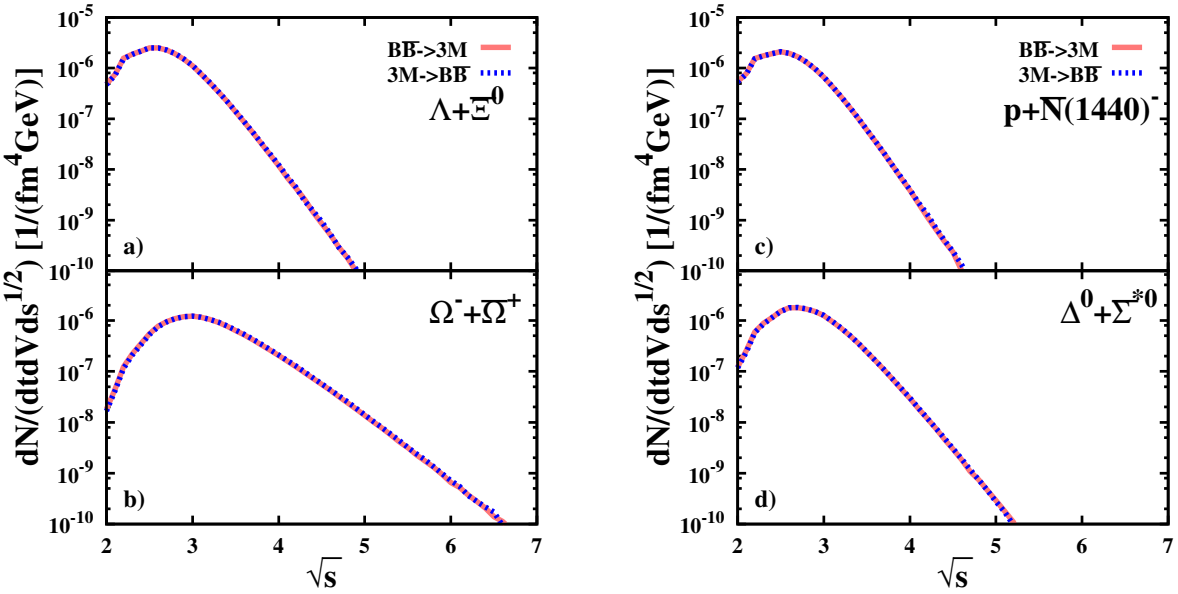

Fig. 4.4 – Total reaction rate as a function of the invariant mass $\sqrt{s}$ in equilibrium for five different initializations. The solid (slightly transparent) red line corresponds to the baryon-antibaryon annihilation and the red dotted line to the formation. The systems are initialized in with only $\Lambda + \bar{\Xi}^0$ (a), $\Omega^- + \bar{\Omega}^+$ (b), $p + \bar{\mathrm{N}}(1440)^-$ (c) and $\Delta^0 + \bar{\Sigma}^{*0}$ (d).

particle densities; thus the generation via ϕ and η should have negligible influence on actual heavy-ion collisions since large densities are needed for a significant contribution from the meson fusion. In a 5% central Pb+Pb collision at 158A GeV the meson fusion dies out at $\approx 13\,\mathrm{fm/c}$ which is insufficient for having a major influence on the strangeness sector, see Fig. 5.1 (discussed in Sec. 5.1 below).

We show in Fig. 4.3 the total reaction rate as a function of time for four exemplary initializations which were initialized with $p + \bar{p}$, $\Delta^0 + \bar{\Lambda}, N(1535)^- + \bar{\Omega}^+$ and $\Xi^{*-} + \bar{\Sigma}^0$, respectively. All systems share a similar evolution of the total reaction rate and they reach detailed balance much faster ($\approx 40\,\mathrm{fm/c}$) than they reach equilibrium ($\approx 1000\,\mathrm{fm/c}$).

Detailed balance should also be valid for the total reaction rate as function of the invariant mass. For this we show in Fig. 4.4 the total reaction rate as a function of the invariant mass $\sqrt{s}$ in the plateau region of Fig. 4.3 which is associated with the equilibrium state. From Fig. 4.4 we see that detailed balance is also fulfilled for this quantity. Note that the maximum achievable invariant mass of particles participating in annihilation or recreation (in equilibrium) is lower in systems initialized with lighter baryons than for systems initialized with heavier ones.

The last most crucial check for detailed balance is the fulfilment on a channel-by-channel

Tab. 4.1 – Deviation from detailed balance δ (4.3) for selected systems and as the average over all 100 investigated systems $\langle\delta\rangle$.

rank	$p+\bar{p}$		$\Delta^0+\bar{\Lambda}$		$\Lambda+\bar{\Xi}^0$		$\langle\delta\rangle$ [%]
	channel	δ [%]	channel	δ [%]	channel	δ [%]	
1	$N\bar{N}\leftrightarrow\pi\pi\rho$	0.17	$N\bar{\Xi}\leftrightarrow\pi KK^*$	1.45	$N\bar{N}\leftrightarrow\pi\pi\rho$	0.13	1.24
2	$N\bar{N}\leftrightarrow\pi\rho\rho$	3.06	$N\bar{\Omega}\leftrightarrow KK^*K^*$	3.59	$N\bar{\Delta}\leftrightarrow\pi\rho\rho$	1.70	1.82
3	$N\bar{\Delta}\leftrightarrow\pi\pi\rho$	1.58	$\Delta\bar{\Xi}\leftrightarrow\pi KK^*$	1.32	$N\bar{\Delta}\leftrightarrow\pi\pi\rho$	2.04	1.70
4	$N\bar{\Delta}\leftrightarrow\pi\rho\rho$	0.84	$\Delta\bar{\Xi}\leftrightarrow KK^*\rho$	0.64	$N\bar{N}\leftrightarrow\pi\rho\rho$	3.31	1.54
5	$\Delta\bar{N}\leftrightarrow\pi\pi\rho$	2.43	$\Delta\bar{\Omega}\leftrightarrow KK^*K^*$	1.08	$\Delta\bar{N}\leftrightarrow\pi\rho\rho$	1.33	1.49
6	$\Delta\bar{N}\leftrightarrow\pi\rho\rho$	0.73	$N\bar{\Sigma}\leftrightarrow\pi K^*\rho$	3.58	$\Delta\bar{N}\leftrightarrow\pi\pi\rho$	2.71	1.97
7	$N\bar{N}\leftrightarrow\pi\pi a_1$	6.52	$\Delta\bar{\Sigma}\leftrightarrow\pi K^*\rho$	2.00	$\Delta\bar{\Delta}\leftrightarrow\pi\pi\rho$	2.69	2.04
8	$N\bar{N}\leftrightarrow\pi\pi\pi$	5.10	$N\bar{N}\leftrightarrow\pi\pi\rho$	0.23	$N\bar{\Sigma}\leftrightarrow\pi K^*\rho$	2.04	2.03
9	$N\bar{\Sigma}\leftrightarrow\pi K\rho$	0.31	$N\bar{\Sigma}\leftrightarrow\pi K\rho$	0.42	$\Delta\bar{\Delta}\leftrightarrow\pi\pi\rho$	2.12	2.11
10	$N\bar{\Sigma}\leftrightarrow\pi K^*\rho$	0.96	$N\bar{\Omega}\leftrightarrow KKK$	0.35	$N\bar{\Sigma}\leftrightarrow\pi K\rho$	0.35	2.11

basis. To this end we define the deviation from detailed balance for each channel by

$$\delta = 1 - \frac{\frac{\mathrm{d}N}{\mathrm{d}t}(B\bar{B}\rightarrow 3M)}{\frac{\mathrm{d}N}{\mathrm{d}t}(3M\rightarrow B\bar{B})}. \tag{4.3}$$

We calculate δ for each of the more than 2000 channels and look at the channels with the largest reaction rates in all 100 investigated systems. In Table 4.1 the 10 most important channels with the largest reaction rates are shown from highest to lowest for 3 of the exemplary systems as well as the average for all 100 investigated systems and the average over all channels. The average over all 100 investigated systems shows that detailed balance is fulfilled better than 97% on a channel-by-channel basis for the 100 most dominant channels. This verifies the correct implementation of the baryon-antibaryon annihilation and recreation within the quark rearrangement model in the PHSD transport approach. Some channels of a system may deviate by more than 5% from detailed balance, however, this is a relict of too low statistics. We found only few channels (≈ 20 for the 10 most dominant channels) that had a deviation of up to 9%. In general these deviations may be neglected as can be seen in the averaged values and the dominant number of channels being very close to detailed balance which gives a proof for the working principle of the implementation presented.

4.3 Chemical equilibration times

This chapter closes with the analysis of chemical equilibration times for the 100 systems. The equilibration times are extracted from the total reaction rates at the point where a plateau emerges and the rates do not change any more. In Fig. 4.5 we present the histogram of the equilibration times which range from 400 to 2000 fm. For a better estimation of the average equilibration time we fit a Gaussian distribution to the histogram

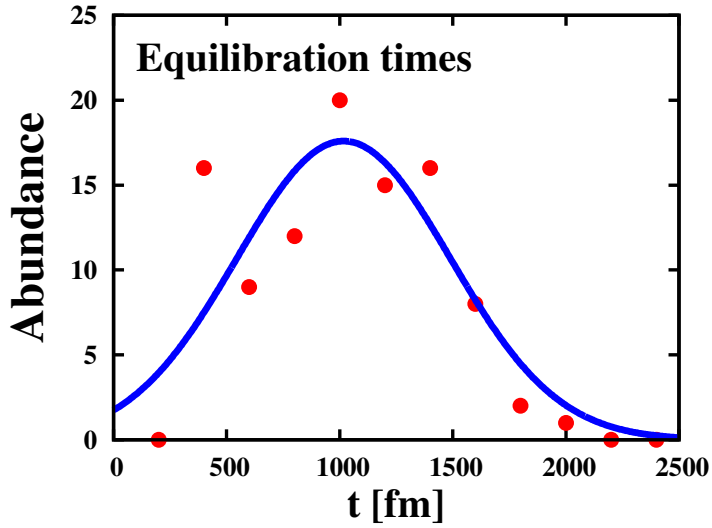

Fig. 4.5 – The histogram of the equilibration times extracted from the total reaction rates (points) and its fit by a Gaussian distribution (line).

and find $\langle t_{\rm eq} \rangle = 1017 \pm 73\,{\rm fm/c}$, which coincides with the highest abundance. The Gaussian gives a reasonable fit, although one might expect a larger spread of the equilibration times due to the large variety of quantum numbers considered. As a result for the different quantum numbers we observe a rather large peak around an equilibration time of 400 fm/c that stems from initializations with multistrange baryons or antibaryons. The highest equilibration time of 2000 fm/c is found for the proton-antiproton initialization. The equilibration times are in general shorter if more strange or antistrange quarks exist in the initial baryons and antibaryons and strange/antistrange hadrons have to be produced by a lower amount to achieve a chemical equilibration.

Chapter 5

PHSD calculations for relativistic heavy-ion collisions

Since our numerical realization of the $2 \leftrightarrow 3$ reactions fulfills the detailed balance relations we insert the routines into the PHSD transport approach and investigate their influence on HICs for different systems and energies. First, we examine the impact of the $2 \leftrightarrow 3$ reactions with [SU(3)] — including a strange quark suppression factor $\lambda = 0.5$ — and without the strangeness sector [SU(2)] on rapidity and transverse mass spectra of antibaryons at top AGS and SPS energies ($11.7A\,\mathrm{GeV} \leq E_{\mathrm{lab}} \leq 158A\,\mathrm{GeV}$). Then we will analyze the influence of the reactions without any strange quark suppression ($\lambda = 1$) at RHIC and LHC and additionally compare calculations without the baryon-antibaryon recreation to results with the full model to estimate the difference to other models that neglect the recreation. We will provide excitation functions — calculated with and without the $2 \leftrightarrow 3$ reactions — for the relevant hadrons and show ratios of hadron yields from calculations with different versions of the model for a better visualization of the effects of the annihilation and recreation of baryon-antibaryon pairs on the final spectra.

5.1 SPS energies

In this section we show the influence of the additional channels in the strangeness sector for $B\bar{B} \leftrightarrow 3M$ reactions for heavy-ion collisions in the energy regime of 11.7-158A GeV. In the calculations the strange quark suppression is taken to be $\lambda = 0.5$. Before coming to the actual results we compare in Fig. 5.1 the reaction rate for the total baryon-antibaryon annihilation (solid line) and formation (dashed line) from PHSD in 5% central Pb+Pb collisions at 158A GeV. Whereas the meson-fusion rate dominates at early times (< 13 fm/c) the annihilation takes over for larger times during the final expansion of the system. Although the time integrals of both rates are about the same (a slightly stronger annihilation is present) there is no appreciable time interval in which both rates are identical. This indicates strong nonequilibrium dynamics of baryon-antibaryon anni-

hilation and reproduction in actual heavy-ion reactions. We note that a similar analysis

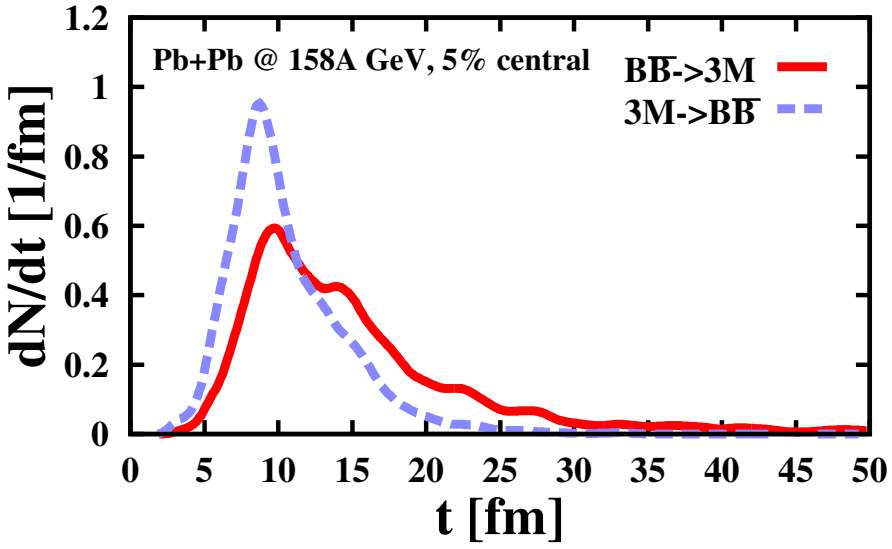

Fig. 5.1 – The reaction rate of the $B\bar{B} \to 3M$ reactions (solid line) as a function of time in 5% central Pb+Pb collisions at $158A$ GeV in comparison to the total three-meson fusion rate (dashed line).

has been performed in the earlier study in Ref. [42] (Fig. 7) on the basis of the HSD transport model for the same system, however, without averaging over the ensembles. The earlier rates differ substantially from the present results from PHSD due to the different degrees of freedom in the initial phase of the collision. In order to quantify the differences we have recalculated the rates within HSD2.3 (from the year 2002) and compared the numbers with those from PHSD4.0, which is the most recent version including also the effects from chiral symmetry restoration [15] (PHSD3.3) and nonperturbative charm dynamics as well as extended $2 \leftrightarrow 3$ reactions. We found that both rates (from HSD2.3 and PHSD4.0) differ only slightly for times $\geq$ 6 fm/c (after contact of Pb+Pb at b=2fm) but the huge rates (from HSD2.3) at the first few fm/c are essentially missing in PHSD4.0. This is due to the fact that at the top SPS energy the initial energy conversion goes to interacting partons in PHSD4.0 and not to strings decaying to hadrons (and partly to $B\bar{B}$ pairs) in HSD2.3. Thus in PHSD4.0 (at the top SPS energy) there are initially no $B\bar{B}$ pairs that might annihilate nor mesons that might fuse! Due to the very high hadron densities in HSD2.3 (after string decay) both the annihilation and reproduction rates are very high and about equal whereas in the hadronic expansion phase the densities are sizeably lower. In this dilute regime the three-body channels first dominate and decrease fast in time whereas the two-body annihilation reactions still continue for some time. However, in both transport calculations — incorporating the $2 \leftrightarrow 3$ reactions — the time integrated rates for annihilation and reproduction turn out to be about equal.

The actual PHSD calculations for relativistic nucleus-nucleus collisions are carried out

in the parallel ensemble method, i.e. in case of the cascade mode a typical number of 100 - 300 ensembles are propagated in time fully independent from each other. However, the calculation of net-baryon densities, scalar densities and energy densities — needed for the full PHSD dynamics — is carried out by averaging over all ensembles. This results in a crosstalk between ensembles due to the propagation of particles in the self-generated mean fields (for partons and baryons/antibaryons) as well as in the baryon/antibaryon formation in the hadronization. A systematic study of all particle spectra in rapidity and transverse mass shows that the results for mesons and baryons well scale with the number of ensembles whereas the antibaryon sector shows small variations with the number of

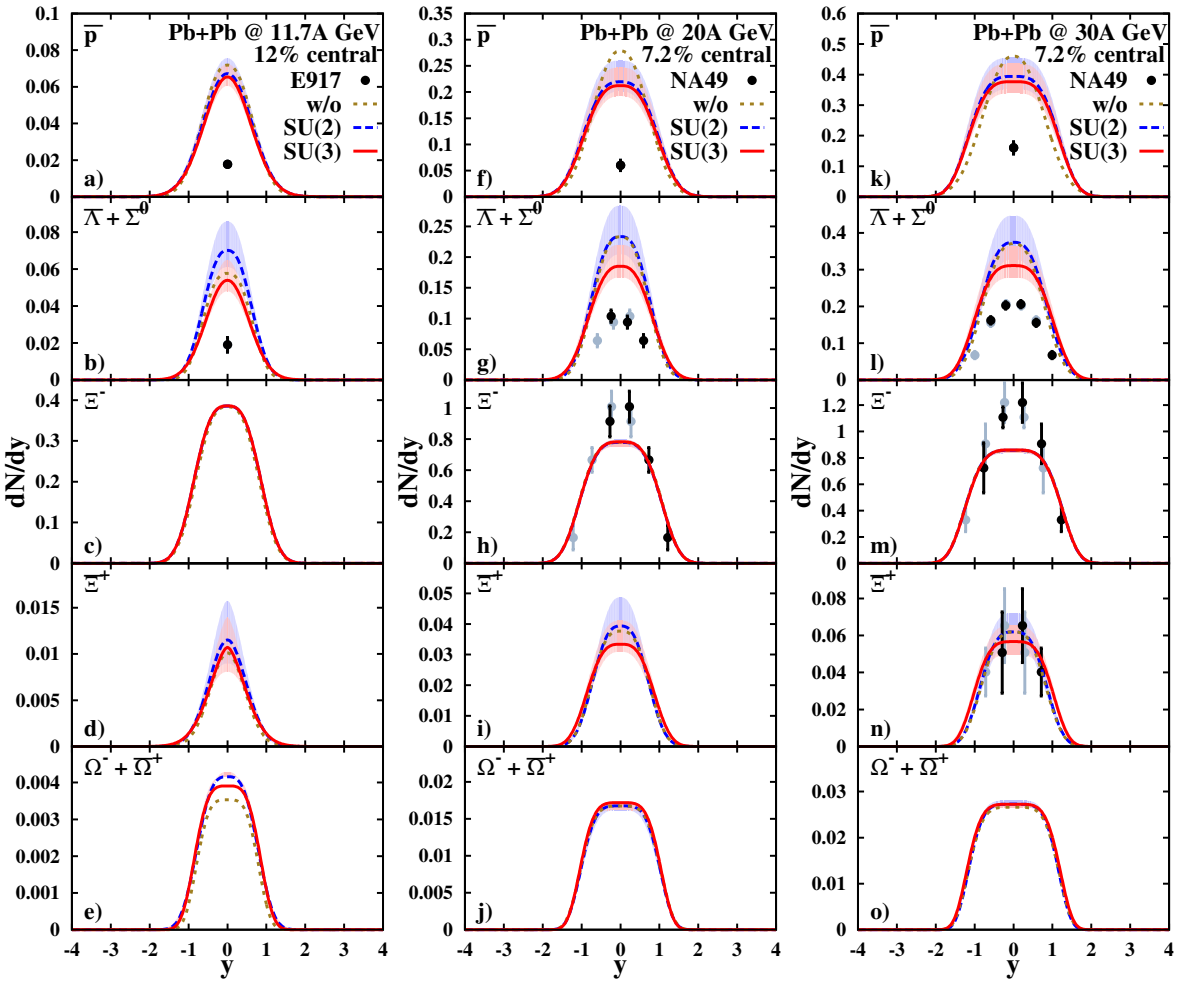

Fig. 5.2 – Rapidity spectra of $\bar{p}, \bar{\Lambda} + \bar{\Sigma}^0, \Xi^-, \bar{\Xi}^+, \Omega^- + \bar{\Omega}^+$ in (12%) 7.2% central Pb+Pb collisions at 11.7, 20 and 30A GeV. The solid lines show the results when including all light and strange quark channels (denoted by SU(3)) while the dashed lines result from discarding strange or antistrange quarks in the reaction channels (denoted by SU(2)). The error bands indicate the systematic uncertainty of the calculations due to a different ensemble size. The dotted lines show the results with $B\bar{B} \leftrightarrow 3M$ reactions switched off. The data points are taken from Refs. [77–79].

ensembles. This scaling violation is essentially due to the numerical approximations that have to be presently introduced in order to keep the huge number of reaction channels manageable. This introduces a systematic error in our calculations for the antibaryon sector which is accounted for by hatched bands in the following figures. The solid or dashed lines correspond to the standard ensemble number of 150 used as default in PHSD calculations in the energy range of interest in this section.

5.1.1 Rapidity and transverse mass spectra

We now discuss the influence of the $B\bar{B} \leftrightarrow 3M$ reactions on observables measured in actual experiments from 11.7 - 158A GeV. We first focus on rapidity spectra and mention that the $B\bar{B} \leftrightarrow 3M$ reactions have practically no influence on baryon and meson spectra (as shown in Ref. [15]) and, hence, we only display the results for the relevant antibaryons and Ξ^- to demonstrate that the influence on baryons is barely visible. For results on meson and baryon spectra we refer the reader to the review [26] and Ref. [15]. As mentioned above the full, dashed and dotted lines show the results for 150 ensembles; the blue and red hatched areas result when employing different ensemble numbers in a wide range.

We first focus on the influence of the newly incorporated strangeness sector. In the following, we compare the implementation with only light quark channels (SU(2)) with the new one including also the strangeness sector (SU(3)). The rapidity spectra of $\bar{p}, \bar{\Lambda}+\bar{\Sigma}^0, \Xi^-, \bar{\Xi}^+, \Omega^- + \bar{\Omega}^+$ for central Pb+Pb collisions from 11.7 to 158A GeV are shown in Figs. 5.2 and 5.3. The rapidity spectra of the anti-hyperons are overall closer to the experimental data when taking into account the strangeness sector for the $B\bar{B} \leftrightarrow 3M$ reactions. However, the antiproton spectra are faintly influenced by the incorporated sector and describe the data only moderately well. In general the investigations suggest that the $B\bar{B} \leftrightarrow 3M$ reactions have the largest impact at energies below 80A GeV. This result shows that the consideration of the strange quarks helps improving the description of a heavy-ion collision in the framework of PHSD. For particles like $\bar{\Xi}^+, \Omega^-$ and $\bar{\Omega}^-$ at lower energies, where currently no experimental data are available, our results should be taken as predictions.

In Fig. 5.2 we, furthermore, show results from calculations neglecting the $B\bar{B} \leftrightarrow 3M$ reactions. We find that the rapidity distribution for $\bar{p}$ has a higher peak and is narrower compared to calculations with $B\bar{B} \leftrightarrow 3M$, while the total number of antiprotons is about the same. The results for the antihyperons — starting from 20A GeV — lie on top of the SU(2) simulations. At 11.7A GeV the hyperon spectra are closer to the SU(3) calculations and for $\Omega^- + \bar{\Omega}^+$ lie even below those.

Another interesting observable measured in experiment is the transverse mass (m_t) spectrum at midrapidity, i.e. $dN/(m_t dy dm_t)$ as displayed in Fig. 5.4. Here the additional strangeness sector has qualitatively the same impact as for the rapidity spectra. Accordingly, we only show results for central Pb+Pb collisions in the energy regime from 20 to 158A GeV including the strangeness sector for the $B\bar{B} \leftrightarrow 3M$ reactions. For the

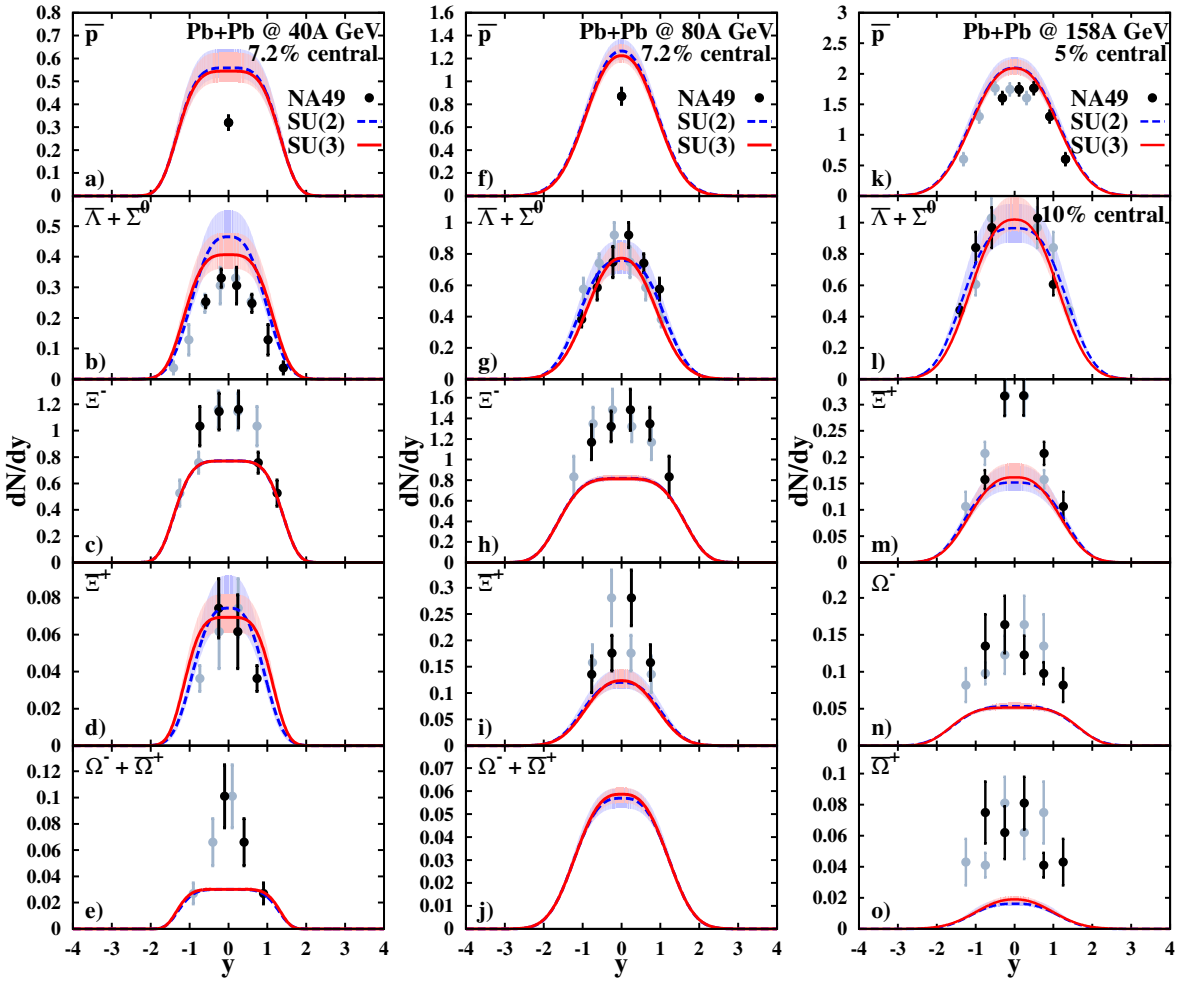

Fig. 5.3 – Rapidity spectra of $\bar{p}, \bar{\Lambda}+\bar{\Sigma}^0, \Xi^-, \bar{\Xi}^+, \Omega^- + \bar{\Omega}^+$ in central Pb+Pb collisions at 40, 80 and 158A GeV for $B\bar{B} \leftrightarrow 3M$ with only light quarks (dashed lines) and including strange quarks (solid lines) compared to experimental measurements. The error bands indicate the systematic uncertainty of the calculations due to a different ensemble size. The data points are taken from Refs. [78–82].

Ξ^- we find that PHSD describes the low m_t regime for energies below 158A GeV rather well. However, for higher m_t the data points are missed due to a harder experimental slope of the spectrum. At 158A GeV some Ξ^-'s are missed in the low m_t regime. The $\bar{\Lambda}+\bar{\Sigma}^0$ spectrum is close to the experimentally measured data for all energies, however, at 158A GeV it falls off too fast. The transverse mass spectra of the antiprotons are overall in very good agreement with experiment, the only drawback is the overproduction at midrapidity which is most visible for 20A GeV. Also, the $\bar{\Xi}^+$ are in close vicinity to the experimental data for energies smaller than 158A GeV, but fall off too quickly at 158A GeV. The production of Ω^- and $\bar{\Omega}^+$ was underestimated already in the rapidity spectra, see Fig. 5.3, but looking at the transverse mass spectra at 158A GeV the results are in reasonable agreement with experiment for $m_t < 0.8$ GeV.

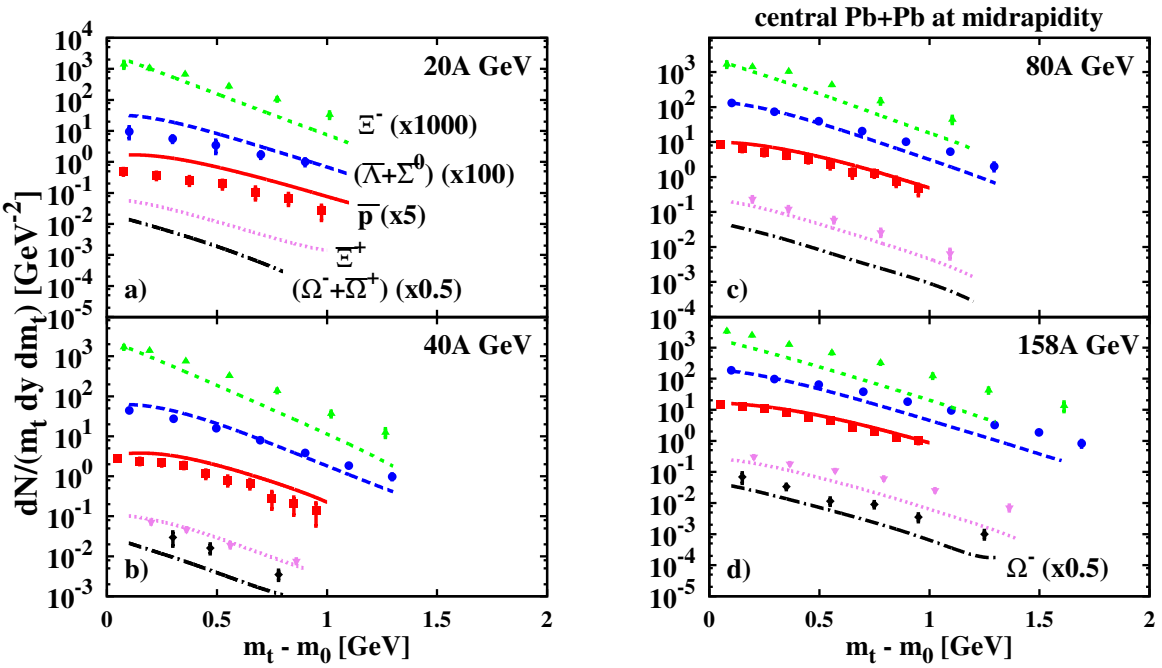

Fig. 5.4 – Transverse mass spectra for central Pb+Pb collisions at midrapidity. The centrality selection for the particles at the different energies is the same as in Figs. 5.2 and 5.3. The particles in each panel are from top to bottom $\Xi^-, \bar{\Lambda} + \bar{\Sigma}^0, \bar{p}, \bar{\Xi}^+$ and $\Omega^- + \bar{\Omega}^+$, only at 158$A$ GeV the lowest lying line corresponds to Ω^-. The data points are taken from Refs. [79–82] whereas the lines give the spectra from PHSD.

5.1.2 Impact of chiral symmetry restoration and deconfinement

We now address the question with respect to traces of chiral symmetry restoration and deconfinement in the antibaryon and multi-strange baryon spectra from central Pb+Pb collisions at SPS energies. We recall that clear signals have been found before in the strange meson and baryon rapidity distributions [15, 83] and one might speculate if a similar signal can be seen in the antibaryon sector. For this aim we perform transport calculations — including the $B\bar{B} \leftrightarrow 3M$ channels specified above — with different settings:

- HSD calculations without chiral symmetry restoration (CSR) and deconfinement since HSD does not include a partonic phase
- HSD calculations with chiral symmetry restoration (CSR) in the hadronic phase but without deconfinement
- PHSD calculations without chiral symmetry restoration (CSR) in the hadronic phase but with a deconfinement transition

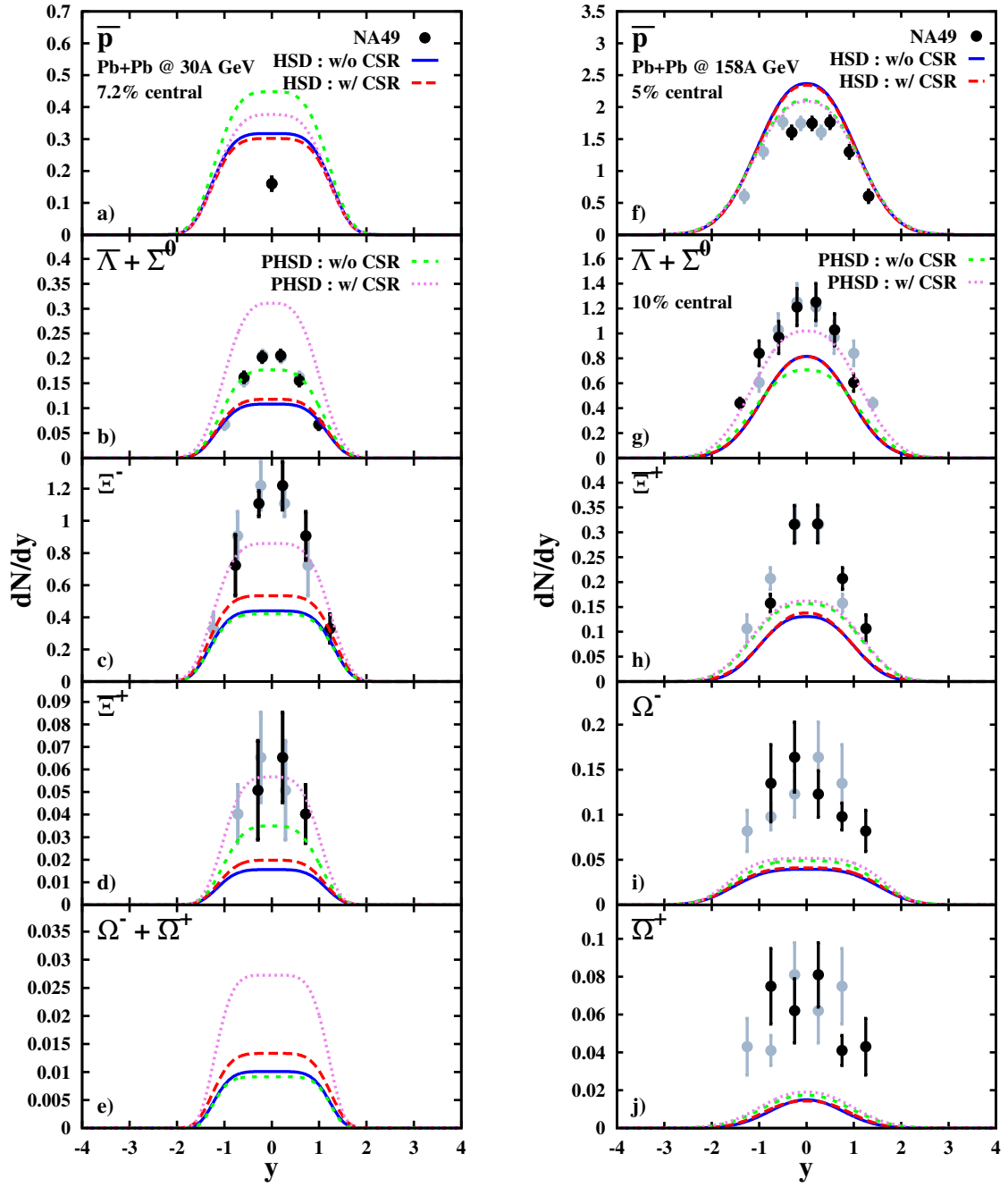

Fig. 5.5 – Rapidity spectra for a central Pb+Pb collision at 30 (left) and 158A GeV (right); comparison between simulations with (PHSD) and without (HSD) the deconfinement transition and with activated and deactivated chiral symmetry restoration (CSR). The data points are taken from Refs. [78–82].

- PHSD calculations with chiral symmetry restoration (CSR) in the hadronic phase and with a deconfinement transition.

The systems addressed are central Pb+Pb collisions at 30 and 158A GeV. The rapidity spectra for antibaryons and Ξ^- are displayed in Fig. 5.5 and show that at 158A GeV the impact of chiral symmetry restoration is very small in the HSD calculations (without deconfinement) as well as for PHSD (including deconfinement) except for the $\bar{\Lambda} + \bar{\Sigma}^0$ spectrum. When comparing HSD and PHSD results including CSR we find a slight reduction of the $\bar{p}$ spectra, a moderate enhancement for the $\bar{\Lambda} + \bar{\Sigma}^0$ spectrum and only a small enhancement for $\Xi^{\pm}$ and $\Omega^- + \bar{\Omega}^+$ when including a partonic phase. Since the reproduction of the multistrange sector by PHSD is very poor one cannot conclude on the presence of a deconfinement transition on the basis of the rapidity spectra shown in Fig. 5.5. Note, however, that a clear signal for deconfinement has been found in the elliptic and triangular flow of charged hadrons before in Ref. [40] at this energy.

At 30A GeV the situation is not much better. The PHSD calculations with CSR perform best for Ξ^- and $\bar{\Xi}^+$, however, overestimate the $\bar{p}$ and $\bar{\Lambda} + \bar{\Sigma}^0$ yield. The HSD calculations are too low in the strange antibaryon sector including/excluding CSR providing some hint that a partonic phase should be present in a moderate space-time volume at this energy. Accordingly, the antibaryons and in particular the multi-strange sector do not give additional information on chiral symmetry restoration or deconfinement within the framework of PHSD calculations.

5.1.3 Comparison to other dynamical models

In this subsection we compare our current PHSD results to those from other dynamical models which have been employed for heavy-ion reactions in the SPS energy regime, in particular from the Ultra-relativistic Quantum Molecular Dynamics model (UrQMD) [32, 33] and the three-fluid dynamics model (3FD) [27]. The UrQMD is a hadronic transport model including a multitude of hadronic resonances as well as strings that are responsible for multi-particle production. The 3FD is a fluid dynamical model describing — within the framework of hydrodynamics — the transition from the initial baryonic fluids (projectile and target) to the newly produced fluid (around midrapidity). For details we refer the reader to the original literature [27, 32, 33]. We show in Fig. 5.6 our actual results in case of the rapidity spectra for a central Pb+Pb collision at 40A GeV with the $B\bar{B} \leftrightarrow 3M$ reactions including the strangeness sector in comparison to results from the UrQMD [34] and the 3FD using a 2-phase equation of state [84]. The 3FD model, like PHSD, overshoots the antiproton yield whereas UrQMD is close to the experimental data. The $\bar{\Lambda} + \bar{\Sigma}^0$ spectrum is described by PHSD and the 3FD model similarly close to the experimental data whereas UrQMD produces too few. For the Ξ^- all models show different behaviors; whereas the 3FD model overpredicts the production, PHSD produces slightly too few Ξ^- at midrapidity but describes otherwise the shape well. UrQMD predicts (just like for $\bar{\Lambda} + \bar{\Sigma}^0$ and $\bar{\Xi}^+$) too few antibaryons since $B\bar{B}$ annihilation is incorporated, however, not the backward channels thus violating detailed balance. PHSD and the 3FD model are close to the experimental data for $\bar{\Xi}^+$, with the 3FD slightly underpredicting the yield. Depending on the particle species of interest one

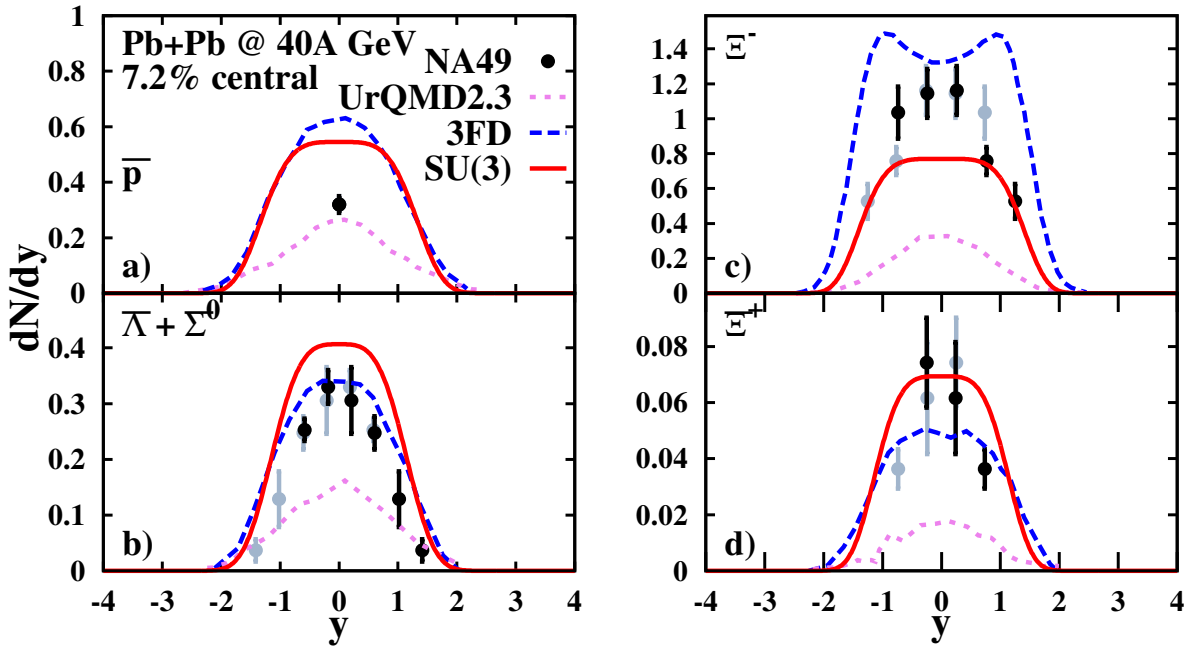

Fig. 5.6 – Rapidity spectra for a central Pb+Pb collision at $40A$ GeV; comparison between PHSD results with the $B\bar{B} \leftrightarrow 3M$ reactions including strangeness (red solid line), UrQMD-2.3 [34] (violet short-dashed line) and 3FD with a 2-phase equation of state [84] (blue dashed line). The experimental data are taken from Refs. [78, 79].

model describes some yield better than the other at higher SPS energies. In general, the 3FD model and PHSD appear to be similarly capable of roughly describing the dynamics of baryons and antibaryons with strangeness content in this energy range.

Another issue relates to the actual value of the strangeness suppression factor λ which had been taken as $\lambda = 0.5$. In order to demonstrate the impact of the parameter λ on antibaryon spectra we show in Fig. 5.7 the rapidity distributions for central Pb+Pb collisions at 30 A GeV for λ=0.5 (dashed lines) and λ=1 (solid lines). Without strangeness suppression in $2 \leftrightarrow 3$ reactions for hadrons with strange/antistrange quarks we find at $30A$ GeV that the rapidity spectra of $\bar{\Lambda} + \bar{\Sigma}^0$ and $\bar{\Xi}^+$ are slightly shifted to lower values and broadened in comparison to the value of $\lambda = 0.5$. The spectrum for $\Omega^- + \bar{\Omega}^+$ very slightly broadens and the $\bar{p}$ spectrum is basically not influenced by the change of λ.

5.2 RHIC and LHC energies

In this section we show the influence of the $B\bar{B} \leftrightarrow 3M$ reactions on heavy-ion collisions at RHIC and LHC energies in extension of the calculations at SPS energies in Sec. 5.1 but without a strange quark suppression ($\lambda = 1$) since the sensitivity of the antibaryon spectra to a reasonable range in λ is very small (cf. Fig. 5.7). Before coming to the actual results for hadron spectra we compare in Fig. 5.8 the reaction rates for the

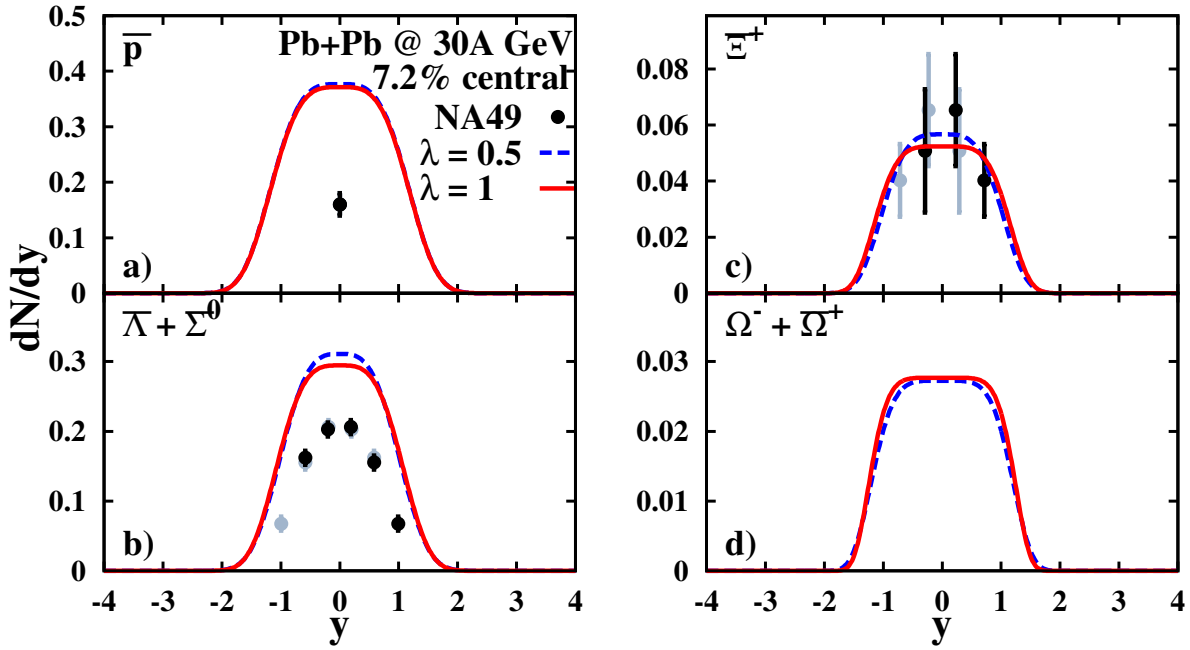

Fig. 5.7 – Rapidity spectra for a central Pb+Pb collision at 30A GeV; comparison between simulations with a strangeness suppression factor $\lambda = 0.5$ (dashed lines) and no strangeness suppression, i.e. $\lambda = 1$ (solid lines).

total baryon-antibaryon annihilation and formation from PHSD in 5% central Pb+Pb (Au+Au) collisions at $\sqrt{s_{NN}} = 200$ GeV (a), and 2.76 TeV (b) integrated over rapidity. The solid blue lines denote the rates for $B\bar{B}$ annihilation when discarding the reproduction channels; the red solid lines stand for the $B\bar{B}$ annihilation rate when including the backward channels whereas the dashed lines display the reproduction rate in the latter case. The meson-fusion rate dominates at early times at the LHC energy over the $B\bar{B}$ annihilation rate (b) while the situation is inverse at the top RHIC energy (a). Without regeneration of $B\bar{B}$ pairs (blue solid lines) the annihilation rates are lower than in case of $B\bar{B}$ reproduction which is, however, an unphysical limit and displayed only for orientation. The explicit dependence of ratios versus $\sqrt{s_{NN}}$ will be discussed in Sec. 5.3.

5.2.1 Hadron transverse-momentum spectra at RHIC and LHC

We continue with PHSD results for antibaryons and mesons in 5% central Pb+Pb (Au+Au) collisions at the top RHIC energy ($\sqrt{s_{NN}}$=200 GeV) and the LHC energy of $\sqrt{s_{NN}}$= 2.76 TeV. In Fig. 5.9 a) - c) we display the calculated transverse momentum spectra for protons, positive pions and kaons in comparison to the data from the PHENIX Collaboration [85]. Whereas the hadron spectra are quite well described at lower transverse momenta there is a deficit at high p_T for all hadron species in the PHSD calculations. We note that the hadron formation at the top RHIC energy at midrapidity

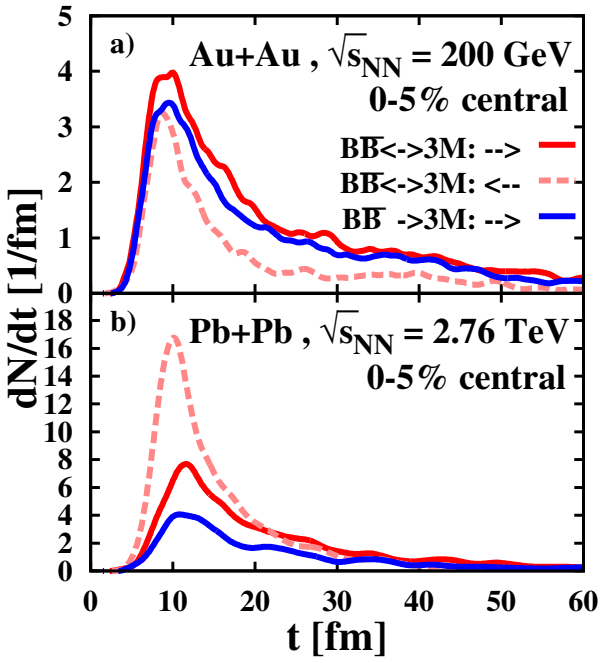

Fig. 5.8 – The reaction rates of the $B\bar{B} \to 3M$ reactions (solid line) as a function of time in 5% central Au+Au collisions at $\sqrt{s_{NN}} = 200$ GeV a) and Pb+Pb collisions at $\sqrt{s_{NN}} = 2.76$ TeV b) integrated over rapidity. The solid blue lines denote the rates for $B\bar{B}$ annihilation when discarding the reproduction channels; the red solid lines stand for the $B\bar{B}$ annihilation rate when including the backward channels whereas the dashed lines display the reproduction rate in the latter case.

proceeds essentially by hadronization, i.e. by dynamical coalescence, which implies that the quarks and antiquarks at hadronization have softer transverse momenta in PHSD than in "experiment". The total hadron densities at midrapidity are only marginally affected by the underestimated high p_T tail and we may conclude that the hadron densities within PHSD are sufficiently realistic such that rather solid results for the annihilation and fusion rates should emerge. The full red lines show the spectra from calculations with the $2 \leftrightarrow 3$ reactions included while the dashed lines correspond to calculations with the $2 \leftrightarrow 3$ reactions discarded. Since there are almost no differences between the lines we can conclude again that the $2 \leftrightarrow 3$ reactions have practically no impact on baryon and meson spectra.

In Fig. 5.9 d)-f) we show the same hadron p_T spectra at midrapidity for 5% central Pb+Pb collisions at $\sqrt{s_{NN}}$=2.76 TeV in comparison to the data from the ALICE Collaboration [69, 86–89]. In this case the description of the data is rather good (except for protons) and again there is no visible impact of the $2 \leftrightarrow 3$ reactions on the transverse momentum spectra of the mesons. We note in passing that the flow coefficients v_n (for $n = 2, 3, 4, 5$) for charged hadrons from PHSD for this system are also in a very good agreement with the experimental measurements as shown in Ref. [90]. Thus we may state that the densities of the most abundant hadrons appear to be well under control

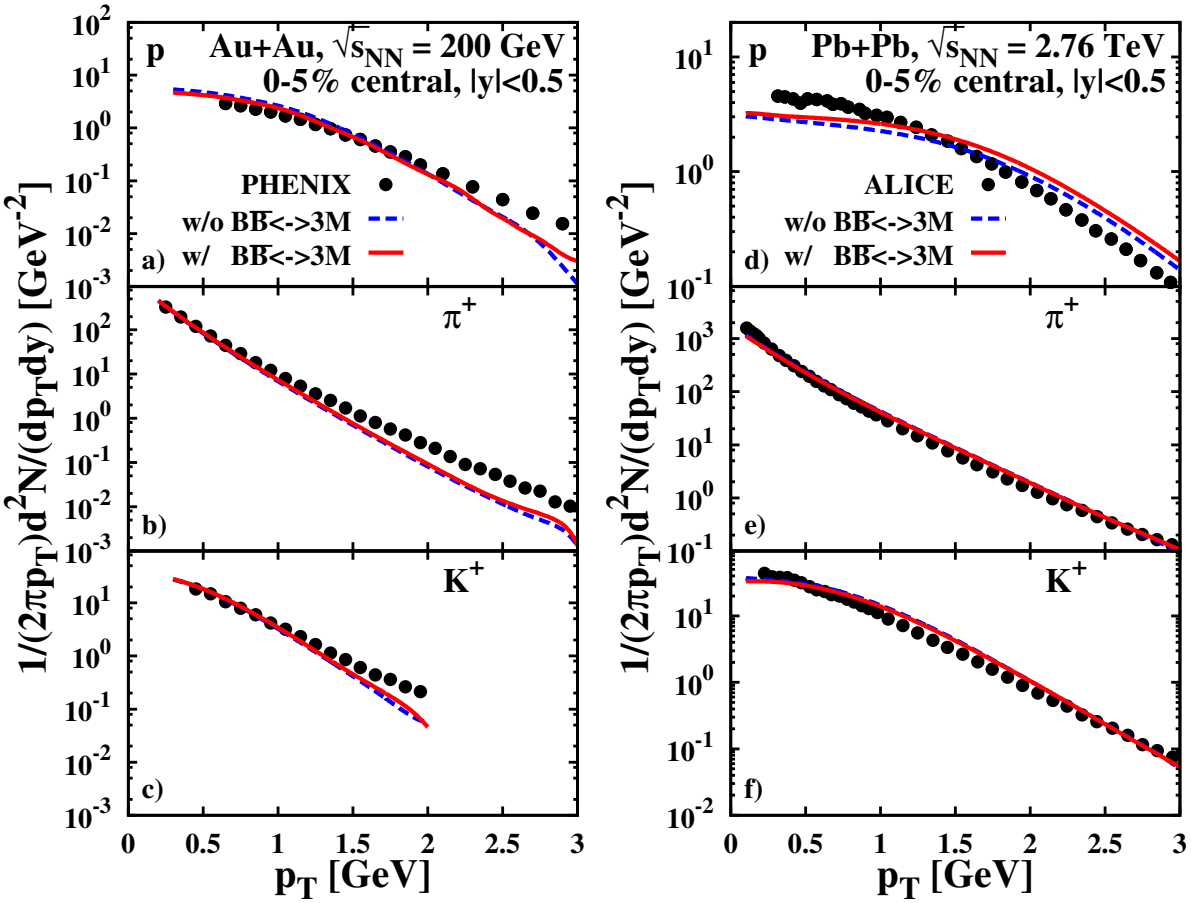

Fig. 5.9 – The transverse momentum spectra for protons, positive pions as well as for kaons from PHSD at midrapidity in comparison to the data from the PHENIX Collaboration [85] for 5% central Au+Au collisions at $\sqrt{s_{NN}}$=200 GeV (a - c), and to the data from the ALICE Collaboration [69, 86–89] for 5% central Pb+Pb collisions at $\sqrt{s_{NN}}$=2.76 TeV (d - f). The full red lines show the results of calculations with the $2 \leftrightarrow 3$ reactions included while dashed lines correspond to calculations with the $2 \leftrightarrow 3$ reactions discarded.

in PHSD in particular at the LHC energy.

We continue with the antibaryon transverse momentum spectra at midrapidity for top RHIC and LHC energies, which are displayed in Fig. 5.10 in comparison with the data from the PHENIX, STAR and ALICE Collaborations [85–88, 91, 92]. Here again the low momentum spectra for $\bar{p}, \bar{\Lambda} + \bar{\Sigma}^0, \Xi^-, \bar{\Xi}^+$ and $\Omega^- + \bar{\Omega}^+$ are roughly described, however, the high p_T tails are missed considerably at $\sqrt{s_{NN}} = 200$ GeV in Fig. 5.10 a) - e) while they look somewhat better at the LHC energy f) - j). We note that again there is no sizeable impact of the $2 \leftrightarrow 3$ reactions on these transverse momentum spectra.

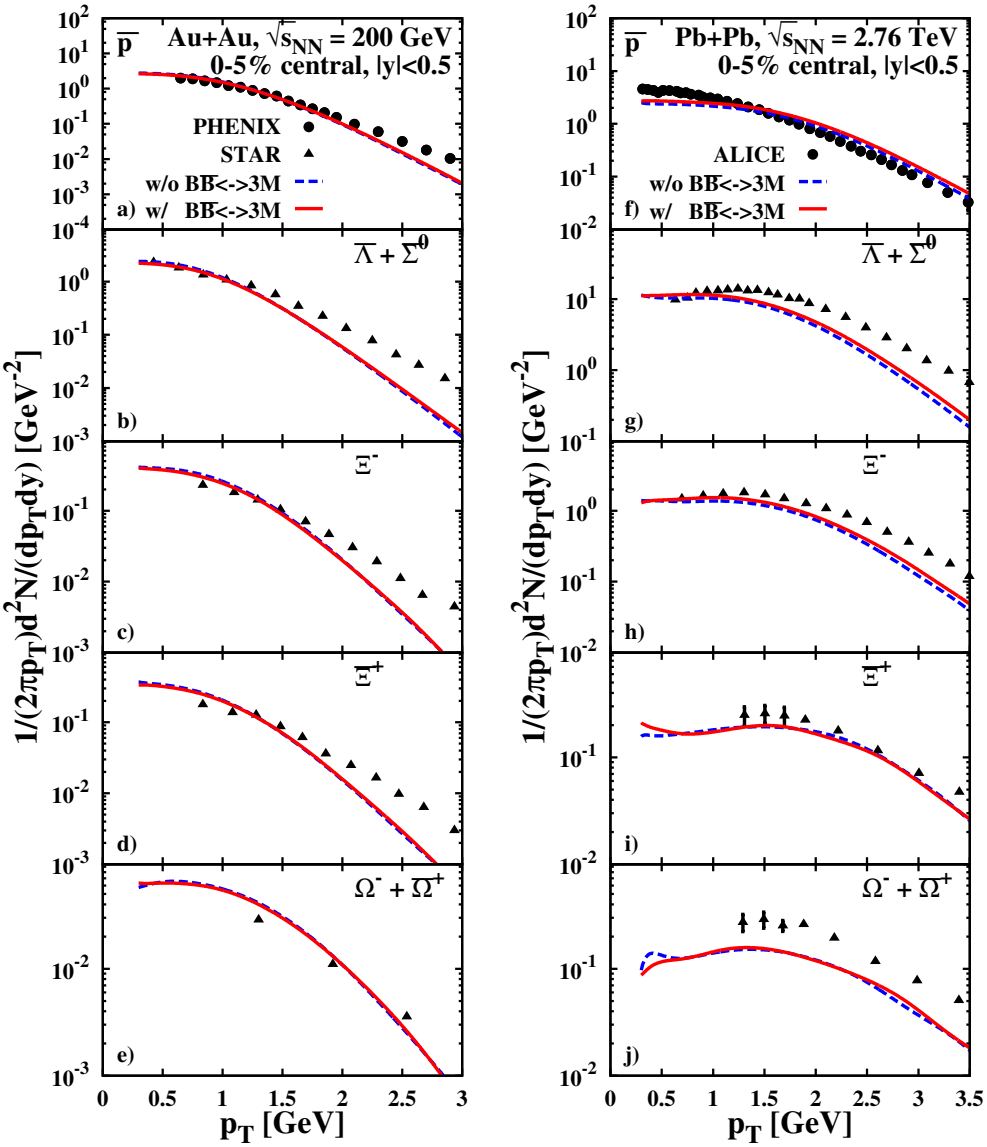

Fig. 5.10 – The transverse momentum spectra for $\bar{p}, \bar{\Lambda} + \bar{\Sigma}^0, \Xi^-, \bar{\Xi}^+$ and $\Omega^- + \bar{\Omega}^+$ from PHSD at midrapidity in comparison to the data from the PHENIX and STAR Collaborations [85, 91, 92] for 5% central Au+Au collisions at $\sqrt{s_{NN}}$=200 GeV a) - e), and to the data from the ALICE Collaboration [86–88] for 5% central Pb+Pb collisions at $\sqrt{s_{NN}}$=2.76 TeV f) - j). The full red lines show the results of calculations with the $2 \leftrightarrow 3$ reactions included while dashed lines correspond to calculations with the $2 \leftrightarrow 3$ reactions discarded.

5.2.2 Centrality dependence at RHIC and LHC

We continue with p_T integrated rapidity densities for baryons and antibaryons as a function of centrality in terms of the number of participating nucleons N_{part} which is calculated within PHSD. Fig. 5.11 shows the rapidity density of baryons and antibaryons from PHSD at midrapidity in comparison to data from the PHENIX and STAR Collabo-

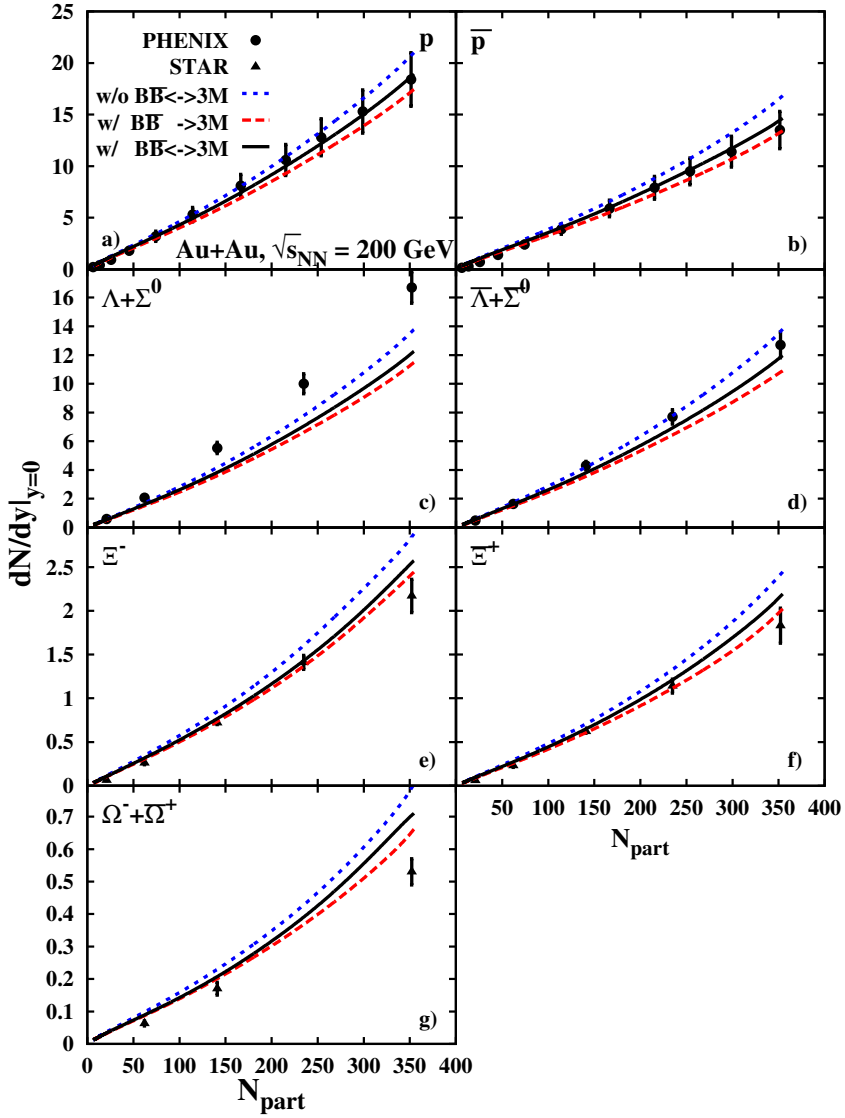

Fig. 5.11 – The rapidity density of baryons and antibaryons from PHSD at midrapidity in comparison to data from the PHENIX and STAR Collaborations [85, 91, 92] for 5% central Au+Au collisions at $\sqrt{s_{NN}}$=200 GeV. The dashed red lines show the results of calculations with only $B\bar{B}$ annihilation, the solid black lines show results with the $2 \leftrightarrow 3$ reactions included while dotted blue lines correspond to calculations with the $2 \leftrightarrow 3$ reactions discarded.

rations [85,91,92] for 5% central Au+Au collisions at $\sqrt{s_{NN}}$=200 GeV. When discarding the $2 \leftrightarrow 3$ reactions (blue dotted lines) the experimental data are slightly overestimated (except for $\Lambda+\Sigma^0$), while calculations with only $B\bar{B}$ annihilation (dashed red lines) show a slight tendency to underestimate the data. The results from PHSD calculations with the $2 \leftrightarrow 3$ reactions included are displayed by the black solid lines and lie in between the other limits. This points towards a small net $B\bar{B}$ annihilation at the top RHIC energy for all baryons/antibaryons considered. We will quantify this net annihilation in Sec.

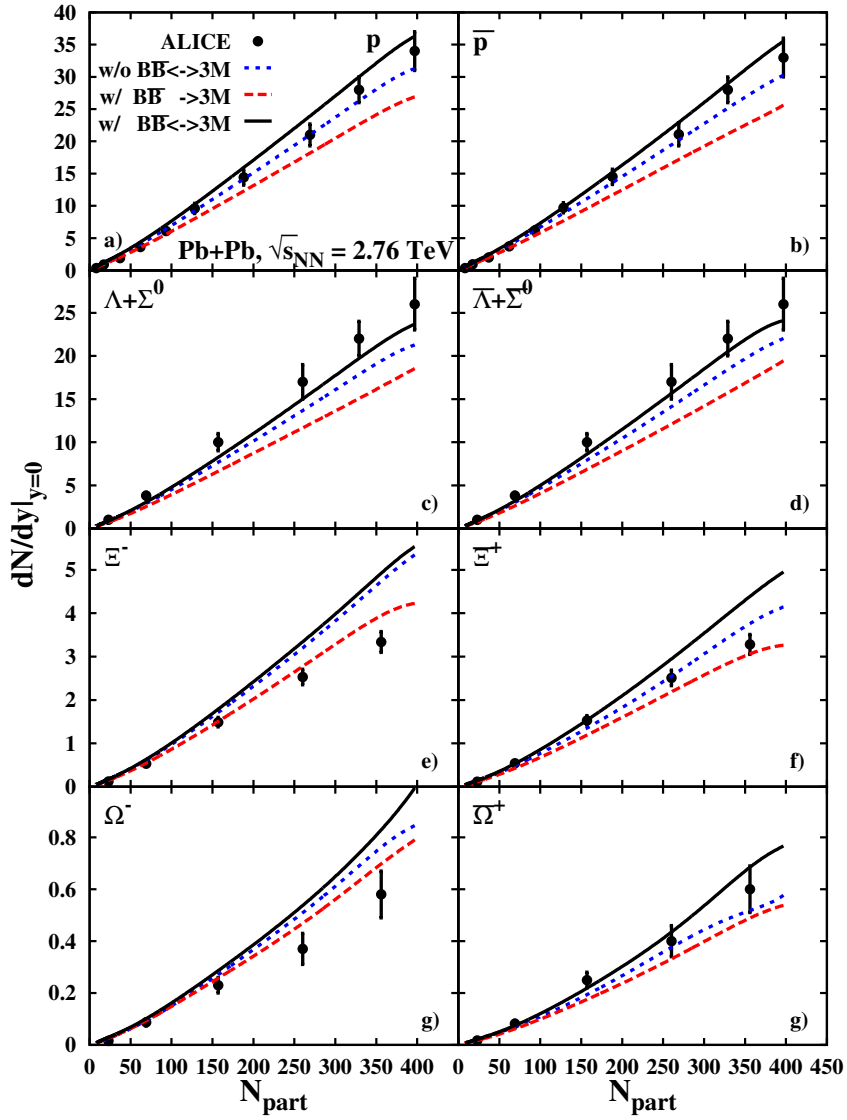

Fig. 5.12 – The rapidity density of baryons and antibaryons from PHSD at midrapidity in comparison to the data from the ALICE Collaboration [69, 86–89] for 5% central Pb+Pb collisions at $\sqrt{s_{NN}}$=2.76 TeV. The dashed red lines show the results of calculations with only $B\bar{B}$ annihilation, the solid black lines show results with the $2 \leftrightarrow 3$ reactions included while dotted blue lines correspond to calculations with the $2 \leftrightarrow 3$ reactions discarded.

5.3.

The situation is somewhat different at LHC energies. Fig. 5.12 shows the rapidity density of baryons and antibaryons from PHSD at midrapidity in comparison to data from the ALICE Collaboration [69,86–89] for 5% central Pb+Pb collisions at $\sqrt{s_{NN}}$=2.76 TeV. The blue dotted lines display the calculated results when discarding the $2 \leftrightarrow 3$ reactions and the dashed red lines correspond to calculations with only $B\bar{B}$ annihilation. The results from PHSD calculations with the $2 \leftrightarrow 3$ reactions included are displayed by

the black solid lines and lie in all cases slightly above the other limits indicating a net $B\bar{B}$ production at the LHC instead of an absorption. The calculations with only $B\bar{B}$ annihilation (red dashed line) underestimate the experimental data (except for Ξ^- and Ω^-). In particular the $p, \bar{p}, \Lambda + \Sigma^0$, and $\bar{\Lambda} + \bar{\Sigma}^0$ multiplicities are (within error bars) in line with experimental observation at all centralities (when including the $B\bar{B} \leftrightarrow 3M$ channels) contrary to the results of the Statistical Hadronization Model (SHM) quoted in Ref. [87]. On the other hand the $\Xi^-, \bar{\Xi}^+, \Omega^-$ and $\bar{\Omega}^+$ baryons are slightly overestimated in more central collisions when including the $B\bar{B} \leftrightarrow 3M$ channels. We attribute these results to a deviation from statistical equilibrium in the hadronization incorporated in PHSD.

5.3 Excitation functions

In this section we will quantify the net effect of the $B\bar{B} \leftrightarrow 3M$ channels for central Pb+Pb (Au+Au) collisions as a function of the bombarding energy or $\sqrt{s_{NN}}$, respectively, summarizing results from Sec. 5.1 and Sec. 5.2.

5.3.1 Hadron yields at midrapidity

In Fig. 5.13 we first show the performance of PHSD4.0 with respect to hadron production (at midrapidity) in central Pb+Pb (Au+Au) collisions from $\sqrt{s_{NN}}$= 3.5 GeV to 2.76 TeV, i.e. by roughly 3 orders of magnitude in invariant energy. The solid lines refer to calculations including the $B\bar{B} \leftrightarrow 3M$ channels while the dashed lines display calculations without these channels. The particle yields at midrapidity from PHSD are connected by lines to draw the eye although experimental data (taken from Refs. [69, 77–80, 85–89, 91–104]) and calculations do not always correspond to the same centrality selection (and system) for different bombarding energies. However, for given $\sqrt{s_{NN}}$ data and calculation correspond to the same centrality and collision system. From Fig. 5.13 a) we see that PHSD essentially reproduces the experimental observations for pions, kaons and antikaons in the whole energy range. We recall that at AGS and SPS energies this is essentially due to the incorporation of chiral symmetry restoration (cf. Refs. [15, 83]). The same holds true for the baryon and antibaryon excitation functions except for the energy regime 20 GeV $< \sqrt{s_{NN}} <$100 GeV where PHSD underestimates the baryons and antibaryons. The reason for this discrepancy is presently not understood. However, by comparing the hadron yields from calculations with (solid lines) and without (dashed lines) the $B\bar{B} \leftrightarrow 3M$ channels we find no essential differences by eye.

5.3.2 Quantitative impact of many-body reactions

In this subsection we will quantify the effect of the $B\bar{B} \leftrightarrow 3M$ channels and $B\bar{B} \rightarrow 3M$ channels in 5% central Pb+Pb collisions for 3.5 GeV $\leq \sqrt{s_{NN}} \leq$ 2.76 TeV. To this end we

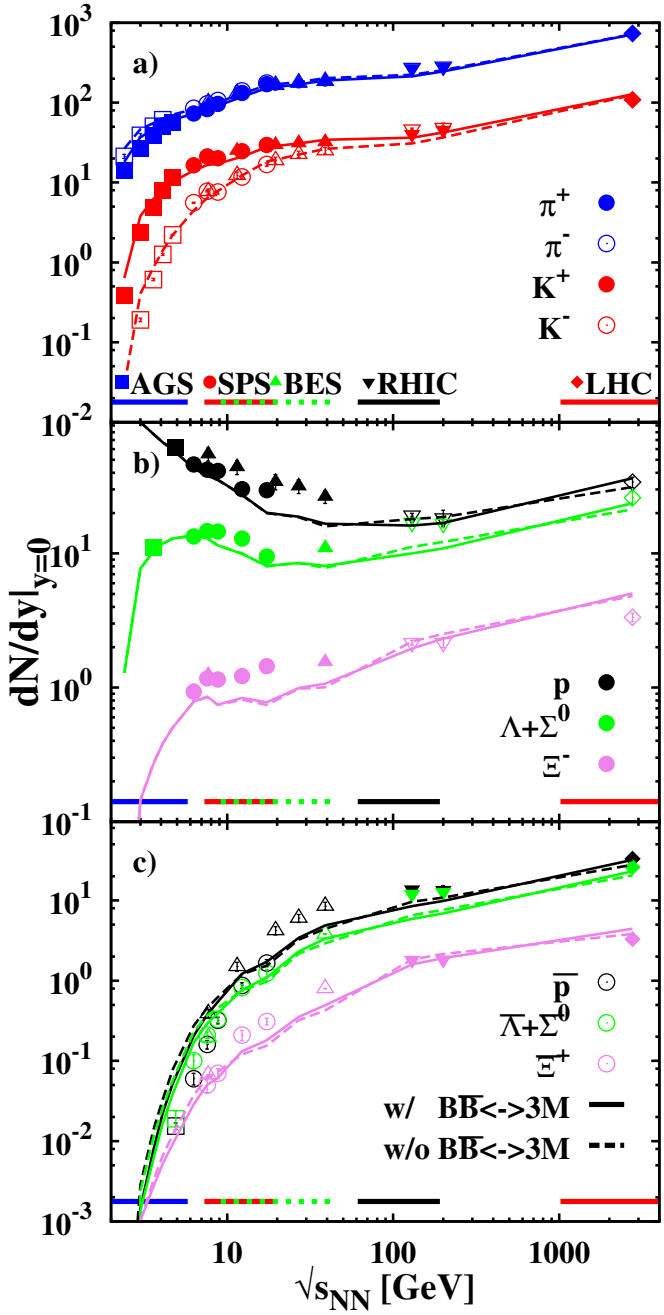

Fig. 5.13 – The midrapidity yields of mesons (a), baryons (b) and antibaryons (c) from PHSD as a function of the invariant energy $\sqrt{s_{NN}}$ for central heavy-ion collisions in comparison with the experimental data taken from Refs. [69, 77–80, 85–89, 91–104]. The solid lines refer to calculations including the $B\bar{B} \leftrightarrow 3M$ channels while the dashed lines display calculations without these channels. The particle yields from PHSD are connected by lines to draw the eye although experimental data and calculations do not always correspond to the same centrality selection (and system) for different bombarding energies.

show in Fig. 5.14 a) - d) the ratio of the antibaryons $\bar{p}, \bar{\lambda} + \bar{\Sigma}^0, \bar{\Xi}$ and $\bar{\Omega}$ (at midrapidity)

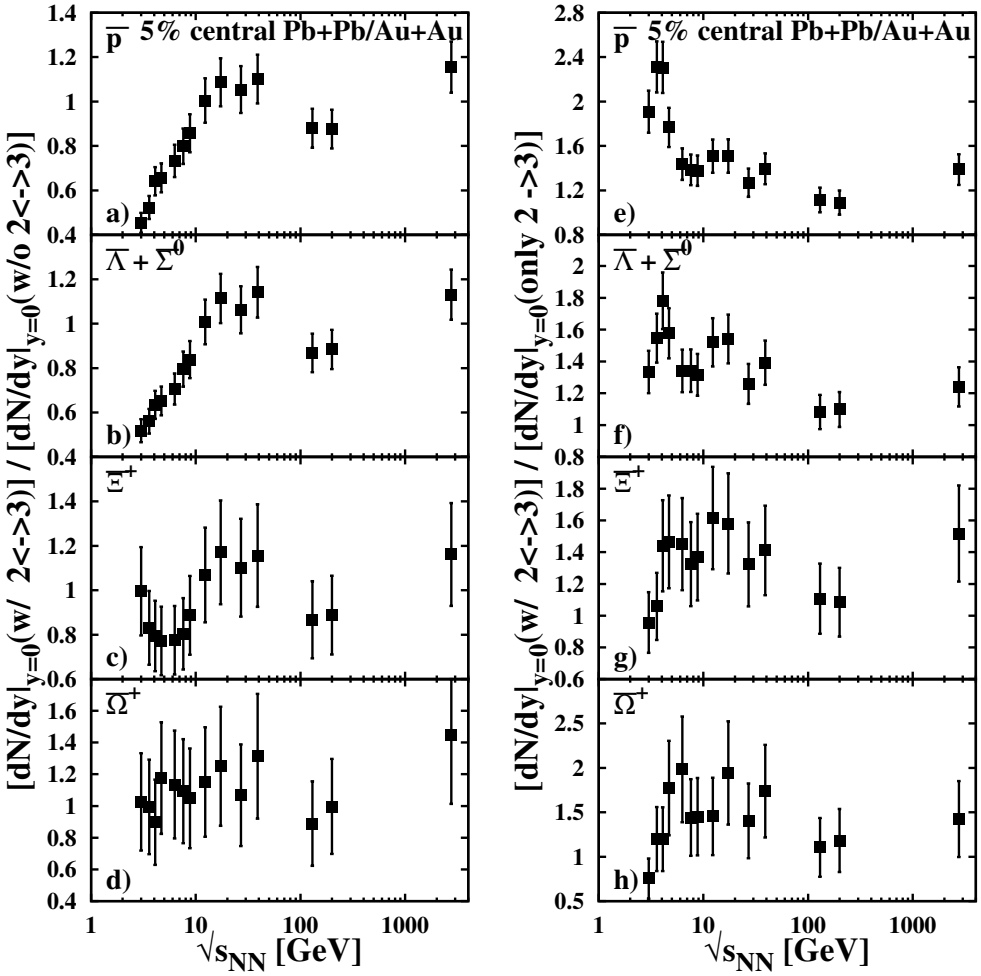

Fig. 5.14 – Ratios of 0-5% central midrapidity yields from calculations with the full $B\bar{B} \leftrightarrow 3M$ reactions to calculations without them for the antibaryons (a - d) and ratios of PHSD calculations with the full $B\bar{B} \leftrightarrow 3M$ reactions to calculations with only annihilation (e - h) as a function of the invariant energy $\sqrt{s_{NN}}$.

from PHSD calculations including the $B\bar{B} \leftrightarrow 3M$ channels to calculations without them. At low $\sqrt{s_{NN}} \approx 3.5\,\mathrm{GeV}$ we observe a sizeable net annihilation of antiprotons and antihyperons by about a factor of two which is essentially due to the fact that here the nucleon density is very large compared to the antinucleon density. Practically the same holds for the strangeness $S = \pm 1$ sector while the net suppression of $\bar{\Xi}^+$ is only 20%. For $\bar{\Omega}^+$'s there is no net suppression within error bars which results from the statistical errors of both calculations. With increasing invariant energy the net annihilation of antiprotons and antihyperons disappears at $\sqrt{s_{NN}} \approx 10$ GeV, i.e. at the top SPS and lower RHIC energies. For $\sqrt{s_{NN}} = 130$ GeV and 200 GeV we find a small net annihilation for $\bar{p}, \bar{\Lambda} + \bar{\Sigma}^0$, and $\bar{\Xi}^+$ which turns to a small enhancement at the LHC energy of $\sqrt{s_{NN}} = 2.76$ TeV as quoted before. This is in contrast to the results of the

model calculations in Refs. [105,106]. The small net suppression of antiprotons at the top RHIC energy, however, is in line with the results from Ref. [107] which also incorporate detailed balance for the annihilation channels. We interpret the tiny enhancement of antibaryons at the LHC energy to result from the huge meson abundances which in phase space are slightly overpopulated in PHSD relative to baryon-antibaryon pairs at hadronization.

In order to investigate the effect of the $B\bar{B}$ annihilation channels we show in Fig. 5.14 e) - h) the ratio of the antibaryons $\bar{p}, \bar{\Lambda} + \bar{\Sigma}^0, \bar{\Xi}^+$ and $\bar{\Omega}^+$ (at midrapidity) from PHSD calculations including the $B\bar{B} \leftrightarrow 3M$ channels to calculations with only the annihilation channels for the same reactions as in a) - d). Although this ratio is an unphysical quantity it allows to shed light on the relative importance of the annihilation channels. For all antibaryons in Fig. 5.14 e) - h) this ratio is larger than unity which implies that the back-reactions have some impact on the final antibaryon multiplicities. This effect is most pronounced at lower SPS energies, where the baryon densities are large compared to the antibaryon densities, and drops below 50% enhancement for invariant energies above $\sqrt{s_{NN}} \approx 10\,\mathrm{GeV}$ (within error bars). At top RHIC and LHC energies these modifications are below the 20% level since baryon and antibaryon densities are comparable and all elastic and inelastic $2 \leftrightarrow 2$ channels are equal for time reversed states. Only the relative weight of baryons to mesons changes slightly resulting in ratios greater than unity.

Chapter 6

Predictions for FAIR and NICA

In the last decades the focus of the heavy-ion accelerator community has been on higher energies in the hope of finding new physics and to validate (or falsify) the standard model. The first facility to reach ultra-relativistic energies was RHIC that started its measurements in the beginning of this millennium and reached a center-of-mass energy of $\sqrt{s_{NN}} = 200\,\text{GeV}$ in Au+Au collisions. The collider with the highest energy currently available is the LHC at CERN that started operation in 2010 and is able to collide two Pb nuclei at a center-of-mass energy up to $\sqrt{s_{NN}} = 5.02\,\text{TeV}$. In July 2012, the LHC was able to proof the existence of the Higgs boson that is responsible for the mass generation [4] of elementary particles. By the end of 2018 one expects a proposal for an extension of the LHC, the so-called Future Circular Collider (FCC) that may achieve $\sqrt{s} = 100\,\text{TeV}$ in p+p collisions. If this project is funded then it would be the epitome of the terrestrial reachable energies in heavy-ion collisions (HICs).

As mentioned in the Introduction the current focus of the community lies in the search for a possible critical endpoint of the confinement-deconfinement phase transition in the QCD phase diagram in order to get a better understanding of the nature of the confinement of quarks in hadrons. Both facilities (RHIC and LHC) address the high temperature, low baryon chemical potential/density part of the phase diagram where lattice calculations rule out a critical endpoint [7–12], which is expected at high densities and lower temperatures [6]. To come to the vicinity of the critical endpoint and possibly pinpoint its location, lower collision energies and heavy nuclei are needed; this is why the main emphasis of the current research is shifted — with the exception of LHC. In this context, at RHIC the Beam Energy Scan (BES) program was brought to life in 2010 that investigates a wide range of energies $\sqrt{s_{NN}} = 5.5,7.7,11.5,19.6,27,38,62.4\,\text{GeV}$ to map part of the phase diagram up to baryon chemical potentials of $\mu_B \approx 450\,\text{MeV}$. Additionally, new heavy-ion facilities were funded and are under construction to support the mapping of the phase diagram at even lower energies with high luminosities. The Facility for Antiprotons and Ion Research (FAIR) at the GSI Helmholtzzentrum für Schwerionenforschung in Germany and the Nuclotron-based Ion Collider fAcility (NICA) at the Joint Institute for Nuclear Research (JINR) in Russia are currently under construction

and will start first operation around 2020. The energy ranges are $\sqrt{s_{NN}} = 4 - 9\,\text{GeV}$ and $\sqrt{s_{NN}} = 4 - 11\,\text{GeV}$, respectively, and will map the high density part of the phase diagram in more detail. Because of the high luminosity particle spectra of rare particles like antibaryons (at these energies) will be measured with high precision.

In this chapter, we will investigate the future energy regime of FAIR and NICA with and without the $2 \leftrightarrow 3$ reactions. We will provide the rapidity spectra of $\bar{p}, \bar{\Lambda} + \bar{\Sigma}^0, \bar{\Xi}^+, \Omega^- + \bar{\Omega}^+$ from 5% central Au+Au, Cu+Cu, C+Au and Cu+Au collisions as well as their centrality dependence for the energies $E_{\text{lab}} = 6, 8$ and $60A\,\text{GeV}$ spanning the relevant energy regime for the two facilities. Furthermore, we investigate the total net annihilation as a function of the number of participants N_{part} for different values for the suppression factor λ of strange quarks in the $2 \leftrightarrow 3$ reactions.

6.1 Rapidity spectra

We investigate in this section again the influence of the $2 \leftrightarrow 3$ reactions on the final particle spectra, and show results from calculations with the $2 \leftrightarrow 3$ channels deactivated and calculations with different values for the strange quark suppression factor λ. The simulations were run with $\lambda = 0, 0.5$ and 1, with $\lambda = 0$ being equivalent to neglecting the strangeness sector and only considering the light quark sector [SU(2)]. We stress that in the current PHSD standard no suppression of strange quarks is considered ($\lambda = 1$).

In Fig. 6.1 we display the rapidity spectra for $\bar{p}, \bar{\Lambda} + \bar{\Sigma}^0, \bar{\Xi}^+, \Omega^- + \bar{\Omega}^+$ for 0-5% central Au+Au collisions at energies of $E_{\text{lab}} = 6, 8$ and $60A\,\text{GeV}$. The centrality class 0-5% is related to the number of participants $N_{\text{part}} = 370 \pm 3$ for 6 and $8A\,\text{GeV}$ and $N_{\text{part}} = 360 \pm 1$ for $60A\,\text{GeV}$ (for future comparison to data). At $6A\,\text{GeV}$ the SU(2) calculations are close to calculations without the $2 \leftrightarrow 3$ reactions, except for the antiprotons. Here, the SU(2) calculations lie on top of the half-suppressed calculations ($\lambda = 0.5$). Looking at the order of the maximum in the yield we find that the strangeness sector pushes the $\Omega^- + \bar{\Omega}^+$ spectra up but for every other particle species the spectra are pushed down for $\lambda \to 1$. The results without the $2 \leftrightarrow 3$ channels give at $8A\,\text{GeV}$ the highest rapidity spectra for all species and are on equal parts to calculations with $2 \leftrightarrow 3$ in SU(2) for $\bar{\Lambda} + \bar{\Sigma}^0$ and $\bar{\Xi}^+$. The antibaryons $\bar{\Lambda} + \bar{\Sigma}^0$ and $\bar{\Xi}^+$ show a very similar behavior such that the calculations without strange quark suppression lie farther below the SU(2) and deactivated results. For the antiproton and $\Omega^- + \bar{\Omega}^+$ all $2 \leftrightarrow 3$ calculations lie close to each other. At $60A\,\text{GeV}$ the difference between calculations with and without $2 \leftrightarrow 3$ reactions for the particle rapidity spectra is primarily found in $\Omega^- + \bar{\Omega}^+$ where the lowest yield is observed when neglecting the $2 \leftrightarrow 3$ reactions and the highest for the non-suppressed case ($\lambda = 1$). For $\bar{p}$ and $\bar{\Lambda} + \bar{\Sigma}^0$ the main deviation between the simulations is the width of the spectra and for $\bar{\Xi}^+$ a slight difference in height.

As in the analysis of Sec. 5.1 we find a larger influence of the $2 \leftrightarrow 3$ interactions at the lower energies of 6 and $8A\,\text{GeV}$. When high statistics data from FAIR and NICA become available the difference between the various calculations will allow to decide whether the

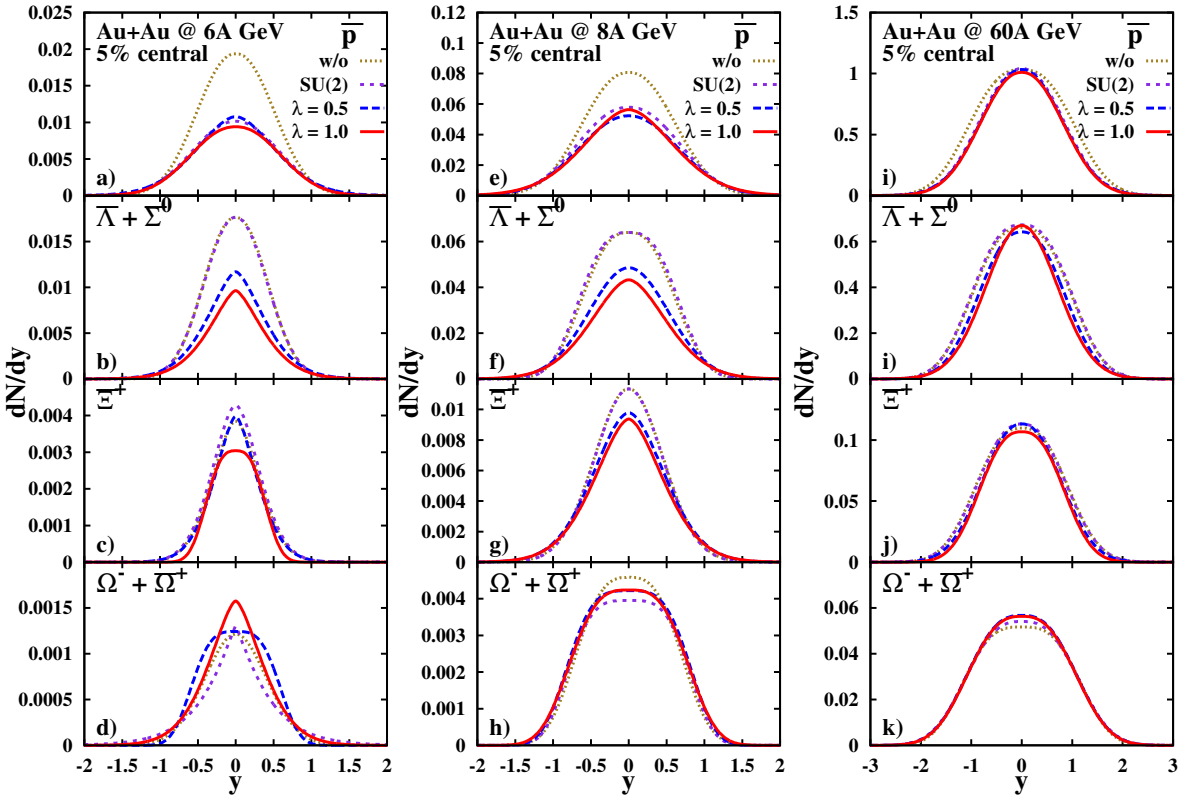

Fig. 6.1 – Rapidity spectra of $\bar{p}, \bar{\Lambda} + \bar{\Sigma}^0, \bar{\Xi}^+, \Omega^- + \bar{\Omega}^+$ in 5% central Au+Au collisions at 6, 8 and 60A GeV for $B\bar{B} \leftrightarrow 3M$ channels deactivated (dotted lines), $B\bar{B} \leftrightarrow 3M$ with only light quarks (short-dashed lines) and including strange quarks with a suppression of $\lambda = 0.5$ (long-dashed lines) and no suppression $\lambda = 1$ (solid lines).

$2 \leftrightarrow 3$ reactions are relevant and if the strangeness sector plays an important role in this energy regime.

6.2 Centrality dependence of Au+Au collisions

We will now focus on the centrality dependence of the rapidity spectra, again for the particles $\bar{p}, \bar{\Lambda} + \bar{\Sigma}^0, \bar{\Xi}^+, \Omega^- + \bar{\Omega}^+$ in central Au+Au collisions at 6, 8 and 60A GeV. For this we show in Fig. 6.2 the rapidity densities for $|y| < 0.2$ as a function of the number of participants N_{part}. At 60A GeV all calculations lie on top of each other for all particle species, only for $\Omega^- + \bar{\Omega}^+$ we find minor deviations. For 6 and 8A GeV the combined centrality dependence clearly distinguishes the different versions and allows for a definite evaluation of the importance of the $2 \leftrightarrow 3$ reactions in HICs in this energy-regime. Furthermore, the antibaryon production at 6 and 8A GeV in peripheral collisions is rather low such that high statistics are needed in the calculations and also in the future experiments. Fortunately, FAIR and NICA will have huge luminosities allowing for precise measurements of antibaryons even in peripheral collisions.

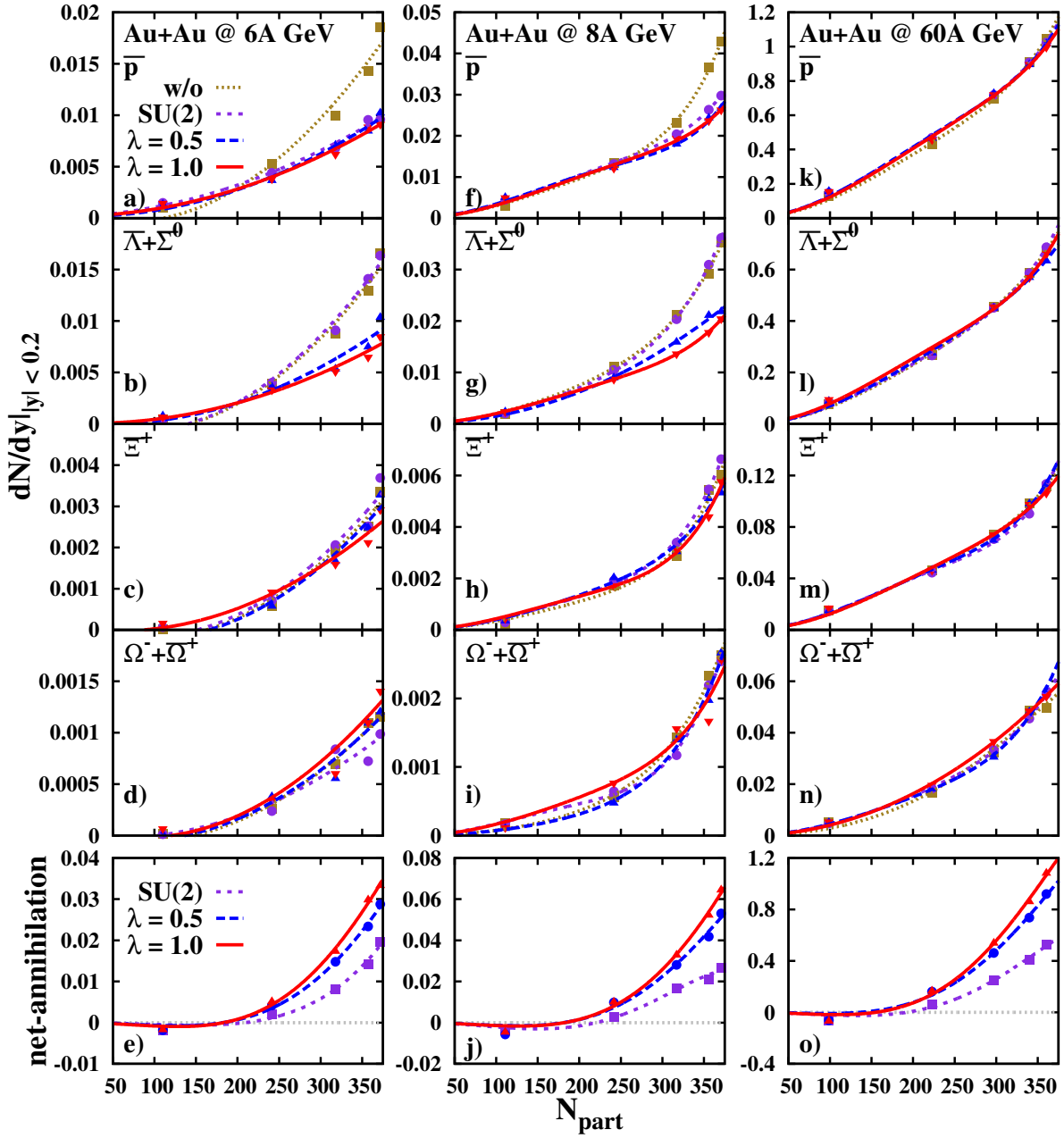

Fig. 6.2 – Rapidity density of $\bar{p}, \bar{\Lambda}+\bar{\Sigma}^0, \bar{\Xi}^+, \Omega^- + \bar{\Omega}^+$ as well as the total net-annihilation (lowest panels) as a function of the number of participants $N_{\rm part}$ in Au+Au collisions at 6, 8 and 60A GeV for $B\bar{B} \leftrightarrow 3M$ channels deactivated (dotted lines), $B\bar{B} \leftrightarrow 3M$ with only light quarks (short-dashed lines) and including strange quarks with a suppression of $\lambda = 0.5$ (long-dashed lines) and no suppression ($\lambda = 1$, solid lines). The dots are the actual PHSD results and the lines are plotted to guide the eye.

In addition to the rapidity densities we show in Fig. 6.2 (lowest panels) the total net-annihilation — which is not a physical quantity but nevertheless interesting — calculated from the time integrated $2 \leftrightarrow 3$ reaction rates as a function of the number of participants

for the different energies and strange quark suppression factors. For all energies we find that more central collisions lead to a larger net-annihilation whereas in peripheral collisions the net-annihilation drops close to zero due to the low abundance of antibaryons in the system and becomes even slightly negative indicating a net-reproduction because of the higher meson abundance. We find a larger net-annihilation for $\lambda \to 1$ and that the difference in λ is not linearly correlated to the net-annihilation but almost in a logarithmic manner for central collisions — attesting the high complexity of a HIC.

6.3 Centrality dependence of light and asymmetric systems

As a complement to the large, symmetric collision systems we show in Fig. 6.3 the centrality dependence of the rapidity density and net-annihilation for the lighter systems C+Au, Cu+Cu and Cu+Au at a bombarding energy of $E_{\mathrm{lab}} = 30A\,\mathrm{GeV}$. At the smallest collision system C+Au only slight deviations in the variety of calculations is found for the antiprotons where the calculations with deactivated $2 \leftrightarrow 3$ channels give lower yields than the calculations with the $2 \leftrightarrow 3$ channels, which lie all on top of each other throughout all centralities . The systems Cu+Cu and Cu+Au have very similar centrality dependences for all particle species, only for Cu+Au higher numbers of participants N_{part} are reached and thus larger yields achieved. Like in the Au+Au collisions a larger suppression of the yields is found for $\lambda \to 1$. A more interesting behavior shows the net-annihilation as a function of N_{part} that is negative for all centralities and systems at $E_{\mathrm{lab}} = 30A\,\mathrm{GeV}$, which signifies a net-recreation of baryon-antibaryon pairs through three-meson fusion. First, the net-annihilation drops as a function of N_{part} and then starts to rise slightly in the most central collisions for the C+Au system . In Cu+Cu and Cu+Au we also find an initial drop that turns into a rise before dropping again in the most central collisions; this deviates from our findings in central Au+Au collisions at $E_{\mathrm{lab}} = 6, 8$ and $60A\,\mathrm{GeV}$. The irregular behavior may stem from more numerous formations of QGP droplets for more central collisions and the resulting interplay between the QGP formation and $2 \leftrightarrow 3$ channels since both reactions happen in the same time interval, see Sec. 2.3.6. This interplay is rather complicated as mesons, baryons and antibaryons are dissolved into the QGP but eventually produced from it again.

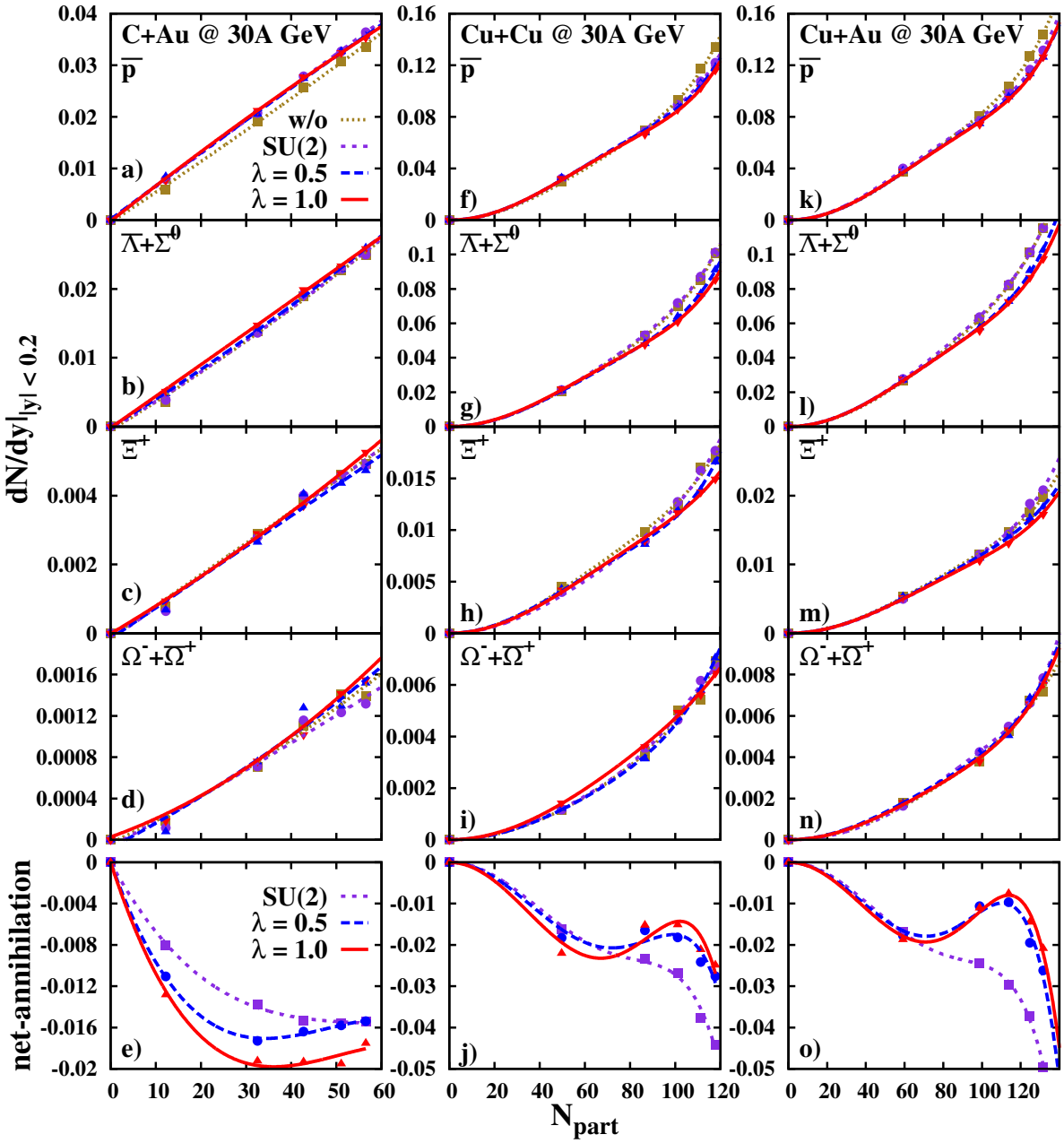

Fig. 6.3 – Rapidity density of $\bar{p}, \bar{\Lambda}+\bar{\Sigma}^0, \bar{\Xi}^+, \Omega^-+\bar{\Omega}^+$ as well as the total net-annihilation (lowest panels) as a function of the number of participants $N_{\rm part}$ in C+Au,Cu+Cu and Cu+Au collisions at $30A\,$GeV for $B\bar{B} \leftrightarrow 3M$ channels deactivated (dotted lines), $B\bar{B} \leftrightarrow 3M$ with only light quarks (short-dashed lines) and including strange quarks with a suppression of $\lambda = 0.5$ (long-dashed lines) and no suppression ($\lambda = 1$, solid lines). The dots are the actual PHSD results and the lines are plotted to guide the eye.

Chapter 7

Conclusions

In this work we have extended the formulation of the baryon-antibaryon annihilation in the Quark Rearrangement Model (QRM) to the strangeness sector in Chapter 3. This extension includes more than 2000 different mass channels and an optional suppression of the transition matrix element for the rearrangement of strange quarks, due to the larger mass of strange quarks compared to the up and down quarks. The transition matrix element was extracted from the experimental $p\bar{p}$ annihilation cross section which is the only measured annihilation cross section (besides $n\bar{p}$).

The correct numerical implementation of the baryon-antibaryon annihilation into three mesons ($2 \leftrightarrow 3$) was validated in Chapter 4 in box simulations with periodic boundary conditions of 100 different baryon-antibaryon initialized systems. In the box simulations all particles from the light and strangeness sector were assumed to be stable and only the $2 \leftrightarrow 3$ reactions were considered (no elastic scattering). The detailed balance relation is fulfilled for the total reaction rate and on a channel-by-channel basis to on average 98% for the ten channels with the highest reaction rates.

In Chapter 5 we implemented the $2 \leftrightarrow 3$ reactions into the Parton-Hadron-String Dynamics (PHSD) approach and investigated their influence on Heavy-Ion Collisions (HIC) from SchwerIonen Synchrotron (SIS) up to Large Hadron Collider (LHC) energies. We first examined the top Alternating Gradient Synchrotron (AGS) and Super Proton Synchrotron (SPS) energies where we found that the $2 \leftrightarrow 3$ channels affect only the antibaryon spectra [15, 108]. At SPS energies the influence of the $2 \leftrightarrow 3$ channels was found to be stronger for lower energies. The additional strangeness sector has virtually no impact on the antiproton spectra while the spectra of $\bar{\Lambda} + \bar{\Sigma}^0, \bar{\Xi}^+$ and $\Omega^- + \bar{\Omega}^+$ are pushed down, closer to the experimental data. This validates that the strangeness sector is an integral part of the $2 \leftrightarrow 3$ reactions which was missing in PHSD so far. At the top SPS energy of $E_{\text{lab}} = 158A\,\text{GeV}$ the $2 \leftrightarrow 3$ reactions induce only minor changes in the rapidity spectra [108].

Additionally, we compared simulations with (PHSD) and without (HSD) the partonic phase as well as simulations including and excluding chiral symmetry restoration (CSR). At $E_{\text{lab}} = 30A\,\text{GeV}$ the description in HSD of the antiprotons is slightly better than in

PHSD, however, any other antibaryon is described better with the partonic phase included. The CSR improves the multistrange antibaryons but overshoots $\bar{\Lambda} + \bar{\Sigma}^0$. At $158A\,\mathrm{GeV}$ we find an overall better description of experimental data from PHSD calculations with CSR effects included so that no energy-independent, concise conclusions can be drawn [108].

Next, we focused on Relativistic Heavy-Ion Collider (RHIC) and LHC energies where we found at $\sqrt{s_{NN}} = 2.76\,\mathrm{TeV}$ a net-reproduction while at $\sqrt{s_{NN}} = 200\,\mathrm{GeV}$ the annihilation is almost balanced out by the reproduction. We compared results from calculations with the full $2 \leftrightarrow 3$ channels to calculations without them and with only the annihilation activated. The latter limit corresponds to other transport models where the recreation of the $B\bar{B}$ pairs is neglected. At $200\,\mathrm{GeV}$ the calculations including the $2 \leftrightarrow 3$ channels lie always in between the other calculations and provide a better description of the experimental data than calculations without them (with the exception of $\Lambda + \Sigma^0$). For the multistrange baryons and antibaryons the results from simulations using only the annihilation lie slightly closer to the data [109].

At the LHC energy of $\sqrt{s_{NN}} = 2.76\,\mathrm{TeV}$ the results from calculations using the full $2 \leftrightarrow 3$ reactions lie above the other two calculations indicating a net $B\bar{B}$ production. Other than $\bar{\Omega}^+$, the multistrange sector is slightly overshot in the full calculations while the calculations with only the annihilation underestimate the experimental data (except for Ξ^- and Ω^-). The overestimation may stem from a deviation from statistical equilibrium in the hadronization.

The yield analysis was completed with the presentation of the excitation functions of the different hadrons where for the baryons and antibaryons the results from calculations including and neglecting the $2 \leftrightarrow 3$ channels were presented in the energy range $\sqrt{s_{NN}} = 3.5 - 2760\,\mathrm{GeV}$. We found that the mesons are well described in PHSD and also that the description of the baryons is good, with the exception of Ξ^- in the SPS energy range where the PHSD results deviate from the experimental data. The description of the $\Lambda + \Sigma^0$ yields is poor at the top RHIC energies. Overall, the antibaryon sector does not deviate too much from the data, only the antiproton yield is overestimated below $\sqrt{s_{NN}} = 10\,\mathrm{GeV}$ for both calculations (with and without the $2 \leftrightarrow 3$ reactions) [109].

Comparing the excitation functions of antibaryons from calculations using the full $2 \leftrightarrow 3$ channels to calculations with only $B\bar{B}$ annihilation we find deviations of up to a factor of 2.5, with the most prominent deviations at lower SPS or FAIR/NICA energies. This shows the importance of the reproduction mechanism that is missing in other transport approaches but is needed for a correct physical description. Depending on the energy and particle species a relative annihilation or reproduction is found when comparing the results from calculations with and without the $2 \leftrightarrow 3$ channels. For lower energies a relative net-annihilation is found that changes into a net reproduction at higher energies ($\sqrt{s_{NN}} \approx 10\,\mathrm{GeV}$) with a dip at RHIC energies where a slight net-annihilation is observed [109].

In Chapter 6 we presented predictions for FAIR and NICA in the antibaryon sector.

First, we investigated the rapidity spectra from 5% central Au+Au collisions at $E_{\mathrm{lab}} = 6, 8$ and $60A\,\mathrm{GeV}$ for a variety of strangeness suppressions λ in the transition matrix element and for calculations without the $2 \leftrightarrow 3$ channels. We found a similar behavior as for the SPS energies. At the lower energies of 6 and $8A\,\mathrm{GeV}$ the influence of the $2 \leftrightarrow 3$ channels on the antibaryon rapidity spectra is more pronounced than at $60A\,\mathrm{GeV}$ and for $\lambda \to 1$ the rapidity spectra of $\bar{p}, \bar{\Lambda} + \bar{\Sigma}^0$ and $\bar{\Xi}^+$ are pushed down, while for $\Omega^- + \bar{\Omega}^+$ the yields are enhanced. Neglecting the $2 \leftrightarrow 3$ channels leads to higher yields that lie on top of the SU(2) ($\lambda = 0$) calculations, except for the antiprotons. The yields show — for all centrality classes — a behavior similar to the observations at 5% centrality.

Furthermore, we studied the total net-annihilation from the integrated $2 \leftrightarrow 3$ rates as a function of centrality for the three energies. For the energies analyzed a slight net-recreation is found for peripheral collisions that turns into a quadratically rising net-annihilation, which is stronger for $\lambda \to 1$ in an almost logarithmic manner.

Next, the same centrality analysis was done for C+Au, Cu+Cu and Cu+Au collisions at $E_{\mathrm{lab}} = 30A\,\mathrm{GeV}$. No major deviations between calculations with and without the $2 \leftrightarrow 3$ channels have been found in these systems, only for the antiprotons in C+Au collisions the yields from calculations without the $2 \leftrightarrow 3$ channels are slightly lower than the other. On the other hand the centrality-dependence of the net-annihilation shows for all systems and centralities negative values, indicating a net-reproduction. For C+Au collisions the net-annihilation first drops until at $N_{\mathrm{part}} \approx 30$ it starts to rise for finite λ, in contrast to the SU(2) calculations that do not show a rise. The net-annihilation in Cu+Cu and Cu+Au systems show up to $N_{\mathrm{part}} \approx 100$ a similar behavior to C+Au but for even more central collisions the net-annihilation starts to drop steeply for all calculations. This behavior is the result of the interplay between the $2 \leftrightarrow 3$ reactions and the formation of QGP droplets in more central collisions.

The comparison to data at SPS energies, where experimental data are available, show that the best description is achieved with the $2 \leftrightarrow 3$ reactions included and $\lambda = 1$ such that this configuration provides reliable predictions for the future facilities FAIR and NICA.

In conclusion, we find that the baryon-antibaryon annihilation and recreation through three mesons has a major impact on HICs in the energy ranges $\sqrt{s_{NN}} \leq 10\,\mathrm{GeV}$ and $\sqrt{s_{NN}} \geq 100\,\mathrm{GeV}$, additionally the strangeness sector improves the description of the experimental data. In contrast to earlier expectations, we do not need to introduce an additional suppression of the strangeness sector in the quark rearrangement model; the $2 \leftrightarrow 3$ reactions appear to be fully described by the $p\bar{p}$ annihilation cross section. Although, the description of a HIC would be further improved if experimental data of more baryon-antibaryon cross sections were available. Furthermore, the neglect of the recreation leads to large deviations with respect to the full calculations and gives a physically incoherent picture of the HIC dynamics and, hence, must be taken into account at least at FAIR/NICA energies. By comparing the future FAIR and NICA data to our predictions the importance of the baryon-antibaryon annihilation at low energies can be directly verified or falsified.

Chapter 8

Acknowledgement

I want to take this moment to thank everybody, who made my three and a half years of PhD studies worthwhile, for their support. First and foremost I want to thank Prof. Wolfgang Cassing from all my heart for his help and guidance that started not just with this PhD but already with my Master's studies. Whenever I had problems or did not understand something he would take the time to listen and clarify in detail what I misunderstood.

I also want to thank Prof. Claudia Höhne for her interest in my work and that she became my second examiner.

To Prof. Elena Bratkovskaya my thanks go out for the fruitful discussions with her in our PHSD group meetings and HGS-HIRe committee meetings where she always made helpful suggestions for the next steps of my thesis. For the easier production of data for my PhD she even gave me access to the Green IT Cube at GSI, which helped me a lot in simulating the sheer number of systems I investigated.

Next, I would like to thank everybody from the PHSD group with whom I worked and who I appreciate Olena Linnyk, Pierre Moreau, Andrej Ilner and Taesoo Song.

I want to thank my office-mates Alessia Palmese and Thorsten Steinert with whom I could always talk to and joke around with. I am grateful for the institute where I found so many friends and had a lot of fun on uncountable occasions. My thanks go out to the secretaries, who always took care of the paper work, and especially to Elke Jung, who always kept me up-to-date with the latest gossip and with whom I shared a bottle of champagne more than once. Many thanks to my close friends Jan Mühlhans, Katja Kleeberg, Christopher Jung, Richard Williams, Johannes Weyrich and Lukas Holicki; see you at the "Späti"!

Last but not least I want to thank my brother Roman and my parents Rudolf and Galina for being always there for me.

Everything that is good has to come to an end.

I will keep these years forever in my heart.

This work was possible thanks to the computational resources of Loewe-CSC and Green IT Cube as well as the support of the Helmholtz International Center for FAIR (HIC for FAIR), the Helmholtz Graduate School for Hadron and Ion Research (HGS-HIRe), the Helmholtz Research School for Quark Matter Studies in Heavy-Ion Collisions (H-QM).

Appendix A

Phase-space integrals

The on-shell phase-space integrals incorporated throughout this work inhibit most of the dynamics of the system. As they play a major role this section is dedicated to some more details of phase-space integrals. We recall that the n-body phase-space integral is generally defined by

$$R_n(P; m_1, \ldots, m_n) = \left(\frac{1}{(2\pi)^3}\right)^n \int \prod_{k=1}^{n} \mathrm{d}^4 p_k \; \rho_k(p_k)(2\pi)^4 \delta^4 \left(P - \sum_{j=1}^{n} p_j\right), \quad \text{(A.1)}$$

with ρ denoting the spectral function of the respective particle. Since the phase-space integrals are Lorentz invariant we will always work in the center-of-mass system. In the on-shell case the spectral function takes the form,

$$\rho(p) = \delta(p^2 - m_1^2), \quad \text{(A.2)}$$

with p denoting the 4-momentum in this case. Inserting the spectral function (A.2) into Eq. (A.1) and integrating over p^0 yields the on-shell phase-space integral of Eq. (3.2). To show (as an example) the behavior of the different n-body phase-space integrals it is instructive to look e.g. at the consecutive decays $p\bar{p} \to \pi\rho\rho \to 3\pi\rho \to 5\pi$ which are essentially the motivation for the QRM. Also, this example connects the 3-,4- and 5-body phase-space integrals as a function of the invariant energy above threshold (see below).

For the sake of completeness, we start with the 1-body phase-space integral,

$$R_1(\sqrt{s}; m) = \frac{1}{(2\pi)^3} \int \frac{\mathrm{d}^3 p}{2E} \; (2\pi)^4 \delta^4(\sqrt{s} - E) = \frac{\pi}{\sqrt{s}}, \quad \text{(A.3)}$$

where E is the on-shell energy $E = \sqrt{m^2 + p^2}$ and the mass m of the particle is equal to the invariant energy $\sqrt{s}$. This result shows that the 1-body phase-space decreases with

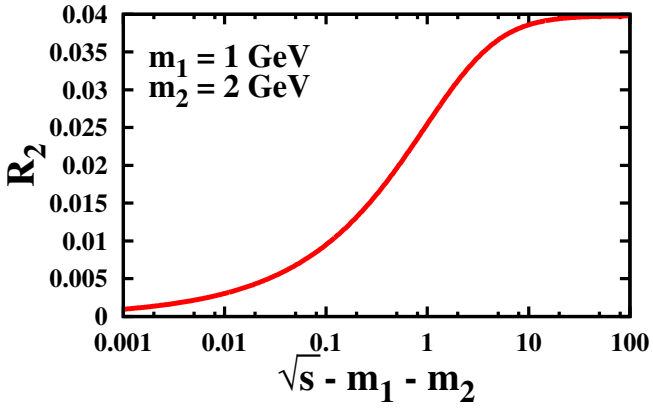

Fig. A.1 – Two-body phase-space integral for particles with masses $m_1 = 1\,\text{GeV}$ and $m_2 = 2\,\text{GeV}$ as a function of the invariant energy above threshold.

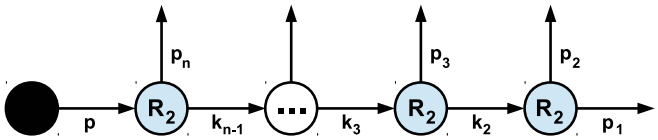

Fig. A.2 – Illustration of the subsequent decay of an initial state (black dot) into n particles. The initial state may consist of m particles as only the invariant mass is relevant for the phase-space integral due to Lorentz invariance.

increasing $\sqrt{s}$. The 2-body phase-space integral can also be evaluated analytically,

$$R_2(\sqrt{s}; m_1, m_2) = \frac{1}{(2\pi)^2} \int\int \frac{\mathrm{d}^3 p_1}{2E_1} \frac{\mathrm{d}^3 p_2}{2E_2}\, \delta^3(\vec{p}_1 + \vec{p}_2)\delta(\sqrt{s} - E_1 - E_2) \tag{A.4}$$

$$= \frac{1}{4(2\pi)^2} \int \frac{\mathrm{d}^3 p_1}{E_1 E_2} \delta(\sqrt{s} - E_1 - E_2) \tag{A.5}$$

$$= \frac{1}{4(2\pi)^2} \int_0^\infty \int_0^\pi \int_0^{2\pi} \frac{\mathrm{d}\phi \mathrm{d}\theta \mathrm{d}p_1\; p_1^2 \sin\theta}{E_1 E_2} \delta(\sqrt{s} - E_1 - E_2) \tag{A.6}$$

$$= \frac{1}{4\pi} \int_0^\infty \frac{\mathrm{d}p_1\; p_1^2}{\sqrt{m_1^2 + p_1^2}\sqrt{m_2^2 + p_1^2}} \delta\left(\sqrt{s} - E_1 - E_2\right). \tag{A.7}$$

The zeros of the delta function are given by

$$p_0 = \pm \frac{\sqrt{\lambda(s, m_1^2, m_2^2)}}{2\sqrt{s}}, \tag{A.8}$$

where only the positive value has to be taken in our calculation. Rewriting the delta

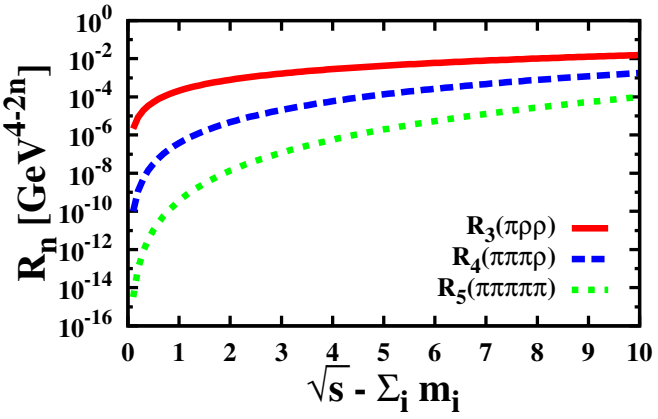

Fig. A.3 – (Color online) Illustration of the 3-, 4-, and 5-body phase-space integrals as a function of the invariant energy above threshold. The red solid line shows the 3-body phase-space integral for $\pi\rho\rho$, the blue dashed line shows the 4-body phase-space integral for $3\pi\rho$ and the green dotted line shows the 5-body phase-space integral for 5 pions.

function as

$$\delta(\sqrt{s} - E_1 - E_2) = \frac{\delta(p_1 - p_0)}{p_1/E_1 + p_1/E_2} \tag{A.9}$$

and plugging Eqs. (A.8) and (A.9) into Eq. (A.7) we obtain the two-body phase-space integral

$$\begin{aligned} R_2(\sqrt{s}; m_1, m_2) =& \frac{1}{4\pi} \int_0^\infty \frac{\mathrm{d}p_1 \; p_1}{E_1 E_2} \frac{E_1 E_2 \delta(p_1 - p_0)}{E_1 + E_2} \\ =& \frac{\sqrt{\lambda(s, m_1^2, m_2^2)}}{8\pi s}, \end{aligned} \tag{A.10}$$

with $E_1 + E_2 = \sqrt{s}$ from the original delta function. The typical shape of $R_2(\sqrt{s}, m_1, m_2)$ is shown in Fig. A.1 for the masses $m_1 = 1\,\mathrm{GeV}$ and $m_2 = 2\,\mathrm{GeV}$ as a function of the invariant energy above threshold. The upper limit is independent of the masses and is given by $1/(8\pi)$.

The on-shell three-body phase-space integral $R_3(\sqrt{s}, m_1, m_2, m_3)$ is the most important one for our work and a good example for the evaluation of phase-space integrals of higher order since the n-body decay can be considered as consecutive 2-body decays, see Fig. A.2 for an illustration. Note that in Fig. A.2 $k_n = p$ and $k_1 = p_1$. A prerequisite in calculating the phase-space integral is that we do not have any incoming momenta in between the first and final 2-body decay. For the calculation of the process we employ the recursion relation for phase-space integrals,

$$R_n(P) = \int \frac{\mathrm{d}^4 p_n}{(2\pi)^3} \rho_n(p_n) R_{n-1}(P - p_n), \tag{A.11}$$

and also insert two identities

$$1 = \int \mathrm{d}M_{n-1}^2 \delta(M_{n-1}^2 - k_{n-1}^2)), \tag{A.12}$$

$$1 = \int \mathrm{d}^4 k_{n-1} \delta^4(P - p_n - k_{n-1}). \tag{A.13}$$

The first identity from Eq. (A.12) gives the mass of the first cluster from which the 4-momentum p_n splits. The second identity ensures energy-momentum conservation in the splitting process. Plugging both identities into Eq. (A.11) we find

$$R_n(P) = \int \mathrm{d}M_{n-1}^2 \underbrace{\int \mathrm{d}^4 k_{n-1} \int \frac{\mathrm{d}^4 p_n}{(2\pi)^3} \delta^4(k_{n-1}^2 - M_{n-1}^2) \delta^4(p_n^2 - m_n^2) \delta^4(P - p_n - k_{n-1})}_{R_2(P; m_n, M_{n-1})/(2\pi)} R_{n-1}(k_{n-1}) \tag{A.14}$$

$$= \int_{(\sum_{i=1}^{n-1} m_i)^2}^{(M_n - m_n)^2} \mathrm{d}M_{n-1}^2 \frac{R_2(P; m_n, M_{n-1})}{2\pi} R_{n-1}(k_{n-1}). \tag{A.15}$$

With this expression any n-particle phase-space integral can be calculated in a straight forward fashion as long as the masses m_i are known. Note that the last R_2, which one gets after applying Eq. (A.15) several times, has no additional factor $1/(2\pi)$. In Fig. A.3 the phase-space integrals for 3, 4 and 5 particles are shown as a function of the invariant energy above threshold for our example of initial $\pi\rho\rho$ with a subsequent decay into $3\pi\rho$ and a final decay to 5 pions. All phase-space integrals share a similar shape, only the magnitudes close to threshold vary substantially with the number of particles.

Since the 3-body phase-space integrals are no longer given analytically and are needed in the PHSD calculations for the 2836 channels incorporated as a function of $\sqrt{s}$ it is very helpful to have an analytical approximation with coefficients that can be fitted and tabulated:

$$R_3(t, m_1, m_2, m_3) = a_1 t^{a_2} \left(1 - \frac{1}{a_3 t + 1 + a_4}\right), \tag{A.16}$$

The parameters a_1, a_2, a_3 and a_4 are fitted to the numerical results for R_3 and stored on file. We discard an explicit representation of the quality of the fits since the lines cannot be distinguished by eye in the range $0\,\mathrm{GeV} < \sqrt{s} - m_1 - m_2 - m_3 \leq 10\,\mathrm{GeV}$.

Appendix B

Numerical implementation

In this appendix we describe how the Quark Rearrangement Model (QRM) is implemented numerically since this is the main numerical work of this thesis and deserves special emphasis. In Sec. 4.1 we already addressed part of the implementation but did not go into detail. This appendix is devoted to a description of our method from the initialization of the arrays — holding information of possible final states for specific initial states — to the selection of actually colliding particles and the final states, respectively.

B.1 Initialization

In Sec. 4.1 it was already mentioned that one has to calculate beforehand the information on possible final states for specific initial $B\bar{B}/3M$ combinations and save the information for a fast access during the run. In the QRM the quark content of the colliding baryons and antibaryons are rearranged into three mesons and vice versa such that for the final meson states one has to ensure the conservation of the quark numbers. We additionally conserve the parity of the particles but do not gate on the spin of the particles due to the relatively high energies we are dealing with. The parity constraint has the interesting property that the combinations $N(1535) + \bar{\Omega}^+$ and $\Omega^- + \bar{N}(1535)$ do not react via the QRM since K and K^* have both negative parity and are the only possible decay candidates.

For the management of the conserved quantities an array is set up that contains the valence quark content, parity and spin of the hadron. The mesons π^0, ρ^0, ω or a_1^0 may have as a quark content either $u\bar{u}$ or $d\bar{d}$ pairs, while η (ϕ) has with 50% (16.9%) probability light quark and 50% (83.1%) $s\bar{s}$ content. These factors have to be taken into account when calculating the multiplicity of a channel. In the case of neutral mesons it is sufficient if one of the possible quark contents ($u\bar{u}, d\bar{d}$ or $s\bar{s}$ depending on the meson) fulfills the quark content constraint. Depending on the combination of $B\bar{B}$ more than a single combination of $q\bar{q}$ pairs may allow a channel and the multiplicity may vary for

the different combinations, e.g.

$$\begin{aligned}\Xi^-[uus] + \bar{\Xi}^+[\bar{u}\bar{u}\bar{s}] \longleftrightarrow \pi^0[u\bar{u}, d\bar{d}] + \eta[0.5(u\bar{u}, d\bar{d}), 0.5\, s\bar{s}] + \phi[0.169(u\bar{u}, d\bar{d}), 0.831\, s\bar{s}],\\ = u\bar{u} + s\bar{s} + u\bar{u}, \quad (i)\\ = u\bar{u} + u\bar{u} + s\bar{s}. \quad (ii)\end{aligned} \tag{B.1}$$

Combination (i) gives a weight factor f from the quark content of $f_{(i)} = 1. \cdot 0.5 \cdot 0.169 = 0.0845$ and combination (ii) of $f_{(ii)} = 1. \cdot 0.5 \cdot 0.831 = 0.4155$. For the calculation of the multiplicity of the channel the weight factor has to be averaged. The multiplicity N is calculated via

$$N = \bar{f} \cdot \begin{cases} (2s_1+1)(2s_2+1) & \text{for baryon} - \text{antibaryon}, \\ \frac{(2s_3+1)(2s_4+1)(2s_5+1)}{N_{\text{id}}!} & \text{for mesons}, \end{cases} \tag{B.2}$$

with $\bar{f}$ as the averaged quark content factor, s_i the spin of the respective particle and N_{id} as the number of identical mesons. The multiplicity N is accumulated for each mass channel and all possible final charge combinations of the mass channels are stored on file.

In PHSD we use for both reaction directions two arrays: one array stores the multiplicity, particle indices and number of final state charge combinations of the mass channel and another array stores the final-state charge combinations. In actual PHSD simulations — depending on the energy/particle densities — these arrays will be accessed by 10^9-10^{12} times per time step and with the wrong array shapes for the programming language the CPU time could be increased by up to a factor of 10.

With the parity and quark content constraint one ends up with the numbers relevant for the arrays displayed in Table B.1 for the $B\bar{B}$ annihilation and three meson fusion. Furthermore, one needs the fit parameters a_i for all meson mass combinations for the three-body phase-space integrals, as mentioned above (A.16).

B.2 Subroutine workflow

We here come to the structure of the subroutine handling the $2 \leftrightarrow 3$ reactions in PHSD. As already described above the subroutine uses the in-cell method where the particles

Tab. B.1 – Values for the relevant entries of the arrays holding the possible mass channels of the $B\bar{B} \leftrightarrow 3M$ reactions.

	$B\bar{B} \to 3M$	$3M \to B\bar{B}$
max. initial particle and charge combinations	484	1771
max. number of final state mass channels per initial particle and charge combination	62	24
max. final state charge combinations	8	4

in the same space-time cell may interact with each other. The subroutine processes one ensemble of the system at a time. For each ensemble the subroutine operates as follows:

- Assign the mesons and baryons to their respective volume cells — store the particle's cell location.
  - Take only particles where the local energy density is below the critical value for the QGP formation $\varepsilon < \varepsilon_c$.
  - Take only particles that are "formed".
  - Save the number of mesons, baryons and antibaryons for each cell.
- Loop over all cells:
  - If there is at least one baryon and one antibaryon in the cell we look for $B\bar{B} \to 3M$ reactions.
    - Loop over the antibaryons.
    - For a specific antibaryon calculate the probability P_i to annihilate — according to Eq. (3.4) — with all other baryons i in the same cell.
    - If the antibaryon was created in a $3 \to 2$ reaction make sure that the reaction partner does not come from the same reaction.
    - Accumulate the probabilities in an array, where the first entry holds P_1, the second entry $P_1 + P_2$, the third $P_1 + P_2 + P_3$, etc.
    - Ensure that for the specific antibaryon the accumulated total annihilation probability is below unity.
    - Choose via Monte Carlo if this antibaryon annihilates with any of the baryons present.
    - The selection of the final state mesons is analogous to the annihilation partner selection:
      - Loop over all possible final states for the $B\bar{B}$ pair and accumulate the probabilities calculated with Eq. (3.7).
      - Consider only those meson triples where the invariant mass of the $B\bar{B}$ pair is larger than the summed mass of the mesons.
      - Select the final state via Monte Carlo
    - If the meson triple was successfully created then delete the $B\bar{B}$ pair.
    - Look at the next antibaryon.
  - If there are at least 3 mesons in the cell we look for $3M \to B\bar{B}$ reactions.
    - For the mesons one has to calculate the probabilities according to Eq. (3.12) for each meson with any other meson and the possible final states.
    - To save computation time we calculate the probabilities for every possible meson combination of the cell with their final states once.

· Depending on the number of mesons per cell, the array holding the probabilities and final states become rather large. Here, the shape of the arrays is crucial as discussed above for the channel arrays.

· In the calculation of the probability for a specific meson channel c fusing to a specific $B\bar{B}$ pair c' the normalization factor $N_3(\sqrt{s}, c')$ needs to be evaluated for every possible $B\bar{B}$ pair and may vary depending on the charge state.

∗ After the calculation loop over the first meson and accumulate the probabilities. Again the total probability should not exceed unity.

∗ Choose via Monte Carlo the mesons fusing and the $B\bar{B}$ pair with the charge constellation created.

∗ Look at the next meson combination in this cell.

- Look at the next cell

In Fig. B.1 a summary of the workflow is sketched in form of a flowchart.

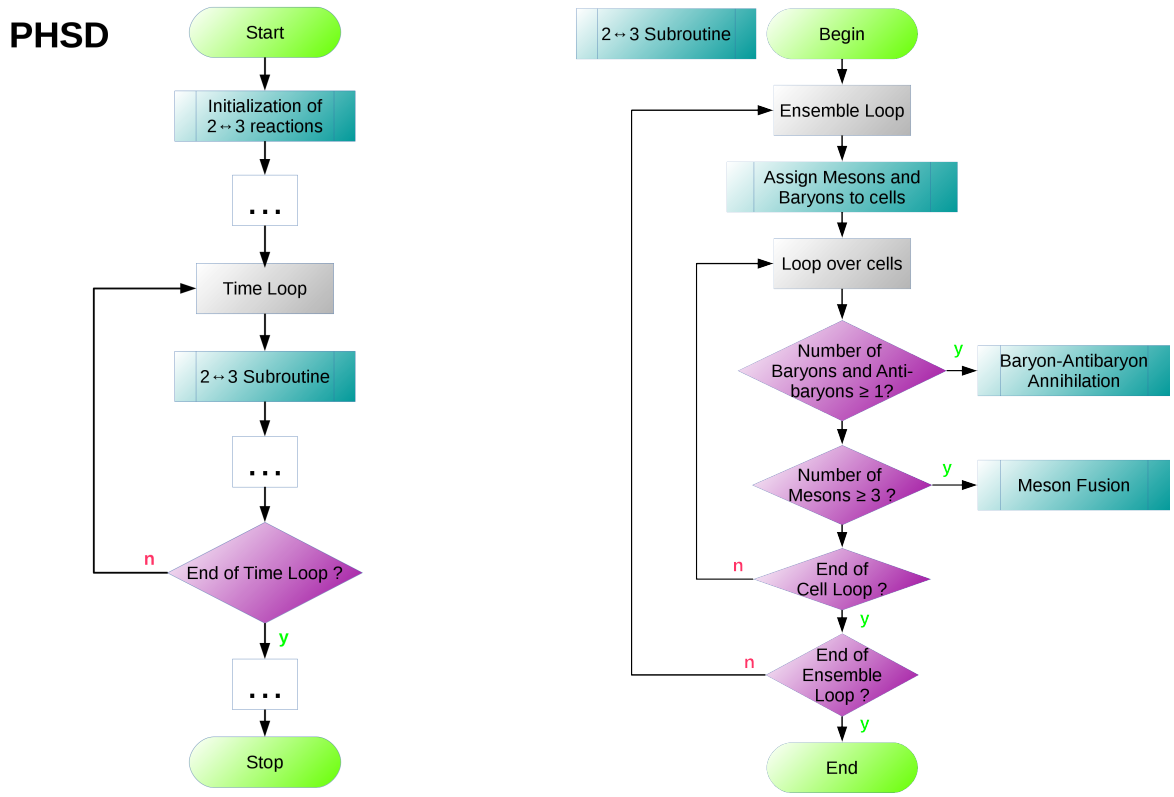

Fig. B.1 – Flowchart of the numerical implementation of the $B\bar{B} \leftrightarrow 3M$ reactions.

Appendix C

Additional box simulations

C.1 In-cell method: cell-size dependence

We here show the stability of our implementation with respect to the equilibrium state when changing the size of the cells. For this investigation we keep the time step dt

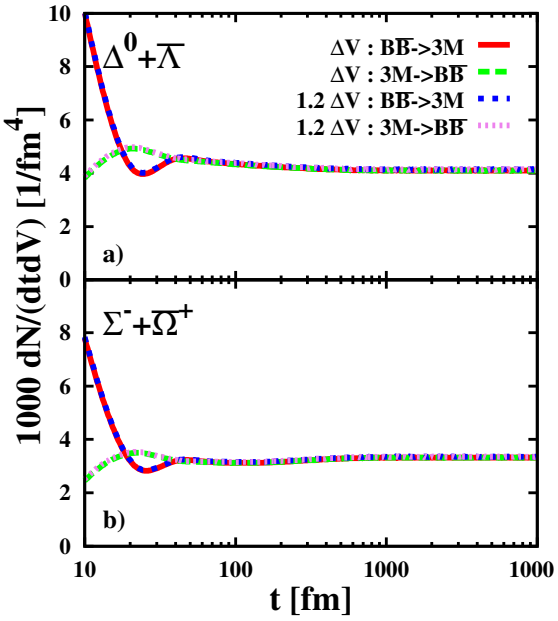

Fig. C.1 – Concistency check for a change in the cell size ΔV by 20%. a) for $\Delta^0 + \bar{\Lambda}$ and b) for $\Sigma^- + \bar{\Omega}^+$ initalizations. The red solid line shows the baryon-antibaryon annihilation for the cell volume ΔV, the green dashed line shows the baryon-antibaryon formation for ΔV, the blue short-dashed line shows the baryon-antibaryon annihilation for $1.2\Delta V$ and the violet dotted line shows the baryon-antibaryon formation for $1.2\Delta V$.

constant but enhance the cell volume ΔV by 20% and compare the reaction rate as a

function of time to the default calculations in Fig. C.1. We observe that the change in the cell size does not have any impact on the equilibration at all. For all times both cell sizes produce the same results giving testimony for the stability of the numerical implementation.

C.2 In-cell method versus next-neighbor interaction

The in-cell method used for the description of the $B\bar{B} \leftrightarrow 3M$ reactions has been implemented cutting effectively the space-time into cells of cell-size $\Delta V \times \Delta t$ and letting only particles of the same cell interact with each other. Another possibility for the implementation of the baryon-antibaryon annihilation (and recreation) is by defining the volume ΔV by a sphere around the first particle and letting all particles in the sphere interact with each other; this implementation we denote by next-neighbor (NN) algorithm in the following. In Fig. C.2 we compare the results of these two choices. Due to the large finite size effects for the NN method the volume of the box had to be enhanced and filled with the same density of hadrons as the standard box but letting only the particles inside the standard box volume be the particles from whose sphere the partners are selected in

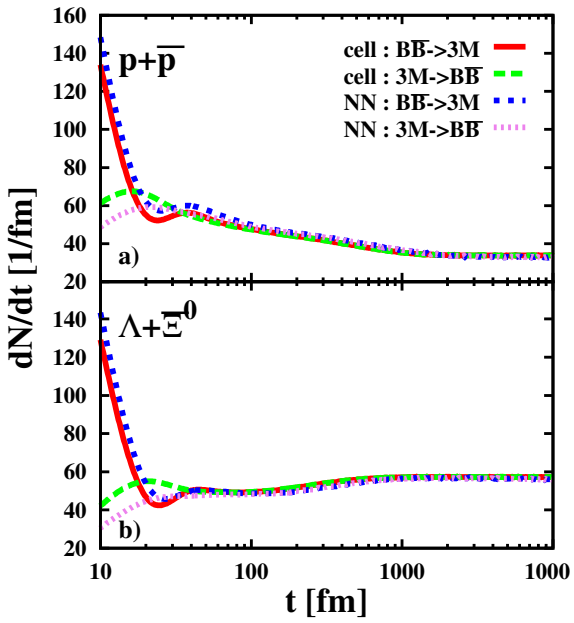

Fig. C.2 – Comparison of the reaction rates between the cell algorithm (cell) and the next-neighbor (NN) realization of the in-cell method. The systems shown are in a) the $p+\bar{p}$ and in b) the $\Lambda+\bar{\Xi}^0$ initialization. The red solid line shows the baryon-antibaryon annihilation for the cell method, the green dashed line shows the baryon-antibaryon formation for the cell method, the blue short-dashed line shows the baryon-antibaryon annihilation for the NN method and the violet dotted line shows the baryon-antibaryon formation for the NN method.

order to avoid surface effects from the finite volume incorporated. After employing this minimization of finite size effects we find that both methods give the same reaction rates for times larger than ≈30 fm. A small deviation between both methods is seen for smaller times. As expected one might use in general also the NN method. The disadvantage of the numerical implementation of the NN method is the larger computational time in comparison to the discretization of space-time. Thus PHSD uses the in-cell method not for the individual cells from the NN method but for the fixed cells of the space-time discretization.

C.3 Strangeness suppression

A further point to discuss in our model is whether to use the sum or the difference of the number of strange and anti-strange quarks in Eq. (3.13) for the strangeness suppression in case of $\lambda < 1$. Fig. C.3 illustrates the deviation between the two suppression models for the total reaction rate in case of $\lambda = 0.5$. For the system consisting initially only of light quarks, $p + \bar{p}$, we see no sizeable differences between the sum and the difference of strange and anti-strange quarks in Eq. (3.13). The system with an initial large difference

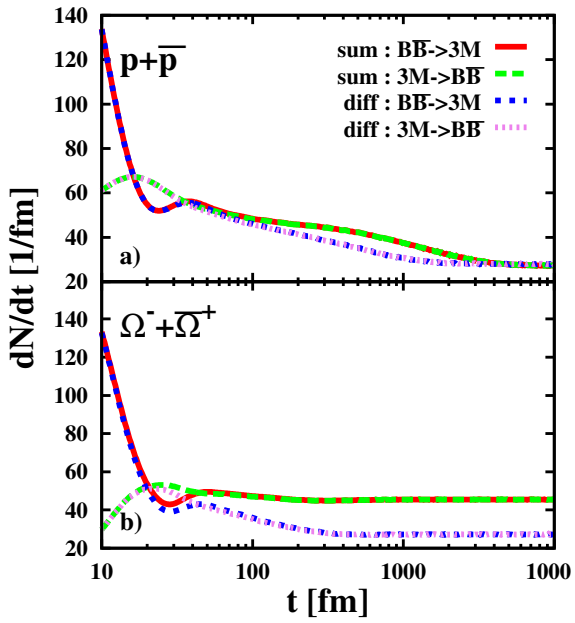

Fig. C.3 – Comparison of the reaction rate between the sum and the difference of the strange and antistrange quarks in the calculation of transition probabilities in $B\bar{B} \leftrightarrow 3M$ reactions (denoted by sum and diff). a) shows the $p + \bar{p}$ and b) the $\Omega^- + \bar{\Omega}^+$ initialization. The red solid line shows the baryon-antibaryon annihilation of the sum, the green dashed line shows the baryon-antibaryon formation of the sum, the blue short-dashed line shows the baryon-antibaryon annihilation of the difference and the violet dotted line shows the baryon-antibaryon formation of the difference.

between the number of strange and anti-strange quarks, $\Omega^- + \bar{\Omega}^+$, converges to rather different equilibrium states for the two assumptions. The suppression with the sum leads to an overall larger total reaction rate and its equilibrium value is twice as large as the suppression with the difference assumption. However, both models produce rather similar results for times $t < 50\,\mathrm{fm}$, which are of relevance for the heavy-ion collisions considered in this work. Accordingly we use in PHSD the suppression with the sum of the number of strange and anti-strange quarks since both models give practically identical results in PHSD simulations of relativistic heavy-ion reactions. We recall that for RHIC and LHC energies we use $\lambda = 1$ and thus have no ambiguity.

Appendix D

Channel list

On the following pages a list of all possible $B\bar{B} \leftrightarrow 3M$ mass channels is presented that conserve the quark numbers and parity and are incorporated in PHSD transport calculations.

Ch. No.	$B_1 + B_2$	$\leftrightarrow$	$M_1+M_2+M_3$
1	$N + \bar{N}$	$\leftrightarrow$	$\pi + \pi + \pi$
2	$N + \bar{N}$	$\leftrightarrow$	$\pi + \pi + \eta$
3	$N + \bar{N}$	$\leftrightarrow$	$\pi + \pi + \rho$
4	$N + \bar{N}$	$\leftrightarrow$	$\pi + \pi + \omega$
5	$N + \bar{N}$	$\leftrightarrow$	$\pi + \pi + \phi$
6	$N + \bar{N}$	$\leftrightarrow$	$\pi + \pi + \eta'$
7	$N + \bar{N}$	$\leftrightarrow$	$\pi + \eta + \eta$
8	$N + \bar{N}$	$\leftrightarrow$	$\pi + \eta + \rho$
9	$N + \bar{N}$	$\leftrightarrow$	$\pi + \eta + \omega$
10	$N + \bar{N}$	$\leftrightarrow$	$\pi + \eta + \phi$
11	$N + \bar{N}$	$\leftrightarrow$	$\pi + \eta + \eta'$
12	$N + \bar{N}$	$\leftrightarrow$	$\pi + \rho + \rho$
13	$N + \bar{N}$	$\leftrightarrow$	$\pi + \rho + \omega$
14	$N + \bar{N}$	$\leftrightarrow$	$\pi + \rho + \phi$
15	$N + \bar{N}$	$\leftrightarrow$	$\pi + \rho + \eta'$
16	$N + \bar{N}$	$\leftrightarrow$	$\pi + \omega + \omega$
17	$N + \bar{N}$	$\leftrightarrow$	$\pi + \omega + \phi$
18	$N + \bar{N}$	$\leftrightarrow$	$\pi + \omega + \eta'$
19	$N + \bar{N}$	$\leftrightarrow$	$\pi + \phi + \phi$
20	$N + \bar{N}$	$\leftrightarrow$	$\pi + \phi + \eta'$
21	$N + \bar{N}$	$\leftrightarrow$	$\pi + \eta' + \eta'$
22	$N + \bar{N}$	$\leftrightarrow$	$\pi + a_1 + a_1$
23	$N + \bar{N}$	$\leftrightarrow$	$\eta + \eta + \eta$
24	$N + \bar{N}$	$\leftrightarrow$	$\eta + \eta + \rho$
25	$N + \bar{N}$	$\leftrightarrow$	$\eta + \eta + \omega$
26	$N + \bar{N}$	$\leftrightarrow$	$\eta + \eta + \phi$
27	$N + \bar{N}$	$\leftrightarrow$	$\eta + \eta + \eta'$
28	$N + \bar{N}$	$\leftrightarrow$	$\eta + \rho + \rho$
29	$N + \bar{N}$	$\leftrightarrow$	$\eta + \rho + \omega$
30	$N + \bar{N}$	$\leftrightarrow$	$\eta + \rho + \phi$
31	$N + \bar{N}$	$\leftrightarrow$	$\eta + \rho + \eta'$
32	$N + \bar{N}$	$\leftrightarrow$	$\eta + \omega + \omega$
33	$N + \bar{N}$	$\leftrightarrow$	$\eta + \omega + \phi$
34	$N + \bar{N}$	$\leftrightarrow$	$\eta + \omega + \eta'$
35	$N + \bar{N}$	$\leftrightarrow$	$\eta + \phi + \phi$
36	$N + \bar{N}$	$\leftrightarrow$	$\eta + \phi + \eta'$
37	$N + \bar{N}$	$\leftrightarrow$	$\eta + \eta' + \eta'$
38	$N + \bar{N}$	$\leftrightarrow$	$\eta + a_1 + a_1$
39	$N + \bar{N}$	$\leftrightarrow$	$\rho + \rho + \rho$
40	$N + \bar{N}$	$\leftrightarrow$	$\rho + \rho + \omega$
41	$N + \bar{N}$	$\leftrightarrow$	$\rho + \rho + \phi$
42	$N + \bar{N}$	$\leftrightarrow$	$\rho + \rho + \eta'$
43	$N + \bar{N}$	$\leftrightarrow$	$\rho + \omega + \omega$
44	$N + \bar{N}$	$\leftrightarrow$	$\rho + \omega + \phi$
45	$N + \bar{N}$	$\leftrightarrow$	$\rho + \omega + \eta'$
46	$N + \bar{N}$	$\leftrightarrow$	$\rho + \phi + \phi$
47	$N + \bar{N}$	$\leftrightarrow$	$\rho + \phi + \eta'$
48	$N + \bar{N}$	$\leftrightarrow$	$\rho + \eta' + \eta'$
49	$N + \bar{N}$	$\leftrightarrow$	$\rho + a_1 + a_1$
50	$N + \bar{N}$	$\leftrightarrow$	$\omega + \omega + \omega$
51	$N + \bar{N}$	$\leftrightarrow$	$\omega + \omega + \phi$
52	$N + \bar{N}$	$\leftrightarrow$	$\omega + \omega + \eta'$
53	$N + \bar{N}$	$\leftrightarrow$	$\omega + \phi + \phi$

Ch. No.	$B_1 + B_2$	$\leftrightarrow$	$M_1+M_2+M_3$
54	$N + \bar{N}$	$\leftrightarrow$	$\omega + \phi + \eta'$
55	$N + \bar{N}$	$\leftrightarrow$	$\omega + \eta' + \eta'$
56	$N + \bar{N}$	$\leftrightarrow$	$\omega + a_1 + a_1$
57	$N + \bar{N}$	$\leftrightarrow$	$\phi + \phi + \phi$
58	$N + \bar{N}$	$\leftrightarrow$	$\phi + \phi + \eta'$
59	$N + \bar{N}$	$\leftrightarrow$	$\phi + \eta' + \eta'$
60	$N + \bar{N}$	$\leftrightarrow$	$\phi + a_1 + a_1$
61	$N + \bar{N}$	$\leftrightarrow$	$\eta' + \eta' + \eta'$
62	$N + \bar{N}$	$\leftrightarrow$	$\eta' + a_1 + a_1$
63	$N + \bar{\Delta}(1232)$	$\leftrightarrow$	$\pi + \pi + \pi$
64	$N + \bar{\Delta}(1232)$	$\leftrightarrow$	$\pi + \pi + \eta$
65	$N + \bar{\Delta}(1232)$	$\leftrightarrow$	$\pi + \pi + \rho$
66	$N + \bar{\Delta}(1232)$	$\leftrightarrow$	$\pi + \pi + \omega$
67	$N + \bar{\Delta}(1232)$	$\leftrightarrow$	$\pi + \pi + \phi$
68	$N + \bar{\Delta}(1232)$	$\leftrightarrow$	$\pi + \pi + \eta'$
69	$N + \bar{\Delta}(1232)$	$\leftrightarrow$	$\pi + \eta + \eta$
70	$N + \bar{\Delta}(1232)$	$\leftrightarrow$	$\pi + \eta + \rho$
71	$N + \bar{\Delta}(1232)$	$\leftrightarrow$	$\pi + \eta + \omega$
72	$N + \bar{\Delta}(1232)$	$\leftrightarrow$	$\pi + \eta + \phi$
73	$N + \bar{\Delta}(1232)$	$\leftrightarrow$	$\pi + \eta + \eta'$
74	$N + \bar{\Delta}(1232)$	$\leftrightarrow$	$\pi + \rho + \rho$
75	$N + \bar{\Delta}(1232)$	$\leftrightarrow$	$\pi + \rho + \omega$
76	$N + \bar{\Delta}(1232)$	$\leftrightarrow$	$\pi + \rho + \phi$
77	$N + \bar{\Delta}(1232)$	$\leftrightarrow$	$\pi + \rho + \eta'$
78	$N + \bar{\Delta}(1232)$	$\leftrightarrow$	$\pi + \omega + \omega$
79	$N + \bar{\Delta}(1232)$	$\leftrightarrow$	$\pi + \omega + \phi$
80	$N + \bar{\Delta}(1232)$	$\leftrightarrow$	$\pi + \omega + \eta'$
81	$N + \bar{\Delta}(1232)$	$\leftrightarrow$	$\pi + \phi + \phi$
82	$N + \bar{\Delta}(1232)$	$\leftrightarrow$	$\pi + \phi + \eta'$
83	$N + \bar{\Delta}(1232)$	$\leftrightarrow$	$\pi + \eta' + \eta'$
84	$N + \bar{\Delta}(1232)$	$\leftrightarrow$	$\pi + a_1 + a_1$
85	$N + \bar{\Delta}(1232)$	$\leftrightarrow$	$\eta + \eta + \eta$
86	$N + \bar{\Delta}(1232)$	$\leftrightarrow$	$\eta + \eta + \rho$
87	$N + \bar{\Delta}(1232)$	$\leftrightarrow$	$\eta + \eta + \omega$
88	$N + \bar{\Delta}(1232)$	$\leftrightarrow$	$\eta + \eta + \phi$
89	$N + \bar{\Delta}(1232)$	$\leftrightarrow$	$\eta + \eta + \eta'$
90	$N + \bar{\Delta}(1232)$	$\leftrightarrow$	$\eta + \rho + \rho$
91	$N + \bar{\Delta}(1232)$	$\leftrightarrow$	$\eta + \rho + \omega$
92	$N + \bar{\Delta}(1232)$	$\leftrightarrow$	$\eta + \rho + \phi$
93	$N + \bar{\Delta}(1232)$	$\leftrightarrow$	$\eta + \rho + \eta'$
94	$N + \bar{\Delta}(1232)$	$\leftrightarrow$	$\eta + \omega + \omega$
95	$N + \bar{\Delta}(1232)$	$\leftrightarrow$	$\eta + \omega + \phi$
96	$N + \bar{\Delta}(1232)$	$\leftrightarrow$	$\eta + \omega + \eta'$
97	$N + \bar{\Delta}(1232)$	$\leftrightarrow$	$\eta + \phi + \phi$
98	$N + \bar{\Delta}(1232)$	$\leftrightarrow$	$\eta + \phi + \eta'$
99	$N + \bar{\Delta}(1232)$	$\leftrightarrow$	$\eta + \eta' + \eta'$
100	$N + \bar{\Delta}(1232)$	$\leftrightarrow$	$\eta + a_1 + a_1$
101	$N + \bar{\Delta}(1232)$	$\leftrightarrow$	$\rho + \rho + \rho$
102	$N + \bar{\Delta}(1232)$	$\leftrightarrow$	$\rho + \rho + \omega$
103	$N + \bar{\Delta}(1232)$	$\leftrightarrow$	$\rho + \rho + \phi$
104	$N + \bar{\Delta}(1232)$	$\leftrightarrow$	$\rho + \rho + \eta'$
105	$N + \bar{\Delta}(1232)$	$\leftrightarrow$	$\rho + \omega + \omega$
106	$N + \bar{\Delta}(1232)$	$\leftrightarrow$	$\rho + \omega + \phi$

Ch. No.	$B_1 + B_2$	$\leftrightarrow$	$M_1+M_2+M_3$
107	$N + \bar{\Delta}(1232)$	$\leftrightarrow$	$\rho + \omega + \eta'$
108	$N + \bar{\Delta}(1232)$	$\leftrightarrow$	$\rho + \phi + \phi$
109	$N + \bar{\Delta}(1232)$	$\leftrightarrow$	$\rho + \phi + \eta'$
110	$N + \bar{\Delta}(1232)$	$\leftrightarrow$	$\rho + \eta' + \eta'$
111	$N + \bar{\Delta}(1232)$	$\leftrightarrow$	$\rho + a_1 + a_1$
112	$N + \bar{\Delta}(1232)$	$\leftrightarrow$	$\omega + \omega + \omega$
113	$N + \bar{\Delta}(1232)$	$\leftrightarrow$	$\omega + \omega + \phi$
114	$N + \bar{\Delta}(1232)$	$\leftrightarrow$	$\omega + \omega + \eta'$
115	$N + \bar{\Delta}(1232)$	$\leftrightarrow$	$\omega + \phi + \phi$
116	$N + \bar{\Delta}(1232)$	$\leftrightarrow$	$\omega + \phi + \eta'$
117	$N + \bar{\Delta}(1232)$	$\leftrightarrow$	$\omega + \eta' + \eta'$
118	$N + \bar{\Delta}(1232)$	$\leftrightarrow$	$\omega + a_1 + a_1$
119	$N + \bar{\Delta}(1232)$	$\leftrightarrow$	$\phi + \phi + \phi$
120	$N + \bar{\Delta}(1232)$	$\leftrightarrow$	$\phi + \phi + \eta'$
121	$N + \bar{\Delta}(1232)$	$\leftrightarrow$	$\phi + \eta' + \eta'$
122	$N + \bar{\Delta}(1232)$	$\leftrightarrow$	$\phi + a_1 + a_1$
123	$N + \bar{\Delta}(1232)$	$\leftrightarrow$	$\eta' + \eta' + \eta'$
124	$N + \bar{\Delta}(1232)$	$\leftrightarrow$	$\eta' + a_1 + a_1$
125	$N + \bar{N}(1440)$	$\leftrightarrow$	$\pi + \pi + \pi$
126	$N + \bar{N}(1440)$	$\leftrightarrow$	$\pi + \pi + \eta$
127	$N + \bar{N}(1440)$	$\leftrightarrow$	$\pi + \pi + \rho$
128	$N + \bar{N}(1440)$	$\leftrightarrow$	$\pi + \pi + \omega$
129	$N + \bar{N}(1440)$	$\leftrightarrow$	$\pi + \pi + \phi$
130	$N + \bar{N}(1440)$	$\leftrightarrow$	$\pi + \pi + \eta'$
131	$N + \bar{N}(1440)$	$\leftrightarrow$	$\pi + \eta + \eta$
132	$N + \bar{N}(1440)$	$\leftrightarrow$	$\pi + \eta + \rho$
133	$N + \bar{N}(1440)$	$\leftrightarrow$	$\pi + \eta + \omega$
134	$N + \bar{N}(1440)$	$\leftrightarrow$	$\pi + \eta + \phi$
135	$N + \bar{N}(1440)$	$\leftrightarrow$	$\pi + \eta + \eta'$
136	$N + \bar{N}(1440)$	$\leftrightarrow$	$\pi + \rho + \rho$
137	$N + \bar{N}(1440)$	$\leftrightarrow$	$\pi + \rho + \omega$
138	$N + \bar{N}(1440)$	$\leftrightarrow$	$\pi + \rho + \phi$
139	$N + \bar{N}(1440)$	$\leftrightarrow$	$\pi + \rho + \eta'$
140	$N + \bar{N}(1440)$	$\leftrightarrow$	$\pi + \omega + \omega$
141	$N + \bar{N}(1440)$	$\leftrightarrow$	$\pi + \omega + \phi$
142	$N + \bar{N}(1440)$	$\leftrightarrow$	$\pi + \omega + \eta'$
143	$N + \bar{N}(1440)$	$\leftrightarrow$	$\pi + \phi + \phi$
144	$N + \bar{N}(1440)$	$\leftrightarrow$	$\pi + \phi + \eta'$
145	$N + \bar{N}(1440)$	$\leftrightarrow$	$\pi + \eta' + \eta'$
146	$N + \bar{N}(1440)$	$\leftrightarrow$	$\pi + a_1 + a_1$
147	$N + \bar{N}(1440)$	$\leftrightarrow$	$\eta + \eta + \eta$
148	$N + \bar{N}(1440)$	$\leftrightarrow$	$\eta + \eta + \rho$
149	$N + \bar{N}(1440)$	$\leftrightarrow$	$\eta + \eta + \omega$
150	$N + \bar{N}(1440)$	$\leftrightarrow$	$\eta + \eta + \phi$
151	$N + \bar{N}(1440)$	$\leftrightarrow$	$\eta + \eta + \eta'$
152	$N + \bar{N}(1440)$	$\leftrightarrow$	$\eta + \rho + \rho$
153	$N + \bar{N}(1440)$	$\leftrightarrow$	$\eta + \rho + \omega$
154	$N + \bar{N}(1440)$	$\leftrightarrow$	$\eta + \rho + \phi$
155	$N + \bar{N}(1440)$	$\leftrightarrow$	$\eta + \rho + \eta'$
156	$N + \bar{N}(1440)$	$\leftrightarrow$	$\eta + \omega + \omega$
157	$N + \bar{N}(1440)$	$\leftrightarrow$	$\eta + \omega + \phi$
158	$N + \bar{N}(1440)$	$\leftrightarrow$	$\eta + \omega + \eta'$
159	$N + \bar{N}(1440)$	$\leftrightarrow$	$\eta + \phi + \phi$
160	$N + \bar{N}(1440)$	$\leftrightarrow$	$\eta + \phi + \eta'$
161	$N + \bar{N}(1440)$	$\leftrightarrow$	$\eta + \eta' + \eta'$
162	$N + \bar{N}(1440)$	$\leftrightarrow$	$\eta + a_1 + a_1$
163	$N + \bar{N}(1440)$	$\leftrightarrow$	$\rho + \rho + \rho$
164	$N + \bar{N}(1440)$	$\leftrightarrow$	$\rho + \rho + \omega$
165	$N + \bar{N}(1440)$	$\leftrightarrow$	$\rho + \rho + \phi$
166	$N + \bar{N}(1440)$	$\leftrightarrow$	$\rho + \rho + \eta'$
167	$N + \bar{N}(1440)$	$\leftrightarrow$	$\rho + \omega + \omega$
168	$N + \bar{N}(1440)$	$\leftrightarrow$	$\rho + \omega + \phi$
169	$N + \bar{N}(1440)$	$\leftrightarrow$	$\rho + \omega + \eta'$
170	$N + \bar{N}(1440)$	$\leftrightarrow$	$\rho + \phi + \phi$
171	$N + \bar{N}(1440)$	$\leftrightarrow$	$\rho + \phi + \eta'$
172	$N + \bar{N}(1440)$	$\leftrightarrow$	$\rho + \eta' + \eta'$
173	$N + \bar{N}(1440)$	$\leftrightarrow$	$\rho + a_1 + a_1$
174	$N + \bar{N}(1440)$	$\leftrightarrow$	$\omega + \omega + \omega$
175	$N + \bar{N}(1440)$	$\leftrightarrow$	$\omega + \omega + \phi$
176	$N + \bar{N}(1440)$	$\leftrightarrow$	$\omega + \omega + \eta'$
177	$N + \bar{N}(1440)$	$\leftrightarrow$	$\omega + \phi + \phi$
178	$N + \bar{N}(1440)$	$\leftrightarrow$	$\omega + \phi + \eta'$
179	$N + \bar{N}(1440)$	$\leftrightarrow$	$\omega + \eta' + \eta'$
180	$N + \bar{N}(1440)$	$\leftrightarrow$	$\omega + a_1 + a_1$
181	$N + \bar{N}(1440)$	$\leftrightarrow$	$\phi + \phi + \phi$
182	$N + \bar{N}(1440)$	$\leftrightarrow$	$\phi + \phi + \eta'$
183	$N + \bar{N}(1440)$	$\leftrightarrow$	$\phi + \eta' + \eta'$
184	$N + \bar{N}(1440)$	$\leftrightarrow$	$\phi + a_1 + a_1$
185	$N + \bar{N}(1440)$	$\leftrightarrow$	$\eta' + \eta' + \eta'$
186	$N + \bar{N}(1440)$	$\leftrightarrow$	$\eta' + a_1 + a_1$
187	$N + \bar{N}(1535)$	$\leftrightarrow$	$\pi + \pi + a_1$
188	$N + \bar{N}(1535)$	$\leftrightarrow$	$\pi + \eta + a_1$
189	$N + \bar{N}(1535)$	$\leftrightarrow$	$\pi + \rho + a_1$
190	$N + \bar{N}(1535)$	$\leftrightarrow$	$\pi + \omega + a_1$
191	$N + \bar{N}(1535)$	$\leftrightarrow$	$\pi + \phi + a_1$
192	$N + \bar{N}(1535)$	$\leftrightarrow$	$\pi + \eta' + a_1$

Ch. No.	$B_1 + B_2$	$\leftrightarrow$	$M_1+M_2+M_3$
193	$N + \bar{N}(1535)$	$\leftrightarrow$	$\eta + \eta + a_1$
194	$N + \bar{N}(1535)$	$\leftrightarrow$	$\eta + \rho + a_1$
195	$N + \bar{N}(1535)$	$\leftrightarrow$	$\eta + \omega + a_1$
196	$N + \bar{N}(1535)$	$\leftrightarrow$	$\eta + \phi + a_1$
197	$N + \bar{N}(1535)$	$\leftrightarrow$	$\eta + \eta' + a_1$
198	$N + \bar{N}(1535)$	$\leftrightarrow$	$\rho + \rho + a_1$
199	$N + \bar{N}(1535)$	$\leftrightarrow$	$\rho + \omega + a_1$
200	$N + \bar{N}(1535)$	$\leftrightarrow$	$\rho + \phi + a_1$
201	$N + \bar{N}(1535)$	$\leftrightarrow$	$\rho + \eta' + a_1$
202	$N + \bar{N}(1535)$	$\leftrightarrow$	$\omega + \omega + a_1$
203	$N + \bar{N}(1535)$	$\leftrightarrow$	$\omega + \phi + a_1$
204	$N + \bar{N}(1535)$	$\leftrightarrow$	$\omega + \eta' + a_1$
205	$N + \bar{N}(1535)$	$\leftrightarrow$	$\phi + \phi + a_1$
206	$N + \bar{N}(1535)$	$\leftrightarrow$	$\phi + \eta' + a_1$
207	$N + \bar{N}(1535)$	$\leftrightarrow$	$\eta' + \eta' + a_1$
208	$N + \bar{N}(1535)$	$\leftrightarrow$	$a_1 + a_1 + a_1$
209	$N + \bar{\Lambda}$	$\leftrightarrow$	$\pi + \pi + K$
210	$N + \bar{\Lambda}$	$\leftrightarrow$	$\pi + \pi + K^*$
211	$N + \bar{\Lambda}$	$\leftrightarrow$	$\pi + \eta + K$
212	$N + \bar{\Lambda}$	$\leftrightarrow$	$\pi + \eta + K^*$
213	$N + \bar{\Lambda}$	$\leftrightarrow$	$\pi + K + \rho$
214	$N + \bar{\Lambda}$	$\leftrightarrow$	$\pi + K + \omega$
215	$N + \bar{\Lambda}$	$\leftrightarrow$	$\pi + K + \phi$
216	$N + \bar{\Lambda}$	$\leftrightarrow$	$\pi + K + \eta'$
217	$N + \bar{\Lambda}$	$\leftrightarrow$	$\pi + K^* + \rho$
218	$N + \bar{\Lambda}$	$\leftrightarrow$	$\pi + K^* + \omega$
219	$N + \bar{\Lambda}$	$\leftrightarrow$	$\pi + K^* + \phi$
220	$N + \bar{\Lambda}$	$\leftrightarrow$	$\pi + K^* + \eta'$
221	$N + \bar{\Lambda}$	$\leftrightarrow$	$\eta + \eta + K$
222	$N + \bar{\Lambda}$	$\leftrightarrow$	$\eta + \eta + K^*$
223	$N + \bar{\Lambda}$	$\leftrightarrow$	$\eta + K + \rho$
224	$N + \bar{\Lambda}$	$\leftrightarrow$	$\eta + K + \omega$
225	$N + \bar{\Lambda}$	$\leftrightarrow$	$\eta + K + \phi$
226	$N + \bar{\Lambda}$	$\leftrightarrow$	$\eta + K + \eta'$
227	$N + \bar{\Lambda}$	$\leftrightarrow$	$\eta + K^* + \rho$
228	$N + \bar{\Lambda}$	$\leftrightarrow$	$\eta + K^* + \omega$
229	$N + \bar{\Lambda}$	$\leftrightarrow$	$\eta + K^* + \phi$
230	$N + \bar{\Lambda}$	$\leftrightarrow$	$\eta + K^* + \eta'$
231	$N + \bar{\Lambda}$	$\leftrightarrow$	$K + \rho + \rho$
232	$N + \bar{\Lambda}$	$\leftrightarrow$	$K + \rho + \omega$
233	$N + \bar{\Lambda}$	$\leftrightarrow$	$K + \rho + \phi$
234	$N + \bar{\Lambda}$	$\leftrightarrow$	$K + \rho + \eta'$
235	$N + \bar{\Lambda}$	$\leftrightarrow$	$K + \omega + \omega$
236	$N + \bar{\Lambda}$	$\leftrightarrow$	$K + \omega + \phi$
237	$N + \bar{\Lambda}$	$\leftrightarrow$	$K + \omega + \eta'$
238	$N + \bar{\Lambda}$	$\leftrightarrow$	$K + \phi + \phi$
239	$N + \bar{\Lambda}$	$\leftrightarrow$	$K + \phi + \eta'$
240	$N + \bar{\Lambda}$	$\leftrightarrow$	$K + \eta' + \eta'$
241	$N + \bar{\Lambda}$	$\leftrightarrow$	$K + a_1 + a_1$
242	$N + \bar{\Lambda}$	$\leftrightarrow$	$K^* + \rho + \rho$
243	$N + \bar{\Lambda}$	$\leftrightarrow$	$K^* + \rho + \omega$
244	$N + \bar{\Lambda}$	$\leftrightarrow$	$K^* + \rho + \phi$
245	$N + \bar{\Lambda}$	$\leftrightarrow$	$K^* + \rho + \eta'$
246	$N + \bar{\Lambda}$	$\leftrightarrow$	$K^* + \omega + \omega$
247	$N + \bar{\Lambda}$	$\leftrightarrow$	$K^* + \omega + \phi$
248	$N + \bar{\Lambda}$	$\leftrightarrow$	$K^* + \omega + \eta'$
249	$N + \bar{\Lambda}$	$\leftrightarrow$	$K^* + \phi + \phi$
250	$N + \bar{\Lambda}$	$\leftrightarrow$	$K^* + \phi + \eta'$
251	$N + \bar{\Lambda}$	$\leftrightarrow$	$K^* + \eta' + \eta'$
252	$N + \bar{\Lambda}$	$\leftrightarrow$	$K^* + a_1 + a_1$
253	$N + \bar{\Sigma}$	$\leftrightarrow$	$\pi + \pi + K$
254	$N + \bar{\Sigma}$	$\leftrightarrow$	$\pi + \pi + K^*$
255	$N + \bar{\Sigma}$	$\leftrightarrow$	$\pi + \eta + K$
256	$N + \bar{\Sigma}$	$\leftrightarrow$	$\pi + \eta + K^*$
257	$N + \bar{\Sigma}$	$\leftrightarrow$	$\pi + K + \rho$
258	$N + \bar{\Sigma}$	$\leftrightarrow$	$\pi + K + \omega$
259	$N + \bar{\Sigma}$	$\leftrightarrow$	$\pi + K + \phi$
260	$N + \bar{\Sigma}$	$\leftrightarrow$	$\pi + K + \eta'$
261	$N + \bar{\Sigma}$	$\leftrightarrow$	$\pi + K^* + \rho$
262	$N + \bar{\Sigma}$	$\leftrightarrow$	$\pi + K^* + \omega$
263	$N + \bar{\Sigma}$	$\leftrightarrow$	$\pi + K^* + \phi$
264	$N + \bar{\Sigma}$	$\leftrightarrow$	$\pi + K^* + \eta'$
265	$N + \bar{\Sigma}$	$\leftrightarrow$	$\eta + \eta + K$
266	$N + \bar{\Sigma}$	$\leftrightarrow$	$\eta + \eta + K^*$
267	$N + \bar{\Sigma}$	$\leftrightarrow$	$\eta + K + \rho$
268	$N + \bar{\Sigma}$	$\leftrightarrow$	$\eta + K + \omega$
269	$N + \bar{\Sigma}$	$\leftrightarrow$	$\eta + K + \phi$
270	$N + \bar{\Sigma}$	$\leftrightarrow$	$\eta + K + \eta'$
271	$N + \bar{\Sigma}$	$\leftrightarrow$	$\eta + K^* + \rho$
272	$N + \bar{\Sigma}$	$\leftrightarrow$	$\eta + K^* + \omega$
273	$N + \bar{\Sigma}$	$\leftrightarrow$	$\eta + K^* + \phi$
274	$N + \bar{\Sigma}$	$\leftrightarrow$	$\eta + K^* + \eta'$
275	$N + \bar{\Sigma}$	$\leftrightarrow$	$K + \rho + \rho$
276	$N + \bar{\Sigma}$	$\leftrightarrow$	$K + \rho + \omega$
277	$N + \bar{\Sigma}$	$\leftrightarrow$	$K + \rho + \phi$
278	$N + \bar{\Sigma}$	$\leftrightarrow$	$K + \rho + \eta'$

Ch. No.	$B_1 + B_2$	$\leftrightarrow$	$M_1+M_2+M_3$
279	$N + \bar{\Sigma}$	$\leftrightarrow$	$K + \omega + \omega$
280	$N + \bar{\Sigma}$	$\leftrightarrow$	$K + \omega + \phi$
281	$N + \bar{\Sigma}$	$\leftrightarrow$	$K + \omega + \eta'$
282	$N + \bar{\Sigma}$	$\leftrightarrow$	$K + \phi + \phi$
283	$N + \bar{\Sigma}$	$\leftrightarrow$	$K + \phi + \eta'$
284	$N + \bar{\Sigma}$	$\leftrightarrow$	$K + \eta' + \eta'$
285	$N + \bar{\Sigma}$	$\leftrightarrow$	$K + a_1 + a_1$
286	$N + \bar{\Sigma}$	$\leftrightarrow$	$K^* + \rho + \rho$
287	$N + \bar{\Sigma}$	$\leftrightarrow$	$K^* + \rho + \omega$
288	$N + \bar{\Sigma}$	$\leftrightarrow$	$K^* + \rho + \phi$
289	$N + \bar{\Sigma}$	$\leftrightarrow$	$K^* + \rho + \eta'$
290	$N + \bar{\Sigma}$	$\leftrightarrow$	$K^* + \omega + \omega$
291	$N + \bar{\Sigma}$	$\leftrightarrow$	$K^* + \omega + \phi$
292	$N + \bar{\Sigma}$	$\leftrightarrow$	$K^* + \omega + \eta'$
293	$N + \bar{\Sigma}$	$\leftrightarrow$	$K^* + \phi + \phi$
294	$N + \bar{\Sigma}$	$\leftrightarrow$	$K^* + \phi + \eta'$
295	$N + \bar{\Sigma}$	$\leftrightarrow$	$K^* + \eta' + \eta'$
296	$N + \bar{\Sigma}$	$\leftrightarrow$	$K^* + a_1 + a_1$
297	$N + \bar{\Sigma}^*$	$\leftrightarrow$	$\pi + \pi + K$
298	$N + \bar{\Sigma}^*$	$\leftrightarrow$	$\pi + \pi + K^*$
299	$N + \bar{\Sigma}^*$	$\leftrightarrow$	$\pi + \eta + K$
300	$N + \bar{\Sigma}^*$	$\leftrightarrow$	$\pi + \eta + K^*$
301	$N + \bar{\Sigma}^*$	$\leftrightarrow$	$\pi + K + \rho$
302	$N + \bar{\Sigma}^*$	$\leftrightarrow$	$\pi + K + \omega$
303	$N + \bar{\Sigma}^*$	$\leftrightarrow$	$\pi + K + \phi$
304	$N + \bar{\Sigma}^*$	$\leftrightarrow$	$\pi + K + \eta'$
305	$N + \bar{\Sigma}^*$	$\leftrightarrow$	$\pi + K^* + \rho$
306	$N + \bar{\Sigma}^*$	$\leftrightarrow$	$\pi + K^* + \omega$
307	$N + \bar{\Sigma}^*$	$\leftrightarrow$	$\pi + K^* + \phi$
308	$N + \bar{\Sigma}^*$	$\leftrightarrow$	$\pi + K^* + \eta'$
309	$N + \bar{\Sigma}^*$	$\leftrightarrow$	$\eta + \eta + K$
310	$N + \bar{\Sigma}^*$	$\leftrightarrow$	$\eta + \eta + K^*$
311	$N + \bar{\Sigma}^*$	$\leftrightarrow$	$\eta + K + \rho$
312	$N + \bar{\Sigma}^*$	$\leftrightarrow$	$\eta + K + \omega$
313	$N + \bar{\Sigma}^*$	$\leftrightarrow$	$\eta + K + \phi$
314	$N + \bar{\Sigma}^*$	$\leftrightarrow$	$\eta + K + \eta'$
315	$N + \bar{\Sigma}^*$	$\leftrightarrow$	$\eta + K^* + \rho$
316	$N + \bar{\Sigma}^*$	$\leftrightarrow$	$\eta + K^* + \omega$
317	$N + \bar{\Sigma}^*$	$\leftrightarrow$	$\eta + K^* + \phi$
318	$N + \bar{\Sigma}^*$	$\leftrightarrow$	$\eta + K^* + \eta'$
319	$N + \bar{\Sigma}^*$	$\leftrightarrow$	$K + \rho + \rho$
320	$N + \bar{\Sigma}^*$	$\leftrightarrow$	$K + \rho + \omega$
321	$N + \bar{\Sigma}^*$	$\leftrightarrow$	$K + \rho + \phi$
322	$N + \bar{\Sigma}^*$	$\leftrightarrow$	$K + \rho + \eta'$
323	$N + \bar{\Sigma}^*$	$\leftrightarrow$	$K + \omega + \omega$
324	$N + \bar{\Sigma}^*$	$\leftrightarrow$	$K + \omega + \phi$
325	$N + \bar{\Sigma}^*$	$\leftrightarrow$	$K + \omega + \eta'$
326	$N + \bar{\Sigma}^*$	$\leftrightarrow$	$K + \phi + \phi$
327	$N + \bar{\Sigma}^*$	$\leftrightarrow$	$K + \phi + \eta'$
328	$N + \bar{\Sigma}^*$	$\leftrightarrow$	$K + \eta' + \eta'$
329	$N + \bar{\Sigma}^*$	$\leftrightarrow$	$K + a_1 + a_1$
330	$N + \bar{\Sigma}^*$	$\leftrightarrow$	$K^* + \rho + \rho$
331	$N + \bar{\Sigma}^*$	$\leftrightarrow$	$K^* + \rho + \omega$
332	$N + \bar{\Sigma}^*$	$\leftrightarrow$	$K^* + \rho + \phi$
333	$N + \bar{\Sigma}^*$	$\leftrightarrow$	$K^* + \rho + \eta'$
334	$N + \bar{\Sigma}^*$	$\leftrightarrow$	$K^* + \omega + \omega$
335	$N + \bar{\Sigma}^*$	$\leftrightarrow$	$K^* + \omega + \phi$
336	$N + \bar{\Sigma}^*$	$\leftrightarrow$	$K^* + \omega + \eta'$
337	$N + \bar{\Sigma}^*$	$\leftrightarrow$	$K^* + \phi + \phi$
338	$N + \bar{\Sigma}^*$	$\leftrightarrow$	$K^* + \phi + \eta'$
339	$N + \bar{\Sigma}^*$	$\leftrightarrow$	$K^* + \eta' + \eta'$
340	$N + \bar{\Sigma}^*$	$\leftrightarrow$	$K^* + a_1 + a_1$
341	$N + \bar{\Xi}$	$\leftrightarrow$	$\pi + K + K$
342	$N + \bar{\Xi}$	$\leftrightarrow$	$\pi + K + K^*$
343	$N + \bar{\Xi}$	$\leftrightarrow$	$\pi + K^* + K^*$
344	$N + \bar{\Xi}$	$\leftrightarrow$	$\eta + K + K$
345	$N + \bar{\Xi}$	$\leftrightarrow$	$\eta + K + K^*$
346	$N + \bar{\Xi}$	$\leftrightarrow$	$\eta + K^* + K^*$
347	$N + \bar{\Xi}$	$\leftrightarrow$	$K + K + \rho$
348	$N + \bar{\Xi}$	$\leftrightarrow$	$K + K + \omega$
349	$N + \bar{\Xi}$	$\leftrightarrow$	$K + K + \phi$
350	$N + \bar{\Xi}$	$\leftrightarrow$	$K + K + \eta'$
351	$N + \bar{\Xi}$	$\leftrightarrow$	$K + K^* + \rho$
352	$N + \bar{\Xi}$	$\leftrightarrow$	$K + K^* + \omega$
353	$N + \bar{\Xi}$	$\leftrightarrow$	$K + K^* + \phi$
354	$N + \bar{\Xi}$	$\leftrightarrow$	$K + K^* + \eta'$
355	$N + \bar{\Xi}$	$\leftrightarrow$	$K^* + K^* + \rho$
356	$N + \bar{\Xi}$	$\leftrightarrow$	$K^* + K^* + \omega$
357	$N + \bar{\Xi}$	$\leftrightarrow$	$K^* + K^* + \phi$
358	$N + \bar{\Xi}$	$\leftrightarrow$	$K^* + K^* + \eta'$
359	$N + \bar{\Xi}^*$	$\leftrightarrow$	$\pi + K + K$
360	$N + \bar{\Xi}^*$	$\leftrightarrow$	$\pi + K + K^*$
361	$N + \bar{\Xi}^*$	$\leftrightarrow$	$\pi + K^* + K^*$
362	$N + \bar{\Xi}^*$	$\leftrightarrow$	$\eta + K + K$
363	$N + \bar{\Xi}^*$	$\leftrightarrow$	$\eta + K + K^*$
364	$N + \bar{\Xi}^*$	$\leftrightarrow$	$\eta + K^* + K^*$

Ch. No.	$B_1 + B_2$	$\leftrightarrow$	$M_1+M_2+M_3$
365	$N + \bar{\Xi}^*$	$\leftrightarrow$	$K + K + \rho$
366	$N + \bar{\Xi}^*$	$\leftrightarrow$	$K + K + \omega$
367	$N + \bar{\Xi}^*$	$\leftrightarrow$	$K + K + \phi$
368	$N + \bar{\Xi}^*$	$\leftrightarrow$	$K + K + \eta'$
369	$N + \bar{\Xi}^*$	$\leftrightarrow$	$K + K^* + \rho$
370	$N + \bar{\Xi}^*$	$\leftrightarrow$	$K + K^* + \omega$
371	$N + \bar{\Xi}^*$	$\leftrightarrow$	$K + K^* + \phi$
372	$N + \bar{\Xi}^*$	$\leftrightarrow$	$K + K^* + \eta'$
373	$N + \bar{\Xi}^*$	$\leftrightarrow$	$K^* + K^* + \rho$
374	$N + \bar{\Xi}^*$	$\leftrightarrow$	$K^* + K^* + \omega$
375	$N + \bar{\Xi}^*$	$\leftrightarrow$	$K^* + K^* + \phi$
376	$N + \bar{\Xi}^*$	$\leftrightarrow$	$K^* + K^* + \eta'$
377	$N + \bar{\Omega}$	$\leftrightarrow$	$K + K + K$
378	$N + \bar{\Omega}$	$\leftrightarrow$	$K + K + K^*$
379	$N + \bar{\Omega}$	$\leftrightarrow$	$K + K^* + K^*$
380	$N + \bar{\Omega}$	$\leftrightarrow$	$K^* + K^* + K^*$
381	$\Delta(1232) + \bar{N}$	$\leftrightarrow$	$\pi + \pi + \pi$
382	$\Delta(1232) + \bar{N}$	$\leftrightarrow$	$\pi + \pi + \eta$
383	$\Delta(1232) + \bar{N}$	$\leftrightarrow$	$\pi + \pi + \rho$
384	$\Delta(1232) + \bar{N}$	$\leftrightarrow$	$\pi + \pi + \omega$
385	$\Delta(1232) + \bar{N}$	$\leftrightarrow$	$\pi + \pi + \phi$
386	$\Delta(1232) + \bar{N}$	$\leftrightarrow$	$\pi + \pi + \eta'$
387	$\Delta(1232) + \bar{N}$	$\leftrightarrow$	$\pi + \eta + \eta$
388	$\Delta(1232) + \bar{N}$	$\leftrightarrow$	$\pi + \eta + \rho$
389	$\Delta(1232) + \bar{N}$	$\leftrightarrow$	$\pi + \eta + \omega$
390	$\Delta(1232) + \bar{N}$	$\leftrightarrow$	$\pi + \eta + \phi$
391	$\Delta(1232) + \bar{N}$	$\leftrightarrow$	$\pi + \eta + \eta'$
392	$\Delta(1232) + \bar{N}$	$\leftrightarrow$	$\pi + \rho + \rho$
393	$\Delta(1232) + \bar{N}$	$\leftrightarrow$	$\pi + \rho + \omega$
394	$\Delta(1232) + \bar{N}$	$\leftrightarrow$	$\pi + \rho + \phi$
395	$\Delta(1232) + \bar{N}$	$\leftrightarrow$	$\pi + \rho + \eta'$
396	$\Delta(1232) + \bar{N}$	$\leftrightarrow$	$\pi + \omega + \omega$
397	$\Delta(1232) + \bar{N}$	$\leftrightarrow$	$\pi + \omega + \phi$
398	$\Delta(1232) + \bar{N}$	$\leftrightarrow$	$\pi + \omega + \eta'$
399	$\Delta(1232) + \bar{N}$	$\leftrightarrow$	$\pi + \phi + \phi$
400	$\Delta(1232) + \bar{N}$	$\leftrightarrow$	$\pi + \phi + \eta'$
401	$\Delta(1232) + \bar{N}$	$\leftrightarrow$	$\pi + \eta' + \eta'$
402	$\Delta(1232) + \bar{N}$	$\leftrightarrow$	$\pi + a_1 + a_1$
403	$\Delta(1232) + \bar{N}$	$\leftrightarrow$	$\eta + \eta + \eta$
404	$\Delta(1232) + \bar{N}$	$\leftrightarrow$	$\eta + \eta + \rho$
405	$\Delta(1232) + \bar{N}$	$\leftrightarrow$	$\eta + \eta + \omega$
406	$\Delta(1232) + \bar{N}$	$\leftrightarrow$	$\eta + \eta + \phi$
407	$\Delta(1232) + \bar{N}$	$\leftrightarrow$	$\eta + \eta + \eta'$
408	$\Delta(1232) + \bar{N}$	$\leftrightarrow$	$\eta + \rho + \rho$
409	$\Delta(1232) + \bar{N}$	$\leftrightarrow$	$\eta + \rho + \omega$
410	$\Delta(1232) + \bar{N}$	$\leftrightarrow$	$\eta + \rho + \phi$
411	$\Delta(1232) + \bar{N}$	$\leftrightarrow$	$\eta + \rho + \eta'$
412	$\Delta(1232) + \bar{N}$	$\leftrightarrow$	$\eta + \omega + \omega$
413	$\Delta(1232) + \bar{N}$	$\leftrightarrow$	$\eta + \omega + \phi$
414	$\Delta(1232) + \bar{N}$	$\leftrightarrow$	$\eta + \omega + \eta'$
415	$\Delta(1232) + \bar{N}$	$\leftrightarrow$	$\eta + \phi + \phi$
416	$\Delta(1232) + \bar{N}$	$\leftrightarrow$	$\eta + \phi + \eta'$
417	$\Delta(1232) + \bar{N}$	$\leftrightarrow$	$\eta + \eta' + \eta'$
418	$\Delta(1232) + \bar{N}$	$\leftrightarrow$	$\eta + a_1 + a_1$
419	$\Delta(1232) + \bar{N}$	$\leftrightarrow$	$\rho + \rho + \rho$
420	$\Delta(1232) + \bar{N}$	$\leftrightarrow$	$\rho + \rho + \omega$
421	$\Delta(1232) + \bar{N}$	$\leftrightarrow$	$\rho + \rho + \phi$
422	$\Delta(1232) + \bar{N}$	$\leftrightarrow$	$\rho + \rho + \eta'$
423	$\Delta(1232) + \bar{N}$	$\leftrightarrow$	$\rho + \omega + \omega$
424	$\Delta(1232) + \bar{N}$	$\leftrightarrow$	$\rho + \omega + \phi$
425	$\Delta(1232) + \bar{N}$	$\leftrightarrow$	$\rho + \omega + \eta'$
426	$\Delta(1232) + \bar{N}$	$\leftrightarrow$	$\rho + \phi + \phi$
427	$\Delta(1232) + \bar{N}$	$\leftrightarrow$	$\rho + \phi + \eta'$
428	$\Delta(1232) + \bar{N}$	$\leftrightarrow$	$\rho + \eta' + \eta'$
429	$\Delta(1232) + \bar{N}$	$\leftrightarrow$	$\rho + a_1 + a_1$
430	$\Delta(1232) + \bar{N}$	$\leftrightarrow$	$\omega + \omega + \omega$
431	$\Delta(1232) + \bar{N}$	$\leftrightarrow$	$\omega + \omega + \phi$
432	$\Delta(1232) + \bar{N}$	$\leftrightarrow$	$\omega + \omega + \eta'$
433	$\Delta(1232) + \bar{N}$	$\leftrightarrow$	$\omega + \phi + \phi$
434	$\Delta(1232) + \bar{N}$	$\leftrightarrow$	$\omega + \phi + \eta'$
435	$\Delta(1232) + \bar{N}$	$\leftrightarrow$	$\omega + \eta' + \eta'$
436	$\Delta(1232) + \bar{N}$	$\leftrightarrow$	$\omega + a_1 + a_1$
437	$\Delta(1232) + \bar{N}$	$\leftrightarrow$	$\phi + \phi + \phi$
438	$\Delta(1232) + \bar{N}$	$\leftrightarrow$	$\phi + \phi + \eta'$
439	$\Delta(1232) + \bar{N}$	$\leftrightarrow$	$\phi + \eta' + \eta'$
440	$\Delta(1232) + \bar{N}$	$\leftrightarrow$	$\phi + a_1 + a_1$
441	$\Delta(1232) + \bar{N}$	$\leftrightarrow$	$\eta' + \eta' + \eta'$
442	$\Delta(1232) + \bar{N}$	$\leftrightarrow$	$\eta' + a_1 + a_1$
443	$\Delta(1232) + \bar{\Delta}(1232)$	$\leftrightarrow$	$\pi + \pi + \pi$
444	$\Delta(1232) + \bar{\Delta}(1232)$	$\leftrightarrow$	$\pi + \pi + \eta$
445	$\Delta(1232) + \bar{\Delta}(1232)$	$\leftrightarrow$	$\pi + \pi + \rho$
446	$\Delta(1232) + \bar{\Delta}(1232)$	$\leftrightarrow$	$\pi + \pi + \omega$
447	$\Delta(1232) + \bar{\Delta}(1232)$	$\leftrightarrow$	$\pi + \pi + \phi$
448	$\Delta(1232) + \bar{\Delta}(1232)$	$\leftrightarrow$	$\pi + \pi + \eta'$
449	$\Delta(1232) + \bar{\Delta}(1232)$	$\leftrightarrow$	$\pi + \eta + \eta$
450	$\Delta(1232) + \bar{\Delta}(1232)$	$\leftrightarrow$	$\pi + \eta + \rho$

Ch. No.	B_1 + B_2	$\leftrightarrow$	M_1+M_2+M_3
451	$\Delta(1232)$ + $\Delta(1232)$	$\leftrightarrow$	$\pi+\eta+\omega$
452	$\Delta(1232)$ + $\bar{\Delta}(1232)$	$\leftrightarrow$	$\pi+\eta+\phi$
453	$\Delta(1232)$ + $\bar{\Delta}(1232)$	$\leftrightarrow$	$\pi+\eta+\eta'$
454	$\Delta(1232)$ + $\bar{\Delta}(1232)$	$\leftrightarrow$	$\pi+\rho+\rho$
455	$\Delta(1232)$ + $\bar{\Delta}(1232)$	$\leftrightarrow$	$\pi+\rho+\omega$
456	$\Delta(1232)$ + $\bar{\Delta}(1232)$	$\leftrightarrow$	$\pi+\rho+\phi$
457	$\Delta(1232)$ + $\bar{\Delta}(1232)$	$\leftrightarrow$	$\pi+\rho+\eta'$
458	$\Delta(1232)$ + $\bar{\Delta}(1232)$	$\leftrightarrow$	$\pi+\omega+\omega$
459	$\Delta(1232)$ + $\bar{\Delta}(1232)$	$\leftrightarrow$	$\pi+\omega+\phi$
460	$\Delta(1232)$ + $\bar{\Delta}(1232)$	$\leftrightarrow$	$\pi+\omega+\eta'$
461	$\Delta(1232)$ + $\bar{\Delta}(1232)$	$\leftrightarrow$	$\pi+\phi+\phi$
462	$\Delta(1232)$ + $\bar{\Delta}(1232)$	$\leftrightarrow$	$\pi+\phi+\eta'$
463	$\Delta(1232)$ + $\bar{\Delta}(1232)$	$\leftrightarrow$	$\pi+\eta'+\eta'$
464	$\Delta(1232)$ + $\bar{\Delta}(1232)$	$\leftrightarrow$	$\pi+a_1+a_1$
465	$\Delta(1232)$ + $\bar{\Delta}(1232)$	$\leftrightarrow$	$\eta+\eta+\eta$
466	$\Delta(1232)$ + $\bar{\Delta}(1232)$	$\leftrightarrow$	$\eta+\eta+\rho$
467	$\Delta(1232)$ + $\bar{\Delta}(1232)$	$\leftrightarrow$	$\eta+\eta+\omega$
468	$\Delta(1232)$ + $\bar{\Delta}(1232)$	$\leftrightarrow$	$\eta+\eta+\phi$
469	$\Delta(1232)$ + $\bar{\Delta}(1232)$	$\leftrightarrow$	$\eta+\eta+\eta'$
470	$\Delta(1232)$ + $\bar{\Delta}(1232)$	$\leftrightarrow$	$\eta+\rho+\rho$
471	$\Delta(1232)$ + $\bar{\Delta}(1232)$	$\leftrightarrow$	$\eta+\rho+\omega$
472	$\Delta(1232)$ + $\bar{\Delta}(1232)$	$\leftrightarrow$	$\eta+\rho+\phi$
473	$\Delta(1232)$ + $\bar{\Delta}(1232)$	$\leftrightarrow$	$\eta+\rho+\eta'$
474	$\Delta(1232)$ + $\bar{\Delta}(1232)$	$\leftrightarrow$	$\eta+\omega+\omega$
475	$\Delta(1232)$ + $\bar{\Delta}(1232)$	$\leftrightarrow$	$\eta+\omega+\phi$
476	$\Delta(1232)$ + $\bar{\Delta}(1232)$	$\leftrightarrow$	$\eta+\omega+\eta'$
477	$\Delta(1232)$ + $\bar{\Delta}(1232)$	$\leftrightarrow$	$\eta+\phi+\phi$
478	$\Delta(1232)$ + $\bar{\Delta}(1232)$	$\leftrightarrow$	$\eta+\phi+\eta'$
479	$\Delta(1232)$ + $\bar{\Delta}(1232)$	$\leftrightarrow$	$\eta+\eta'+\eta'$
480	$\Delta(1232)$ + $\bar{\Delta}(1232)$	$\leftrightarrow$	$\eta+a_1+a_1$
481	$\Delta(1232)$ + $\bar{\Delta}(1232)$	$\leftrightarrow$	$\rho+\rho+\rho$
482	$\Delta(1232)$ + $\bar{\Delta}(1232)$	$\leftrightarrow$	$\rho+\rho+\omega$
483	$\Delta(1232)$ + $\bar{\Delta}(1232)$	$\leftrightarrow$	$\rho+\rho+\phi$
484	$\Delta(1232)$ + $\bar{\Delta}(1232)$	$\leftrightarrow$	$\rho+\rho+\eta'$
485	$\Delta(1232)$ + $\bar{\Delta}(1232)$	$\leftrightarrow$	$\rho+\omega+\omega$
486	$\Delta(1232)$ + $\bar{\Delta}(1232)$	$\leftrightarrow$	$\rho+\omega+\phi$
487	$\Delta(1232)$ + $\bar{\Delta}(1232)$	$\leftrightarrow$	$\rho+\omega+\eta'$
488	$\Delta(1232)$ + $\bar{\Delta}(1232)$	$\leftrightarrow$	$\rho+\phi+\phi$
489	$\Delta(1232)$ + $\bar{\Delta}(1232)$	$\leftrightarrow$	$\rho+\phi+\eta'$
490	$\Delta(1232)$ + $\bar{\Delta}(1232)$	$\leftrightarrow$	$\rho+\eta'+\eta'$
491	$\Delta(1232)$ + $\bar{\Delta}(1232)$	$\leftrightarrow$	$\rho+a_1+a_1$
492	$\Delta(1232)$ + $\bar{\Delta}(1232)$	$\leftrightarrow$	$\omega+\omega+\omega$
493	$\Delta(1232)$ + $\bar{\Delta}(1232)$	$\leftrightarrow$	$\omega+\omega+\phi$
494	$\Delta(1232)$ + $\bar{\Delta}(1232)$	$\leftrightarrow$	$\omega+\omega+\eta'$
495	$\Delta(1232)$ + $\bar{\Delta}(1232)$	$\leftrightarrow$	$\omega+\phi+\phi$
496	$\Delta(1232)$ + $\bar{\Delta}(1232)$	$\leftrightarrow$	$\omega+\phi+\eta'$
497	$\Delta(1232)$ + $\bar{\Delta}(1232)$	$\leftrightarrow$	$\omega+\eta'+\eta'$
498	$\Delta(1232)$ + $\bar{\Delta}(1232)$	$\leftrightarrow$	$\omega+a_1+a_1$
499	$\Delta(1232)$ + $\bar{\Delta}(1232)$	$\leftrightarrow$	$\phi+\phi+\phi$
500	$\Delta(1232)$ + $\bar{\Delta}(1232)$	$\leftrightarrow$	$\phi+\phi+\eta'$
501	$\Delta(1232)$ + $\bar{\Delta}(1232)$	$\leftrightarrow$	$\phi+\eta'+\eta'$
502	$\Delta(1232)$ + $\bar{\Delta}(1232)$	$\leftrightarrow$	$\phi+a_1+a_1$
503	$\Delta(1232)$ + $\bar{\Delta}(1232)$	$\leftrightarrow$	$\eta'+\eta'+\eta'$
504	$\Delta(1232)$ + $\bar{\Delta}(1232)$	$\leftrightarrow$	$\eta'+a_1+a_1$
505	$\Delta(1232)$ + $\bar{\mathrm{N}}(1440)$	$\leftrightarrow$	$\pi+\pi+\pi$
506	$\Delta(1232)$ + $\bar{\mathrm{N}}(1440)$	$\leftrightarrow$	$\pi+\pi+\eta$
507	$\Delta(1232)$ + $\bar{\mathrm{N}}(1440)$	$\leftrightarrow$	$\pi+\pi+\rho$
508	$\Delta(1232)$ + $\bar{\mathrm{N}}(1440)$	$\leftrightarrow$	$\pi+\pi+\omega$
509	$\Delta(1232)$ + $\bar{\mathrm{N}}(1440)$	$\leftrightarrow$	$\pi+\pi+\phi$
510	$\Delta(1232)$ + $\bar{\mathrm{N}}(1440)$	$\leftrightarrow$	$\pi+\pi+\eta'$
511	$\Delta(1232)$ + $\bar{\mathrm{N}}(1440)$	$\leftrightarrow$	$\pi+\eta+\eta$
512	$\Delta(1232)$ + $\bar{\mathrm{N}}(1440)$	$\leftrightarrow$	$\pi+\eta+\rho$
513	$\Delta(1232)$ + $\bar{\mathrm{N}}(1440)$	$\leftrightarrow$	$\pi+\eta+\omega$
514	$\Delta(1232)$ + $\bar{\mathrm{N}}(1440)$	$\leftrightarrow$	$\pi+\eta+\phi$
515	$\Delta(1232)$ + $\bar{\mathrm{N}}(1440)$	$\leftrightarrow$	$\pi+\eta+\eta'$
516	$\Delta(1232)$ + $\bar{\mathrm{N}}(1440)$	$\leftrightarrow$	$\pi+\rho+\rho$
517	$\Delta(1232)$ + $\bar{\mathrm{N}}(1440)$	$\leftrightarrow$	$\pi+\rho+\omega$
518	$\Delta(1232)$ + $\bar{\mathrm{N}}(1440)$	$\leftrightarrow$	$\pi+\rho+\phi$
519	$\Delta(1232)$ + $\bar{\mathrm{N}}(1440)$	$\leftrightarrow$	$\pi+\rho+\eta'$
520	$\Delta(1232)$ + $\bar{\mathrm{N}}(1440)$	$\leftrightarrow$	$\pi+\omega+\omega$
521	$\Delta(1232)$ + $\bar{\mathrm{N}}(1440)$	$\leftrightarrow$	$\pi+\omega+\phi$
522	$\Delta(1232)$ + $\bar{\mathrm{N}}(1440)$	$\leftrightarrow$	$\pi+\omega+\eta'$
523	$\Delta(1232)$ + $\bar{\mathrm{N}}(1440)$	$\leftrightarrow$	$\pi+\phi+\phi$
524	$\Delta(1232)$ + $\bar{\mathrm{N}}(1440)$	$\leftrightarrow$	$\pi+\phi+\eta'$
525	$\Delta(1232)$ + $\bar{\mathrm{N}}(1440)$	$\leftrightarrow$	$\pi+\eta'+\eta'$
526	$\Delta(1232)$ + $\bar{\mathrm{N}}(1440)$	$\leftrightarrow$	$\pi+a_1+a_1$
527	$\Delta(1232)$ + $\bar{\mathrm{N}}(1440)$	$\leftrightarrow$	$\eta+\eta+\eta$
528	$\Delta(1232)$ + $\bar{\mathrm{N}}(1440)$	$\leftrightarrow$	$\eta+\eta+\rho$
529	$\Delta(1232)$ + $\bar{\mathrm{N}}(1440)$	$\leftrightarrow$	$\eta+\eta+\omega$
530	$\Delta(1232)$ + $\bar{\mathrm{N}}(1440)$	$\leftrightarrow$	$\eta+\eta+\phi$
531	$\Delta(1232)$ + $\bar{\mathrm{N}}(1440)$	$\leftrightarrow$	$\eta+\eta+\eta'$
532	$\Delta(1232)$ + $\bar{\mathrm{N}}(1440)$	$\leftrightarrow$	$\eta+\rho+\rho$
533	$\Delta(1232)$ + $\bar{\mathrm{N}}(1440)$	$\leftrightarrow$	$\eta+\rho+\omega$
534	$\Delta(1232)$ + $\bar{\mathrm{N}}(1440)$	$\leftrightarrow$	$\eta+\rho+\phi$
535	$\Delta(1232)$ + $\bar{\mathrm{N}}(1440)$	$\leftrightarrow$	$\eta+\rho+\eta'$
536	$\Delta(1232)$ + $\bar{\mathrm{N}}(1440)$	$\leftrightarrow$	$\eta+\omega+\omega$

Ch. No.	B_1 + B_2	$\leftrightarrow$	M_1+M_2+M_3
537	$\Delta(1232)$ + $\bar{\mathrm{N}}(1440)$	$\leftrightarrow$	$\eta+\omega+\phi$
538	$\Delta(1232)$ + $\bar{\mathrm{N}}(1440)$	$\leftrightarrow$	$\eta+\omega+\eta'$
539	$\Delta(1232)$ + $\bar{\mathrm{N}}(1440)$	$\leftrightarrow$	$\eta+\phi+\phi$
540	$\Delta(1232)$ + $\bar{\mathrm{N}}(1440)$	$\leftrightarrow$	$\eta+\phi+\eta'$
541	$\Delta(1232)$ + $\bar{\mathrm{N}}(1440)$	$\leftrightarrow$	$\eta+\eta'+\eta'$
542	$\Delta(1232)$ + $\bar{\mathrm{N}}(1440)$	$\leftrightarrow$	$\eta+a_1+a_1$
543	$\Delta(1232)$ + $\bar{\mathrm{N}}(1440)$	$\leftrightarrow$	$\rho+\rho+\rho$
544	$\Delta(1232)$ + $\bar{\mathrm{N}}(1440)$	$\leftrightarrow$	$\rho+\rho+\omega$
545	$\Delta(1232)$ + $\bar{\mathrm{N}}(1440)$	$\leftrightarrow$	$\rho+\rho+\phi$
546	$\Delta(1232)$ + $\bar{\mathrm{N}}(1440)$	$\leftrightarrow$	$\rho+\rho+\eta'$
547	$\Delta(1232)$ + $\bar{\mathrm{N}}(1440)$	$\leftrightarrow$	$\rho+\omega+\omega$
548	$\Delta(1232)$ + $\bar{\mathrm{N}}(1440)$	$\leftrightarrow$	$\rho+\omega+\phi$
549	$\Delta(1232)$ + $\bar{\mathrm{N}}(1440)$	$\leftrightarrow$	$\rho+\omega+\eta'$
550	$\Delta(1232)$ + $\bar{\mathrm{N}}(1440)$	$\leftrightarrow$	$\rho+\phi+\phi$
551	$\Delta(1232)$ + $\bar{\mathrm{N}}(1440)$	$\leftrightarrow$	$\rho+\phi+\eta'$
552	$\Delta(1232)$ + $\bar{\mathrm{N}}(1440)$	$\leftrightarrow$	$\rho+\eta'+\eta'$
553	$\Delta(1232)$ + $\bar{\mathrm{N}}(1440)$	$\leftrightarrow$	$\rho+a_1+a_1$
554	$\Delta(1232)$ + $\bar{\mathrm{N}}(1440)$	$\leftrightarrow$	$\omega+\omega+\omega$
555	$\Delta(1232)$ + $\bar{\mathrm{N}}(1440)$	$\leftrightarrow$	$\omega+\omega+\phi$
556	$\Delta(1232)$ + $\bar{\mathrm{N}}(1440)$	$\leftrightarrow$	$\omega+\omega+\eta'$
557	$\Delta(1232)$ + $\bar{\mathrm{N}}(1440)$	$\leftrightarrow$	$\omega+\phi+\phi$
558	$\Delta(1232)$ + $\bar{\mathrm{N}}(1440)$	$\leftrightarrow$	$\omega+\phi+\eta'$
559	$\Delta(1232)$ + $\bar{\mathrm{N}}(1440)$	$\leftrightarrow$	$\omega+\eta'+\eta'$
560	$\Delta(1232)$ + $\bar{\mathrm{N}}(1440)$	$\leftrightarrow$	$\omega+a_1+a_1$
561	$\Delta(1232)$ + $\bar{\mathrm{N}}(1440)$	$\leftrightarrow$	$\phi+\phi+\phi$
562	$\Delta(1232)$ + $\bar{\mathrm{N}}(1440)$	$\leftrightarrow$	$\phi+\phi+\eta'$
563	$\Delta(1232)$ + $\bar{\mathrm{N}}(1440)$	$\leftrightarrow$	$\phi+\eta'+\eta'$
564	$\Delta(1232)$ + $\bar{\mathrm{N}}(1440)$	$\leftrightarrow$	$\phi+a_1+a_1$
565	$\Delta(1232)$ + $\bar{\mathrm{N}}(1440)$	$\leftrightarrow$	$\eta'+\eta'+\eta'$
566	$\Delta(1232)$ + $\bar{\mathrm{N}}(1440)$	$\leftrightarrow$	$\eta'+a_1+a_1$
567	$\Delta(1232)$ + $\bar{\mathrm{N}}(1535)$	$\leftrightarrow$	$\pi+\pi+a_1$
568	$\Delta(1232)$ + $\bar{\mathrm{N}}(1535)$	$\leftrightarrow$	$\pi+\eta+a_1$
569	$\Delta(1232)$ + $\bar{\mathrm{N}}(1535)$	$\leftrightarrow$	$\pi+\rho+a_1$
570	$\Delta(1232)$ + $\bar{\mathrm{N}}(1535)$	$\leftrightarrow$	$\pi+\omega+a_1$
571	$\Delta(1232)$ + $\bar{\mathrm{N}}(1535)$	$\leftrightarrow$	$\pi+\phi+a_1$
572	$\Delta(1232)$ + $\bar{\mathrm{N}}(1535)$	$\leftrightarrow$	$\pi+\eta'+a_1$
573	$\Delta(1232)$ + $\bar{\mathrm{N}}(1535)$	$\leftrightarrow$	$\eta+\eta+a_1$
574	$\Delta(1232)$ + $\bar{\mathrm{N}}(1535)$	$\leftrightarrow$	$\eta+\rho+a_1$
575	$\Delta(1232)$ + $\bar{\mathrm{N}}(1535)$	$\leftrightarrow$	$\eta+\omega+a_1$
576	$\Delta(1232)$ + $\bar{\mathrm{N}}(1535)$	$\leftrightarrow$	$\eta+\phi+a_1$
577	$\Delta(1232)$ + $\bar{\mathrm{N}}(1535)$	$\leftrightarrow$	$\eta+\eta'+a_1$
578	$\Delta(1232)$ + $\bar{\mathrm{N}}(1535)$	$\leftrightarrow$	$\rho+\rho+a_1$
579	$\Delta(1232)$ + $\bar{\mathrm{N}}(1535)$	$\leftrightarrow$	$\rho+\omega+a_1$
580	$\Delta(1232)$ + $\bar{\mathrm{N}}(1535)$	$\leftrightarrow$	$\rho+\phi+a_1$
581	$\Delta(1232)$ + $\bar{\mathrm{N}}(1535)$	$\leftrightarrow$	$\rho+\eta'+a_1$
582	$\Delta(1232)$ + $\bar{\mathrm{N}}(1535)$	$\leftrightarrow$	$\omega+\omega+a_1$
583	$\Delta(1232)$ + $\bar{\mathrm{N}}(1535)$	$\leftrightarrow$	$\omega+\phi+a_1$
584	$\Delta(1232)$ + $\bar{\mathrm{N}}(1535)$	$\leftrightarrow$	$\omega+\eta'+a_1$
585	$\Delta(1232)$ + $\bar{\mathrm{N}}(1535)$	$\leftrightarrow$	$\phi+\phi+a_1$
586	$\Delta(1232)$ + $\bar{\mathrm{N}}(1535)$	$\leftrightarrow$	$\phi+\eta'+a_1$
587	$\Delta(1232)$ + $\bar{\mathrm{N}}(1535)$	$\leftrightarrow$	$\eta'+\eta'+a_1$
588	$\Delta(1232)$ + $\bar{\mathrm{N}}(1535)$	$\leftrightarrow$	$a_1+a_1+a_1$
589	$\Delta(1232)$ + $\bar{\Lambda}$	$\leftrightarrow$	$\pi+\pi+K$
590	$\Delta(1232)$ + $\bar{\Lambda}$	$\leftrightarrow$	$\pi+\pi+K^*$
591	$\Delta(1232)$ + $\bar{\Lambda}$	$\leftrightarrow$	$\pi+\eta+K$
592	$\Delta(1232)$ + $\bar{\Lambda}$	$\leftrightarrow$	$\pi+\eta+K^*$
593	$\Delta(1232)$ + $\bar{\Lambda}$	$\leftrightarrow$	$\pi+K+\rho$
594	$\Delta(1232)$ + $\bar{\Lambda}$	$\leftrightarrow$	$\pi+K+\omega$
595	$\Delta(1232)$ + $\bar{\Lambda}$	$\leftrightarrow$	$\pi+K+\phi$
596	$\Delta(1232)$ + $\bar{\Lambda}$	$\leftrightarrow$	$\pi+K+\eta'$
597	$\Delta(1232)$ + $\bar{\Lambda}$	$\leftrightarrow$	$\pi+K^*+\rho$
598	$\Delta(1232)$ + $\bar{\Lambda}$	$\leftrightarrow$	$\pi+K^*+\omega$
599	$\Delta(1232)$ + $\bar{\Lambda}$	$\leftrightarrow$	$\pi+K^*+\phi$
600	$\Delta(1232)$ + $\bar{\Lambda}$	$\leftrightarrow$	$\pi+K^*+\eta'$
601	$\Delta(1232)$ + $\bar{\Lambda}$	$\leftrightarrow$	$\eta+\eta+K$
602	$\Delta(1232)$ + $\bar{\Lambda}$	$\leftrightarrow$	$\eta+\eta+K^*$
603	$\Delta(1232)$ + $\bar{\Lambda}$	$\leftrightarrow$	$\eta+K+\rho$
604	$\Delta(1232)$ + $\bar{\Lambda}$	$\leftrightarrow$	$\eta+K+\omega$
605	$\Delta(1232)$ + $\bar{\Lambda}$	$\leftrightarrow$	$\eta+K+\phi$
606	$\Delta(1232)$ + $\bar{\Lambda}$	$\leftrightarrow$	$\eta+K+\eta'$
607	$\Delta(1232)$ + $\bar{\Lambda}$	$\leftrightarrow$	$\eta+K^*+\rho$
608	$\Delta(1232)$ + $\bar{\Lambda}$	$\leftrightarrow$	$\eta+K^*+\omega$
609	$\Delta(1232)$ + $\bar{\Lambda}$	$\leftrightarrow$	$\eta+K^*+\phi$
610	$\Delta(1232)$ + $\bar{\Lambda}$	$\leftrightarrow$	$\eta+K^*+\eta'$
611	$\Delta(1232)$ + $\bar{\Lambda}$	$\leftrightarrow$	$K+\rho+\rho$
612	$\Delta(1232)$ + $\bar{\Lambda}$	$\leftrightarrow$	$K+\rho+\omega$
613	$\Delta(1232)$ + $\bar{\Lambda}$	$\leftrightarrow$	$K+\rho+\phi$
614	$\Delta(1232)$ + $\bar{\Lambda}$	$\leftrightarrow$	$K+\rho+\eta'$
615	$\Delta(1232)$ + $\bar{\Lambda}$	$\leftrightarrow$	$K+\omega+\omega$
616	$\Delta(1232)$ + $\bar{\Lambda}$	$\leftrightarrow$	$K+\omega+\phi$
617	$\Delta(1232)$ + $\bar{\Lambda}$	$\leftrightarrow$	$K+\omega+\eta'$
618	$\Delta(1232)$ + $\bar{\Lambda}$	$\leftrightarrow$	$K+\phi+\phi$
619	$\Delta(1232)$ + $\bar{\Lambda}$	$\leftrightarrow$	$K+\phi+\eta'$
620	$\Delta(1232)$ + $\bar{\Lambda}$	$\leftrightarrow$	$K+\eta'+\eta'$
621	$\Delta(1232)$ + $\bar{\Lambda}$	$\leftrightarrow$	$K+a_1+a_1$
622	$\Delta(1232)$ + $\bar{\Lambda}$	$\leftrightarrow$	$K^*+\rho+\rho$

Ch. No.	$B_1 + B_2$	$\leftrightarrow$	$M_1+M_2+M_3$
623	$\Delta(1232) + \bar{\Lambda}$	$\leftrightarrow$	$K^* + \rho + \omega$
624	$\Delta(1232) + \bar{\Lambda}$	$\leftrightarrow$	$K^* + \rho + \phi$
625	$\Delta(1232) + \bar{\Lambda}$	$\leftrightarrow$	$K^* + \rho + \eta'$
626	$\Delta(1232) + \bar{\Lambda}$	$\leftrightarrow$	$K^* + \omega + \omega$
627	$\Delta(1232) + \bar{\Lambda}$	$\leftrightarrow$	$K^* + \omega + \phi$
628	$\Delta(1232) + \bar{\Lambda}$	$\leftrightarrow$	$K^* + \omega + \eta'$
629	$\Delta(1232) + \bar{\Lambda}$	$\leftrightarrow$	$K^* + \phi + \phi$
630	$\Delta(1232) + \bar{\Lambda}$	$\leftrightarrow$	$K^* + \phi + \eta'$
631	$\Delta(1232) + \bar{\Lambda}$	$\leftrightarrow$	$K^* + \eta' + \eta'$
632	$\Delta(1232) + \bar{\Lambda}$	$\leftrightarrow$	$K^* + a_1 + a_1$
633	$\Delta(1232) + \bar{\Sigma}$	$\leftrightarrow$	$\pi + \pi + K$
634	$\Delta(1232) + \bar{\Sigma}$	$\leftrightarrow$	$\pi + \pi + K^*$
635	$\Delta(1232) + \bar{\Sigma}$	$\leftrightarrow$	$\pi + \eta + K$
636	$\Delta(1232) + \bar{\Sigma}$	$\leftrightarrow$	$\pi + \eta + K^*$
637	$\Delta(1232) + \bar{\Sigma}$	$\leftrightarrow$	$\pi + K + \rho$
638	$\Delta(1232) + \bar{\Sigma}$	$\leftrightarrow$	$\pi + K + \omega$
639	$\Delta(1232) + \bar{\Sigma}$	$\leftrightarrow$	$\pi + K + \phi$
640	$\Delta(1232) + \bar{\Sigma}$	$\leftrightarrow$	$\pi + K + \eta'$
641	$\Delta(1232) + \bar{\Sigma}$	$\leftrightarrow$	$\pi + K^* + \rho$
642	$\Delta(1232) + \bar{\Sigma}$	$\leftrightarrow$	$\pi + K^* + \omega$
643	$\Delta(1232) + \bar{\Sigma}$	$\leftrightarrow$	$\pi + K^* + \phi$
644	$\Delta(1232) + \bar{\Sigma}$	$\leftrightarrow$	$\pi + K^* + \eta'$
645	$\Delta(1232) + \bar{\Sigma}$	$\leftrightarrow$	$\eta + \eta + K$
646	$\Delta(1232) + \bar{\Sigma}$	$\leftrightarrow$	$\eta + \eta + K^*$
647	$\Delta(1232) + \bar{\Sigma}$	$\leftrightarrow$	$\eta + K + \rho$
648	$\Delta(1232) + \bar{\Sigma}$	$\leftrightarrow$	$\eta + K + \omega$
649	$\Delta(1232) + \bar{\Sigma}$	$\leftrightarrow$	$\eta + K + \phi$
650	$\Delta(1232) + \bar{\Sigma}$	$\leftrightarrow$	$\eta + K + \eta'$
651	$\Delta(1232) + \bar{\Sigma}$	$\leftrightarrow$	$\eta + K^* + \rho$
652	$\Delta(1232) + \bar{\Sigma}$	$\leftrightarrow$	$\eta + K^* + \omega$
653	$\Delta(1232) + \bar{\Sigma}$	$\leftrightarrow$	$\eta + K^* + \phi$
654	$\Delta(1232) + \bar{\Sigma}$	$\leftrightarrow$	$\eta + K^* + \eta'$
655	$\Delta(1232) + \bar{\Sigma}$	$\leftrightarrow$	$K + \rho + \rho$
656	$\Delta(1232) + \bar{\Sigma}$	$\leftrightarrow$	$K + \rho + \omega$
657	$\Delta(1232) + \bar{\Sigma}$	$\leftrightarrow$	$K + \rho + \phi$
658	$\Delta(1232) + \bar{\Sigma}$	$\leftrightarrow$	$K + \rho + \eta'$
659	$\Delta(1232) + \bar{\Sigma}$	$\leftrightarrow$	$K + \omega + \omega$
660	$\Delta(1232) + \bar{\Sigma}$	$\leftrightarrow$	$K + \omega + \phi$
661	$\Delta(1232) + \bar{\Sigma}$	$\leftrightarrow$	$K + \omega + \eta'$
662	$\Delta(1232) + \bar{\Sigma}$	$\leftrightarrow$	$K + \phi + \phi$
663	$\Delta(1232) + \bar{\Sigma}$	$\leftrightarrow$	$K + \phi + \eta'$
664	$\Delta(1232) + \bar{\Sigma}$	$\leftrightarrow$	$K + \eta' + \eta'$
665	$\Delta(1232) + \bar{\Sigma}$	$\leftrightarrow$	$K + a_1 + a_1$
666	$\Delta(1232) + \bar{\Sigma}$	$\leftrightarrow$	$K^* + \rho + \rho$
667	$\Delta(1232) + \bar{\Sigma}$	$\leftrightarrow$	$K^* + \rho + \omega$
668	$\Delta(1232) + \bar{\Sigma}$	$\leftrightarrow$	$K^* + \rho + \phi$
669	$\Delta(1232) + \bar{\Sigma}$	$\leftrightarrow$	$K^* + \rho + \eta'$
670	$\Delta(1232) + \bar{\Sigma}$	$\leftrightarrow$	$K^* + \omega + \omega$
671	$\Delta(1232) + \bar{\Sigma}$	$\leftrightarrow$	$K^* + \omega + \phi$
672	$\Delta(1232) + \bar{\Sigma}$	$\leftrightarrow$	$K^* + \omega + \eta'$
673	$\Delta(1232) + \bar{\Sigma}$	$\leftrightarrow$	$K^* + \phi + \phi$
674	$\Delta(1232) + \bar{\Sigma}$	$\leftrightarrow$	$K^* + \phi + \eta'$
675	$\Delta(1232) + \bar{\Sigma}$	$\leftrightarrow$	$K^* + \eta' + \eta'$
676	$\Delta(1232) + \bar{\Sigma}$	$\leftrightarrow$	$K^* + a_1 + a_1$
677	$\Delta(1232) + \bar{\Sigma}^*$	$\leftrightarrow$	$\pi + \pi + K$
678	$\Delta(1232) + \bar{\Sigma}^*$	$\leftrightarrow$	$\pi + \pi + K^*$
679	$\Delta(1232) + \bar{\Sigma}^*$	$\leftrightarrow$	$\pi + \eta + K$
680	$\Delta(1232) + \bar{\Sigma}^*$	$\leftrightarrow$	$\pi + \eta + K^*$
681	$\Delta(1232) + \bar{\Sigma}^*$	$\leftrightarrow$	$\pi + K + \rho$
682	$\Delta(1232) + \bar{\Sigma}^*$	$\leftrightarrow$	$\pi + K + \omega$
683	$\Delta(1232) + \bar{\Sigma}^*$	$\leftrightarrow$	$\pi + K + \phi$
684	$\Delta(1232) + \bar{\Sigma}^*$	$\leftrightarrow$	$\pi + K + \eta'$
685	$\Delta(1232) + \bar{\Sigma}^*$	$\leftrightarrow$	$\pi + K^* + \rho$
686	$\Delta(1232) + \bar{\Sigma}^*$	$\leftrightarrow$	$\pi + K^* + \omega$
687	$\Delta(1232) + \bar{\Sigma}^*$	$\leftrightarrow$	$\pi + K^* + \phi$
688	$\Delta(1232) + \bar{\Sigma}^*$	$\leftrightarrow$	$\pi + K^* + \eta'$
689	$\Delta(1232) + \bar{\Sigma}^*$	$\leftrightarrow$	$\eta + \eta + K$
690	$\Delta(1232) + \bar{\Sigma}^*$	$\leftrightarrow$	$\eta + \eta + K^*$
691	$\Delta(1232) + \bar{\Sigma}^*$	$\leftrightarrow$	$\eta + K + \rho$
692	$\Delta(1232) + \bar{\Sigma}^*$	$\leftrightarrow$	$\eta + K + \omega$
693	$\Delta(1232) + \bar{\Sigma}^*$	$\leftrightarrow$	$\eta + K + \phi$
694	$\Delta(1232) + \bar{\Sigma}^*$	$\leftrightarrow$	$\eta + K + \eta'$
695	$\Delta(1232) + \bar{\Sigma}^*$	$\leftrightarrow$	$\eta + K^* + \rho$
696	$\Delta(1232) + \bar{\Sigma}^*$	$\leftrightarrow$	$\eta + K^* + \omega$
697	$\Delta(1232) + \bar{\Sigma}^*$	$\leftrightarrow$	$\eta + K^* + \phi$
698	$\Delta(1232) + \bar{\Sigma}^*$	$\leftrightarrow$	$\eta + K^* + \eta'$
699	$\Delta(1232) + \bar{\Sigma}^*$	$\leftrightarrow$	$K + \rho + \rho$
700	$\Delta(1232) + \bar{\Sigma}^*$	$\leftrightarrow$	$K + \rho + \omega$
701	$\Delta(1232) + \bar{\Sigma}^*$	$\leftrightarrow$	$K + \rho + \phi$
702	$\Delta(1232) + \bar{\Sigma}^*$	$\leftrightarrow$	$K + \rho + \eta'$
703	$\Delta(1232) + \bar{\Sigma}^*$	$\leftrightarrow$	$K + \omega + \omega$
704	$\Delta(1232) + \bar{\Sigma}^*$	$\leftrightarrow$	$K + \omega + \phi$
705	$\Delta(1232) + \bar{\Sigma}^*$	$\leftrightarrow$	$K + \omega + \eta'$
706	$\Delta(1232) + \bar{\Sigma}^*$	$\leftrightarrow$	$K + \phi + \phi$
707	$\Delta(1232) + \bar{\Sigma}^*$	$\leftrightarrow$	$K + \phi + \eta'$
708	$\Delta(1232) + \bar{\Sigma}^*$	$\leftrightarrow$	$K + \eta' + \eta'$

Ch. No.	$B_1 + B_2$	$\leftrightarrow$	$M_1+M_2+M_3$
709	$\Delta(1232) + \bar{\Sigma}^*$	$\leftrightarrow$	$K + a_1 + a_1$
710	$\Delta(1232) + \bar{\Sigma}^*$	$\leftrightarrow$	$K^* + \rho + \rho$
711	$\Delta(1232) + \bar{\Sigma}^*$	$\leftrightarrow$	$K^* + \rho + \omega$
712	$\Delta(1232) + \bar{\Sigma}^*$	$\leftrightarrow$	$K^* + \rho + \phi$
713	$\Delta(1232) + \bar{\Sigma}^*$	$\leftrightarrow$	$K^* + \rho + \eta'$
714	$\Delta(1232) + \bar{\Sigma}^*$	$\leftrightarrow$	$K^* + \omega + \omega$
715	$\Delta(1232) + \bar{\Sigma}^*$	$\leftrightarrow$	$K^* + \omega + \phi$
716	$\Delta(1232) + \bar{\Sigma}^*$	$\leftrightarrow$	$K^* + \omega + \eta'$
717	$\Delta(1232) + \bar{\Sigma}^*$	$\leftrightarrow$	$K^* + \phi + \phi$
718	$\Delta(1232) + \bar{\Sigma}^*$	$\leftrightarrow$	$K^* + \phi + \eta'$
719	$\Delta(1232) + \bar{\Sigma}^*$	$\leftrightarrow$	$K^* + \eta' + \eta'$
720	$\Delta(1232) + \bar{\Sigma}^*$	$\leftrightarrow$	$K^* + a_1 + a_1$
721	$\Delta(1232) + \bar{\Xi}$	$\leftrightarrow$	$\pi + K + K$
722	$\Delta(1232) + \bar{\Xi}$	$\leftrightarrow$	$\pi + K + K^*$
723	$\Delta(1232) + \bar{\Xi}$	$\leftrightarrow$	$\pi + K^* + K^*$
724	$\Delta(1232) + \bar{\Xi}$	$\leftrightarrow$	$\eta + K + K$
725	$\Delta(1232) + \bar{\Xi}$	$\leftrightarrow$	$\eta + K + K^*$
726	$\Delta(1232) + \bar{\Xi}$	$\leftrightarrow$	$\eta + K^* + K^*$
727	$\Delta(1232) + \bar{\Xi}$	$\leftrightarrow$	$K + K + \rho$
728	$\Delta(1232) + \bar{\Xi}$	$\leftrightarrow$	$K + K + \omega$
729	$\Delta(1232) + \bar{\Xi}$	$\leftrightarrow$	$K + K + \phi$
730	$\Delta(1232) + \bar{\Xi}$	$\leftrightarrow$	$K + K + \eta'$
731	$\Delta(1232) + \bar{\Xi}$	$\leftrightarrow$	$K + K^* + \rho$
732	$\Delta(1232) + \bar{\Xi}$	$\leftrightarrow$	$K + K^* + \omega$
733	$\Delta(1232) + \bar{\Xi}$	$\leftrightarrow$	$K + K^* + \phi$
734	$\Delta(1232) + \bar{\Xi}$	$\leftrightarrow$	$K + K^* + \eta'$
735	$\Delta(1232) + \bar{\Xi}$	$\leftrightarrow$	$K^* + K^* + \rho$
736	$\Delta(1232) + \bar{\Xi}$	$\leftrightarrow$	$K^* + K^* + \omega$
737	$\Delta(1232) + \bar{\Xi}$	$\leftrightarrow$	$K^* + K^* + \phi$
738	$\Delta(1232) + \bar{\Xi}$	$\leftrightarrow$	$K^* + K^* + \eta'$
739	$\Delta(1232) + \bar{\Xi}^*$	$\leftrightarrow$	$\pi + K + K$
740	$\Delta(1232) + \bar{\Xi}^*$	$\leftrightarrow$	$\pi + K + K^*$
741	$\Delta(1232) + \bar{\Xi}^*$	$\leftrightarrow$	$\pi + K^* + K^*$
742	$\Delta(1232) + \bar{\Xi}^*$	$\leftrightarrow$	$\eta + K + K$
743	$\Delta(1232) + \bar{\Xi}^*$	$\leftrightarrow$	$\eta + K + K^*$
744	$\Delta(1232) + \bar{\Xi}^*$	$\leftrightarrow$	$\eta + K^* + K^*$
745	$\Delta(1232) + \bar{\Xi}^*$	$\leftrightarrow$	$K + K + \rho$
746	$\Delta(1232) + \bar{\Xi}^*$	$\leftrightarrow$	$K + K + \omega$
747	$\Delta(1232) + \bar{\Xi}^*$	$\leftrightarrow$	$K + K + \phi$
748	$\Delta(1232) + \bar{\Xi}^*$	$\leftrightarrow$	$K + K + \eta'$
749	$\Delta(1232) + \bar{\Xi}^*$	$\leftrightarrow$	$K + K^* + \rho$
750	$\Delta(1232) + \bar{\Xi}^*$	$\leftrightarrow$	$K + K^* + \omega$
751	$\Delta(1232) + \bar{\Xi}^*$	$\leftrightarrow$	$K + K^* + \phi$
752	$\Delta(1232) + \bar{\Xi}^*$	$\leftrightarrow$	$K + K^* + \eta'$
753	$\Delta(1232) + \bar{\Xi}^*$	$\leftrightarrow$	$K^* + K^* + \rho$
754	$\Delta(1232) + \bar{\Xi}^*$	$\leftrightarrow$	$K^* + K^* + \omega$
755	$\Delta(1232) + \bar{\Xi}^*$	$\leftrightarrow$	$K^* + K^* + \phi$
756	$\Delta(1232) + \bar{\Xi}^*$	$\leftrightarrow$	$K^* + K^* + \eta'$
757	$\Delta(1232) + \bar{\Omega}$	$\leftrightarrow$	$K + K + K$
758	$\Delta(1232) + \bar{\Omega}$	$\leftrightarrow$	$K + K + K^*$
759	$\Delta(1232) + \bar{\Omega}$	$\leftrightarrow$	$K + K^* + K^*$
760	$\Delta(1232) + \bar{\Omega}$	$\leftrightarrow$	$K^* + K^* + K^*$
761	$N(1440) + \bar{N}$	$\leftrightarrow$	$\pi + \pi + \pi$
762	$N(1440) + \bar{N}$	$\leftrightarrow$	$\pi + \pi + \eta$
763	$N(1440) + \bar{N}$	$\leftrightarrow$	$\pi + \pi + \rho$
764	$N(1440) + \bar{N}$	$\leftrightarrow$	$\pi + \pi + \omega$
765	$N(1440) + \bar{N}$	$\leftrightarrow$	$\pi + \pi + \phi$
766	$N(1440) + \bar{N}$	$\leftrightarrow$	$\pi + \pi + \eta'$
767	$N(1440) + \bar{N}$	$\leftrightarrow$	$\pi + \eta + \eta$
768	$N(1440) + \bar{N}$	$\leftrightarrow$	$\pi + \eta + \rho$
769	$N(1440) + \bar{N}$	$\leftrightarrow$	$\pi + \eta + \omega$
770	$N(1440) + \bar{N}$	$\leftrightarrow$	$\pi + \eta + \phi$
771	$N(1440) + \bar{N}$	$\leftrightarrow$	$\pi + \eta + \eta'$
772	$N(1440) + \bar{N}$	$\leftrightarrow$	$\pi + \rho + \rho$
773	$N(1440) + \bar{N}$	$\leftrightarrow$	$\pi + \rho + \omega$
774	$N(1440) + \bar{N}$	$\leftrightarrow$	$\pi + \rho + \phi$
775	$N(1440) + \bar{N}$	$\leftrightarrow$	$\pi + \rho + \eta'$
776	$N(1440) + \bar{N}$	$\leftrightarrow$	$\pi + \omega + \omega$
777	$N(1440) + \bar{N}$	$\leftrightarrow$	$\pi + \omega + \phi$
778	$N(1440) + \bar{N}$	$\leftrightarrow$	$\pi + \omega + \eta'$
779	$N(1440) + \bar{N}$	$\leftrightarrow$	$\pi + \phi + \phi$
780	$N(1440) + \bar{N}$	$\leftrightarrow$	$\pi + \phi + \eta'$
781	$N(1440) + \bar{N}$	$\leftrightarrow$	$\pi + \eta' + \eta'$
782	$N(1440) + \bar{N}$	$\leftrightarrow$	$\pi + a_1 + a_1$
783	$N(1440) + \bar{N}$	$\leftrightarrow$	$\eta + \eta + \eta$
784	$N(1440) + \bar{N}$	$\leftrightarrow$	$\eta + \eta + \rho$
785	$N(1440) + \bar{N}$	$\leftrightarrow$	$\eta + \eta + \omega$
786	$N(1440) + \bar{N}$	$\leftrightarrow$	$\eta + \eta + \phi$
787	$N(1440) + \bar{N}$	$\leftrightarrow$	$\eta + \eta + \eta'$
788	$N(1440) + \bar{N}$	$\leftrightarrow$	$\eta + \rho + \rho$
789	$N(1440) + \bar{N}$	$\leftrightarrow$	$\eta + \rho + \omega$
790	$N(1440) + \bar{N}$	$\leftrightarrow$	$\eta + \rho + \phi$
791	$N(1440) + \bar{N}$	$\leftrightarrow$	$\eta + \rho + \eta'$
792	$N(1440) + \bar{N}$	$\leftrightarrow$	$\eta + \omega + \omega$
793	$N(1440) + \bar{N}$	$\leftrightarrow$	$\eta + \omega + \phi$
794	$N(1440) + \bar{N}$	$\leftrightarrow$	$\eta + \omega + \eta'$

Ch. No.	B_1 + B_2	$\leftrightarrow$	M_1+M_2+M_3
795	N(1440) + $\bar{\text{N}}$	$\leftrightarrow$	$\eta + \phi + \phi$
796	N(1440) + $\bar{\text{N}}$	$\leftrightarrow$	$\eta + \phi + \eta'$
797	N(1440) + $\bar{\text{N}}$	$\leftrightarrow$	$\eta + \eta' + \eta'$
798	N(1440) + $\bar{\text{N}}$	$\leftrightarrow$	$\eta + a_1 + a_1$
799	N(1440) + $\bar{\text{N}}$	$\leftrightarrow$	$\rho + \rho + \rho$
800	N(1440) + $\bar{\text{N}}$	$\leftrightarrow$	$\rho + \rho + \omega$
801	N(1440) + $\bar{\text{N}}$	$\leftrightarrow$	$\rho + \rho + \phi$
802	N(1440) + $\bar{\text{N}}$	$\leftrightarrow$	$\rho + \rho + \eta'$
803	N(1440) + $\bar{\text{N}}$	$\leftrightarrow$	$\rho + \omega + \omega$
804	N(1440) + $\bar{\text{N}}$	$\leftrightarrow$	$\rho + \omega + \phi$
805	N(1440) + $\bar{\text{N}}$	$\leftrightarrow$	$\rho + \omega + \eta'$
806	N(1440) + $\bar{\text{N}}$	$\leftrightarrow$	$\rho + \phi + \phi$
807	N(1440) + $\bar{\text{N}}$	$\leftrightarrow$	$\rho + \phi + \eta'$
808	N(1440) + $\bar{\text{N}}$	$\leftrightarrow$	$\rho + \eta' + \eta'$
809	N(1440) + $\bar{\text{N}}$	$\leftrightarrow$	$\rho + a_1 + a_1$
810	N(1440) + $\bar{\text{N}}$	$\leftrightarrow$	$\omega + \omega + \omega$
811	N(1440) + $\bar{\text{N}}$	$\leftrightarrow$	$\omega + \omega + \phi$
812	N(1440) + $\bar{\text{N}}$	$\leftrightarrow$	$\omega + \omega + \eta'$
813	N(1440) + $\bar{\text{N}}$	$\leftrightarrow$	$\omega + \phi + \phi$
814	N(1440) + $\bar{\text{N}}$	$\leftrightarrow$	$\omega + \phi + \eta'$
815	N(1440) + $\bar{\text{N}}$	$\leftrightarrow$	$\omega + \eta' + \eta'$
816	N(1440) + $\bar{\text{N}}$	$\leftrightarrow$	$\omega + a_1 + a_1$
817	N(1440) + $\bar{\text{N}}$	$\leftrightarrow$	$\phi + \phi + \phi$
818	N(1440) + $\bar{\text{N}}$	$\leftrightarrow$	$\phi + \phi + \eta'$
819	N(1440) + $\bar{\text{N}}$	$\leftrightarrow$	$\phi + \eta' + \eta'$
820	N(1440) + $\bar{\text{N}}$	$\leftrightarrow$	$\phi + a_1 + a_1$
821	N(1440) + $\bar{\text{N}}$	$\leftrightarrow$	$\eta' + \eta' + \eta'$
822	N(1440) + $\bar{\text{N}}$	$\leftrightarrow$	$\eta' + a_1 + a_1$
823	N(1440) + $\bar{\Delta}$(1232)	$\leftrightarrow$	$\pi + \pi + \pi$
824	N(1440) + $\bar{\Delta}$(1232)	$\leftrightarrow$	$\pi + \pi + \eta$
825	N(1440) + $\bar{\Delta}$(1232)	$\leftrightarrow$	$\pi + \pi + \rho$
826	N(1440) + $\bar{\Delta}$(1232)	$\leftrightarrow$	$\pi + \pi + \omega$
827	N(1440) + $\bar{\Delta}$(1232)	$\leftrightarrow$	$\pi + \pi + \phi$
828	N(1440) + $\bar{\Delta}$(1232)	$\leftrightarrow$	$\pi + \pi + \eta'$
829	N(1440) + $\bar{\Delta}$(1232)	$\leftrightarrow$	$\pi + \eta + \eta$
830	N(1440) + $\bar{\Delta}$(1232)	$\leftrightarrow$	$\pi + \eta + \rho$
831	N(1440) + $\bar{\Delta}$(1232)	$\leftrightarrow$	$\pi + \eta + \omega$
832	N(1440) + $\bar{\Delta}$(1232)	$\leftrightarrow$	$\pi + \eta + \phi$
833	N(1440) + $\bar{\Delta}$(1232)	$\leftrightarrow$	$\pi + \eta + \eta'$
834	N(1440) + $\bar{\Delta}$(1232)	$\leftrightarrow$	$\pi + \rho + \rho$
835	N(1440) + $\bar{\Delta}$(1232)	$\leftrightarrow$	$\pi + \rho + \omega$
836	N(1440) + $\bar{\Delta}$(1232)	$\leftrightarrow$	$\pi + \rho + \phi$
837	N(1440) + $\bar{\Delta}$(1232)	$\leftrightarrow$	$\pi + \rho + \eta'$
838	N(1440) + $\bar{\Delta}$(1232)	$\leftrightarrow$	$\pi + \omega + \omega$
839	N(1440) + $\bar{\Delta}$(1232)	$\leftrightarrow$	$\pi + \omega + \phi$
840	N(1440) + $\bar{\Delta}$(1232)	$\leftrightarrow$	$\pi + \omega + \eta'$
841	N(1440) + $\bar{\Delta}$(1232)	$\leftrightarrow$	$\pi + \phi + \phi$
842	N(1440) + $\bar{\Delta}$(1232)	$\leftrightarrow$	$\pi + \phi + \eta'$
843	N(1440) + $\bar{\Delta}$(1232)	$\leftrightarrow$	$\pi + \eta' + \eta'$
844	N(1440) + $\bar{\Delta}$(1232)	$\leftrightarrow$	$\pi + a_1 + a_1$
845	N(1440) + $\bar{\Delta}$(1232)	$\leftrightarrow$	$\eta + \eta + \eta$
846	N(1440) + $\bar{\Delta}$(1232)	$\leftrightarrow$	$\eta + \eta + \rho$
847	N(1440) + $\bar{\Delta}$(1232)	$\leftrightarrow$	$\eta + \eta + \omega$
848	N(1440) + $\bar{\Delta}$(1232)	$\leftrightarrow$	$\eta + \eta + \phi$
849	N(1440) + $\bar{\Delta}$(1232)	$\leftrightarrow$	$\eta + \eta + \eta'$
850	N(1440) + $\bar{\Delta}$(1232)	$\leftrightarrow$	$\eta + \rho + \rho$
851	N(1440) + $\bar{\Delta}$(1232)	$\leftrightarrow$	$\eta + \rho + \omega$
852	N(1440) + $\bar{\Delta}$(1232)	$\leftrightarrow$	$\eta + \rho + \phi$
853	N(1440) + $\bar{\Delta}$(1232)	$\leftrightarrow$	$\eta + \rho + \eta'$
854	N(1440) + $\bar{\Delta}$(1232)	$\leftrightarrow$	$\eta + \omega + \omega$
855	N(1440) + $\bar{\Delta}$(1232)	$\leftrightarrow$	$\eta + \omega + \phi$
856	N(1440) + $\bar{\Delta}$(1232)	$\leftrightarrow$	$\eta + \omega + \eta'$
857	N(1440) + $\bar{\Delta}$(1232)	$\leftrightarrow$	$\eta + \phi + \phi$
858	N(1440) + $\bar{\Delta}$(1232)	$\leftrightarrow$	$\eta + \phi + \eta'$
859	N(1440) + $\bar{\Delta}$(1232)	$\leftrightarrow$	$\eta + \eta' + \eta'$
860	N(1440) + $\bar{\Delta}$(1232)	$\leftrightarrow$	$\eta + a_1 + a_1$
861	N(1440) + $\bar{\Delta}$(1232)	$\leftrightarrow$	$\rho + \rho + \rho$
862	N(1440) + $\bar{\Delta}$(1232)	$\leftrightarrow$	$\rho + \rho + \omega$
863	N(1440) + $\bar{\Delta}$(1232)	$\leftrightarrow$	$\rho + \rho + \phi$
864	N(1440) + $\bar{\Delta}$(1232)	$\leftrightarrow$	$\rho + \rho + \eta'$
865	N(1440) + $\bar{\Delta}$(1232)	$\leftrightarrow$	$\rho + \omega + \omega$
866	N(1440) + $\bar{\Delta}$(1232)	$\leftrightarrow$	$\rho + \omega + \phi$
867	N(1440) + $\bar{\Delta}$(1232)	$\leftrightarrow$	$\rho + \omega + \eta'$
868	N(1440) + $\bar{\Delta}$(1232)	$\leftrightarrow$	$\rho + \phi + \phi$
869	N(1440) + $\bar{\Delta}$(1232)	$\leftrightarrow$	$\rho + \phi + \eta'$
870	N(1440) + $\bar{\Delta}$(1232)	$\leftrightarrow$	$\rho + \eta' + \eta'$
871	N(1440) + $\bar{\Delta}$(1232)	$\leftrightarrow$	$\rho + a_1 + a_1$
872	N(1440) + $\bar{\Delta}$(1232)	$\leftrightarrow$	$\omega + \omega + \omega$
873	N(1440) + $\bar{\Delta}$(1232)	$\leftrightarrow$	$\omega + \omega + \phi$
874	N(1440) + $\bar{\Delta}$(1232)	$\leftrightarrow$	$\omega + \omega + \eta'$
875	N(1440) + $\bar{\Delta}$(1232)	$\leftrightarrow$	$\omega + \phi + \phi$
876	N(1440) + $\bar{\Delta}$(1232)	$\leftrightarrow$	$\omega + \phi + \eta'$
877	N(1440) + $\bar{\Delta}$(1232)	$\leftrightarrow$	$\omega + \eta' + \eta'$
878	N(1440) + $\bar{\Delta}$(1232)	$\leftrightarrow$	$\omega + a_1 + a_1$
879	N(1440) + $\bar{\Delta}$(1232)	$\leftrightarrow$	$\phi + \phi + \phi$
880	N(1440) + $\bar{\Delta}$(1232)	$\leftrightarrow$	$\phi + \phi + \eta'$

Ch. No.	B_1 + B_2	$\leftrightarrow$	M_1+M_2+M_3
881	N(1440) + $\bar{\Delta}$(1232)	$\leftrightarrow$	$\phi + \eta' + \eta'$
882	N(1440) + $\bar{\Delta}$(1232)	$\leftrightarrow$	$\phi + a_1 + a_1$
883	N(1440) + $\bar{\Delta}$(1232)	$\leftrightarrow$	$\eta' + \eta' + \eta'$
884	N(1440) + $\bar{\Delta}$(1232)	$\leftrightarrow$	$\eta' + a_1 + a_1$
885	N(1440) + $\bar{\text{N}}$(1440)	$\leftrightarrow$	$\pi + \pi + \pi$
886	N(1440) + $\bar{\text{N}}$(1440)	$\leftrightarrow$	$\pi + \pi + \eta$
887	N(1440) + $\bar{\text{N}}$(1440)	$\leftrightarrow$	$\pi + \pi + \rho$
888	N(1440) + $\bar{\text{N}}$(1440)	$\leftrightarrow$	$\pi + \pi + \omega$
889	N(1440) + $\bar{\text{N}}$(1440)	$\leftrightarrow$	$\pi + \pi + \phi$
890	N(1440) + $\bar{\text{N}}$(1440)	$\leftrightarrow$	$\pi + \pi + \eta'$
891	N(1440) + $\bar{\text{N}}$(1440)	$\leftrightarrow$	$\pi + \eta + \eta$
892	N(1440) + $\bar{\text{N}}$(1440)	$\leftrightarrow$	$\pi + \eta + \rho$
893	N(1440) + $\bar{\text{N}}$(1440)	$\leftrightarrow$	$\pi + \eta + \omega$
894	N(1440) + $\bar{\text{N}}$(1440)	$\leftrightarrow$	$\pi + \eta + \phi$
895	N(1440) + $\bar{\text{N}}$(1440)	$\leftrightarrow$	$\pi + \eta + \eta'$
896	N(1440) + $\bar{\text{N}}$(1440)	$\leftrightarrow$	$\pi + \rho + \rho$
897	N(1440) + $\bar{\text{N}}$(1440)	$\leftrightarrow$	$\pi + \rho + \omega$
898	N(1440) + $\bar{\text{N}}$(1440)	$\leftrightarrow$	$\pi + \rho + \phi$
899	N(1440) + $\bar{\text{N}}$(1440)	$\leftrightarrow$	$\pi + \rho + \eta'$
900	N(1440) + $\bar{\text{N}}$(1440)	$\leftrightarrow$	$\pi + \omega + \omega$
901	N(1440) + $\bar{\text{N}}$(1440)	$\leftrightarrow$	$\pi + \omega + \phi$
902	N(1440) + $\bar{\text{N}}$(1440)	$\leftrightarrow$	$\pi + \omega + \eta'$
903	N(1440) + $\bar{\text{N}}$(1440)	$\leftrightarrow$	$\pi + \phi + \phi$
904	N(1440) + $\bar{\text{N}}$(1440)	$\leftrightarrow$	$\pi + \phi + \eta'$
905	N(1440) + $\bar{\text{N}}$(1440)	$\leftrightarrow$	$\pi + \eta' + \eta'$
906	N(1440) + $\bar{\text{N}}$(1440)	$\leftrightarrow$	$\pi + a_1 + a_1$
907	N(1440) + $\bar{\text{N}}$(1440)	$\leftrightarrow$	$\eta + \eta + \eta$
908	N(1440) + $\bar{\text{N}}$(1440)	$\leftrightarrow$	$\eta + \eta + \rho$
909	N(1440) + $\bar{\text{N}}$(1440)	$\leftrightarrow$	$\eta + \eta + \omega$
910	N(1440) + $\bar{\text{N}}$(1440)	$\leftrightarrow$	$\eta + \eta + \phi$
911	N(1440) + $\bar{\text{N}}$(1440)	$\leftrightarrow$	$\eta + \eta + \eta'$
912	N(1440) + $\bar{\text{N}}$(1440)	$\leftrightarrow$	$\eta + \rho + \rho$
913	N(1440) + $\bar{\text{N}}$(1440)	$\leftrightarrow$	$\eta + \rho + \omega$
914	N(1440) + $\bar{\text{N}}$(1440)	$\leftrightarrow$	$\eta + \rho + \phi$
915	N(1440) + $\bar{\text{N}}$(1440)	$\leftrightarrow$	$\eta + \rho + \eta'$
916	N(1440) + $\bar{\text{N}}$(1440)	$\leftrightarrow$	$\eta + \omega + \omega$
917	N(1440) + $\bar{\text{N}}$(1440)	$\leftrightarrow$	$\eta + \omega + \phi$
918	N(1440) + $\bar{\text{N}}$(1440)	$\leftrightarrow$	$\eta + \omega + \eta'$
919	N(1440) + $\bar{\text{N}}$(1440)	$\leftrightarrow$	$\eta + \phi + \phi$
920	N(1440) + $\bar{\text{N}}$(1440)	$\leftrightarrow$	$\eta + \phi + \eta'$
921	N(1440) + $\bar{\text{N}}$(1440)	$\leftrightarrow$	$\eta + \eta' + \eta'$
922	N(1440) + $\bar{\text{N}}$(1440)	$\leftrightarrow$	$\eta + a_1 + a_1$
923	N(1440) + $\bar{\text{N}}$(1440)	$\leftrightarrow$	$\rho + \rho + \rho$
924	N(1440) + $\bar{\text{N}}$(1440)	$\leftrightarrow$	$\rho + \rho + \omega$
925	N(1440) + $\bar{\text{N}}$(1440)	$\leftrightarrow$	$\rho + \rho + \phi$
926	N(1440) + $\bar{\text{N}}$(1440)	$\leftrightarrow$	$\rho + \rho + \eta'$
927	N(1440) + $\bar{\text{N}}$(1440)	$\leftrightarrow$	$\rho + \omega + \omega$
928	N(1440) + $\bar{\text{N}}$(1440)	$\leftrightarrow$	$\rho + \omega + \phi$
929	N(1440) + $\bar{\text{N}}$(1440)	$\leftrightarrow$	$\rho + \omega + \eta'$
930	N(1440) + $\bar{\text{N}}$(1440)	$\leftrightarrow$	$\rho + \phi + \phi$
931	N(1440) + $\bar{\text{N}}$(1440)	$\leftrightarrow$	$\rho + \phi + \eta'$
932	N(1440) + $\bar{\text{N}}$(1440)	$\leftrightarrow$	$\rho + \eta' + \eta'$
933	N(1440) + $\bar{\text{N}}$(1440)	$\leftrightarrow$	$\rho + a_1 + a_1$
934	N(1440) + $\bar{\text{N}}$(1440)	$\leftrightarrow$	$\omega + \omega + \omega$
935	N(1440) + $\bar{\text{N}}$(1440)	$\leftrightarrow$	$\omega + \omega + \phi$
936	N(1440) + $\bar{\text{N}}$(1440)	$\leftrightarrow$	$\omega + \omega + \eta'$
937	N(1440) + $\bar{\text{N}}$(1440)	$\leftrightarrow$	$\omega + \phi + \phi$
938	N(1440) + $\bar{\text{N}}$(1440)	$\leftrightarrow$	$\omega + \phi + \eta'$
939	N(1440) + $\bar{\text{N}}$(1440)	$\leftrightarrow$	$\omega + \eta' + \eta'$
940	N(1440) + $\bar{\text{N}}$(1440)	$\leftrightarrow$	$\omega + a_1 + a_1$
941	N(1440) + $\bar{\text{N}}$(1440)	$\leftrightarrow$	$\phi + \phi + \phi$
942	N(1440) + $\bar{\text{N}}$(1440)	$\leftrightarrow$	$\phi + \phi + \eta'$
943	N(1440) + $\bar{\text{N}}$(1440)	$\leftrightarrow$	$\phi + \eta' + \eta'$
944	N(1440) + $\bar{\text{N}}$(1440)	$\leftrightarrow$	$\phi + a_1 + a_1$
945	N(1440) + $\bar{\text{N}}$(1440)	$\leftrightarrow$	$\eta' + \eta' + \eta'$
946	N(1440) + $\bar{\text{N}}$(1440)	$\leftrightarrow$	$\eta' + a_1 + a_1$
947	N(1440) + $\bar{\text{N}}$(1535)	$\leftrightarrow$	$\pi + \pi + a_1$
948	N(1440) + $\bar{\text{N}}$(1535)	$\leftrightarrow$	$\pi + \eta + a_1$
949	N(1440) + $\bar{\text{N}}$(1535)	$\leftrightarrow$	$\pi + \rho + a_1$
950	N(1440) + $\bar{\text{N}}$(1535)	$\leftrightarrow$	$\pi + \omega + a_1$
951	N(1440) + $\bar{\text{N}}$(1535)	$\leftrightarrow$	$\pi + \phi + a_1$
952	N(1440) + $\bar{\text{N}}$(1535)	$\leftrightarrow$	$\pi + \eta' + a_1$
953	N(1440) + $\bar{\text{N}}$(1535)	$\leftrightarrow$	$\eta + \eta + a_1$
954	N(1440) + $\bar{\text{N}}$(1535)	$\leftrightarrow$	$\eta + \rho + a_1$
955	N(1440) + $\bar{\text{N}}$(1535)	$\leftrightarrow$	$\eta + \omega + a_1$
956	N(1440) + $\bar{\text{N}}$(1535)	$\leftrightarrow$	$\eta + \phi + a_1$
957	N(1440) + $\bar{\text{N}}$(1535)	$\leftrightarrow$	$\eta + \eta' + a_1$
958	N(1440) + $\bar{\text{N}}$(1535)	$\leftrightarrow$	$\rho + \rho + a_1$
959	N(1440) + $\bar{\text{N}}$(1535)	$\leftrightarrow$	$\rho + \omega + a_1$
960	N(1440) + $\bar{\text{N}}$(1535)	$\leftrightarrow$	$\rho + \phi + a_1$
961	N(1440) + $\bar{\text{N}}$(1535)	$\leftrightarrow$	$\rho + \eta' + a_1$
962	N(1440) + $\bar{\text{N}}$(1535)	$\leftrightarrow$	$\omega + \omega + a_1$
963	N(1440) + $\bar{\text{N}}$(1535)	$\leftrightarrow$	$\omega + \phi + a_1$
964	N(1440) + $\bar{\text{N}}$(1535)	$\leftrightarrow$	$\omega + \eta' + a_1$
965	N(1440) + $\bar{\text{N}}$(1535)	$\leftrightarrow$	$\phi + \phi + a_1$
966	N(1440) + $\bar{\text{N}}$(1535)	$\leftrightarrow$	$\phi + \eta' + a_1$

Ch. No.	$B_1 + B_2$	$\leftrightarrow$	$M_1+M_2+M_3$
967	$N(1440) + \bar{N}(1535)$	$\leftrightarrow$	$\eta' + \eta' + a_1$
968	$N(1440) + \bar{N}(1535)$	$\leftrightarrow$	$a_1 + a_1 + a_1$
969	$N(1440) + \bar{\Lambda}$	$\leftrightarrow$	$\pi + \pi + K$
970	$N(1440) + \bar{\Lambda}$	$\leftrightarrow$	$\pi + \pi + K^*$
971	$N(1440) + \bar{\Lambda}$	$\leftrightarrow$	$\pi + \eta + K$
972	$N(1440) + \bar{\Lambda}$	$\leftrightarrow$	$\pi + \eta + K^*$
973	$N(1440) + \bar{\Lambda}$	$\leftrightarrow$	$\pi + K + \rho$
974	$N(1440) + \bar{\Lambda}$	$\leftrightarrow$	$\pi + K + \omega$
975	$N(1440) + \bar{\Lambda}$	$\leftrightarrow$	$\pi + K + \phi$
976	$N(1440) + \bar{\Lambda}$	$\leftrightarrow$	$\pi + K + \eta'$
977	$N(1440) + \bar{\Lambda}$	$\leftrightarrow$	$\pi + K^* + \rho$
978	$N(1440) + \bar{\Lambda}$	$\leftrightarrow$	$\pi + K^* + \omega$
979	$N(1440) + \bar{\Lambda}$	$\leftrightarrow$	$\pi + K^* + \phi$
980	$N(1440) + \bar{\Lambda}$	$\leftrightarrow$	$\pi + K^* + \eta'$
981	$N(1440) + \bar{\Lambda}$	$\leftrightarrow$	$\eta + \eta + K$
982	$N(1440) + \bar{\Lambda}$	$\leftrightarrow$	$\eta + \eta + K^*$
983	$N(1440) + \bar{\Lambda}$	$\leftrightarrow$	$\eta + K + \rho$
984	$N(1440) + \bar{\Lambda}$	$\leftrightarrow$	$\eta + K + \omega$
985	$N(1440) + \bar{\Lambda}$	$\leftrightarrow$	$\eta + K + \phi$
986	$N(1440) + \bar{\Lambda}$	$\leftrightarrow$	$\eta + K + \eta'$
987	$N(1440) + \bar{\Lambda}$	$\leftrightarrow$	$\eta + K^* + \rho$
988	$N(1440) + \bar{\Lambda}$	$\leftrightarrow$	$\eta + K^* + \omega$
989	$N(1440) + \bar{\Lambda}$	$\leftrightarrow$	$\eta + K^* + \phi$
990	$N(1440) + \bar{\Lambda}$	$\leftrightarrow$	$\eta + K^* + \eta'$
991	$N(1440) + \bar{\Lambda}$	$\leftrightarrow$	$K + \rho + \rho$
992	$N(1440) + \bar{\Lambda}$	$\leftrightarrow$	$K + \rho + \omega$
993	$N(1440) + \bar{\Lambda}$	$\leftrightarrow$	$K + \rho + \phi$
994	$N(1440) + \bar{\Lambda}$	$\leftrightarrow$	$K + \rho + \eta'$
995	$N(1440) + \bar{\Lambda}$	$\leftrightarrow$	$K + \omega + \omega$
996	$N(1440) + \bar{\Lambda}$	$\leftrightarrow$	$K + \omega + \phi$
997	$N(1440) + \bar{\Lambda}$	$\leftrightarrow$	$K + \omega + \eta'$
998	$N(1440) + \bar{\Lambda}$	$\leftrightarrow$	$K + \phi + \phi$
999	$N(1440) + \bar{\Lambda}$	$\leftrightarrow$	$K + \phi + \eta'$
1000	$N(1440) + \bar{\Lambda}$	$\leftrightarrow$	$K + \eta' + \eta'$
1001	$N(1440) + \bar{\Lambda}$	$\leftrightarrow$	$K + a_1 + a_1$
1002	$N(1440) + \bar{\Lambda}$	$\leftrightarrow$	$K^* + \rho + \rho$
1003	$N(1440) + \bar{\Lambda}$	$\leftrightarrow$	$K^* + \rho + \omega$
1004	$N(1440) + \bar{\Lambda}$	$\leftrightarrow$	$K^* + \rho + \phi$
1005	$N(1440) + \bar{\Lambda}$	$\leftrightarrow$	$K^* + \rho + \eta'$
1006	$N(1440) + \bar{\Lambda}$	$\leftrightarrow$	$K^* + \omega + \omega$
1007	$N(1440) + \bar{\Lambda}$	$\leftrightarrow$	$K^* + \omega + \phi$
1008	$N(1440) + \bar{\Lambda}$	$\leftrightarrow$	$K^* + \omega + \eta'$
1009	$N(1440) + \bar{\Lambda}$	$\leftrightarrow$	$K^* + \phi + \phi$
1010	$N(1440) + \bar{\Lambda}$	$\leftrightarrow$	$K^* + \phi + \eta'$
1011	$N(1440) + \bar{\Lambda}$	$\leftrightarrow$	$K^* + \eta' + \eta'$
1012	$N(1440) + \bar{\Lambda}$	$\leftrightarrow$	$K^* + a_1 + a_1$
1013	$N(1440) + \bar{\Sigma}$	$\leftrightarrow$	$\pi + \pi + K$
1014	$N(1440) + \bar{\Sigma}$	$\leftrightarrow$	$\pi + \pi + K^*$
1015	$N(1440) + \bar{\Sigma}$	$\leftrightarrow$	$\pi + \eta + K$
1016	$N(1440) + \bar{\Sigma}$	$\leftrightarrow$	$\pi + \eta + K^*$
1017	$N(1440) + \bar{\Sigma}$	$\leftrightarrow$	$\pi + K + \rho$
1018	$N(1440) + \bar{\Sigma}$	$\leftrightarrow$	$\pi + K + \omega$
1019	$N(1440) + \bar{\Sigma}$	$\leftrightarrow$	$\pi + K + \phi$
1020	$N(1440) + \bar{\Sigma}$	$\leftrightarrow$	$\pi + K + \eta'$
1021	$N(1440) + \bar{\Sigma}$	$\leftrightarrow$	$\pi + K^* + \rho$
1022	$N(1440) + \bar{\Sigma}$	$\leftrightarrow$	$\pi + K^* + \omega$
1023	$N(1440) + \bar{\Sigma}$	$\leftrightarrow$	$\pi + K^* + \phi$
1024	$N(1440) + \bar{\Sigma}$	$\leftrightarrow$	$\pi + K^* + \eta'$
1025	$N(1440) + \bar{\Sigma}$	$\leftrightarrow$	$\eta + \eta + K$
1026	$N(1440) + \bar{\Sigma}$	$\leftrightarrow$	$\eta + \eta + K^*$
1027	$N(1440) + \bar{\Sigma}$	$\leftrightarrow$	$\eta + K + \rho$
1028	$N(1440) + \bar{\Sigma}$	$\leftrightarrow$	$\eta + K + \omega$
1029	$N(1440) + \bar{\Sigma}$	$\leftrightarrow$	$\eta + K + \phi$
1030	$N(1440) + \bar{\Sigma}$	$\leftrightarrow$	$\eta + K + \eta'$
1031	$N(1440) + \bar{\Sigma}$	$\leftrightarrow$	$\eta + K^* + \rho$
1032	$N(1440) + \bar{\Sigma}$	$\leftrightarrow$	$\eta + K^* + \omega$
1033	$N(1440) + \bar{\Sigma}$	$\leftrightarrow$	$\eta + K^* + \phi$
1034	$N(1440) + \bar{\Sigma}$	$\leftrightarrow$	$\eta + K^* + \eta'$
1035	$N(1440) + \bar{\Sigma}$	$\leftrightarrow$	$K + \rho + \rho$
1036	$N(1440) + \bar{\Sigma}$	$\leftrightarrow$	$K + \rho + \omega$
1037	$N(1440) + \bar{\Sigma}$	$\leftrightarrow$	$K + \rho + \phi$
1038	$N(1440) + \bar{\Sigma}$	$\leftrightarrow$	$K + \rho + \eta'$
1039	$N(1440) + \bar{\Sigma}$	$\leftrightarrow$	$K + \omega + \omega$
1040	$N(1440) + \bar{\Sigma}$	$\leftrightarrow$	$K + \omega + \phi$
1041	$N(1440) + \bar{\Sigma}$	$\leftrightarrow$	$K + \omega + \eta'$
1042	$N(1440) + \bar{\Sigma}$	$\leftrightarrow$	$K + \phi + \phi$
1043	$N(1440) + \bar{\Sigma}$	$\leftrightarrow$	$K + \phi + \eta'$
1044	$N(1440) + \bar{\Sigma}$	$\leftrightarrow$	$K + \eta' + \eta'$
1045	$N(1440) + \bar{\Sigma}$	$\leftrightarrow$	$K + a_1 + a_1$
1046	$N(1440) + \bar{\Sigma}$	$\leftrightarrow$	$K^* + \rho + \rho$
1047	$N(1440) + \bar{\Sigma}$	$\leftrightarrow$	$K^* + \rho + \omega$
1048	$N(1440) + \bar{\Sigma}$	$\leftrightarrow$	$K^* + \rho + \phi$
1049	$N(1440) + \bar{\Sigma}$	$\leftrightarrow$	$K^* + \rho + \eta'$
1050	$N(1440) + \bar{\Sigma}$	$\leftrightarrow$	$K^* + \omega + \omega$
1051	$N(1440) + \bar{\Sigma}$	$\leftrightarrow$	$K^* + \omega + \phi$
1052	$N(1440) + \bar{\Sigma}$	$\leftrightarrow$	$K^* + \omega + \eta'$

Ch. No.	$B_1 + B_2$	$\leftrightarrow$	$M_1+M_2+M_3$
1053	$N(1440) + \bar{\Sigma}$	$\leftrightarrow$	$K^* + \phi + \phi$
1054	$N(1440) + \bar{\Sigma}$	$\leftrightarrow$	$K^* + \phi + \eta'$
1055	$N(1440) + \bar{\Sigma}$	$\leftrightarrow$	$K^* + \eta' + \eta'$
1056	$N(1440) + \bar{\Sigma}$	$\leftrightarrow$	$K^* + a_1 + a_1$
1057	$N(1440) + \bar{\Sigma}^*$	$\leftrightarrow$	$\pi + \pi + K$
1058	$N(1440) + \bar{\Sigma}^*$	$\leftrightarrow$	$\pi + \pi + K^*$
1059	$N(1440) + \bar{\Sigma}^*$	$\leftrightarrow$	$\pi + \eta + K$
1060	$N(1440) + \bar{\Sigma}^*$	$\leftrightarrow$	$\pi + \eta + K^*$
1061	$N(1440) + \bar{\Sigma}^*$	$\leftrightarrow$	$\pi + K + \rho$
1062	$N(1440) + \bar{\Sigma}^*$	$\leftrightarrow$	$\pi + K + \omega$
1063	$N(1440) + \bar{\Sigma}^*$	$\leftrightarrow$	$\pi + K + \phi$
1064	$N(1440) + \bar{\Sigma}^*$	$\leftrightarrow$	$\pi + K + \eta'$
1065	$N(1440) + \bar{\Sigma}^*$	$\leftrightarrow$	$\pi + K^* + \rho$
1066	$N(1440) + \bar{\Sigma}^*$	$\leftrightarrow$	$\pi + K^* + \omega$
1067	$N(1440) + \bar{\Sigma}^*$	$\leftrightarrow$	$\pi + K^* + \phi$
1068	$N(1440) + \bar{\Sigma}^*$	$\leftrightarrow$	$\pi + K^* + \eta'$
1069	$N(1440) + \bar{\Sigma}^*$	$\leftrightarrow$	$\eta + \eta + K$
1070	$N(1440) + \bar{\Sigma}^*$	$\leftrightarrow$	$\eta + \eta + K^*$
1071	$N(1440) + \bar{\Sigma}^*$	$\leftrightarrow$	$\eta + K + \rho$
1072	$N(1440) + \bar{\Sigma}^*$	$\leftrightarrow$	$\eta + K + \omega$
1073	$N(1440) + \bar{\Sigma}^*$	$\leftrightarrow$	$\eta + K + \phi$
1074	$N(1440) + \bar{\Sigma}^*$	$\leftrightarrow$	$\eta + K + \eta'$
1075	$N(1440) + \bar{\Sigma}^*$	$\leftrightarrow$	$\eta + K^* + \rho$
1076	$N(1440) + \bar{\Sigma}^*$	$\leftrightarrow$	$\eta + K^* + \omega$
1077	$N(1440) + \bar{\Sigma}^*$	$\leftrightarrow$	$\eta + K^* + \phi$
1078	$N(1440) + \bar{\Sigma}^*$	$\leftrightarrow$	$\eta + K^* + \eta'$
1079	$N(1440) + \bar{\Sigma}^*$	$\leftrightarrow$	$K + \rho + \rho$
1080	$N(1440) + \bar{\Sigma}^*$	$\leftrightarrow$	$K + \rho + \omega$
1081	$N(1440) + \bar{\Sigma}^*$	$\leftrightarrow$	$K + \rho + \phi$
1082	$N(1440) + \bar{\Sigma}^*$	$\leftrightarrow$	$K + \rho + \eta'$
1083	$N(1440) + \bar{\Sigma}^*$	$\leftrightarrow$	$K + \omega + \omega$
1084	$N(1440) + \bar{\Sigma}^*$	$\leftrightarrow$	$K + \omega + \phi$
1085	$N(1440) + \bar{\Sigma}^*$	$\leftrightarrow$	$K + \omega + \eta'$
1086	$N(1440) + \bar{\Sigma}^*$	$\leftrightarrow$	$K + \phi + \phi$
1087	$N(1440) + \bar{\Sigma}^*$	$\leftrightarrow$	$K + \phi + \eta'$
1088	$N(1440) + \bar{\Sigma}^*$	$\leftrightarrow$	$K + \eta' + \eta'$
1089	$N(1440) + \bar{\Sigma}^*$	$\leftrightarrow$	$K + a_1 + a_1$
1090	$N(1440) + \bar{\Sigma}^*$	$\leftrightarrow$	$K^* + \rho + \rho$
1091	$N(1440) + \bar{\Sigma}^*$	$\leftrightarrow$	$K^* + \rho + \omega$
1092	$N(1440) + \bar{\Sigma}^*$	$\leftrightarrow$	$K^* + \rho + \phi$
1093	$N(1440) + \bar{\Sigma}^*$	$\leftrightarrow$	$K^* + \rho + \eta'$
1094	$N(1440) + \bar{\Sigma}^*$	$\leftrightarrow$	$K^* + \omega + \omega$
1095	$N(1440) + \bar{\Sigma}^*$	$\leftrightarrow$	$K^* + \omega + \phi$
1096	$N(1440) + \bar{\Sigma}^*$	$\leftrightarrow$	$K^* + \omega + \eta'$
1097	$N(1440) + \bar{\Sigma}^*$	$\leftrightarrow$	$K^* + \phi + \phi$
1098	$N(1440) + \bar{\Sigma}^*$	$\leftrightarrow$	$K^* + \phi + \eta'$
1099	$N(1440) + \bar{\Sigma}^*$	$\leftrightarrow$	$K^* + \eta' + \eta'$
1100	$N(1440) + \bar{\Sigma}^*$	$\leftrightarrow$	$K^* + a_1 + a_1$
1101	$N(1440) + \bar{\Xi}$	$\leftrightarrow$	$\pi + K + K$
1102	$N(1440) + \bar{\Xi}$	$\leftrightarrow$	$\pi + K + K^*$
1103	$N(1440) + \bar{\Xi}$	$\leftrightarrow$	$\pi + K^* + K^*$
1104	$N(1440) + \bar{\Xi}$	$\leftrightarrow$	$\eta + K + K$
1105	$N(1440) + \bar{\Xi}$	$\leftrightarrow$	$\eta + K + K^*$
1106	$N(1440) + \bar{\Xi}$	$\leftrightarrow$	$\eta + K^* + K^*$
1107	$N(1440) + \bar{\Xi}$	$\leftrightarrow$	$K + K + \rho$
1108	$N(1440) + \bar{\Xi}$	$\leftrightarrow$	$K + K + \omega$
1109	$N(1440) + \bar{\Xi}$	$\leftrightarrow$	$K + K + \phi$
1110	$N(1440) + \bar{\Xi}$	$\leftrightarrow$	$K + K + \eta'$
1111	$N(1440) + \bar{\Xi}$	$\leftrightarrow$	$K + K^* + \rho$
1112	$N(1440) + \bar{\Xi}$	$\leftrightarrow$	$K + K^* + \omega$
1113	$N(1440) + \bar{\Xi}$	$\leftrightarrow$	$K + K^* + \phi$
1114	$N(1440) + \bar{\Xi}$	$\leftrightarrow$	$K + K^* + \eta'$
1115	$N(1440) + \bar{\Xi}$	$\leftrightarrow$	$K^* + K^* + \rho$
1116	$N(1440) + \bar{\Xi}$	$\leftrightarrow$	$K^* + K^* + \omega$
1117	$N(1440) + \bar{\Xi}$	$\leftrightarrow$	$K^* + K^* + \phi$
1118	$N(1440) + \bar{\Xi}$	$\leftrightarrow$	$K^* + K^* + \eta'$
1119	$N(1440) + \bar{\Xi}^*$	$\leftrightarrow$	$\pi + K + K$
1120	$N(1440) + \bar{\Xi}^*$	$\leftrightarrow$	$\pi + K + K^*$
1121	$N(1440) + \bar{\Xi}^*$	$\leftrightarrow$	$\pi + K^* + K^*$
1122	$N(1440) + \bar{\Xi}^*$	$\leftrightarrow$	$\eta + K + K$
1123	$N(1440) + \bar{\Xi}^*$	$\leftrightarrow$	$\eta + K + K^*$
1124	$N(1440) + \bar{\Xi}^*$	$\leftrightarrow$	$\eta + K^* + K^*$
1125	$N(1440) + \bar{\Xi}^*$	$\leftrightarrow$	$K + K + \rho$
1126	$N(1440) + \bar{\Xi}^*$	$\leftrightarrow$	$K + K + \omega$
1127	$N(1440) + \bar{\Xi}^*$	$\leftrightarrow$	$K + K + \phi$
1128	$N(1440) + \bar{\Xi}^*$	$\leftrightarrow$	$K + K + \eta'$
1129	$N(1440) + \bar{\Xi}^*$	$\leftrightarrow$	$K + K^* + \rho$
1130	$N(1440) + \bar{\Xi}^*$	$\leftrightarrow$	$K + K^* + \omega$
1131	$N(1440) + \bar{\Xi}^*$	$\leftrightarrow$	$K + K^* + \phi$
1132	$N(1440) + \bar{\Xi}^*$	$\leftrightarrow$	$K + K^* + \eta'$
1133	$N(1440) + \bar{\Xi}^*$	$\leftrightarrow$	$K^* + K^* + \rho$
1134	$N(1440) + \bar{\Xi}^*$	$\leftrightarrow$	$K^* + K^* + \omega$
1135	$N(1440) + \bar{\Xi}^*$	$\leftrightarrow$	$K^* + K^* + \phi$
1136	$N(1440) + \bar{\Xi}^*$	$\leftrightarrow$	$K^* + K^* + \eta'$
1137	$N(1440) + \bar{\Omega}$	$\leftrightarrow$	$K + K + K$
1138	$N(1440) + \bar{\Omega}$	$\leftrightarrow$	$K + K + K^*$

Ch. No.	$B_1 + B_2$	$\leftrightarrow$	$M_1+M_2+M_3$
1139	$N(1440) + \Omega$	$\leftrightarrow$	$K + K^* + K^*$
1140	$N(1440) + \bar{\Omega}$	$\leftrightarrow$	$K^* + K^* + K^*$
1141	$N(1535) + \bar{N}$	$\leftrightarrow$	$\pi + \pi + a_1$
1142	$N(1535) + \bar{N}$	$\leftrightarrow$	$\pi + \eta + a_1$
1143	$N(1535) + \bar{N}$	$\leftrightarrow$	$\pi + \rho + a_1$
1144	$N(1535) + \bar{N}$	$\leftrightarrow$	$\pi + \omega + a_1$
1145	$N(1535) + \bar{N}$	$\leftrightarrow$	$\pi + \phi + a_1$
1146	$N(1535) + \bar{N}$	$\leftrightarrow$	$\pi + \eta' + a_1$
1147	$N(1535) + \bar{N}$	$\leftrightarrow$	$\eta + \eta + a_1$
1148	$N(1535) + \bar{N}$	$\leftrightarrow$	$\eta + \rho + a_1$
1149	$N(1535) + \bar{N}$	$\leftrightarrow$	$\eta + \omega + a_1$
1150	$N(1535) + \bar{N}$	$\leftrightarrow$	$\eta + \phi + a_1$
1151	$N(1535) + \bar{N}$	$\leftrightarrow$	$\eta + \eta' + a_1$
1152	$N(1535) + \bar{N}$	$\leftrightarrow$	$\rho + \rho + a_1$
1153	$N(1535) + \bar{N}$	$\leftrightarrow$	$\rho + \omega + a_1$
1154	$N(1535) + \bar{N}$	$\leftrightarrow$	$\rho + \phi + a_1$
1155	$N(1535) + \bar{N}$	$\leftrightarrow$	$\rho + \eta' + a_1$
1156	$N(1535) + \bar{N}$	$\leftrightarrow$	$\omega + \omega + a_1$
1157	$N(1535) + \bar{N}$	$\leftrightarrow$	$\omega + \phi + a_1$
1158	$N(1535) + \bar{N}$	$\leftrightarrow$	$\omega + \eta' + a_1$
1159	$N(1535) + \bar{N}$	$\leftrightarrow$	$\phi + \phi + a_1$
1160	$N(1535) + \bar{N}$	$\leftrightarrow$	$\phi + \eta' + a_1$
1161	$N(1535) + \bar{N}$	$\leftrightarrow$	$\eta' + \eta' + a_1$
1162	$N(1535) + \bar{N}$	$\leftrightarrow$	$a_1 + a_1 + a_1$
1163	$N(1535) + \bar{\Delta}(1232)$	$\leftrightarrow$	$\pi + \pi + a_1$
1164	$N(1535) + \bar{\Delta}(1232)$	$\leftrightarrow$	$\pi + \eta + a_1$
1165	$N(1535) + \bar{\Delta}(1232)$	$\leftrightarrow$	$\pi + \rho + a_1$
1166	$N(1535) + \bar{\Delta}(1232)$	$\leftrightarrow$	$\pi + \omega + a_1$
1167	$N(1535) + \bar{\Delta}(1232)$	$\leftrightarrow$	$\pi + \phi + a_1$
1168	$N(1535) + \bar{\Delta}(1232)$	$\leftrightarrow$	$\pi + \eta' + a_1$
1169	$N(1535) + \bar{\Delta}(1232)$	$\leftrightarrow$	$\eta + \eta + a_1$
1170	$N(1535) + \bar{\Delta}(1232)$	$\leftrightarrow$	$\eta + \rho + a_1$
1171	$N(1535) + \bar{\Delta}(1232)$	$\leftrightarrow$	$\eta + \omega + a_1$
1172	$N(1535) + \bar{\Delta}(1232)$	$\leftrightarrow$	$\eta + \phi + a_1$
1173	$N(1535) + \bar{\Delta}(1232)$	$\leftrightarrow$	$\eta + \eta' + a_1$
1174	$N(1535) + \bar{\Delta}(1232)$	$\leftrightarrow$	$\rho + \rho + a_1$
1175	$N(1535) + \bar{\Delta}(1232)$	$\leftrightarrow$	$\rho + \omega + a_1$
1176	$N(1535) + \bar{\Delta}(1232)$	$\leftrightarrow$	$\rho + \phi + a_1$
1177	$N(1535) + \bar{\Delta}(1232)$	$\leftrightarrow$	$\rho + \eta' + a_1$
1178	$N(1535) + \bar{\Delta}(1232)$	$\leftrightarrow$	$\omega + \omega + a_1$
1179	$N(1535) + \bar{\Delta}(1232)$	$\leftrightarrow$	$\omega + \phi + a_1$
1180	$N(1535) + \bar{\Delta}(1232)$	$\leftrightarrow$	$\omega + \eta' + a_1$
1181	$N(1535) + \bar{\Delta}(1232)$	$\leftrightarrow$	$\phi + \phi + a_1$
1182	$N(1535) + \bar{\Delta}(1232)$	$\leftrightarrow$	$\phi + \eta' + a_1$
1183	$N(1535) + \bar{\Delta}(1232)$	$\leftrightarrow$	$\eta' + \eta' + a_1$
1184	$N(1535) + \bar{\Delta}(1232)$	$\leftrightarrow$	$a_1 + a_1 + a_1$
1185	$N(1535) + \bar{N}(1440)$	$\leftrightarrow$	$\pi + \pi + a_1$
1186	$N(1535) + \bar{N}(1440)$	$\leftrightarrow$	$\pi + \eta + a_1$
1187	$N(1535) + \bar{N}(1440)$	$\leftrightarrow$	$\pi + \rho + a_1$
1188	$N(1535) + \bar{N}(1440)$	$\leftrightarrow$	$\pi + \omega + a_1$
1189	$N(1535) + \bar{N}(1440)$	$\leftrightarrow$	$\pi + \phi + a_1$
1190	$N(1535) + \bar{N}(1440)$	$\leftrightarrow$	$\pi + \eta' + a_1$
1191	$N(1535) + \bar{N}(1440)$	$\leftrightarrow$	$\eta + \eta + a_1$
1192	$N(1535) + \bar{N}(1440)$	$\leftrightarrow$	$\eta + \rho + a_1$
1193	$N(1535) + \bar{N}(1440)$	$\leftrightarrow$	$\eta + \omega + a_1$
1194	$N(1535) + \bar{N}(1440)$	$\leftrightarrow$	$\eta + \phi + a_1$
1195	$N(1535) + \bar{N}(1440)$	$\leftrightarrow$	$\eta + \eta' + a_1$
1196	$N(1535) + \bar{N}(1440)$	$\leftrightarrow$	$\rho + \rho + a_1$
1197	$N(1535) + \bar{N}(1440)$	$\leftrightarrow$	$\rho + \omega + a_1$
1198	$N(1535) + \bar{N}(1440)$	$\leftrightarrow$	$\rho + \phi + a_1$
1199	$N(1535) + \bar{N}(1440)$	$\leftrightarrow$	$\rho + \eta' + a_1$
1200	$N(1535) + \bar{N}(1440)$	$\leftrightarrow$	$\omega + \omega + a_1$
1201	$N(1535) + \bar{N}(1440)$	$\leftrightarrow$	$\omega + \phi + a_1$
1202	$N(1535) + \bar{N}(1440)$	$\leftrightarrow$	$\omega + \eta' + a_1$
1203	$N(1535) + \bar{N}(1440)$	$\leftrightarrow$	$\phi + \phi + a_1$
1204	$N(1535) + \bar{N}(1440)$	$\leftrightarrow$	$\phi + \eta' + a_1$
1205	$N(1535) + \bar{N}(1440)$	$\leftrightarrow$	$\eta' + \eta' + a_1$
1206	$N(1535) + \bar{N}(1440)$	$\leftrightarrow$	$a_1 + a_1 + a_1$
1207	$N(1535) + \bar{N}(1535)$	$\leftrightarrow$	$\pi + \pi + \pi$
1208	$N(1535) + \bar{N}(1535)$	$\leftrightarrow$	$\pi + \pi + \eta$
1209	$N(1535) + \bar{N}(1535)$	$\leftrightarrow$	$\pi + \pi + \rho$
1210	$N(1535) + \bar{N}(1535)$	$\leftrightarrow$	$\pi + \pi + \omega$
1211	$N(1535) + \bar{N}(1535)$	$\leftrightarrow$	$\pi + \pi + \phi$
1212	$N(1535) + \bar{N}(1535)$	$\leftrightarrow$	$\pi + \pi + \eta'$
1213	$N(1535) + \bar{N}(1535)$	$\leftrightarrow$	$\pi + \eta + \eta$
1214	$N(1535) + \bar{N}(1535)$	$\leftrightarrow$	$\pi + \eta + \rho$
1215	$N(1535) + \bar{N}(1535)$	$\leftrightarrow$	$\pi + \eta + \omega$
1216	$N(1535) + \bar{N}(1535)$	$\leftrightarrow$	$\pi + \eta + \phi$
1217	$N(1535) + \bar{N}(1535)$	$\leftrightarrow$	$\pi + \eta + \eta'$
1218	$N(1535) + \bar{N}(1535)$	$\leftrightarrow$	$\pi + \rho + \rho$
1219	$N(1535) + \bar{N}(1535)$	$\leftrightarrow$	$\pi + \rho + \omega$
1220	$N(1535) + \bar{N}(1535)$	$\leftrightarrow$	$\pi + \rho + \phi$
1221	$N(1535) + \bar{N}(1535)$	$\leftrightarrow$	$\pi + \rho + \eta'$
1222	$N(1535) + \bar{N}(1535)$	$\leftrightarrow$	$\pi + \omega + \omega$
1223	$N(1535) + \bar{N}(1535)$	$\leftrightarrow$	$\pi + \omega + \phi$
1224	$N(1535) + \bar{N}(1535)$	$\leftrightarrow$	$\pi + \omega + \eta'$

Ch. No.	$B_1 + B_2$	$\leftrightarrow$	$M_1+M_2+M_3$
1225	$N(1535) + \bar{N}(1535)$	$\leftrightarrow$	$\pi + \phi + \phi$
1226	$N(1535) + \bar{N}(1535)$	$\leftrightarrow$	$\pi + \phi + \eta'$
1227	$N(1535) + \bar{N}(1535)$	$\leftrightarrow$	$\pi + \eta' + \eta'$
1228	$N(1535) + \bar{N}(1535)$	$\leftrightarrow$	$\pi + a_1 + a_1$
1229	$N(1535) + \bar{N}(1535)$	$\leftrightarrow$	$\eta + \eta + \eta$
1230	$N(1535) + \bar{N}(1535)$	$\leftrightarrow$	$\eta + \eta + \rho$
1231	$N(1535) + \bar{N}(1535)$	$\leftrightarrow$	$\eta + \eta + \omega$
1232	$N(1535) + \bar{N}(1535)$	$\leftrightarrow$	$\eta + \eta + \phi$
1233	$N(1535) + \bar{N}(1535)$	$\leftrightarrow$	$\eta + \eta + \eta'$
1234	$N(1535) + \bar{N}(1535)$	$\leftrightarrow$	$\eta + \rho + \rho$
1235	$N(1535) + \bar{N}(1535)$	$\leftrightarrow$	$\eta + \rho + \omega$
1236	$N(1535) + \bar{N}(1535)$	$\leftrightarrow$	$\eta + \rho + \phi$
1237	$N(1535) + \bar{N}(1535)$	$\leftrightarrow$	$\eta + \rho + \eta'$
1238	$N(1535) + \bar{N}(1535)$	$\leftrightarrow$	$\eta + \omega + \omega$
1239	$N(1535) + \bar{N}(1535)$	$\leftrightarrow$	$\eta + \omega + \phi$
1240	$N(1535) + \bar{N}(1535)$	$\leftrightarrow$	$\eta + \omega + \eta'$
1241	$N(1535) + \bar{N}(1535)$	$\leftrightarrow$	$\eta + \phi + \phi$
1242	$N(1535) + \bar{N}(1535)$	$\leftrightarrow$	$\eta + \phi + \eta'$
1243	$N(1535) + \bar{N}(1535)$	$\leftrightarrow$	$\eta + \eta' + \eta'$
1244	$N(1535) + \bar{N}(1535)$	$\leftrightarrow$	$\eta + a_1 + a_1$
1245	$N(1535) + \bar{N}(1535)$	$\leftrightarrow$	$\rho + \rho + \rho$
1246	$N(1535) + \bar{N}(1535)$	$\leftrightarrow$	$\rho + \rho + \omega$
1247	$N(1535) + \bar{N}(1535)$	$\leftrightarrow$	$\rho + \rho + \phi$
1248	$N(1535) + \bar{N}(1535)$	$\leftrightarrow$	$\rho + \rho + \eta'$
1249	$N(1535) + \bar{N}(1535)$	$\leftrightarrow$	$\rho + \omega + \omega$
1250	$N(1535) + \bar{N}(1535)$	$\leftrightarrow$	$\rho + \omega + \phi$
1251	$N(1535) + \bar{N}(1535)$	$\leftrightarrow$	$\rho + \omega + \eta'$
1252	$N(1535) + \bar{N}(1535)$	$\leftrightarrow$	$\rho + \phi + \phi$
1253	$N(1535) + \bar{N}(1535)$	$\leftrightarrow$	$\rho + \phi + \eta'$
1254	$N(1535) + \bar{N}(1535)$	$\leftrightarrow$	$\rho + \eta' + \eta'$
1255	$N(1535) + \bar{N}(1535)$	$\leftrightarrow$	$\rho + a_1 + a_1$
1256	$N(1535) + \bar{N}(1535)$	$\leftrightarrow$	$\omega + \omega + \omega$
1257	$N(1535) + \bar{N}(1535)$	$\leftrightarrow$	$\omega + \omega + \phi$
1258	$N(1535) + \bar{N}(1535)$	$\leftrightarrow$	$\omega + \omega + \eta'$
1259	$N(1535) + \bar{N}(1535)$	$\leftrightarrow$	$\omega + \phi + \phi$
1260	$N(1535) + \bar{N}(1535)$	$\leftrightarrow$	$\omega + \phi + \eta'$
1261	$N(1535) + \bar{N}(1535)$	$\leftrightarrow$	$\omega + \eta' + \eta'$
1262	$N(1535) + \bar{N}(1535)$	$\leftrightarrow$	$\omega + a_1 + a_1$
1263	$N(1535) + \bar{N}(1535)$	$\leftrightarrow$	$\phi + \phi + \phi$
1264	$N(1535) + \bar{N}(1535)$	$\leftrightarrow$	$\phi + \phi + \eta'$
1265	$N(1535) + \bar{N}(1535)$	$\leftrightarrow$	$\phi + \eta' + \eta'$
1266	$N(1535) + \bar{N}(1535)$	$\leftrightarrow$	$\phi + a_1 + a_1$
1267	$N(1535) + \bar{N}(1535)$	$\leftrightarrow$	$\eta' + \eta' + \eta'$
1268	$N(1535) + \bar{N}(1535)$	$\leftrightarrow$	$\eta' + a_1 + a_1$
1269	$N(1535) + \bar{\Lambda}$	$\leftrightarrow$	$\pi + K + a_1$
1270	$N(1535) + \bar{\Lambda}$	$\leftrightarrow$	$\pi + K^* + a_1$
1271	$N(1535) + \bar{\Lambda}$	$\leftrightarrow$	$\eta + K + a_1$
1272	$N(1535) + \bar{\Lambda}$	$\leftrightarrow$	$\eta + K^* + a_1$
1273	$N(1535) + \bar{\Lambda}$	$\leftrightarrow$	$K + \rho + a_1$
1274	$N(1535) + \bar{\Lambda}$	$\leftrightarrow$	$K + \omega + a_1$
1275	$N(1535) + \bar{\Lambda}$	$\leftrightarrow$	$K + \phi + a_1$
1276	$N(1535) + \bar{\Lambda}$	$\leftrightarrow$	$K + \eta' + a_1$
1277	$N(1535) + \bar{\Lambda}$	$\leftrightarrow$	$K^* + \rho + a_1$
1278	$N(1535) + \bar{\Lambda}$	$\leftrightarrow$	$K^* + \omega + a_1$
1279	$N(1535) + \bar{\Lambda}$	$\leftrightarrow$	$K^* + \phi + a_1$
1280	$N(1535) + \bar{\Lambda}$	$\leftrightarrow$	$K^* + \eta' + a_1$
1281	$N(1535) + \bar{\Sigma}$	$\leftrightarrow$	$\pi + K + a_1$
1282	$N(1535) + \bar{\Sigma}$	$\leftrightarrow$	$\pi + K^* + a_1$
1283	$N(1535) + \bar{\Sigma}$	$\leftrightarrow$	$\eta + K + a_1$
1284	$N(1535) + \bar{\Sigma}$	$\leftrightarrow$	$\eta + K^* + a_1$
1285	$N(1535) + \bar{\Sigma}$	$\leftrightarrow$	$K + \rho + a_1$
1286	$N(1535) + \bar{\Sigma}$	$\leftrightarrow$	$K + \omega + a_1$
1287	$N(1535) + \bar{\Sigma}$	$\leftrightarrow$	$K + \phi + a_1$
1288	$N(1535) + \bar{\Sigma}$	$\leftrightarrow$	$K + \eta' + a_1$
1289	$N(1535) + \bar{\Sigma}$	$\leftrightarrow$	$K^* + \rho + a_1$
1290	$N(1535) + \bar{\Sigma}$	$\leftrightarrow$	$K^* + \omega + a_1$
1291	$N(1535) + \bar{\Sigma}$	$\leftrightarrow$	$K^* + \phi + a_1$
1292	$N(1535) + \bar{\Sigma}$	$\leftrightarrow$	$K^* + \eta' + a_1$
1293	$N(1535) + \bar{\Sigma}^*$	$\leftrightarrow$	$\pi + K + a_1$
1294	$N(1535) + \bar{\Sigma}^*$	$\leftrightarrow$	$\pi + K^* + a_1$
1295	$N(1535) + \bar{\Sigma}^*$	$\leftrightarrow$	$\eta + K + a_1$
1296	$N(1535) + \bar{\Sigma}^*$	$\leftrightarrow$	$\eta + K^* + a_1$
1297	$N(1535) + \bar{\Sigma}^*$	$\leftrightarrow$	$K + \rho + a_1$
1298	$N(1535) + \bar{\Sigma}^*$	$\leftrightarrow$	$K + \omega + a_1$
1299	$N(1535) + \bar{\Sigma}^*$	$\leftrightarrow$	$K + \phi + a_1$
1300	$N(1535) + \bar{\Sigma}^*$	$\leftrightarrow$	$K + \eta' + a_1$
1301	$N(1535) + \bar{\Sigma}^*$	$\leftrightarrow$	$K^* + \rho + a_1$
1302	$N(1535) + \bar{\Sigma}^*$	$\leftrightarrow$	$K^* + \omega + a_1$
1303	$N(1535) + \bar{\Sigma}^*$	$\leftrightarrow$	$K^* + \phi + a_1$
1304	$N(1535) + \bar{\Sigma}^*$	$\leftrightarrow$	$K^* + \eta' + a_1$
1305	$N(1535) + \bar{\Xi}$	$\leftrightarrow$	$K + K + a_1$
1306	$N(1535) + \bar{\Xi}$	$\leftrightarrow$	$K + K^* + a_1$
1307	$N(1535) + \bar{\Xi}$	$\leftrightarrow$	$K^* + K^* + a_1$
1308	$N(1535) + \bar{\Xi}^*$	$\leftrightarrow$	$K + K + a_1$
1309	$N(1535) + \bar{\Xi}^*$	$\leftrightarrow$	$K + K^* + a_1$
1310	$N(1535) + \bar{\Xi}^*$	$\leftrightarrow$	$K^* + K^* + a_1$

Ch. No.	$B_1 + B_2$	$\leftrightarrow$	$M_1+M_2+M_3$
1311	$\Lambda + \bar{N}$	$\leftrightarrow$	$\pi + \pi + K$
1312	$\Lambda + \bar{N}$	$\leftrightarrow$	$\pi + \pi + K^*$
1313	$\Lambda + \bar{N}$	$\leftrightarrow$	$\pi + \eta + K$
1314	$\Lambda + \bar{N}$	$\leftrightarrow$	$\pi + \eta + K^*$
1315	$\Lambda + \bar{N}$	$\leftrightarrow$	$\pi + K + \rho$
1316	$\Lambda + \bar{N}$	$\leftrightarrow$	$\pi + K + \omega$
1317	$\Lambda + \bar{N}$	$\leftrightarrow$	$\pi + K + \phi$
1318	$\Lambda + \bar{N}$	$\leftrightarrow$	$\pi + K + \eta'$
1319	$\Lambda + \bar{N}$	$\leftrightarrow$	$\pi + K^* + \rho$
1320	$\Lambda + \bar{N}$	$\leftrightarrow$	$\pi + K^* + \omega$
1321	$\Lambda + \bar{N}$	$\leftrightarrow$	$\pi + K^* + \phi$
1322	$\Lambda + \bar{N}$	$\leftrightarrow$	$\pi + K^* + \eta'$
1323	$\Lambda + \bar{N}$	$\leftrightarrow$	$\eta + \eta + K$
1324	$\Lambda + \bar{N}$	$\leftrightarrow$	$\eta + \eta + K^*$
1325	$\Lambda + \bar{N}$	$\leftrightarrow$	$\eta + K + \rho$
1326	$\Lambda + \bar{N}$	$\leftrightarrow$	$\eta + K + \omega$
1327	$\Lambda + \bar{N}$	$\leftrightarrow$	$\eta + K + \phi$
1328	$\Lambda + \bar{N}$	$\leftrightarrow$	$\eta + K + \eta'$
1329	$\Lambda + \bar{N}$	$\leftrightarrow$	$\eta + K^* + \rho$
1330	$\Lambda + \bar{N}$	$\leftrightarrow$	$\eta + K^* + \omega$
1331	$\Lambda + \bar{N}$	$\leftrightarrow$	$\eta + K^* + \phi$
1332	$\Lambda + \bar{N}$	$\leftrightarrow$	$\eta + K^* + \eta'$
1333	$\Lambda + \bar{N}$	$\leftrightarrow$	$K + \rho + \rho$
1334	$\Lambda + \bar{N}$	$\leftrightarrow$	$K + \rho + \omega$
1335	$\Lambda + \bar{N}$	$\leftrightarrow$	$K + \rho + \phi$
1336	$\Lambda + \bar{N}$	$\leftrightarrow$	$K + \rho + \eta'$
1337	$\Lambda + \bar{N}$	$\leftrightarrow$	$K + \omega + \omega$
1338	$\Lambda + \bar{N}$	$\leftrightarrow$	$K + \omega + \phi$
1339	$\Lambda + \bar{N}$	$\leftrightarrow$	$K + \omega + \eta'$
1340	$\Lambda + \bar{N}$	$\leftrightarrow$	$K + \phi + \phi$
1341	$\Lambda + \bar{N}$	$\leftrightarrow$	$K + \phi + \eta'$
1342	$\Lambda + \bar{N}$	$\leftrightarrow$	$K + \eta' + \eta'$
1343	$\Lambda + \bar{N}$	$\leftrightarrow$	$K + a_1 + a_1$
1344	$\Lambda + \bar{N}$	$\leftrightarrow$	$K^* + \rho + \rho$
1345	$\Lambda + \bar{N}$	$\leftrightarrow$	$K^* + \rho + \omega$
1346	$\Lambda + \bar{N}$	$\leftrightarrow$	$K^* + \rho + \phi$
1347	$\Lambda + \bar{N}$	$\leftrightarrow$	$K^* + \rho + \eta'$
1348	$\Lambda + \bar{N}$	$\leftrightarrow$	$K^* + \omega + \omega$
1349	$\Lambda + \bar{N}$	$\leftrightarrow$	$K^* + \omega + \phi$
1350	$\Lambda + \bar{N}$	$\leftrightarrow$	$K^* + \omega + \eta'$
1351	$\Lambda + \bar{N}$	$\leftrightarrow$	$K^* + \phi + \phi$
1352	$\Lambda + \bar{N}$	$\leftrightarrow$	$K^* + \phi + \eta'$
1353	$\Lambda + \bar{N}$	$\leftrightarrow$	$K^* + \eta' + \eta'$
1354	$\Lambda + \bar{N}$	$\leftrightarrow$	$K^* + a_1 + a_1$
1355	$\Lambda + \bar{\Delta}(1232)$	$\leftrightarrow$	$\pi + \pi + K$
1356	$\Lambda + \bar{\Delta}(1232)$	$\leftrightarrow$	$\pi + \pi + K^*$
1357	$\Lambda + \bar{\Delta}(1232)$	$\leftrightarrow$	$\pi + \eta + K$
1358	$\Lambda + \bar{\Delta}(1232)$	$\leftrightarrow$	$\pi + \eta + K^*$
1359	$\Lambda + \bar{\Delta}(1232)$	$\leftrightarrow$	$\pi + K + \rho$
1360	$\Lambda + \bar{\Delta}(1232)$	$\leftrightarrow$	$\pi + K + \omega$
1361	$\Lambda + \bar{\Delta}(1232)$	$\leftrightarrow$	$\pi + K + \phi$
1362	$\Lambda + \bar{\Delta}(1232)$	$\leftrightarrow$	$\pi + K + \eta'$
1363	$\Lambda + \bar{\Delta}(1232)$	$\leftrightarrow$	$\pi + K^* + \rho$
1364	$\Lambda + \bar{\Delta}(1232)$	$\leftrightarrow$	$\pi + K^* + \omega$
1365	$\Lambda + \bar{\Delta}(1232)$	$\leftrightarrow$	$\pi + K^* + \phi$
1366	$\Lambda + \bar{\Delta}(1232)$	$\leftrightarrow$	$\pi + K^* + \eta'$
1367	$\Lambda + \bar{\Delta}(1232)$	$\leftrightarrow$	$\eta + \eta + K$
1368	$\Lambda + \bar{\Delta}(1232)$	$\leftrightarrow$	$\eta + \eta + K^*$
1369	$\Lambda + \bar{\Delta}(1232)$	$\leftrightarrow$	$\eta + K + \rho$
1370	$\Lambda + \bar{\Delta}(1232)$	$\leftrightarrow$	$\eta + K + \omega$
1371	$\Lambda + \bar{\Delta}(1232)$	$\leftrightarrow$	$\eta + K + \phi$
1372	$\Lambda + \bar{\Delta}(1232)$	$\leftrightarrow$	$\eta + K + \eta'$
1373	$\Lambda + \bar{\Delta}(1232)$	$\leftrightarrow$	$\eta + K^* + \rho$
1374	$\Lambda + \bar{\Delta}(1232)$	$\leftrightarrow$	$\eta + K^* + \omega$
1375	$\Lambda + \bar{\Delta}(1232)$	$\leftrightarrow$	$\eta + K^* + \phi$
1376	$\Lambda + \bar{\Delta}(1232)$	$\leftrightarrow$	$\eta + K^* + \eta'$
1377	$\Lambda + \bar{\Delta}(1232)$	$\leftrightarrow$	$K + \rho + \rho$
1378	$\Lambda + \bar{\Delta}(1232)$	$\leftrightarrow$	$K + \rho + \omega$
1379	$\Lambda + \bar{\Delta}(1232)$	$\leftrightarrow$	$K + \rho + \phi$
1380	$\Lambda + \bar{\Delta}(1232)$	$\leftrightarrow$	$K + \rho + \eta'$
1381	$\Lambda + \bar{\Delta}(1232)$	$\leftrightarrow$	$K + \omega + \omega$
1382	$\Lambda + \bar{\Delta}(1232)$	$\leftrightarrow$	$K + \omega + \phi$
1383	$\Lambda + \bar{\Delta}(1232)$	$\leftrightarrow$	$K + \omega + \eta'$
1384	$\Lambda + \bar{\Delta}(1232)$	$\leftrightarrow$	$K + \phi + \phi$
1385	$\Lambda + \bar{\Delta}(1232)$	$\leftrightarrow$	$K + \phi + \eta'$
1386	$\Lambda + \bar{\Delta}(1232)$	$\leftrightarrow$	$K + \eta' + \eta'$
1387	$\Lambda + \bar{\Delta}(1232)$	$\leftrightarrow$	$K + a_1 + a_1$
1388	$\Lambda + \bar{\Delta}(1232)$	$\leftrightarrow$	$K^* + \rho + \rho$
1389	$\Lambda + \bar{\Delta}(1232)$	$\leftrightarrow$	$K^* + \rho + \omega$
1390	$\Lambda + \bar{\Delta}(1232)$	$\leftrightarrow$	$K^* + \rho + \phi$
1391	$\Lambda + \bar{\Delta}(1232)$	$\leftrightarrow$	$K^* + \rho + \eta'$
1392	$\Lambda + \bar{\Delta}(1232)$	$\leftrightarrow$	$K^* + \omega + \omega$
1393	$\Lambda + \bar{\Delta}(1232)$	$\leftrightarrow$	$K^* + \omega + \phi$
1394	$\Lambda + \bar{\Delta}(1232)$	$\leftrightarrow$	$K^* + \omega + \eta'$
1395	$\Lambda + \bar{\Delta}(1232)$	$\leftrightarrow$	$K^* + \phi + \phi$
1396	$\Lambda + \bar{\Delta}(1232)$	$\leftrightarrow$	$K^* + \phi + \eta'$

Ch. No.	$B_1 + B_2$	$\leftrightarrow$	$M_1+M_2+M_3$
1397	$\Lambda + \bar{\Delta}(1232)$	$\leftrightarrow$	$K^* + \eta' + \eta'$
1398	$\Lambda + \bar{\Delta}(1232)$	$\leftrightarrow$	$K^* + a_1 + a_1$
1399	$\Lambda + \bar{N}(1440)$	$\leftrightarrow$	$\pi + \pi + K$
1400	$\Lambda + \bar{N}(1440)$	$\leftrightarrow$	$\pi + \pi + K^*$
1401	$\Lambda + \bar{N}(1440)$	$\leftrightarrow$	$\pi + \eta + K$
1402	$\Lambda + \bar{N}(1440)$	$\leftrightarrow$	$\pi + \eta + K^*$
1403	$\Lambda + \bar{N}(1440)$	$\leftrightarrow$	$\pi + K + \rho$
1404	$\Lambda + \bar{N}(1440)$	$\leftrightarrow$	$\pi + K + \omega$
1405	$\Lambda + \bar{N}(1440)$	$\leftrightarrow$	$\pi + K + \phi$
1406	$\Lambda + \bar{N}(1440)$	$\leftrightarrow$	$\pi + K + \eta'$
1407	$\Lambda + \bar{N}(1440)$	$\leftrightarrow$	$\pi + K^* + \rho$
1408	$\Lambda + \bar{N}(1440)$	$\leftrightarrow$	$\pi + K^* + \omega$
1409	$\Lambda + \bar{N}(1440)$	$\leftrightarrow$	$\pi + K^* + \phi$
1410	$\Lambda + \bar{N}(1440)$	$\leftrightarrow$	$\pi + K^* + \eta'$
1411	$\Lambda + \bar{N}(1440)$	$\leftrightarrow$	$\eta + \eta + K$
1412	$\Lambda + \bar{N}(1440)$	$\leftrightarrow$	$\eta + \eta + K^*$
1413	$\Lambda + \bar{N}(1440)$	$\leftrightarrow$	$\eta + K + \rho$
1414	$\Lambda + \bar{N}(1440)$	$\leftrightarrow$	$\eta + K + \omega$
1415	$\Lambda + \bar{N}(1440)$	$\leftrightarrow$	$\eta + K + \phi$
1416	$\Lambda + \bar{N}(1440)$	$\leftrightarrow$	$\eta + K + \eta'$
1417	$\Lambda + \bar{N}(1440)$	$\leftrightarrow$	$\eta + K^* + \rho$
1418	$\Lambda + \bar{N}(1440)$	$\leftrightarrow$	$\eta + K^* + \omega$
1419	$\Lambda + \bar{N}(1440)$	$\leftrightarrow$	$\eta + K^* + \phi$
1420	$\Lambda + \bar{N}(1440)$	$\leftrightarrow$	$\eta + K^* + \eta'$
1421	$\Lambda + \bar{N}(1440)$	$\leftrightarrow$	$K + \rho + \rho$
1422	$\Lambda + \bar{N}(1440)$	$\leftrightarrow$	$K + \rho + \omega$
1423	$\Lambda + \bar{N}(1440)$	$\leftrightarrow$	$K + \rho + \phi$
1424	$\Lambda + \bar{N}(1440)$	$\leftrightarrow$	$K + \rho + \eta'$
1425	$\Lambda + \bar{N}(1440)$	$\leftrightarrow$	$K + \omega + \omega$
1426	$\Lambda + \bar{N}(1440)$	$\leftrightarrow$	$K + \omega + \phi$
1427	$\Lambda + \bar{N}(1440)$	$\leftrightarrow$	$K + \omega + \eta'$
1428	$\Lambda + \bar{N}(1440)$	$\leftrightarrow$	$K + \phi + \phi$
1429	$\Lambda + \bar{N}(1440)$	$\leftrightarrow$	$K + \phi + \eta'$
1430	$\Lambda + \bar{N}(1440)$	$\leftrightarrow$	$K + \eta' + \eta'$
1431	$\Lambda + \bar{N}(1440)$	$\leftrightarrow$	$K + a_1 + a_1$
1432	$\Lambda + \bar{N}(1440)$	$\leftrightarrow$	$K^* + \rho + \rho$
1433	$\Lambda + \bar{N}(1440)$	$\leftrightarrow$	$K^* + \rho + \omega$
1434	$\Lambda + \bar{N}(1440)$	$\leftrightarrow$	$K^* + \rho + \phi$
1435	$\Lambda + \bar{N}(1440)$	$\leftrightarrow$	$K^* + \rho + \eta'$
1436	$\Lambda + \bar{N}(1440)$	$\leftrightarrow$	$K^* + \omega + \omega$
1437	$\Lambda + \bar{N}(1440)$	$\leftrightarrow$	$K^* + \omega + \phi$
1438	$\Lambda + \bar{N}(1440)$	$\leftrightarrow$	$K^* + \omega + \eta'$
1439	$\Lambda + \bar{N}(1440)$	$\leftrightarrow$	$K^* + \phi + \phi$
1440	$\Lambda + \bar{N}(1440)$	$\leftrightarrow$	$K^* + \phi + \eta'$
1441	$\Lambda + \bar{N}(1440)$	$\leftrightarrow$	$K^* + \eta' + \eta'$
1442	$\Lambda + \bar{N}(1440)$	$\leftrightarrow$	$K^* + a_1 + a_1$
1443	$\Lambda + \bar{N}(1535)$	$\leftrightarrow$	$\pi + K + a_1$
1444	$\Lambda + \bar{N}(1535)$	$\leftrightarrow$	$\pi + K^* + a_1$
1445	$\Lambda + \bar{N}(1535)$	$\leftrightarrow$	$\eta + K + a_1$
1446	$\Lambda + \bar{N}(1535)$	$\leftrightarrow$	$\eta + K^* + a_1$
1447	$\Lambda + \bar{N}(1535)$	$\leftrightarrow$	$K + \rho + a_1$
1448	$\Lambda + \bar{N}(1535)$	$\leftrightarrow$	$K + \omega + a_1$
1449	$\Lambda + \bar{N}(1535)$	$\leftrightarrow$	$K + \phi + a_1$
1450	$\Lambda + \bar{N}(1535)$	$\leftrightarrow$	$K + \eta' + a_1$
1451	$\Lambda + \bar{N}(1535)$	$\leftrightarrow$	$K^* + \rho + a_1$
1452	$\Lambda + \bar{N}(1535)$	$\leftrightarrow$	$K^* + \omega + a_1$
1453	$\Lambda + \bar{N}(1535)$	$\leftrightarrow$	$K^* + \phi + a_1$
1454	$\Lambda + \bar{N}(1535)$	$\leftrightarrow$	$K^* + \eta' + a_1$
1455	$\Lambda + \bar{\Lambda}$	$\leftrightarrow$	$\pi + \pi + \eta$
1456	$\Lambda + \bar{\Lambda}$	$\leftrightarrow$	$\pi + \pi + \phi$
1457	$\Lambda + \bar{\Lambda}$	$\leftrightarrow$	$\pi + \eta + \eta$
1458	$\Lambda + \bar{\Lambda}$	$\leftrightarrow$	$\pi + \eta + \rho$
1459	$\Lambda + \bar{\Lambda}$	$\leftrightarrow$	$\pi + \eta + \omega$
1460	$\Lambda + \bar{\Lambda}$	$\leftrightarrow$	$\pi + \eta + \phi$
1461	$\Lambda + \bar{\Lambda}$	$\leftrightarrow$	$\pi + \eta + \eta'$
1462	$\Lambda + \bar{\Lambda}$	$\leftrightarrow$	$\pi + K + K$
1463	$\Lambda + \bar{\Lambda}$	$\leftrightarrow$	$\pi + K + K^*$
1464	$\Lambda + \bar{\Lambda}$	$\leftrightarrow$	$\pi + K^* + K^*$
1465	$\Lambda + \bar{\Lambda}$	$\leftrightarrow$	$\pi + \rho + \phi$
1466	$\Lambda + \bar{\Lambda}$	$\leftrightarrow$	$\pi + \omega + \phi$
1467	$\Lambda + \bar{\Lambda}$	$\leftrightarrow$	$\pi + \phi + \phi$
1468	$\Lambda + \bar{\Lambda}$	$\leftrightarrow$	$\pi + \phi + \eta'$
1469	$\Lambda + \bar{\Lambda}$	$\leftrightarrow$	$\eta + \eta + \eta$
1470	$\Lambda + \bar{\Lambda}$	$\leftrightarrow$	$\eta + \eta + \rho$
1471	$\Lambda + \bar{\Lambda}$	$\leftrightarrow$	$\eta + \eta + \omega$
1472	$\Lambda + \bar{\Lambda}$	$\leftrightarrow$	$\eta + \eta + \phi$
1473	$\Lambda + \bar{\Lambda}$	$\leftrightarrow$	$\eta + \eta + \eta'$
1474	$\Lambda + \bar{\Lambda}$	$\leftrightarrow$	$\eta + K + K$
1475	$\Lambda + \bar{\Lambda}$	$\leftrightarrow$	$\eta + K + K^*$
1476	$\Lambda + \bar{\Lambda}$	$\leftrightarrow$	$\eta + K^* + K^*$
1477	$\Lambda + \bar{\Lambda}$	$\leftrightarrow$	$\eta + \rho + \rho$
1478	$\Lambda + \bar{\Lambda}$	$\leftrightarrow$	$\eta + \rho + \omega$
1479	$\Lambda + \bar{\Lambda}$	$\leftrightarrow$	$\eta + \rho + \phi$
1480	$\Lambda + \bar{\Lambda}$	$\leftrightarrow$	$\eta + \rho + \eta'$
1481	$\Lambda + \bar{\Lambda}$	$\leftrightarrow$	$\eta + \omega + \omega$
1482	$\Lambda + \bar{\Lambda}$	$\leftrightarrow$	$\eta + \omega + \phi$

Ch. No.	$B_1 + B_2$	$\leftrightarrow$	$M_1+M_2+M_3$
1483	$\Lambda + \bar{\Lambda}$	$\leftrightarrow$	$\eta + \omega + \eta'$
1484	$\Lambda + \bar{\Lambda}$	$\leftrightarrow$	$\eta + \phi + \phi$
1485	$\Lambda + \bar{\Lambda}$	$\leftrightarrow$	$\eta + \phi + \eta'$
1486	$\Lambda + \bar{\Lambda}$	$\leftrightarrow$	$\eta + \eta' + \eta'$
1487	$\Lambda + \bar{\Lambda}$	$\leftrightarrow$	$\eta + a_1 + a_1$
1488	$\Lambda + \bar{\Lambda}$	$\leftrightarrow$	$K + K + \rho$
1489	$\Lambda + \bar{\Lambda}$	$\leftrightarrow$	$K + K + \omega$
1490	$\Lambda + \bar{\Lambda}$	$\leftrightarrow$	$K + K + \phi$
1491	$\Lambda + \bar{\Lambda}$	$\leftrightarrow$	$K + K + \eta'$
1492	$\Lambda + \bar{\Lambda}$	$\leftrightarrow$	$K + K^* + \rho$
1493	$\Lambda + \bar{\Lambda}$	$\leftrightarrow$	$K + K^* + \omega$
1494	$\Lambda + \bar{\Lambda}$	$\leftrightarrow$	$K + K^* + \phi$
1495	$\Lambda + \bar{\Lambda}$	$\leftrightarrow$	$K + K^* + \eta'$
1496	$\Lambda + \bar{\Lambda}$	$\leftrightarrow$	$K^* + K^* + \rho$
1497	$\Lambda + \bar{\Lambda}$	$\leftrightarrow$	$K^* + K^* + \omega$
1498	$\Lambda + \bar{\Lambda}$	$\leftrightarrow$	$K^* + K^* + \phi$
1499	$\Lambda + \bar{\Lambda}$	$\leftrightarrow$	$K^* + K^* + \eta'$
1500	$\Lambda + \bar{\Lambda}$	$\leftrightarrow$	$\rho + \rho + \phi$
1501	$\Lambda + \bar{\Lambda}$	$\leftrightarrow$	$\rho + \omega + \phi$
1502	$\Lambda + \bar{\Lambda}$	$\leftrightarrow$	$\rho + \phi + \phi$
1503	$\Lambda + \bar{\Lambda}$	$\leftrightarrow$	$\rho + \phi + \eta'$
1504	$\Lambda + \bar{\Lambda}$	$\leftrightarrow$	$\omega + \omega + \phi$
1505	$\Lambda + \bar{\Lambda}$	$\leftrightarrow$	$\omega + \phi + \phi$
1506	$\Lambda + \bar{\Lambda}$	$\leftrightarrow$	$\omega + \phi + \eta'$
1507	$\Lambda + \bar{\Lambda}$	$\leftrightarrow$	$\phi + \phi + \phi$
1508	$\Lambda + \bar{\Lambda}$	$\leftrightarrow$	$\phi + \phi + \eta'$
1509	$\Lambda + \bar{\Lambda}$	$\leftrightarrow$	$\phi + \eta' + \eta'$
1510	$\Lambda + \bar{\Lambda}$	$\leftrightarrow$	$\phi + a_1 + a_1$
1511	$\Lambda + \bar{\Sigma}$	$\leftrightarrow$	$\pi + \pi + \eta$
1512	$\Lambda + \bar{\Sigma}$	$\leftrightarrow$	$\pi + \pi + \phi$
1513	$\Lambda + \bar{\Sigma}$	$\leftrightarrow$	$\pi + \eta + \eta$
1514	$\Lambda + \bar{\Sigma}$	$\leftrightarrow$	$\pi + \eta + \rho$
1515	$\Lambda + \bar{\Sigma}$	$\leftrightarrow$	$\pi + \eta + \omega$
1516	$\Lambda + \bar{\Sigma}$	$\leftrightarrow$	$\pi + \eta + \phi$
1517	$\Lambda + \bar{\Sigma}$	$\leftrightarrow$	$\pi + \eta + \eta'$
1518	$\Lambda + \bar{\Sigma}$	$\leftrightarrow$	$\pi + K + K$
1519	$\Lambda + \bar{\Sigma}$	$\leftrightarrow$	$\pi + K + K^*$
1520	$\Lambda + \bar{\Sigma}$	$\leftrightarrow$	$\pi + K^* + K^*$
1521	$\Lambda + \bar{\Sigma}$	$\leftrightarrow$	$\pi + \rho + \phi$
1522	$\Lambda + \bar{\Sigma}$	$\leftrightarrow$	$\pi + \omega + \phi$
1523	$\Lambda + \bar{\Sigma}$	$\leftrightarrow$	$\pi + \phi + \phi$
1524	$\Lambda + \bar{\Sigma}$	$\leftrightarrow$	$\pi + \phi + \eta'$
1525	$\Lambda + \bar{\Sigma}$	$\leftrightarrow$	$\eta + \eta + \eta$
1526	$\Lambda + \bar{\Sigma}$	$\leftrightarrow$	$\eta + \eta + \rho$
1527	$\Lambda + \bar{\Sigma}$	$\leftrightarrow$	$\eta + \eta + \omega$
1528	$\Lambda + \bar{\Sigma}$	$\leftrightarrow$	$\eta + \eta + \phi$
1529	$\Lambda + \bar{\Sigma}$	$\leftrightarrow$	$\eta + \eta + \eta'$
1530	$\Lambda + \bar{\Sigma}$	$\leftrightarrow$	$\eta + K + K$
1531	$\Lambda + \bar{\Sigma}$	$\leftrightarrow$	$\eta + K + K^*$
1532	$\Lambda + \bar{\Sigma}$	$\leftrightarrow$	$\eta + K^* + K^*$
1533	$\Lambda + \bar{\Sigma}$	$\leftrightarrow$	$\eta + \rho + \rho$
1534	$\Lambda + \bar{\Sigma}$	$\leftrightarrow$	$\eta + \rho + \omega$
1535	$\Lambda + \bar{\Sigma}$	$\leftrightarrow$	$\eta + \rho + \phi$
1536	$\Lambda + \bar{\Sigma}$	$\leftrightarrow$	$\eta + \rho + \eta'$
1537	$\Lambda + \bar{\Sigma}$	$\leftrightarrow$	$\eta + \omega + \omega$
1538	$\Lambda + \bar{\Sigma}$	$\leftrightarrow$	$\eta + \omega + \phi$
1539	$\Lambda + \bar{\Sigma}$	$\leftrightarrow$	$\eta + \omega + \eta'$
1540	$\Lambda + \bar{\Sigma}$	$\leftrightarrow$	$\eta + \phi + \phi$
1541	$\Lambda + \bar{\Sigma}$	$\leftrightarrow$	$\eta + \phi + \eta'$
1542	$\Lambda + \bar{\Sigma}$	$\leftrightarrow$	$\eta + \eta' + \eta'$
1543	$\Lambda + \bar{\Sigma}$	$\leftrightarrow$	$\eta + a_1 + a_1$
1544	$\Lambda + \bar{\Sigma}$	$\leftrightarrow$	$K + K + \rho$
1545	$\Lambda + \bar{\Sigma}$	$\leftrightarrow$	$K + K + \omega$
1546	$\Lambda + \bar{\Sigma}$	$\leftrightarrow$	$K + K + \phi$
1547	$\Lambda + \bar{\Sigma}$	$\leftrightarrow$	$K + K + \eta'$
1548	$\Lambda + \bar{\Sigma}$	$\leftrightarrow$	$K + K^* + \rho$
1549	$\Lambda + \bar{\Sigma}$	$\leftrightarrow$	$K + K^* + \omega$
1550	$\Lambda + \bar{\Sigma}$	$\leftrightarrow$	$K + K^* + \phi$
1551	$\Lambda + \bar{\Sigma}$	$\leftrightarrow$	$K + K^* + \eta'$
1552	$\Lambda + \bar{\Sigma}$	$\leftrightarrow$	$K^* + K^* + \rho$
1553	$\Lambda + \bar{\Sigma}$	$\leftrightarrow$	$K^* + K^* + \omega$
1554	$\Lambda + \bar{\Sigma}$	$\leftrightarrow$	$K^* + K^* + \phi$
1555	$\Lambda + \bar{\Sigma}$	$\leftrightarrow$	$K^* + K^* + \eta'$
1556	$\Lambda + \bar{\Sigma}$	$\leftrightarrow$	$\rho + \rho + \phi$
1557	$\Lambda + \bar{\Sigma}$	$\leftrightarrow$	$\rho + \omega + \phi$
1558	$\Lambda + \bar{\Sigma}$	$\leftrightarrow$	$\rho + \phi + \phi$
1559	$\Lambda + \bar{\Sigma}$	$\leftrightarrow$	$\rho + \phi + \eta'$
1560	$\Lambda + \bar{\Sigma}$	$\leftrightarrow$	$\omega + \omega + \phi$
1561	$\Lambda + \bar{\Sigma}$	$\leftrightarrow$	$\omega + \phi + \phi$
1562	$\Lambda + \bar{\Sigma}$	$\leftrightarrow$	$\omega + \phi + \eta'$
1563	$\Lambda + \bar{\Sigma}$	$\leftrightarrow$	$\phi + \phi + \phi$
1564	$\Lambda + \bar{\Sigma}$	$\leftrightarrow$	$\phi + \phi + \eta'$
1565	$\Lambda + \bar{\Sigma}$	$\leftrightarrow$	$\phi + \eta' + \eta'$
1566	$\Lambda + \bar{\Sigma}$	$\leftrightarrow$	$\phi + a_1 + a_1$
1567	$\Lambda + \bar{\Sigma}^*$	$\leftrightarrow$	$\pi + \pi + \eta$
1568	$\Lambda + \bar{\Sigma}^*$	$\leftrightarrow$	$\pi + \pi + \phi$

Ch. No.	$B_1 + B_2$	$\leftrightarrow$	$M_1+M_2+M_3$
1569	$\Lambda + \bar{\Sigma}^*$	$\leftrightarrow$	$\pi + \eta + \eta$
1570	$\Lambda + \bar{\Sigma}^*$	$\leftrightarrow$	$\pi + \eta + \rho$
1571	$\Lambda + \bar{\Sigma}^*$	$\leftrightarrow$	$\pi + \eta + \omega$
1572	$\Lambda + \bar{\Sigma}^*$	$\leftrightarrow$	$\pi + \eta + \phi$
1573	$\Lambda + \bar{\Sigma}^*$	$\leftrightarrow$	$\pi + \eta + \eta'$
1574	$\Lambda + \bar{\Sigma}^*$	$\leftrightarrow$	$\pi + K + K$
1575	$\Lambda + \bar{\Sigma}^*$	$\leftrightarrow$	$\pi + K + K^*$
1576	$\Lambda + \bar{\Sigma}^*$	$\leftrightarrow$	$\pi + K^* + K^*$
1577	$\Lambda + \bar{\Sigma}^*$	$\leftrightarrow$	$\pi + \rho + \phi$
1578	$\Lambda + \bar{\Sigma}^*$	$\leftrightarrow$	$\pi + \omega + \phi$
1579	$\Lambda + \bar{\Sigma}^*$	$\leftrightarrow$	$\pi + \phi + \phi$
1580	$\Lambda + \bar{\Sigma}^*$	$\leftrightarrow$	$\pi + \phi + \eta'$
1581	$\Lambda + \bar{\Sigma}^*$	$\leftrightarrow$	$\eta + \eta + \eta$
1582	$\Lambda + \bar{\Sigma}^*$	$\leftrightarrow$	$\eta + \eta + \rho$
1583	$\Lambda + \bar{\Sigma}^*$	$\leftrightarrow$	$\eta + \eta + \omega$
1584	$\Lambda + \bar{\Sigma}^*$	$\leftrightarrow$	$\eta + \eta + \phi$
1585	$\Lambda + \bar{\Sigma}^*$	$\leftrightarrow$	$\eta + \eta + \eta'$
1586	$\Lambda + \bar{\Sigma}^*$	$\leftrightarrow$	$\eta + K + K$
1587	$\Lambda + \bar{\Sigma}^*$	$\leftrightarrow$	$\eta + K + K^*$
1588	$\Lambda + \bar{\Sigma}^*$	$\leftrightarrow$	$\eta + K^* + K^*$
1589	$\Lambda + \bar{\Sigma}^*$	$\leftrightarrow$	$\eta + \rho + \rho$
1590	$\Lambda + \bar{\Sigma}^*$	$\leftrightarrow$	$\eta + \rho + \omega$
1591	$\Lambda + \bar{\Sigma}^*$	$\leftrightarrow$	$\eta + \rho + \phi$
1592	$\Lambda + \bar{\Sigma}^*$	$\leftrightarrow$	$\eta + \rho + \eta'$
1593	$\Lambda + \bar{\Sigma}^*$	$\leftrightarrow$	$\eta + \omega + \omega$
1594	$\Lambda + \bar{\Sigma}^*$	$\leftrightarrow$	$\eta + \omega + \phi$
1595	$\Lambda + \bar{\Sigma}^*$	$\leftrightarrow$	$\eta + \omega + \eta'$
1596	$\Lambda + \bar{\Sigma}^*$	$\leftrightarrow$	$\eta + \phi + \phi$
1597	$\Lambda + \bar{\Sigma}^*$	$\leftrightarrow$	$\eta + \phi + \eta'$
1598	$\Lambda + \bar{\Sigma}^*$	$\leftrightarrow$	$\eta + \eta' + \eta'$
1599	$\Lambda + \bar{\Sigma}^*$	$\leftrightarrow$	$\eta + a_1 + a_1$
1600	$\Lambda + \bar{\Sigma}^*$	$\leftrightarrow$	$K + K + \rho$
1601	$\Lambda + \bar{\Sigma}^*$	$\leftrightarrow$	$K + K + \omega$
1602	$\Lambda + \bar{\Sigma}^*$	$\leftrightarrow$	$K + K + \phi$
1603	$\Lambda + \bar{\Sigma}^*$	$\leftrightarrow$	$K + K + \eta'$
1604	$\Lambda + \bar{\Sigma}^*$	$\leftrightarrow$	$K + K^* + \rho$
1605	$\Lambda + \bar{\Sigma}^*$	$\leftrightarrow$	$K + K^* + \omega$
1606	$\Lambda + \bar{\Sigma}^*$	$\leftrightarrow$	$K + K^* + \phi$
1607	$\Lambda + \bar{\Sigma}^*$	$\leftrightarrow$	$K + K^* + \eta'$
1608	$\Lambda + \bar{\Sigma}^*$	$\leftrightarrow$	$K^* + K^* + \rho$
1609	$\Lambda + \bar{\Sigma}^*$	$\leftrightarrow$	$K^* + K^* + \omega$
1610	$\Lambda + \bar{\Sigma}^*$	$\leftrightarrow$	$K^* + K^* + \phi$
1611	$\Lambda + \bar{\Sigma}^*$	$\leftrightarrow$	$K^* + K^* + \eta'$
1612	$\Lambda + \bar{\Sigma}^*$	$\leftrightarrow$	$\rho + \rho + \phi$
1613	$\Lambda + \bar{\Sigma}^*$	$\leftrightarrow$	$\rho + \omega + \phi$
1614	$\Lambda + \bar{\Sigma}^*$	$\leftrightarrow$	$\rho + \phi + \phi$
1615	$\Lambda + \bar{\Sigma}^*$	$\leftrightarrow$	$\rho + \phi + \eta'$
1616	$\Lambda + \bar{\Sigma}^*$	$\leftrightarrow$	$\omega + \omega + \phi$
1617	$\Lambda + \bar{\Sigma}^*$	$\leftrightarrow$	$\omega + \phi + \phi$
1618	$\Lambda + \bar{\Sigma}^*$	$\leftrightarrow$	$\omega + \phi + \eta'$
1619	$\Lambda + \bar{\Sigma}^*$	$\leftrightarrow$	$\phi + \phi + \phi$
1620	$\Lambda + \bar{\Sigma}^*$	$\leftrightarrow$	$\phi + \phi + \eta'$
1621	$\Lambda + \bar{\Sigma}^*$	$\leftrightarrow$	$\phi + \eta' + \eta'$
1622	$\Lambda + \bar{\Sigma}^*$	$\leftrightarrow$	$\phi + a_1 + a_1$
1623	$\Lambda + \bar{\Xi}$	$\leftrightarrow$	$\pi + \eta + K$
1624	$\Lambda + \bar{\Xi}$	$\leftrightarrow$	$\pi + \eta + K^*$
1625	$\Lambda + \bar{\Xi}$	$\leftrightarrow$	$\pi + K + \phi$
1626	$\Lambda + \bar{\Xi}$	$\leftrightarrow$	$\pi + K^* + \phi$
1627	$\Lambda + \bar{\Xi}$	$\leftrightarrow$	$\eta + \eta + K$
1628	$\Lambda + \bar{\Xi}$	$\leftrightarrow$	$\eta + \eta + K^*$
1629	$\Lambda + \bar{\Xi}$	$\leftrightarrow$	$\eta + K + \rho$
1630	$\Lambda + \bar{\Xi}$	$\leftrightarrow$	$\eta + K + \omega$
1631	$\Lambda + \bar{\Xi}$	$\leftrightarrow$	$\eta + K + \phi$
1632	$\Lambda + \bar{\Xi}$	$\leftrightarrow$	$\eta + K + \eta'$
1633	$\Lambda + \bar{\Xi}$	$\leftrightarrow$	$\eta + K^* + \rho$
1634	$\Lambda + \bar{\Xi}$	$\leftrightarrow$	$\eta + K^* + \omega$
1635	$\Lambda + \bar{\Xi}$	$\leftrightarrow$	$\eta + K^* + \phi$
1636	$\Lambda + \bar{\Xi}$	$\leftrightarrow$	$\eta + K^* + \eta'$
1637	$\Lambda + \bar{\Xi}$	$\leftrightarrow$	$K + K + K$
1638	$\Lambda + \bar{\Xi}$	$\leftrightarrow$	$K + K + K^*$
1639	$\Lambda + \bar{\Xi}$	$\leftrightarrow$	$K + K^* + K^*$
1640	$\Lambda + \bar{\Xi}$	$\leftrightarrow$	$K + \rho + \phi$
1641	$\Lambda + \bar{\Xi}$	$\leftrightarrow$	$K + \omega + \phi$
1642	$\Lambda + \bar{\Xi}$	$\leftrightarrow$	$K + \phi + \phi$
1643	$\Lambda + \bar{\Xi}$	$\leftrightarrow$	$K + \phi + \eta'$
1644	$\Lambda + \bar{\Xi}$	$\leftrightarrow$	$K^* + K^* + K^*$
1645	$\Lambda + \bar{\Xi}$	$\leftrightarrow$	$K^* + \rho + \phi$
1646	$\Lambda + \bar{\Xi}$	$\leftrightarrow$	$K^* + \omega + \phi$
1647	$\Lambda + \bar{\Xi}$	$\leftrightarrow$	$K^* + \phi + \phi$
1648	$\Lambda + \bar{\Xi}$	$\leftrightarrow$	$K^* + \phi + \eta'$
1649	$\Lambda + \bar{\Xi}^*$	$\leftrightarrow$	$\pi + \eta + K$
1650	$\Lambda + \bar{\Xi}^*$	$\leftrightarrow$	$\pi + \eta + K^*$
1651	$\Lambda + \bar{\Xi}^*$	$\leftrightarrow$	$\pi + K + \phi$
1652	$\Lambda + \bar{\Xi}^*$	$\leftrightarrow$	$\pi + K^* + \phi$
1653	$\Lambda + \bar{\Xi}^*$	$\leftrightarrow$	$\eta + \eta + K$
1654	$\Lambda + \bar{\Xi}^*$	$\leftrightarrow$	$\eta + \eta + K^*$

Ch. No.	$B_1 + B_2$	$\leftrightarrow$	$M_1+M_2+M_3$
1655	$\Lambda + \bar{\Xi}^*$	$\leftrightarrow$	$\eta + K + \rho$
1656	$\Lambda + \bar{\Xi}^*$	$\leftrightarrow$	$\eta + K + \omega$
1657	$\Lambda + \bar{\Xi}^*$	$\leftrightarrow$	$\eta + K + \phi$
1658	$\Lambda + \bar{\Xi}^*$	$\leftrightarrow$	$\eta + K + \eta'$
1659	$\Lambda + \bar{\Xi}^*$	$\leftrightarrow$	$\eta + K^* + \rho$
1660	$\Lambda + \bar{\Xi}^*$	$\leftrightarrow$	$\eta + K^* + \omega$
1661	$\Lambda + \bar{\Xi}^*$	$\leftrightarrow$	$\eta + K^* + \phi$
1662	$\Lambda + \bar{\Xi}^*$	$\leftrightarrow$	$\eta + K^* + \eta'$
1663	$\Lambda + \bar{\Xi}^*$	$\leftrightarrow$	$K + K + K$
1664	$\Lambda + \bar{\Xi}^*$	$\leftrightarrow$	$K + K + K^*$
1665	$\Lambda + \bar{\Xi}^*$	$\leftrightarrow$	$K + K^* + K^*$
1666	$\Lambda + \bar{\Xi}^*$	$\leftrightarrow$	$K + \rho + \phi$
1667	$\Lambda + \bar{\Xi}^*$	$\leftrightarrow$	$K + \omega + \phi$
1668	$\Lambda + \bar{\Xi}^*$	$\leftrightarrow$	$K + \phi + \phi$
1669	$\Lambda + \bar{\Xi}^*$	$\leftrightarrow$	$K + \phi + \eta'$
1670	$\Lambda + \bar{\Xi}^*$	$\leftrightarrow$	$K^* + K^* + K^*$
1671	$\Lambda + \bar{\Xi}^*$	$\leftrightarrow$	$K^* + \rho + \phi$
1672	$\Lambda + \bar{\Xi}^*$	$\leftrightarrow$	$K^* + \omega + \phi$
1673	$\Lambda + \bar{\Xi}^*$	$\leftrightarrow$	$K^* + \phi + \phi$
1674	$\Lambda + \bar{\Xi}^*$	$\leftrightarrow$	$K^* + \phi + \eta'$
1675	$\Lambda + \bar{\Omega}$	$\leftrightarrow$	$\eta + K + K$
1676	$\Lambda + \bar{\Omega}$	$\leftrightarrow$	$\eta + K + K^*$
1677	$\Lambda + \bar{\Omega}$	$\leftrightarrow$	$\eta + K^* + K^*$
1678	$\Lambda + \bar{\Omega}$	$\leftrightarrow$	$K + K + \phi$
1679	$\Lambda + \bar{\Omega}$	$\leftrightarrow$	$K + K^* + \phi$
1680	$\Lambda + \bar{\Omega}$	$\leftrightarrow$	$K^* + K^* + \phi$
1681	$\Sigma + \bar{\mathrm{N}}$	$\leftrightarrow$	$\pi + \pi + K$
1682	$\Sigma + \bar{\mathrm{N}}$	$\leftrightarrow$	$\pi + \pi + K^*$
1683	$\Sigma + \bar{\mathrm{N}}$	$\leftrightarrow$	$\pi + \eta + K$
1684	$\Sigma + \bar{\mathrm{N}}$	$\leftrightarrow$	$\pi + \eta + K^*$
1685	$\Sigma + \bar{\mathrm{N}}$	$\leftrightarrow$	$\pi + K + \rho$
1686	$\Sigma + \bar{\mathrm{N}}$	$\leftrightarrow$	$\pi + K + \omega$
1687	$\Sigma + \bar{\mathrm{N}}$	$\leftrightarrow$	$\pi + K + \phi$
1688	$\Sigma + \bar{\mathrm{N}}$	$\leftrightarrow$	$\pi + K + \eta'$
1689	$\Sigma + \bar{\mathrm{N}}$	$\leftrightarrow$	$\pi + K^* + \rho$
1690	$\Sigma + \bar{\mathrm{N}}$	$\leftrightarrow$	$\pi + K^* + \omega$
1691	$\Sigma + \bar{\mathrm{N}}$	$\leftrightarrow$	$\pi + K^* + \phi$
1692	$\Sigma + \bar{\mathrm{N}}$	$\leftrightarrow$	$\pi + K^* + \eta'$
1693	$\Sigma + \bar{\mathrm{N}}$	$\leftrightarrow$	$\eta + \eta + K$
1694	$\Sigma + \bar{\mathrm{N}}$	$\leftrightarrow$	$\eta + \eta + K^*$
1695	$\Sigma + \bar{\mathrm{N}}$	$\leftrightarrow$	$\eta + K + \rho$
1696	$\Sigma + \bar{\mathrm{N}}$	$\leftrightarrow$	$\eta + K + \omega$
1697	$\Sigma + \bar{\mathrm{N}}$	$\leftrightarrow$	$\eta + K + \phi$
1698	$\Sigma + \bar{\mathrm{N}}$	$\leftrightarrow$	$\eta + K + \eta'$
1699	$\Sigma + \bar{\mathrm{N}}$	$\leftrightarrow$	$\eta + K^* + \rho$
1700	$\Sigma + \bar{\mathrm{N}}$	$\leftrightarrow$	$\eta + K^* + \omega$
1701	$\Sigma + \bar{\mathrm{N}}$	$\leftrightarrow$	$\eta + K^* + \phi$
1702	$\Sigma + \bar{\mathrm{N}}$	$\leftrightarrow$	$\eta + K^* + \eta'$
1703	$\Sigma + \bar{\mathrm{N}}$	$\leftrightarrow$	$K + \rho + \rho$
1704	$\Sigma + \bar{\mathrm{N}}$	$\leftrightarrow$	$K + \rho + \omega$
1705	$\Sigma + \bar{\mathrm{N}}$	$\leftrightarrow$	$K + \rho + \phi$
1706	$\Sigma + \bar{\mathrm{N}}$	$\leftrightarrow$	$K + \rho + \eta'$
1707	$\Sigma + \bar{\mathrm{N}}$	$\leftrightarrow$	$K + \omega + \omega$
1708	$\Sigma + \bar{\mathrm{N}}$	$\leftrightarrow$	$K + \omega + \phi$
1709	$\Sigma + \bar{\mathrm{N}}$	$\leftrightarrow$	$K + \omega + \eta'$
1710	$\Sigma + \bar{\mathrm{N}}$	$\leftrightarrow$	$K + \phi + \phi$
1711	$\Sigma + \bar{\mathrm{N}}$	$\leftrightarrow$	$K + \phi + \eta'$
1712	$\Sigma + \bar{\mathrm{N}}$	$\leftrightarrow$	$K + \eta' + \eta'$
1713	$\Sigma + \bar{\mathrm{N}}$	$\leftrightarrow$	$K + a_1 + a_1$
1714	$\Sigma + \bar{\mathrm{N}}$	$\leftrightarrow$	$K^* + \rho + \rho$
1715	$\Sigma + \bar{\mathrm{N}}$	$\leftrightarrow$	$K^* + \rho + \omega$
1716	$\Sigma + \bar{\mathrm{N}}$	$\leftrightarrow$	$K^* + \rho + \phi$
1717	$\Sigma + \bar{\mathrm{N}}$	$\leftrightarrow$	$K^* + \rho + \eta'$
1718	$\Sigma + \bar{\mathrm{N}}$	$\leftrightarrow$	$K^* + \omega + \omega$
1719	$\Sigma + \bar{\mathrm{N}}$	$\leftrightarrow$	$K^* + \omega + \phi$
1720	$\Sigma + \bar{\mathrm{N}}$	$\leftrightarrow$	$K^* + \omega + \eta'$
1721	$\Sigma + \bar{\mathrm{N}}$	$\leftrightarrow$	$K^* + \phi + \phi$
1722	$\Sigma + \bar{\mathrm{N}}$	$\leftrightarrow$	$K^* + \phi + \eta'$
1723	$\Sigma + \bar{\mathrm{N}}$	$\leftrightarrow$	$K^* + \eta' + \eta'$
1724	$\Sigma + \bar{\mathrm{N}}$	$\leftrightarrow$	$K^* + a_1 + a_1$
1725	$\Sigma + \bar{\Delta}(1232)$	$\leftrightarrow$	$\pi + \pi + K$
1726	$\Sigma + \bar{\Delta}(1232)$	$\leftrightarrow$	$\pi + \pi + K^*$
1727	$\Sigma + \bar{\Delta}(1232)$	$\leftrightarrow$	$\pi + \eta + K$
1728	$\Sigma + \bar{\Delta}(1232)$	$\leftrightarrow$	$\pi + \eta + K^*$
1729	$\Sigma + \bar{\Delta}(1232)$	$\leftrightarrow$	$\pi + K + \rho$
1730	$\Sigma + \bar{\Delta}(1232)$	$\leftrightarrow$	$\pi + K + \omega$
1731	$\Sigma + \bar{\Delta}(1232)$	$\leftrightarrow$	$\pi + K + \phi$
1732	$\Sigma + \bar{\Delta}(1232)$	$\leftrightarrow$	$\pi + K + \eta'$
1733	$\Sigma + \bar{\Delta}(1232)$	$\leftrightarrow$	$\pi + K^* + \rho$
1734	$\Sigma + \bar{\Delta}(1232)$	$\leftrightarrow$	$\pi + K^* + \omega$
1735	$\Sigma + \bar{\Delta}(1232)$	$\leftrightarrow$	$\pi + K^* + \phi$
1736	$\Sigma + \bar{\Delta}(1232)$	$\leftrightarrow$	$\pi + K^* + \eta'$
1737	$\Sigma + \bar{\Delta}(1232)$	$\leftrightarrow$	$\eta + \eta + K$
1738	$\Sigma + \bar{\Delta}(1232)$	$\leftrightarrow$	$\eta + \eta + K^*$
1739	$\Sigma + \bar{\Delta}(1232)$	$\leftrightarrow$	$\eta + K + \rho$
1740	$\Sigma + \bar{\Delta}(1232)$	$\leftrightarrow$	$\eta + K + \omega$

Ch. No.	$B_1 + B_2$	$\leftrightarrow$	$M_1+M_2+M_3$
1741	$\Sigma + \bar{\Delta}(1232)$	$\leftrightarrow$	$\eta + K + \phi$
1742	$\Sigma + \bar{\Delta}(1232)$	$\leftrightarrow$	$\eta + K + \eta'$
1743	$\Sigma + \bar{\Delta}(1232)$	$\leftrightarrow$	$\eta + K^* + \rho$
1744	$\Sigma + \bar{\Delta}(1232)$	$\leftrightarrow$	$\eta + K^* + \omega$
1745	$\Sigma + \bar{\Delta}(1232)$	$\leftrightarrow$	$\eta + K^* + \phi$
1746	$\Sigma + \bar{\Delta}(1232)$	$\leftrightarrow$	$\eta + K^* + \eta'$
1747	$\Sigma + \bar{\Delta}(1232)$	$\leftrightarrow$	$K + \rho + \rho$
1748	$\Sigma + \bar{\Delta}(1232)$	$\leftrightarrow$	$K + \rho + \omega$
1749	$\Sigma + \bar{\Delta}(1232)$	$\leftrightarrow$	$K + \rho + \phi$
1750	$\Sigma + \bar{\Delta}(1232)$	$\leftrightarrow$	$K + \rho + \eta'$
1751	$\Sigma + \bar{\Delta}(1232)$	$\leftrightarrow$	$K + \omega + \omega$
1752	$\Sigma + \bar{\Delta}(1232)$	$\leftrightarrow$	$K + \omega + \phi$
1753	$\Sigma + \bar{\Delta}(1232)$	$\leftrightarrow$	$K + \omega + \eta'$
1754	$\Sigma + \bar{\Delta}(1232)$	$\leftrightarrow$	$K + \phi + \phi$
1755	$\Sigma + \bar{\Delta}(1232)$	$\leftrightarrow$	$K + \phi + \eta'$
1756	$\Sigma + \bar{\Delta}(1232)$	$\leftrightarrow$	$K + \eta' + \eta'$
1757	$\Sigma + \bar{\Delta}(1232)$	$\leftrightarrow$	$K + a_1 + a_1$
1758	$\Sigma + \bar{\Delta}(1232)$	$\leftrightarrow$	$K^* + \rho + \rho$
1759	$\Sigma + \bar{\Delta}(1232)$	$\leftrightarrow$	$K^* + \rho + \omega$
1760	$\Sigma + \bar{\Delta}(1232)$	$\leftrightarrow$	$K^* + \rho + \phi$
1761	$\Sigma + \bar{\Delta}(1232)$	$\leftrightarrow$	$K^* + \rho + \eta'$
1762	$\Sigma + \bar{\Delta}(1232)$	$\leftrightarrow$	$K^* + \omega + \omega$
1763	$\Sigma + \bar{\Delta}(1232)$	$\leftrightarrow$	$K^* + \omega + \phi$
1764	$\Sigma + \bar{\Delta}(1232)$	$\leftrightarrow$	$K^* + \omega + \eta'$
1765	$\Sigma + \bar{\Delta}(1232)$	$\leftrightarrow$	$K^* + \phi + \phi$
1766	$\Sigma + \bar{\Delta}(1232)$	$\leftrightarrow$	$K^* + \phi + \eta'$
1767	$\Sigma + \bar{\Delta}(1232)$	$\leftrightarrow$	$K^* + \eta' + \eta'$
1768	$\Sigma + \bar{\Delta}(1232)$	$\leftrightarrow$	$K^* + a_1 + a_1$
1769	$\Sigma + \bar{\mathrm{N}}(1440)$	$\leftrightarrow$	$\pi + \pi + K$
1770	$\Sigma + \bar{\mathrm{N}}(1440)$	$\leftrightarrow$	$\pi + \pi + K^*$
1771	$\Sigma + \bar{\mathrm{N}}(1440)$	$\leftrightarrow$	$\pi + \eta + K$
1772	$\Sigma + \bar{\mathrm{N}}(1440)$	$\leftrightarrow$	$\pi + \eta + K^*$
1773	$\Sigma + \bar{\mathrm{N}}(1440)$	$\leftrightarrow$	$\pi + K + \rho$
1774	$\Sigma + \bar{\mathrm{N}}(1440)$	$\leftrightarrow$	$\pi + K + \omega$
1775	$\Sigma + \bar{\mathrm{N}}(1440)$	$\leftrightarrow$	$\pi + K + \phi$
1776	$\Sigma + \bar{\mathrm{N}}(1440)$	$\leftrightarrow$	$\pi + K + \eta'$
1777	$\Sigma + \bar{\mathrm{N}}(1440)$	$\leftrightarrow$	$\pi + K^* + \rho$
1778	$\Sigma + \bar{\mathrm{N}}(1440)$	$\leftrightarrow$	$\pi + K^* + \omega$
1779	$\Sigma + \bar{\mathrm{N}}(1440)$	$\leftrightarrow$	$\pi + K^* + \phi$
1780	$\Sigma + \bar{\mathrm{N}}(1440)$	$\leftrightarrow$	$\pi + K^* + \eta'$
1781	$\Sigma + \bar{\mathrm{N}}(1440)$	$\leftrightarrow$	$\eta + \eta + K$
1782	$\Sigma + \bar{\mathrm{N}}(1440)$	$\leftrightarrow$	$\eta + \eta + K^*$
1783	$\Sigma + \bar{\mathrm{N}}(1440)$	$\leftrightarrow$	$\eta + K + \rho$
1784	$\Sigma + \bar{\mathrm{N}}(1440)$	$\leftrightarrow$	$\eta + K + \omega$
1785	$\Sigma + \bar{\mathrm{N}}(1440)$	$\leftrightarrow$	$\eta + K + \phi$
1786	$\Sigma + \bar{\mathrm{N}}(1440)$	$\leftrightarrow$	$\eta + K + \eta'$
1787	$\Sigma + \bar{\mathrm{N}}(1440)$	$\leftrightarrow$	$\eta + K^* + \rho$
1788	$\Sigma + \bar{\mathrm{N}}(1440)$	$\leftrightarrow$	$\eta + K^* + \omega$
1789	$\Sigma + \bar{\mathrm{N}}(1440)$	$\leftrightarrow$	$\eta + K^* + \phi$
1790	$\Sigma + \bar{\mathrm{N}}(1440)$	$\leftrightarrow$	$\eta + K^* + \eta'$
1791	$\Sigma + \bar{\mathrm{N}}(1440)$	$\leftrightarrow$	$K + \rho + \rho$
1792	$\Sigma + \bar{\mathrm{N}}(1440)$	$\leftrightarrow$	$K + \rho + \omega$
1793	$\Sigma + \bar{\mathrm{N}}(1440)$	$\leftrightarrow$	$K + \rho + \phi$
1794	$\Sigma + \bar{\mathrm{N}}(1440)$	$\leftrightarrow$	$K + \rho + \eta'$
1795	$\Sigma + \bar{\mathrm{N}}(1440)$	$\leftrightarrow$	$K + \omega + \omega$
1796	$\Sigma + \bar{\mathrm{N}}(1440)$	$\leftrightarrow$	$K + \omega + \phi$
1797	$\Sigma + \bar{\mathrm{N}}(1440)$	$\leftrightarrow$	$K + \omega + \eta'$
1798	$\Sigma + \bar{\mathrm{N}}(1440)$	$\leftrightarrow$	$K + \phi + \phi$
1799	$\Sigma + \bar{\mathrm{N}}(1440)$	$\leftrightarrow$	$K + \phi + \eta'$
1800	$\Sigma + \bar{\mathrm{N}}(1440)$	$\leftrightarrow$	$K + \eta' + \eta'$
1801	$\Sigma + \bar{\mathrm{N}}(1440)$	$\leftrightarrow$	$K + a_1 + a_1$
1802	$\Sigma + \bar{\mathrm{N}}(1440)$	$\leftrightarrow$	$K^* + \rho + \rho$
1803	$\Sigma + \bar{\mathrm{N}}(1440)$	$\leftrightarrow$	$K^* + \rho + \omega$
1804	$\Sigma + \bar{\mathrm{N}}(1440)$	$\leftrightarrow$	$K^* + \rho + \phi$
1805	$\Sigma + \bar{\mathrm{N}}(1440)$	$\leftrightarrow$	$K^* + \rho + \eta'$
1806	$\Sigma + \bar{\mathrm{N}}(1440)$	$\leftrightarrow$	$K^* + \omega + \omega$
1807	$\Sigma + \bar{\mathrm{N}}(1440)$	$\leftrightarrow$	$K^* + \omega + \phi$
1808	$\Sigma + \bar{\mathrm{N}}(1440)$	$\leftrightarrow$	$K^* + \omega + \eta'$
1809	$\Sigma + \bar{\mathrm{N}}(1440)$	$\leftrightarrow$	$K^* + \phi + \phi$
1810	$\Sigma + \bar{\mathrm{N}}(1440)$	$\leftrightarrow$	$K^* + \phi + \eta'$
1811	$\Sigma + \bar{\mathrm{N}}(1440)$	$\leftrightarrow$	$K^* + \eta' + \eta'$
1812	$\Sigma + \bar{\mathrm{N}}(1440)$	$\leftrightarrow$	$K^* + a_1 + a_1$
1813	$\Sigma + \bar{\mathrm{N}}(1535)$	$\leftrightarrow$	$\pi + K + a_1$
1814	$\Sigma + \bar{\mathrm{N}}(1535)$	$\leftrightarrow$	$\pi + K^* + a_1$
1815	$\Sigma + \bar{\mathrm{N}}(1535)$	$\leftrightarrow$	$\eta + K + a_1$
1816	$\Sigma + \bar{\mathrm{N}}(1535)$	$\leftrightarrow$	$\eta + K^* + a_1$
1817	$\Sigma + \bar{\mathrm{N}}(1535)$	$\leftrightarrow$	$K + \rho + a_1$
1818	$\Sigma + \bar{\mathrm{N}}(1535)$	$\leftrightarrow$	$K + \omega + a_1$
1819	$\Sigma + \bar{\mathrm{N}}(1535)$	$\leftrightarrow$	$K + \phi + a_1$
1820	$\Sigma + \bar{\mathrm{N}}(1535)$	$\leftrightarrow$	$K + \eta' + a_1$
1821	$\Sigma + \bar{\mathrm{N}}(1535)$	$\leftrightarrow$	$K^* + \rho + a_1$
1822	$\Sigma + \bar{\mathrm{N}}(1535)$	$\leftrightarrow$	$K^* + \omega + a_1$
1823	$\Sigma + \bar{\mathrm{N}}(1535)$	$\leftrightarrow$	$K^* + \phi + a_1$
1824	$\Sigma + \bar{\mathrm{N}}(1535)$	$\leftrightarrow$	$K^* + \eta' + a_1$
1825	$\Sigma + \bar{\Lambda}$	$\leftrightarrow$	$\pi + \pi + \eta$
1826	$\Sigma + \bar{\Lambda}$	$\leftrightarrow$	$\pi + \pi + \phi$

Ch. No.	$B_1 + B_2$	$\leftrightarrow$	$M_1+M_2+M_3$
1827	$\bar{\Sigma} + \bar{\Lambda}$	$\leftrightarrow$	$\pi + \eta + \eta$
1828	$\Sigma + \bar{\Lambda}$	$\leftrightarrow$	$\pi + \eta + \rho$
1829	$\Sigma + \bar{\Lambda}$	$\leftrightarrow$	$\pi + \eta + \omega$
1830	$\Sigma + \bar{\Lambda}$	$\leftrightarrow$	$\pi + \eta + \phi$
1831	$\Sigma + \bar{\Lambda}$	$\leftrightarrow$	$\pi + \eta + \eta'$
1832	$\Sigma + \bar{\Lambda}$	$\leftrightarrow$	$\pi + K + K$
1833	$\Sigma + \bar{\Lambda}$	$\leftrightarrow$	$\pi + K + K^*$
1834	$\Sigma + \bar{\Lambda}$	$\leftrightarrow$	$\pi + K^* + K^*$
1835	$\Sigma + \bar{\Lambda}$	$\leftrightarrow$	$\pi + \rho + \phi$
1836	$\Sigma + \bar{\Lambda}$	$\leftrightarrow$	$\pi + \omega + \phi$
1837	$\Sigma + \bar{\Lambda}$	$\leftrightarrow$	$\pi + \phi + \phi$
1838	$\Sigma + \bar{\Lambda}$	$\leftrightarrow$	$\pi + \phi + \eta'$
1839	$\Sigma + \bar{\Lambda}$	$\leftrightarrow$	$\eta + \eta + \eta$
1840	$\Sigma + \bar{\Lambda}$	$\leftrightarrow$	$\eta + \eta + \rho$
1841	$\Sigma + \bar{\Lambda}$	$\leftrightarrow$	$\eta + \eta + \omega$
1842	$\Sigma + \bar{\Lambda}$	$\leftrightarrow$	$\eta + \eta + \phi$
1843	$\Sigma + \bar{\Lambda}$	$\leftrightarrow$	$\eta + \eta + \eta'$
1844	$\Sigma + \bar{\Lambda}$	$\leftrightarrow$	$\eta + K + K$
1845	$\Sigma + \bar{\Lambda}$	$\leftrightarrow$	$\eta + K + K^*$
1846	$\Sigma + \bar{\Lambda}$	$\leftrightarrow$	$\eta + K^* + K^*$
1847	$\Sigma + \bar{\Lambda}$	$\leftrightarrow$	$\eta + \rho + \rho$
1848	$\Sigma + \bar{\Lambda}$	$\leftrightarrow$	$\eta + \rho + \omega$
1849	$\Sigma + \bar{\Lambda}$	$\leftrightarrow$	$\eta + \rho + \phi$
1850	$\Sigma + \bar{\Lambda}$	$\leftrightarrow$	$\eta + \rho + \eta'$
1851	$\Sigma + \bar{\Lambda}$	$\leftrightarrow$	$\eta + \omega + \omega$
1852	$\Sigma + \bar{\Lambda}$	$\leftrightarrow$	$\eta + \omega + \phi$
1853	$\Sigma + \bar{\Lambda}$	$\leftrightarrow$	$\eta + \omega + \eta'$
1854	$\Sigma + \bar{\Lambda}$	$\leftrightarrow$	$\eta + \phi + \phi$
1855	$\Sigma + \bar{\Lambda}$	$\leftrightarrow$	$\eta + \phi + \eta'$
1856	$\Sigma + \bar{\Lambda}$	$\leftrightarrow$	$\eta + \eta' + \eta'$
1857	$\Sigma + \bar{\Lambda}$	$\leftrightarrow$	$\eta + a_1 + a_1$
1858	$\Sigma + \bar{\Lambda}$	$\leftrightarrow$	$K + K + \rho$
1859	$\Sigma + \bar{\Lambda}$	$\leftrightarrow$	$K + K + \omega$
1860	$\Sigma + \bar{\Lambda}$	$\leftrightarrow$	$K + K + \phi$
1861	$\Sigma + \bar{\Lambda}$	$\leftrightarrow$	$K + K + \eta'$
1862	$\Sigma + \bar{\Lambda}$	$\leftrightarrow$	$K + K^* + \rho$
1863	$\Sigma + \bar{\Lambda}$	$\leftrightarrow$	$K + K^* + \omega$
1864	$\Sigma + \bar{\Lambda}$	$\leftrightarrow$	$K + K^* + \phi$
1865	$\Sigma + \bar{\Lambda}$	$\leftrightarrow$	$K + K^* + \eta'$
1866	$\Sigma + \bar{\Lambda}$	$\leftrightarrow$	$K^* + K^* + \rho$
1867	$\Sigma + \bar{\Lambda}$	$\leftrightarrow$	$K^* + K^* + \omega$
1868	$\Sigma + \bar{\Lambda}$	$\leftrightarrow$	$K^* + K^* + \phi$
1869	$\Sigma + \bar{\Lambda}$	$\leftrightarrow$	$K^* + K^* + \eta'$
1870	$\Sigma + \bar{\Lambda}$	$\leftrightarrow$	$\rho + \rho + \phi$
1871	$\Sigma + \bar{\Lambda}$	$\leftrightarrow$	$\rho + \omega + \phi$
1872	$\Sigma + \bar{\Lambda}$	$\leftrightarrow$	$\rho + \phi + \phi$
1873	$\Sigma + \bar{\Lambda}$	$\leftrightarrow$	$\rho + \phi + \eta'$
1874	$\Sigma + \bar{\Lambda}$	$\leftrightarrow$	$\omega + \omega + \phi$
1875	$\Sigma + \bar{\Lambda}$	$\leftrightarrow$	$\omega + \phi + \phi$
1876	$\Sigma + \bar{\Lambda}$	$\leftrightarrow$	$\omega + \phi + \eta'$
1877	$\Sigma + \bar{\Lambda}$	$\leftrightarrow$	$\phi + \phi + \phi$
1878	$\Sigma + \bar{\Lambda}$	$\leftrightarrow$	$\phi + \phi + \eta'$
1879	$\Sigma + \bar{\Lambda}$	$\leftrightarrow$	$\phi + \eta' + \eta'$
1880	$\Sigma + \bar{\Lambda}$	$\leftrightarrow$	$\phi + a_1 + a_1$
1881	$\Sigma + \bar{\Sigma}$	$\leftrightarrow$	$\pi + \pi + \eta$
1882	$\Sigma + \bar{\Sigma}$	$\leftrightarrow$	$\pi + \pi + \phi$
1883	$\Sigma + \bar{\Sigma}$	$\leftrightarrow$	$\pi + \eta + \eta$
1884	$\Sigma + \bar{\Sigma}$	$\leftrightarrow$	$\pi + \eta + \rho$
1885	$\Sigma + \bar{\Sigma}$	$\leftrightarrow$	$\pi + \eta + \omega$
1886	$\Sigma + \bar{\Sigma}$	$\leftrightarrow$	$\pi + \eta + \phi$
1887	$\Sigma + \bar{\Sigma}$	$\leftrightarrow$	$\pi + \eta + \eta'$
1888	$\Sigma + \bar{\Sigma}$	$\leftrightarrow$	$\pi + K + K$
1889	$\Sigma + \bar{\Sigma}$	$\leftrightarrow$	$\pi + K + K^*$
1890	$\Sigma + \bar{\Sigma}$	$\leftrightarrow$	$\pi + K^* + K^*$
1891	$\Sigma + \bar{\Sigma}$	$\leftrightarrow$	$\pi + \rho + \phi$
1892	$\Sigma + \bar{\Sigma}$	$\leftrightarrow$	$\pi + \omega + \phi$
1893	$\Sigma + \bar{\Sigma}$	$\leftrightarrow$	$\pi + \phi + \phi$
1894	$\Sigma + \bar{\Sigma}$	$\leftrightarrow$	$\pi + \phi + \eta'$
1895	$\Sigma + \bar{\Sigma}$	$\leftrightarrow$	$\eta + \eta + \eta$
1896	$\Sigma + \bar{\Sigma}$	$\leftrightarrow$	$\eta + \eta + \rho$
1897	$\Sigma + \bar{\Sigma}$	$\leftrightarrow$	$\eta + \eta + \omega$
1898	$\Sigma + \bar{\Sigma}$	$\leftrightarrow$	$\eta + \eta + \phi$
1899	$\Sigma + \bar{\Sigma}$	$\leftrightarrow$	$\eta + \eta + \eta'$
1900	$\Sigma + \bar{\Sigma}$	$\leftrightarrow$	$\eta + K + K$
1901	$\Sigma + \bar{\Sigma}$	$\leftrightarrow$	$\eta + K + K^*$
1902	$\Sigma + \bar{\Sigma}$	$\leftrightarrow$	$\eta + K^* + K^*$
1903	$\Sigma + \bar{\Sigma}$	$\leftrightarrow$	$\eta + \rho + \rho$
1904	$\Sigma + \bar{\Sigma}$	$\leftrightarrow$	$\eta + \rho + \omega$
1905	$\Sigma + \bar{\Sigma}$	$\leftrightarrow$	$\eta + \rho + \phi$
1906	$\Sigma + \bar{\Sigma}$	$\leftrightarrow$	$\eta + \rho + \eta'$
1907	$\Sigma + \bar{\Sigma}$	$\leftrightarrow$	$\eta + \omega + \omega$
1908	$\Sigma + \bar{\Sigma}$	$\leftrightarrow$	$\eta + \omega + \phi$
1909	$\Sigma + \bar{\Sigma}$	$\leftrightarrow$	$\eta + \omega + \eta'$
1910	$\Sigma + \bar{\Sigma}$	$\leftrightarrow$	$\eta + \phi + \phi$
1911	$\Sigma + \bar{\Sigma}$	$\leftrightarrow$	$\eta + \phi + \eta'$
1912	$\Sigma + \bar{\Sigma}$	$\leftrightarrow$	$\eta + \eta' + \eta'$

Ch. No.	$B_1 + B_2$	$\leftrightarrow$	$M_1+M_2+M_3$
1913	$\Sigma + \bar{\Sigma}$	$\leftrightarrow$	$\eta + a_1 + a_1$
1914	$\Sigma + \bar{\Sigma}$	$\leftrightarrow$	$K + K + \rho$
1915	$\Sigma + \bar{\Sigma}$	$\leftrightarrow$	$K + K + \omega$
1916	$\Sigma + \bar{\Sigma}$	$\leftrightarrow$	$K + K + \phi$
1917	$\Sigma + \bar{\Sigma}$	$\leftrightarrow$	$K + K + \eta'$
1918	$\Sigma + \bar{\Sigma}$	$\leftrightarrow$	$K + K^* + \rho$
1919	$\Sigma + \bar{\Sigma}$	$\leftrightarrow$	$K + K^* + \omega$
1920	$\Sigma + \bar{\Sigma}$	$\leftrightarrow$	$K + K^* + \phi$
1921	$\Sigma + \bar{\Sigma}$	$\leftrightarrow$	$K + K^* + \eta'$
1922	$\Sigma + \bar{\Sigma}$	$\leftrightarrow$	$K^* + K^* + \rho$
1923	$\Sigma + \bar{\Sigma}$	$\leftrightarrow$	$K^* + K^* + \omega$
1924	$\Sigma + \bar{\Sigma}$	$\leftrightarrow$	$K^* + K^* + \phi$
1925	$\Sigma + \bar{\Sigma}$	$\leftrightarrow$	$K^* + K^* + \eta'$
1926	$\Sigma + \bar{\Sigma}$	$\leftrightarrow$	$\rho + \rho + \phi$
1927	$\Sigma + \bar{\Sigma}$	$\leftrightarrow$	$\rho + \omega + \phi$
1928	$\Sigma + \bar{\Sigma}$	$\leftrightarrow$	$\rho + \phi + \phi$
1929	$\Sigma + \bar{\Sigma}$	$\leftrightarrow$	$\rho + \phi + \eta'$
1930	$\Sigma + \bar{\Sigma}$	$\leftrightarrow$	$\omega + \omega + \phi$
1931	$\Sigma + \bar{\Sigma}$	$\leftrightarrow$	$\omega + \phi + \phi$
1932	$\Sigma + \bar{\Sigma}$	$\leftrightarrow$	$\omega + \phi + \eta'$
1933	$\Sigma + \bar{\Sigma}$	$\leftrightarrow$	$\phi + \phi + \phi$
1934	$\Sigma + \bar{\Sigma}$	$\leftrightarrow$	$\phi + \phi + \eta'$
1935	$\Sigma + \bar{\Sigma}$	$\leftrightarrow$	$\phi + \eta' + \eta'$
1936	$\Sigma + \bar{\Sigma}$	$\leftrightarrow$	$\phi + a_1 + a_1$
1937	$\Sigma + \bar{\Sigma}^*$	$\leftrightarrow$	$\pi + \pi + \eta$
1938	$\Sigma + \bar{\Sigma}^*$	$\leftrightarrow$	$\pi + \pi + \phi$
1939	$\Sigma + \bar{\Sigma}^*$	$\leftrightarrow$	$\pi + \eta + \eta$
1940	$\Sigma + \bar{\Sigma}^*$	$\leftrightarrow$	$\pi + \eta + \rho$
1941	$\Sigma + \bar{\Sigma}^*$	$\leftrightarrow$	$\pi + \eta + \omega$
1942	$\Sigma + \bar{\Sigma}^*$	$\leftrightarrow$	$\pi + \eta + \phi$
1943	$\Sigma + \bar{\Sigma}^*$	$\leftrightarrow$	$\pi + \eta + \eta'$
1944	$\Sigma + \bar{\Sigma}^*$	$\leftrightarrow$	$\pi + K + K$
1945	$\Sigma + \bar{\Sigma}^*$	$\leftrightarrow$	$\pi + K + K^*$
1946	$\Sigma + \bar{\Sigma}^*$	$\leftrightarrow$	$\pi + K^* + K^*$
1947	$\Sigma + \bar{\Sigma}^*$	$\leftrightarrow$	$\pi + \rho + \phi$
1948	$\Sigma + \bar{\Sigma}^*$	$\leftrightarrow$	$\pi + \omega + \phi$
1949	$\Sigma + \bar{\Sigma}^*$	$\leftrightarrow$	$\pi + \phi + \phi$
1950	$\Sigma + \bar{\Sigma}^*$	$\leftrightarrow$	$\pi + \phi + \eta'$
1951	$\Sigma + \bar{\Sigma}^*$	$\leftrightarrow$	$\eta + \eta + \eta$
1952	$\Sigma + \bar{\Sigma}^*$	$\leftrightarrow$	$\eta + \eta + \rho$
1953	$\Sigma + \bar{\Sigma}^*$	$\leftrightarrow$	$\eta + \eta + \omega$
1954	$\Sigma + \bar{\Sigma}^*$	$\leftrightarrow$	$\eta + \eta + \phi$
1955	$\Sigma + \bar{\Sigma}^*$	$\leftrightarrow$	$\eta + \eta + \eta'$
1956	$\Sigma + \bar{\Sigma}^*$	$\leftrightarrow$	$\eta + K + K$
1957	$\Sigma + \bar{\Sigma}^*$	$\leftrightarrow$	$\eta + K + K^*$
1958	$\Sigma + \bar{\Sigma}^*$	$\leftrightarrow$	$\eta + K^* + K^*$
1959	$\Sigma + \bar{\Sigma}^*$	$\leftrightarrow$	$\eta + \rho + \rho$
1960	$\Sigma + \bar{\Sigma}^*$	$\leftrightarrow$	$\eta + \rho + \omega$
1961	$\Sigma + \bar{\Sigma}^*$	$\leftrightarrow$	$\eta + \rho + \phi$
1962	$\Sigma + \bar{\Sigma}^*$	$\leftrightarrow$	$\eta + \rho + \eta'$
1963	$\Sigma + \bar{\Sigma}^*$	$\leftrightarrow$	$\eta + \omega + \omega$
1964	$\Sigma + \bar{\Sigma}^*$	$\leftrightarrow$	$\eta + \omega + \phi$
1965	$\Sigma + \bar{\Sigma}^*$	$\leftrightarrow$	$\eta + \omega + \eta'$
1966	$\Sigma + \bar{\Sigma}^*$	$\leftrightarrow$	$\eta + \phi + \phi$
1967	$\Sigma + \bar{\Sigma}^*$	$\leftrightarrow$	$\eta + \phi + \eta'$
1968	$\Sigma + \bar{\Sigma}^*$	$\leftrightarrow$	$\eta + \eta' + \eta'$
1969	$\Sigma + \bar{\Sigma}^*$	$\leftrightarrow$	$\eta + a_1 + a_1$
1970	$\Sigma + \bar{\Sigma}^*$	$\leftrightarrow$	$K + K + \rho$
1971	$\Sigma + \bar{\Sigma}^*$	$\leftrightarrow$	$K + K + \omega$
1972	$\Sigma + \bar{\Sigma}^*$	$\leftrightarrow$	$K + K + \phi$
1973	$\Sigma + \bar{\Sigma}^*$	$\leftrightarrow$	$K + K + \eta'$
1974	$\Sigma + \bar{\Sigma}^*$	$\leftrightarrow$	$K + K^* + \rho$
1975	$\Sigma + \bar{\Sigma}^*$	$\leftrightarrow$	$K + K^* + \omega$
1976	$\Sigma + \bar{\Sigma}^*$	$\leftrightarrow$	$K + K^* + \phi$
1977	$\Sigma + \bar{\Sigma}^*$	$\leftrightarrow$	$K + K^* + \eta'$
1978	$\Sigma + \bar{\Sigma}^*$	$\leftrightarrow$	$K^* + K^* + \rho$
1979	$\Sigma + \bar{\Sigma}^*$	$\leftrightarrow$	$K^* + K^* + \omega$
1980	$\Sigma + \bar{\Sigma}^*$	$\leftrightarrow$	$K^* + K^* + \phi$
1981	$\Sigma + \bar{\Sigma}^*$	$\leftrightarrow$	$K^* + K^* + \eta'$
1982	$\Sigma + \bar{\Sigma}^*$	$\leftrightarrow$	$\rho + \rho + \phi$
1983	$\Sigma + \bar{\Sigma}^*$	$\leftrightarrow$	$\rho + \omega + \phi$
1984	$\Sigma + \bar{\Sigma}^*$	$\leftrightarrow$	$\rho + \phi + \phi$
1985	$\Sigma + \bar{\Sigma}^*$	$\leftrightarrow$	$\rho + \phi + \eta'$
1986	$\Sigma + \bar{\Sigma}^*$	$\leftrightarrow$	$\omega + \omega + \phi$
1987	$\Sigma + \bar{\Sigma}^*$	$\leftrightarrow$	$\omega + \phi + \phi$
1988	$\Sigma + \bar{\Sigma}^*$	$\leftrightarrow$	$\omega + \phi + \eta'$
1989	$\Sigma + \bar{\Sigma}^*$	$\leftrightarrow$	$\phi + \phi + \phi$
1990	$\Sigma + \bar{\Sigma}^*$	$\leftrightarrow$	$\phi + \phi + \eta'$
1991	$\Sigma + \bar{\Sigma}^*$	$\leftrightarrow$	$\phi + \eta' + \eta'$
1992	$\Sigma + \bar{\Sigma}^*$	$\leftrightarrow$	$\phi + a_1 + a_1$
1993	$\Sigma + \bar{\Xi}$	$\leftrightarrow$	$\pi + \eta + K$
1994	$\Sigma + \bar{\Xi}$	$\leftrightarrow$	$\pi + \eta + K^*$
1995	$\Sigma + \bar{\Xi}$	$\leftrightarrow$	$\pi + K + \phi$
1996	$\Sigma + \bar{\Xi}$	$\leftrightarrow$	$\pi + K^* + \phi$
1997	$\Sigma + \bar{\Xi}$	$\leftrightarrow$	$\eta + \eta + K$
1998	$\Sigma + \bar{\Xi}$	$\leftrightarrow$	$\eta + \eta + K^*$

Ch. No.	$B_1 + B_2$	$\leftrightarrow$	$M_1+M_2+M_3$
1999	$\Sigma + \bar{\Xi}$	$\leftrightarrow$	$\eta + K + \rho$
2000	$\Sigma + \bar{\Xi}$	$\leftrightarrow$	$\eta + K + \omega$
2001	$\Sigma + \bar{\Xi}$	$\leftrightarrow$	$\eta + K + \phi$
2002	$\Sigma + \bar{\Xi}$	$\leftrightarrow$	$\eta + K + \eta'$
2003	$\Sigma + \bar{\Xi}$	$\leftrightarrow$	$\eta + K^* + \rho$
2004	$\Sigma + \bar{\Xi}$	$\leftrightarrow$	$\eta + K^* + \omega$
2005	$\Sigma + \bar{\Xi}$	$\leftrightarrow$	$\eta + K^* + \phi$
2006	$\Sigma + \bar{\Xi}$	$\leftrightarrow$	$\eta + K^* + \eta'$
2007	$\Sigma + \bar{\Xi}$	$\leftrightarrow$	$K + K + K$
2008	$\Sigma + \bar{\Xi}$	$\leftrightarrow$	$K + K + K^*$
2009	$\Sigma + \bar{\Xi}$	$\leftrightarrow$	$K + K^* + K^*$
2010	$\Sigma + \bar{\Xi}$	$\leftrightarrow$	$K + \rho + \phi$
2011	$\Sigma + \bar{\Xi}$	$\leftrightarrow$	$K + \omega + \phi$
2012	$\Sigma + \bar{\Xi}$	$\leftrightarrow$	$K + \phi + \phi$
2013	$\Sigma + \bar{\Xi}$	$\leftrightarrow$	$K + \phi + \eta'$
2014	$\Sigma + \bar{\Xi}$	$\leftrightarrow$	$K^* + K^* + K^*$
2015	$\Sigma + \bar{\Xi}$	$\leftrightarrow$	$K^* + \rho + \phi$
2016	$\Sigma + \bar{\Xi}$	$\leftrightarrow$	$K^* + \omega + \phi$
2017	$\Sigma + \bar{\Xi}$	$\leftrightarrow$	$K^* + \phi + \phi$
2018	$\Sigma + \bar{\Xi}$	$\leftrightarrow$	$K^* + \phi + \eta'$
2019	$\Sigma + \bar{\Xi}^*$	$\leftrightarrow$	$\pi + \eta + K$
2020	$\Sigma + \bar{\Xi}^*$	$\leftrightarrow$	$\pi + \eta + K^*$
2021	$\Sigma + \bar{\Xi}^*$	$\leftrightarrow$	$\pi + K + \phi$
2022	$\Sigma + \bar{\Xi}^*$	$\leftrightarrow$	$\pi + K^* + \phi$
2023	$\Sigma + \bar{\Xi}^*$	$\leftrightarrow$	$\eta + \eta + K$
2024	$\Sigma + \bar{\Xi}^*$	$\leftrightarrow$	$\eta + \eta + K^*$
2025	$\Sigma + \bar{\Xi}^*$	$\leftrightarrow$	$\eta + K + \rho$
2026	$\Sigma + \bar{\Xi}^*$	$\leftrightarrow$	$\eta + K + \omega$
2027	$\Sigma + \bar{\Xi}^*$	$\leftrightarrow$	$\eta + K + \phi$
2028	$\Sigma + \bar{\Xi}^*$	$\leftrightarrow$	$\eta + K + \eta'$
2029	$\Sigma + \bar{\Xi}^*$	$\leftrightarrow$	$\eta + K^* + \rho$
2030	$\Sigma + \bar{\Xi}^*$	$\leftrightarrow$	$\eta + K^* + \omega$
2031	$\Sigma + \bar{\Xi}^*$	$\leftrightarrow$	$\eta + K^* + \phi$
2032	$\Sigma + \bar{\Xi}^*$	$\leftrightarrow$	$\eta + K^* + \eta'$
2033	$\Sigma + \bar{\Xi}^*$	$\leftrightarrow$	$K + K + K$
2034	$\Sigma + \bar{\Xi}^*$	$\leftrightarrow$	$K + K + K^*$
2035	$\Sigma + \bar{\Xi}^*$	$\leftrightarrow$	$K + K^* + K^*$
2036	$\Sigma + \bar{\Xi}^*$	$\leftrightarrow$	$K + \rho + \phi$
2037	$\Sigma + \bar{\Xi}^*$	$\leftrightarrow$	$K + \omega + \phi$
2038	$\Sigma + \bar{\Xi}^*$	$\leftrightarrow$	$K + \phi + \phi$
2039	$\Sigma + \bar{\Xi}^*$	$\leftrightarrow$	$K + \phi + \eta'$
2040	$\Sigma + \bar{\Xi}^*$	$\leftrightarrow$	$K^* + K^* + K^*$
2041	$\Sigma + \bar{\Xi}^*$	$\leftrightarrow$	$K^* + \rho + \phi$
2042	$\Sigma + \bar{\Xi}^*$	$\leftrightarrow$	$K^* + \omega + \phi$
2043	$\Sigma + \bar{\Xi}^*$	$\leftrightarrow$	$K^* + \phi + \phi$
2044	$\Sigma + \bar{\Xi}^*$	$\leftrightarrow$	$K^* + \phi + \eta'$
2045	$\Sigma + \bar{\Omega}$	$\leftrightarrow$	$\eta + K + K$
2046	$\Sigma + \bar{\Omega}$	$\leftrightarrow$	$\eta + K + K^*$
2047	$\Sigma + \bar{\Omega}$	$\leftrightarrow$	$\eta + K^* + K^*$
2048	$\Sigma + \bar{\Omega}$	$\leftrightarrow$	$K + K + \phi$
2049	$\Sigma + \bar{\Omega}$	$\leftrightarrow$	$K + K^* + \phi$
2050	$\Sigma + \bar{\Omega}$	$\leftrightarrow$	$K^* + K^* + \phi$
2051	$\Sigma^* + \bar{\mathrm{N}}$	$\leftrightarrow$	$\pi + \pi + K$
2052	$\Sigma^* + \bar{\mathrm{N}}$	$\leftrightarrow$	$\pi + \pi + K^*$
2053	$\Sigma^* + \bar{\mathrm{N}}$	$\leftrightarrow$	$\pi + \eta + K$
2054	$\Sigma^* + \bar{\mathrm{N}}$	$\leftrightarrow$	$\pi + \eta + K^*$
2055	$\Sigma^* + \bar{\mathrm{N}}$	$\leftrightarrow$	$\pi + K + \rho$
2056	$\Sigma^* + \bar{\mathrm{N}}$	$\leftrightarrow$	$\pi + K + \omega$
2057	$\Sigma^* + \bar{\mathrm{N}}$	$\leftrightarrow$	$\pi + K + \phi$
2058	$\Sigma^* + \bar{\mathrm{N}}$	$\leftrightarrow$	$\pi + K + \eta'$
2059	$\Sigma^* + \bar{\mathrm{N}}$	$\leftrightarrow$	$\pi + K^* + \rho$
2060	$\Sigma^* + \bar{\mathrm{N}}$	$\leftrightarrow$	$\pi + K^* + \omega$
2061	$\Sigma^* + \bar{\mathrm{N}}$	$\leftrightarrow$	$\pi + K^* + \phi$
2062	$\Sigma^* + \bar{\mathrm{N}}$	$\leftrightarrow$	$\pi + K^* + \eta'$
2063	$\Sigma^* + \bar{\mathrm{N}}$	$\leftrightarrow$	$\eta + \eta + K$
2064	$\Sigma^* + \bar{\mathrm{N}}$	$\leftrightarrow$	$\eta + \eta + K^*$
2065	$\Sigma^* + \bar{\mathrm{N}}$	$\leftrightarrow$	$\eta + K + \rho$
2066	$\Sigma^* + \bar{\mathrm{N}}$	$\leftrightarrow$	$\eta + K + \omega$
2067	$\Sigma^* + \bar{\mathrm{N}}$	$\leftrightarrow$	$\eta + K + \phi$
2068	$\Sigma^* + \bar{\mathrm{N}}$	$\leftrightarrow$	$\eta + K + \eta'$
2069	$\Sigma^* + \bar{\mathrm{N}}$	$\leftrightarrow$	$\eta + K^* + \rho$
2070	$\Sigma^* + \bar{\mathrm{N}}$	$\leftrightarrow$	$\eta + K^* + \omega$
2071	$\Sigma^* + \bar{\mathrm{N}}$	$\leftrightarrow$	$\eta + K^* + \phi$
2072	$\Sigma^* + \bar{\mathrm{N}}$	$\leftrightarrow$	$\eta + K^* + \eta'$
2073	$\Sigma^* + \bar{\mathrm{N}}$	$\leftrightarrow$	$K + \rho + \rho$
2074	$\Sigma^* + \bar{\mathrm{N}}$	$\leftrightarrow$	$K + \rho + \omega$
2075	$\Sigma^* + \bar{\mathrm{N}}$	$\leftrightarrow$	$K + \rho + \phi$
2076	$\Sigma^* + \bar{\mathrm{N}}$	$\leftrightarrow$	$K + \rho + \eta'$
2077	$\Sigma^* + \bar{\mathrm{N}}$	$\leftrightarrow$	$K + \omega + \omega$
2078	$\Sigma^* + \bar{\mathrm{N}}$	$\leftrightarrow$	$K + \omega + \phi$
2079	$\Sigma^* + \bar{\mathrm{N}}$	$\leftrightarrow$	$K + \omega + \eta'$
2080	$\Sigma^* + \bar{\mathrm{N}}$	$\leftrightarrow$	$K + \phi + \phi$
2081	$\Sigma^* + \bar{\mathrm{N}}$	$\leftrightarrow$	$K + \phi + \eta'$
2082	$\Sigma^* + \bar{\mathrm{N}}$	$\leftrightarrow$	$K + \eta' + \eta'$
2083	$\Sigma^* + \bar{\mathrm{N}}$	$\leftrightarrow$	$K + a_1 + a_1$
2084	$\Sigma^* + \bar{\mathrm{N}}$	$\leftrightarrow$	$K^* + \rho + \rho$

Ch. No.	$B_1 + B_2$	$\leftrightarrow$	$M_1+M_2+M_3$
2085	$\Sigma^* + \bar{\mathrm{N}}$	$\leftrightarrow$	$K^* + \rho + \omega$
2086	$\Sigma^* + \bar{\mathrm{N}}$	$\leftrightarrow$	$K^* + \rho + \phi$
2087	$\Sigma^* + \bar{\mathrm{N}}$	$\leftrightarrow$	$K^* + \rho + \eta'$
2088	$\Sigma^* + \bar{\mathrm{N}}$	$\leftrightarrow$	$K^* + \omega + \omega$
2089	$\Sigma^* + \bar{\mathrm{N}}$	$\leftrightarrow$	$K^* + \omega + \phi$
2090	$\Sigma^* + \bar{\mathrm{N}}$	$\leftrightarrow$	$K^* + \omega + \eta'$
2091	$\Sigma^* + \bar{\mathrm{N}}$	$\leftrightarrow$	$K^* + \phi + \phi$
2092	$\Sigma^* + \bar{\mathrm{N}}$	$\leftrightarrow$	$K^* + \phi + \eta'$
2093	$\Sigma^* + \bar{\mathrm{N}}$	$\leftrightarrow$	$K^* + \eta' + \eta'$
2094	$\Sigma^* + \bar{\mathrm{N}}$	$\leftrightarrow$	$K^* + a_1 + a_1$
2095	$\Sigma^* + \bar{\Delta}(1232)$	$\leftrightarrow$	$\pi + \pi + K$
2096	$\Sigma^* + \bar{\Delta}(1232)$	$\leftrightarrow$	$\pi + \pi + K^*$
2097	$\Sigma^* + \bar{\Delta}(1232)$	$\leftrightarrow$	$\pi + \eta + K$
2098	$\Sigma^* + \bar{\Delta}(1232)$	$\leftrightarrow$	$\pi + \eta + K^*$
2099	$\Sigma^* + \bar{\Delta}(1232)$	$\leftrightarrow$	$\pi + K + \rho$
2100	$\Sigma^* + \bar{\Delta}(1232)$	$\leftrightarrow$	$\pi + K + \omega$
2101	$\Sigma^* + \bar{\Delta}(1232)$	$\leftrightarrow$	$\pi + K + \phi$
2102	$\Sigma^* + \bar{\Delta}(1232)$	$\leftrightarrow$	$\pi + K + \eta'$
2103	$\Sigma^* + \bar{\Delta}(1232)$	$\leftrightarrow$	$\pi + K^* + \rho$
2104	$\Sigma^* + \bar{\Delta}(1232)$	$\leftrightarrow$	$\pi + K^* + \omega$
2105	$\Sigma^* + \bar{\Delta}(1232)$	$\leftrightarrow$	$\pi + K^* + \phi$
2106	$\Sigma^* + \bar{\Delta}(1232)$	$\leftrightarrow$	$\pi + K^* + \eta'$
2107	$\Sigma^* + \bar{\Delta}(1232)$	$\leftrightarrow$	$\eta + \eta + K$
2108	$\Sigma^* + \bar{\Delta}(1232)$	$\leftrightarrow$	$\eta + \eta + K^*$
2109	$\Sigma^* + \bar{\Delta}(1232)$	$\leftrightarrow$	$\eta + K + \rho$
2110	$\Sigma^* + \bar{\Delta}(1232)$	$\leftrightarrow$	$\eta + K + \omega$
2111	$\Sigma^* + \bar{\Delta}(1232)$	$\leftrightarrow$	$\eta + K + \phi$
2112	$\Sigma^* + \bar{\Delta}(1232)$	$\leftrightarrow$	$\eta + K + \eta'$
2113	$\Sigma^* + \bar{\Delta}(1232)$	$\leftrightarrow$	$\eta + K^* + \rho$
2114	$\Sigma^* + \bar{\Delta}(1232)$	$\leftrightarrow$	$\eta + K^* + \omega$
2115	$\Sigma^* + \bar{\Delta}(1232)$	$\leftrightarrow$	$\eta + K^* + \phi$
2116	$\Sigma^* + \bar{\Delta}(1232)$	$\leftrightarrow$	$\eta + K^* + \eta'$
2117	$\Sigma^* + \bar{\Delta}(1232)$	$\leftrightarrow$	$K + \rho + \rho$
2118	$\Sigma^* + \bar{\Delta}(1232)$	$\leftrightarrow$	$K + \rho + \omega$
2119	$\Sigma^* + \bar{\Delta}(1232)$	$\leftrightarrow$	$K + \rho + \phi$
2120	$\Sigma^* + \bar{\Delta}(1232)$	$\leftrightarrow$	$K + \rho + \eta'$
2121	$\Sigma^* + \bar{\Delta}(1232)$	$\leftrightarrow$	$K + \omega + \omega$
2122	$\Sigma^* + \bar{\Delta}(1232)$	$\leftrightarrow$	$K + \omega + \phi$
2123	$\Sigma^* + \bar{\Delta}(1232)$	$\leftrightarrow$	$K + \omega + \eta'$
2124	$\Sigma^* + \bar{\Delta}(1232)$	$\leftrightarrow$	$K + \phi + \phi$
2125	$\Sigma^* + \bar{\Delta}(1232)$	$\leftrightarrow$	$K + \phi + \eta'$
2126	$\Sigma^* + \bar{\Delta}(1232)$	$\leftrightarrow$	$K + \eta' + \eta'$
2127	$\Sigma^* + \bar{\Delta}(1232)$	$\leftrightarrow$	$K + a_1 + a_1$
2128	$\Sigma^* + \bar{\Delta}(1232)$	$\leftrightarrow$	$K^* + \rho + \rho$
2129	$\Sigma^* + \bar{\Delta}(1232)$	$\leftrightarrow$	$K^* + \rho + \omega$
2130	$\Sigma^* + \bar{\Delta}(1232)$	$\leftrightarrow$	$K^* + \rho + \phi$
2131	$\Sigma^* + \bar{\Delta}(1232)$	$\leftrightarrow$	$K^* + \rho + \eta'$
2132	$\Sigma^* + \bar{\Delta}(1232)$	$\leftrightarrow$	$K^* + \omega + \omega$
2133	$\Sigma^* + \bar{\Delta}(1232)$	$\leftrightarrow$	$K^* + \omega + \phi$
2134	$\Sigma^* + \bar{\Delta}(1232)$	$\leftrightarrow$	$K^* + \omega + \eta'$
2135	$\Sigma^* + \bar{\Delta}(1232)$	$\leftrightarrow$	$K^* + \phi + \phi$
2136	$\Sigma^* + \bar{\Delta}(1232)$	$\leftrightarrow$	$K^* + \phi + \eta'$
2137	$\Sigma^* + \bar{\Delta}(1232)$	$\leftrightarrow$	$K^* + \eta' + \eta'$
2138	$\Sigma^* + \bar{\Delta}(1232)$	$\leftrightarrow$	$K^* + a_1 + a_1$
2139	$\Sigma^* + \bar{\mathrm{N}}(1440)$	$\leftrightarrow$	$\pi + \pi + K$
2140	$\Sigma^* + \bar{\mathrm{N}}(1440)$	$\leftrightarrow$	$\pi + \pi + K^*$
2141	$\Sigma^* + \bar{\mathrm{N}}(1440)$	$\leftrightarrow$	$\pi + \eta + K$
2142	$\Sigma^* + \bar{\mathrm{N}}(1440)$	$\leftrightarrow$	$\pi + \eta + K^*$
2143	$\Sigma^* + \bar{\mathrm{N}}(1440)$	$\leftrightarrow$	$\pi + K + \rho$
2144	$\Sigma^* + \bar{\mathrm{N}}(1440)$	$\leftrightarrow$	$\pi + K + \omega$
2145	$\Sigma^* + \bar{\mathrm{N}}(1440)$	$\leftrightarrow$	$\pi + K + \phi$
2146	$\Sigma^* + \bar{\mathrm{N}}(1440)$	$\leftrightarrow$	$\pi + K + \eta'$
2147	$\Sigma^* + \bar{\mathrm{N}}(1440)$	$\leftrightarrow$	$\pi + K^* + \rho$
2148	$\Sigma^* + \bar{\mathrm{N}}(1440)$	$\leftrightarrow$	$\pi + K^* + \omega$
2149	$\Sigma^* + \bar{\mathrm{N}}(1440)$	$\leftrightarrow$	$\pi + K^* + \phi$
2150	$\Sigma^* + \bar{\mathrm{N}}(1440)$	$\leftrightarrow$	$\pi + K^* + \eta'$
2151	$\Sigma^* + \bar{\mathrm{N}}(1440)$	$\leftrightarrow$	$\eta + \eta + K$
2152	$\Sigma^* + \bar{\mathrm{N}}(1440)$	$\leftrightarrow$	$\eta + \eta + K^*$
2153	$\Sigma^* + \bar{\mathrm{N}}(1440)$	$\leftrightarrow$	$\eta + K + \rho$
2154	$\Sigma^* + \bar{\mathrm{N}}(1440)$	$\leftrightarrow$	$\eta + K + \omega$
2155	$\Sigma^* + \bar{\mathrm{N}}(1440)$	$\leftrightarrow$	$\eta + K + \phi$
2156	$\Sigma^* + \bar{\mathrm{N}}(1440)$	$\leftrightarrow$	$\eta + K + \eta'$
2157	$\Sigma^* + \bar{\mathrm{N}}(1440)$	$\leftrightarrow$	$\eta + K^* + \rho$
2158	$\Sigma^* + \bar{\mathrm{N}}(1440)$	$\leftrightarrow$	$\eta + K^* + \omega$
2159	$\Sigma^* + \bar{\mathrm{N}}(1440)$	$\leftrightarrow$	$\eta + K^* + \phi$
2160	$\Sigma^* + \bar{\mathrm{N}}(1440)$	$\leftrightarrow$	$\eta + K^* + \eta'$
2161	$\Sigma^* + \bar{\mathrm{N}}(1440)$	$\leftrightarrow$	$K + \rho + \rho$
2162	$\Sigma^* + \bar{\mathrm{N}}(1440)$	$\leftrightarrow$	$K + \rho + \omega$
2163	$\Sigma^* + \bar{\mathrm{N}}(1440)$	$\leftrightarrow$	$K + \rho + \phi$
2164	$\Sigma^* + \bar{\mathrm{N}}(1440)$	$\leftrightarrow$	$K + \rho + \eta'$
2165	$\Sigma^* + \bar{\mathrm{N}}(1440)$	$\leftrightarrow$	$K + \omega + \omega$
2166	$\Sigma^* + \bar{\mathrm{N}}(1440)$	$\leftrightarrow$	$K + \omega + \phi$
2167	$\Sigma^* + \bar{\mathrm{N}}(1440)$	$\leftrightarrow$	$K + \omega + \eta'$
2168	$\Sigma^* + \bar{\mathrm{N}}(1440)$	$\leftrightarrow$	$K + \phi + \phi$
2169	$\Sigma^* + \bar{\mathrm{N}}(1440)$	$\leftrightarrow$	$K + \phi + \eta'$
2170	$\Sigma^* + \bar{\mathrm{N}}(1440)$	$\leftrightarrow$	$K + \eta' + \eta'$

Ch. No.	$B_1 + B_2$	$\leftrightarrow$	$M_1+M_2+M_3$
2171	$\Sigma^* + \bar{N}(1440)$	$\leftrightarrow$	$K + a_1 + a_1$
2172	$\Sigma^* + \bar{N}(1440)$	$\leftrightarrow$	$K^* + \rho + \rho$
2173	$\Sigma^* + \bar{N}(1440)$	$\leftrightarrow$	$K^* + \rho + \omega$
2174	$\Sigma^* + \bar{N}(1440)$	$\leftrightarrow$	$K^* + \rho + \phi$
2175	$\Sigma^* + \bar{N}(1440)$	$\leftrightarrow$	$K^* + \rho + \eta'$
2176	$\Sigma^* + \bar{N}(1440)$	$\leftrightarrow$	$K^* + \omega + \omega$
2177	$\Sigma^* + \bar{N}(1440)$	$\leftrightarrow$	$K^* + \omega + \phi$
2178	$\Sigma^* + \bar{N}(1440)$	$\leftrightarrow$	$K^* + \omega + \eta'$
2179	$\Sigma^* + \bar{N}(1440)$	$\leftrightarrow$	$K^* + \phi + \phi$
2180	$\Sigma^* + \bar{N}(1440)$	$\leftrightarrow$	$K^* + \phi + \eta'$
2181	$\Sigma^* + \bar{N}(1440)$	$\leftrightarrow$	$K^* + \eta' + \eta'$
2182	$\Sigma^* + \bar{N}(1440)$	$\leftrightarrow$	$K^* + a_1 + a_1$
2183	$\Sigma^* + \bar{N}(1535)$	$\leftrightarrow$	$\pi + K + a_1$
2184	$\Sigma^* + \bar{N}(1535)$	$\leftrightarrow$	$\pi + K^* + a_1$
2185	$\Sigma^* + \bar{N}(1535)$	$\leftrightarrow$	$\eta + K + a_1$
2186	$\Sigma^* + \bar{N}(1535)$	$\leftrightarrow$	$\eta + K^* + a_1$
2187	$\Sigma^* + \bar{N}(1535)$	$\leftrightarrow$	$K + \rho + a_1$
2188	$\Sigma^* + \bar{N}(1535)$	$\leftrightarrow$	$K + \omega + a_1$
2189	$\Sigma^* + \bar{N}(1535)$	$\leftrightarrow$	$K + \phi + a_1$
2190	$\Sigma^* + \bar{N}(1535)$	$\leftrightarrow$	$K + \eta' + a_1$
2191	$\Sigma^* + \bar{N}(1535)$	$\leftrightarrow$	$K^* + \rho + a_1$
2192	$\Sigma^* + \bar{N}(1535)$	$\leftrightarrow$	$K^* + \omega + a_1$
2193	$\Sigma^* + \bar{N}(1535)$	$\leftrightarrow$	$K^* + \phi + a_1$
2194	$\Sigma^* + \bar{N}(1535)$	$\leftrightarrow$	$K^* + \eta' + a_1$
2195	$\Sigma^* + \bar{\Lambda}$	$\leftrightarrow$	$\pi + \pi + \eta$
2196	$\Sigma^* + \bar{\Lambda}$	$\leftrightarrow$	$\pi + \pi + \phi$
2197	$\Sigma^* + \bar{\Lambda}$	$\leftrightarrow$	$\pi + \eta + \eta$
2198	$\Sigma^* + \bar{\Lambda}$	$\leftrightarrow$	$\pi + \eta + \rho$
2199	$\Sigma^* + \bar{\Lambda}$	$\leftrightarrow$	$\pi + \eta + \omega$
2200	$\Sigma^* + \bar{\Lambda}$	$\leftrightarrow$	$\pi + \eta + \phi$
2201	$\Sigma^* + \bar{\Lambda}$	$\leftrightarrow$	$\pi + \eta + \eta'$
2202	$\Sigma^* + \bar{\Lambda}$	$\leftrightarrow$	$\pi + K + K$
2203	$\Sigma^* + \bar{\Lambda}$	$\leftrightarrow$	$\pi + K + K^*$
2204	$\Sigma^* + \bar{\Lambda}$	$\leftrightarrow$	$\pi + K^* + K^*$
2205	$\Sigma^* + \bar{\Lambda}$	$\leftrightarrow$	$\pi + \rho + \phi$
2206	$\Sigma^* + \bar{\Lambda}$	$\leftrightarrow$	$\pi + \omega + \phi$
2207	$\Sigma^* + \bar{\Lambda}$	$\leftrightarrow$	$\pi + \phi + \phi$
2208	$\Sigma^* + \bar{\Lambda}$	$\leftrightarrow$	$\pi + \phi + \eta'$
2209	$\Sigma^* + \bar{\Lambda}$	$\leftrightarrow$	$\eta + \eta + \eta$
2210	$\Sigma^* + \bar{\Lambda}$	$\leftrightarrow$	$\eta + \eta + \rho$
2211	$\Sigma^* + \bar{\Lambda}$	$\leftrightarrow$	$\eta + \eta + \omega$
2212	$\Sigma^* + \bar{\Lambda}$	$\leftrightarrow$	$\eta + \eta + \phi$
2213	$\Sigma^* + \bar{\Lambda}$	$\leftrightarrow$	$\eta + \eta + \eta'$
2214	$\Sigma^* + \bar{\Lambda}$	$\leftrightarrow$	$\eta + K + K$
2215	$\Sigma^* + \bar{\Lambda}$	$\leftrightarrow$	$\eta + K + K^*$
2216	$\Sigma^* + \bar{\Lambda}$	$\leftrightarrow$	$\eta + K^* + K^*$
2217	$\Sigma^* + \bar{\Lambda}$	$\leftrightarrow$	$\eta + \rho + \rho$
2218	$\Sigma^* + \bar{\Lambda}$	$\leftrightarrow$	$\eta + \rho + \omega$
2219	$\Sigma^* + \bar{\Lambda}$	$\leftrightarrow$	$\eta + \rho + \phi$
2220	$\Sigma^* + \bar{\Lambda}$	$\leftrightarrow$	$\eta + \rho + \eta'$
2221	$\Sigma^* + \bar{\Lambda}$	$\leftrightarrow$	$\eta + \omega + \omega$
2222	$\Sigma^* + \bar{\Lambda}$	$\leftrightarrow$	$\eta + \omega + \phi$
2223	$\Sigma^* + \bar{\Lambda}$	$\leftrightarrow$	$\eta + \omega + \eta'$
2224	$\Sigma^* + \bar{\Lambda}$	$\leftrightarrow$	$\eta + \phi + \phi$
2225	$\Sigma^* + \bar{\Lambda}$	$\leftrightarrow$	$\eta + \phi + \eta'$
2226	$\Sigma^* + \bar{\Lambda}$	$\leftrightarrow$	$\eta + \eta' + \eta'$
2227	$\Sigma^* + \bar{\Lambda}$	$\leftrightarrow$	$\eta + a_1 + a_1$
2228	$\Sigma^* + \bar{\Lambda}$	$\leftrightarrow$	$K + K + \rho$
2229	$\Sigma^* + \bar{\Lambda}$	$\leftrightarrow$	$K + K + \omega$
2230	$\Sigma^* + \bar{\Lambda}$	$\leftrightarrow$	$K + K + \phi$
2231	$\Sigma^* + \bar{\Lambda}$	$\leftrightarrow$	$K + K + \eta'$
2232	$\Sigma^* + \bar{\Lambda}$	$\leftrightarrow$	$K + K^* + \rho$
2233	$\Sigma^* + \bar{\Lambda}$	$\leftrightarrow$	$K + K^* + \omega$
2234	$\Sigma^* + \bar{\Lambda}$	$\leftrightarrow$	$K + K^* + \phi$
2235	$\Sigma^* + \bar{\Lambda}$	$\leftrightarrow$	$K + K^* + \eta'$
2236	$\Sigma^* + \bar{\Lambda}$	$\leftrightarrow$	$K^* + K^* + \rho$
2237	$\Sigma^* + \bar{\Lambda}$	$\leftrightarrow$	$K^* + K^* + \omega$
2238	$\Sigma^* + \bar{\Lambda}$	$\leftrightarrow$	$K^* + K^* + \phi$
2239	$\Sigma^* + \bar{\Lambda}$	$\leftrightarrow$	$K^* + K^* + \eta'$
2240	$\Sigma^* + \bar{\Lambda}$	$\leftrightarrow$	$\rho + \rho + \phi$
2241	$\Sigma^* + \bar{\Lambda}$	$\leftrightarrow$	$\rho + \omega + \phi$
2242	$\Sigma^* + \bar{\Lambda}$	$\leftrightarrow$	$\rho + \phi + \phi$
2243	$\Sigma^* + \bar{\Lambda}$	$\leftrightarrow$	$\rho + \phi + \eta'$
2244	$\Sigma^* + \bar{\Lambda}$	$\leftrightarrow$	$\omega + \omega + \phi$
2245	$\Sigma^* + \bar{\Lambda}$	$\leftrightarrow$	$\omega + \phi + \phi$
2246	$\Sigma^* + \bar{\Lambda}$	$\leftrightarrow$	$\omega + \phi + \eta'$
2247	$\Sigma^* + \bar{\Lambda}$	$\leftrightarrow$	$\phi + \phi + \phi$
2248	$\Sigma^* + \bar{\Lambda}$	$\leftrightarrow$	$\phi + \phi + \eta'$
2249	$\Sigma^* + \bar{\Lambda}$	$\leftrightarrow$	$\phi + \eta' + \eta'$
2250	$\Sigma^* + \bar{\Lambda}$	$\leftrightarrow$	$\phi + a_1 + a_1$
2251	$\Sigma^* + \bar{\Sigma}$	$\leftrightarrow$	$\pi + \pi + \eta$
2252	$\Sigma^* + \bar{\Sigma}$	$\leftrightarrow$	$\pi + \pi + \phi$
2253	$\Sigma^* + \bar{\Sigma}$	$\leftrightarrow$	$\pi + \eta + \eta$
2254	$\Sigma^* + \bar{\Sigma}$	$\leftrightarrow$	$\pi + \eta + \rho$
2255	$\Sigma^* + \bar{\Sigma}$	$\leftrightarrow$	$\pi + \eta + \omega$
2256	$\Sigma^* + \bar{\Sigma}$	$\leftrightarrow$	$\pi + \eta + \phi$

Ch. No.	$B_1 + B_2$	$\leftrightarrow$	$M_1+M_2+M_3$
2257	$\Sigma^* + \bar{\Sigma}$	$\leftrightarrow$	$\pi + \eta + \eta'$
2258	$\Sigma^* + \bar{\Sigma}$	$\leftrightarrow$	$\pi + K + K$
2259	$\Sigma^* + \bar{\Sigma}$	$\leftrightarrow$	$\pi + K + K^*$
2260	$\Sigma^* + \bar{\Sigma}$	$\leftrightarrow$	$\pi + K^* + K^*$
2261	$\Sigma^* + \bar{\Sigma}$	$\leftrightarrow$	$\pi + \rho + \phi$
2262	$\Sigma^* + \bar{\Sigma}$	$\leftrightarrow$	$\pi + \omega + \phi$
2263	$\Sigma^* + \bar{\Sigma}$	$\leftrightarrow$	$\pi + \phi + \phi$
2264	$\Sigma^* + \bar{\Sigma}$	$\leftrightarrow$	$\pi + \phi + \eta'$
2265	$\Sigma^* + \bar{\Sigma}$	$\leftrightarrow$	$\eta + \eta + \eta$
2266	$\Sigma^* + \bar{\Sigma}$	$\leftrightarrow$	$\eta + \eta + \rho$
2267	$\Sigma^* + \bar{\Sigma}$	$\leftrightarrow$	$\eta + \eta + \omega$
2268	$\Sigma^* + \bar{\Sigma}$	$\leftrightarrow$	$\eta + \eta + \phi$
2269	$\Sigma^* + \bar{\Sigma}$	$\leftrightarrow$	$\eta + \eta + \eta'$
2270	$\Sigma^* + \bar{\Sigma}$	$\leftrightarrow$	$\eta + K + K$
2271	$\Sigma^* + \bar{\Sigma}$	$\leftrightarrow$	$\eta + K + K^*$
2272	$\Sigma^* + \bar{\Sigma}$	$\leftrightarrow$	$\eta + K^* + K^*$
2273	$\Sigma^* + \bar{\Sigma}$	$\leftrightarrow$	$\eta + \rho + \rho$
2274	$\Sigma^* + \bar{\Sigma}$	$\leftrightarrow$	$\eta + \rho + \omega$
2275	$\Sigma^* + \bar{\Sigma}$	$\leftrightarrow$	$\eta + \rho + \phi$
2276	$\Sigma^* + \bar{\Sigma}$	$\leftrightarrow$	$\eta + \rho + \eta'$
2277	$\Sigma^* + \bar{\Sigma}$	$\leftrightarrow$	$\eta + \omega + \omega$
2278	$\Sigma^* + \bar{\Sigma}$	$\leftrightarrow$	$\eta + \omega + \phi$
2279	$\Sigma^* + \bar{\Sigma}$	$\leftrightarrow$	$\eta + \omega + \eta'$
2280	$\Sigma^* + \bar{\Sigma}$	$\leftrightarrow$	$\eta + \phi + \phi$
2281	$\Sigma^* + \bar{\Sigma}$	$\leftrightarrow$	$\eta + \phi + \eta'$
2282	$\Sigma^* + \bar{\Sigma}$	$\leftrightarrow$	$\eta + \eta' + \eta'$
2283	$\Sigma^* + \bar{\Sigma}$	$\leftrightarrow$	$\eta + a_1 + a_1$
2284	$\Sigma^* + \bar{\Sigma}$	$\leftrightarrow$	$K + K + \rho$
2285	$\Sigma^* + \bar{\Sigma}$	$\leftrightarrow$	$K + K + \omega$
2286	$\Sigma^* + \bar{\Sigma}$	$\leftrightarrow$	$K + K + \phi$
2287	$\Sigma^* + \bar{\Sigma}$	$\leftrightarrow$	$K + K + \eta'$
2288	$\Sigma^* + \bar{\Sigma}$	$\leftrightarrow$	$K + K^* + \rho$
2289	$\Sigma^* + \bar{\Sigma}$	$\leftrightarrow$	$K + K^* + \omega$
2290	$\Sigma^* + \bar{\Sigma}$	$\leftrightarrow$	$K + K^* + \phi$
2291	$\Sigma^* + \bar{\Sigma}$	$\leftrightarrow$	$K + K^* + \eta'$
2292	$\Sigma^* + \bar{\Sigma}$	$\leftrightarrow$	$K^* + K^* + \rho$
2293	$\Sigma^* + \bar{\Sigma}$	$\leftrightarrow$	$K^* + K^* + \omega$
2294	$\Sigma^* + \bar{\Sigma}$	$\leftrightarrow$	$K^* + K^* + \phi$
2295	$\Sigma^* + \bar{\Sigma}$	$\leftrightarrow$	$K^* + K^* + \eta'$
2296	$\Sigma^* + \bar{\Sigma}$	$\leftrightarrow$	$\rho + \rho + \phi$
2297	$\Sigma^* + \bar{\Sigma}$	$\leftrightarrow$	$\rho + \omega + \phi$
2298	$\Sigma^* + \bar{\Sigma}$	$\leftrightarrow$	$\rho + \phi + \phi$
2299	$\Sigma^* + \bar{\Sigma}$	$\leftrightarrow$	$\rho + \phi + \eta'$
2300	$\Sigma^* + \bar{\Sigma}$	$\leftrightarrow$	$\omega + \omega + \phi$
2301	$\Sigma^* + \bar{\Sigma}$	$\leftrightarrow$	$\omega + \phi + \phi$
2302	$\Sigma^* + \bar{\Sigma}$	$\leftrightarrow$	$\omega + \phi + \eta'$
2303	$\Sigma^* + \bar{\Sigma}$	$\leftrightarrow$	$\phi + \phi + \phi$
2304	$\Sigma^* + \bar{\Sigma}$	$\leftrightarrow$	$\phi + \phi + \eta'$
2305	$\Sigma^* + \bar{\Sigma}$	$\leftrightarrow$	$\phi + \eta' + \eta'$
2306	$\Sigma^* + \bar{\Sigma}$	$\leftrightarrow$	$\phi + a_1 + a_1$
2307	$\Sigma^* + \bar{\Sigma}^*$	$\leftrightarrow$	$\pi + \pi + \eta$
2308	$\Sigma^* + \bar{\Sigma}^*$	$\leftrightarrow$	$\pi + \pi + \phi$
2309	$\Sigma^* + \bar{\Sigma}^*$	$\leftrightarrow$	$\pi + \eta + \eta$
2310	$\Sigma^* + \bar{\Sigma}^*$	$\leftrightarrow$	$\pi + \eta + \rho$
2311	$\Sigma^* + \bar{\Sigma}^*$	$\leftrightarrow$	$\pi + \eta + \omega$
2312	$\Sigma^* + \bar{\Sigma}^*$	$\leftrightarrow$	$\pi + \eta + \phi$
2313	$\Sigma^* + \bar{\Sigma}^*$	$\leftrightarrow$	$\pi + \eta + \eta'$
2314	$\Sigma^* + \bar{\Sigma}^*$	$\leftrightarrow$	$\pi + K + K$
2315	$\Sigma^* + \bar{\Sigma}^*$	$\leftrightarrow$	$\pi + K + K^*$
2316	$\Sigma^* + \bar{\Sigma}^*$	$\leftrightarrow$	$\pi + K^* + K^*$
2317	$\Sigma^* + \bar{\Sigma}^*$	$\leftrightarrow$	$\pi + \rho + \phi$
2318	$\Sigma^* + \bar{\Sigma}^*$	$\leftrightarrow$	$\pi + \omega + \phi$
2319	$\Sigma^* + \bar{\Sigma}^*$	$\leftrightarrow$	$\pi + \phi + \phi$
2320	$\Sigma^* + \bar{\Sigma}^*$	$\leftrightarrow$	$\pi + \phi + \eta'$
2321	$\Sigma^* + \bar{\Sigma}^*$	$\leftrightarrow$	$\eta + \eta + \eta$
2322	$\Sigma^* + \bar{\Sigma}^*$	$\leftrightarrow$	$\eta + \eta + \rho$
2323	$\Sigma^* + \bar{\Sigma}^*$	$\leftrightarrow$	$\eta + \eta + \omega$
2324	$\Sigma^* + \bar{\Sigma}^*$	$\leftrightarrow$	$\eta + \eta + \phi$
2325	$\Sigma^* + \bar{\Sigma}^*$	$\leftrightarrow$	$\eta + \eta + \eta'$
2326	$\Sigma^* + \bar{\Sigma}^*$	$\leftrightarrow$	$\eta + K + K$
2327	$\Sigma^* + \bar{\Sigma}^*$	$\leftrightarrow$	$\eta + K + K^*$
2328	$\Sigma^* + \bar{\Sigma}^*$	$\leftrightarrow$	$\eta + K^* + K^*$
2329	$\Sigma^* + \bar{\Sigma}^*$	$\leftrightarrow$	$\eta + \rho + \rho$
2330	$\Sigma^* + \bar{\Sigma}^*$	$\leftrightarrow$	$\eta + \rho + \omega$
2331	$\Sigma^* + \bar{\Sigma}^*$	$\leftrightarrow$	$\eta + \rho + \phi$
2332	$\Sigma^* + \bar{\Sigma}^*$	$\leftrightarrow$	$\eta + \rho + \eta'$
2333	$\Sigma^* + \bar{\Sigma}^*$	$\leftrightarrow$	$\eta + \omega + \omega$
2334	$\Sigma^* + \bar{\Sigma}^*$	$\leftrightarrow$	$\eta + \omega + \phi$
2335	$\Sigma^* + \bar{\Sigma}^*$	$\leftrightarrow$	$\eta + \omega + \eta'$
2336	$\Sigma^* + \bar{\Sigma}^*$	$\leftrightarrow$	$\eta + \phi + \phi$
2337	$\Sigma^* + \bar{\Sigma}^*$	$\leftrightarrow$	$\eta + \phi + \eta'$
2338	$\Sigma^* + \bar{\Sigma}^*$	$\leftrightarrow$	$\eta + \eta' + \eta'$
2339	$\Sigma^* + \bar{\Sigma}^*$	$\leftrightarrow$	$\eta + a_1 + a_1$
2340	$\Sigma^* + \bar{\Sigma}^*$	$\leftrightarrow$	$K + K + \rho$
2341	$\Sigma^* + \bar{\Sigma}^*$	$\leftrightarrow$	$K + K + \omega$
2342	$\Sigma^* + \bar{\Sigma}^*$	$\leftrightarrow$	$K + K + \phi$

Ch. No.	$B_1 + B_2$	$\leftrightarrow$	$M_1+M_2+M_3$
2343	$\Sigma^* + \bar{\Sigma}^*$	$\leftrightarrow$	$K + K + \eta'$
2344	$\Sigma^* + \bar{\Sigma}^*$	$\leftrightarrow$	$K + K^* + \rho$
2345	$\Sigma^* + \bar{\Sigma}^*$	$\leftrightarrow$	$K + K^* + \omega$
2346	$\Sigma^* + \bar{\Sigma}^*$	$\leftrightarrow$	$K + K^* + \phi$
2347	$\Sigma^* + \bar{\Sigma}^*$	$\leftrightarrow$	$K + K^* + \eta'$
2348	$\Sigma^* + \bar{\Sigma}^*$	$\leftrightarrow$	$K^* + K^* + \rho$
2349	$\Sigma^* + \bar{\Sigma}^*$	$\leftrightarrow$	$K^* + K^* + \omega$
2350	$\Sigma^* + \bar{\Sigma}^*$	$\leftrightarrow$	$K^* + K^* + \phi$
2351	$\Sigma^* + \bar{\Sigma}^*$	$\leftrightarrow$	$K^* + K^* + \eta'$
2352	$\Sigma^* + \bar{\Sigma}^*$	$\leftrightarrow$	$\rho + \rho + \phi$
2353	$\Sigma^* + \bar{\Sigma}^*$	$\leftrightarrow$	$\rho + \omega + \phi$
2354	$\Sigma^* + \bar{\Sigma}^*$	$\leftrightarrow$	$\rho + \phi + \phi$
2355	$\Sigma^* + \bar{\Sigma}^*$	$\leftrightarrow$	$\rho + \phi + \eta'$
2356	$\Sigma^* + \bar{\Sigma}^*$	$\leftrightarrow$	$\omega + \omega + \phi$
2357	$\Sigma^* + \bar{\Sigma}^*$	$\leftrightarrow$	$\omega + \phi + \phi$
2358	$\Sigma^* + \bar{\Sigma}^*$	$\leftrightarrow$	$\omega + \phi + \eta'$
2359	$\Sigma^* + \bar{\Sigma}^*$	$\leftrightarrow$	$\phi + \phi + \phi$
2360	$\Sigma^* + \bar{\Sigma}^*$	$\leftrightarrow$	$\phi + \phi + \eta'$
2361	$\Sigma^* + \bar{\Sigma}^*$	$\leftrightarrow$	$\phi + \eta' + \eta'$
2362	$\Sigma^* + \bar{\Sigma}^*$	$\leftrightarrow$	$\phi + a_1 + a_1$
2363	$\Sigma^* + \bar{\Xi}$	$\leftrightarrow$	$\pi + \eta + K$
2364	$\Sigma^* + \bar{\Xi}$	$\leftrightarrow$	$\pi + \eta + K^*$
2365	$\Sigma^* + \bar{\Xi}$	$\leftrightarrow$	$\pi + K + \phi$
2366	$\Sigma^* + \bar{\Xi}$	$\leftrightarrow$	$\pi + K^* + \phi$
2367	$\Sigma^* + \bar{\Xi}$	$\leftrightarrow$	$\eta + \eta + K$
2368	$\Sigma^* + \bar{\Xi}$	$\leftrightarrow$	$\eta + \eta + K^*$
2369	$\Sigma^* + \bar{\Xi}$	$\leftrightarrow$	$\eta + K + \rho$
2370	$\Sigma^* + \bar{\Xi}$	$\leftrightarrow$	$\eta + K + \omega$
2371	$\Sigma^* + \bar{\Xi}$	$\leftrightarrow$	$\eta + K + \phi$
2372	$\Sigma^* + \bar{\Xi}$	$\leftrightarrow$	$\eta + K + \eta'$
2373	$\Sigma^* + \bar{\Xi}$	$\leftrightarrow$	$\eta + K^* + \rho$
2374	$\Sigma^* + \bar{\Xi}$	$\leftrightarrow$	$\eta + K^* + \omega$
2375	$\Sigma^* + \bar{\Xi}$	$\leftrightarrow$	$\eta + K^* + \phi$
2376	$\Sigma^* + \bar{\Xi}$	$\leftrightarrow$	$\eta + K^* + \eta'$
2377	$\Sigma^* + \bar{\Xi}$	$\leftrightarrow$	$K + K + K$
2378	$\Sigma^* + \bar{\Xi}$	$\leftrightarrow$	$K + K + K^*$
2379	$\Sigma^* + \bar{\Xi}$	$\leftrightarrow$	$K + K^* + K^*$
2380	$\Sigma^* + \bar{\Xi}$	$\leftrightarrow$	$K + \rho + \phi$
2381	$\Sigma^* + \bar{\Xi}$	$\leftrightarrow$	$K + \omega + \phi$
2382	$\Sigma^* + \bar{\Xi}$	$\leftrightarrow$	$K + \phi + \phi$
2383	$\Sigma^* + \bar{\Xi}$	$\leftrightarrow$	$K + \phi + \eta'$
2384	$\Sigma^* + \bar{\Xi}$	$\leftrightarrow$	$K^* + K^* + K^*$
2385	$\Sigma^* + \bar{\Xi}$	$\leftrightarrow$	$K^* + \rho + \phi$
2386	$\Sigma^* + \bar{\Xi}$	$\leftrightarrow$	$K^* + \omega + \phi$
2387	$\Sigma^* + \bar{\Xi}$	$\leftrightarrow$	$K^* + \phi + \phi$
2388	$\Sigma^* + \bar{\Xi}$	$\leftrightarrow$	$K^* + \phi + \eta'$
2389	$\Sigma^* + \bar{\Xi}^*$	$\leftrightarrow$	$\pi + \eta + K$
2390	$\Sigma^* + \bar{\Xi}^*$	$\leftrightarrow$	$\pi + \eta + K^*$
2391	$\Sigma^* + \bar{\Xi}^*$	$\leftrightarrow$	$\pi + K + \phi$
2392	$\Sigma^* + \bar{\Xi}^*$	$\leftrightarrow$	$\pi + K^* + \phi$
2393	$\Sigma^* + \bar{\Xi}^*$	$\leftrightarrow$	$\eta + \eta + K$
2394	$\Sigma^* + \bar{\Xi}^*$	$\leftrightarrow$	$\eta + \eta + K^*$
2395	$\Sigma^* + \bar{\Xi}^*$	$\leftrightarrow$	$\eta + K + \rho$
2396	$\Sigma^* + \bar{\Xi}^*$	$\leftrightarrow$	$\eta + K + \omega$
2397	$\Sigma^* + \bar{\Xi}^*$	$\leftrightarrow$	$\eta + K + \phi$
2398	$\Sigma^* + \bar{\Xi}^*$	$\leftrightarrow$	$\eta + K + \eta'$
2399	$\Sigma^* + \bar{\Xi}^*$	$\leftrightarrow$	$\eta + K^* + \rho$
2400	$\Sigma^* + \bar{\Xi}^*$	$\leftrightarrow$	$\eta + K^* + \omega$
2401	$\Sigma^* + \bar{\Xi}^*$	$\leftrightarrow$	$\eta + K^* + \phi$
2402	$\Sigma^* + \bar{\Xi}^*$	$\leftrightarrow$	$\eta + K^* + \eta'$
2403	$\Sigma^* + \bar{\Xi}^*$	$\leftrightarrow$	$K + K + K$
2404	$\Sigma^* + \bar{\Xi}^*$	$\leftrightarrow$	$K + K + K^*$
2405	$\Sigma^* + \bar{\Xi}^*$	$\leftrightarrow$	$K + K^* + K^*$
2406	$\Sigma^* + \bar{\Xi}^*$	$\leftrightarrow$	$K + \rho + \phi$
2407	$\Sigma^* + \bar{\Xi}^*$	$\leftrightarrow$	$K + \omega + \phi$
2408	$\Sigma^* + \bar{\Xi}^*$	$\leftrightarrow$	$K + \phi + \phi$
2409	$\Sigma^* + \bar{\Xi}^*$	$\leftrightarrow$	$K + \phi + \eta'$
2410	$\Sigma^* + \bar{\Xi}^*$	$\leftrightarrow$	$K^* + K^* + K^*$
2411	$\Sigma^* + \bar{\Xi}^*$	$\leftrightarrow$	$K^* + \rho + \phi$
2412	$\Sigma^* + \bar{\Xi}^*$	$\leftrightarrow$	$K^* + \omega + \phi$
2413	$\Sigma^* + \bar{\Xi}^*$	$\leftrightarrow$	$K^* + \phi + \phi$
2414	$\Sigma^* + \bar{\Xi}^*$	$\leftrightarrow$	$K^* + \phi + \eta'$
2415	$\Sigma^* + \bar{\Omega}$	$\leftrightarrow$	$\eta + K + K$
2416	$\Sigma^* + \bar{\Omega}$	$\leftrightarrow$	$\eta + K + K^*$
2417	$\Sigma^* + \bar{\Omega}$	$\leftrightarrow$	$\eta + K^* + K^*$
2418	$\Sigma^* + \bar{\Omega}$	$\leftrightarrow$	$K + K + \phi$
2419	$\Sigma^* + \bar{\Omega}$	$\leftrightarrow$	$K + K^* + \phi$
2420	$\Sigma^* + \bar{\Omega}$	$\leftrightarrow$	$K^* + K^* + \phi$
2421	$\Xi + \bar{\mathrm{N}}$	$\leftrightarrow$	$\pi + K + K$
2422	$\Xi + \bar{\mathrm{N}}$	$\leftrightarrow$	$\pi + K + K^*$
2423	$\Xi + \bar{\mathrm{N}}$	$\leftrightarrow$	$\pi + K^* + K^*$
2424	$\Xi + \bar{\mathrm{N}}$	$\leftrightarrow$	$\eta + K + K$
2425	$\Xi + \bar{\mathrm{N}}$	$\leftrightarrow$	$\eta + K + K^*$
2426	$\Xi + \bar{\mathrm{N}}$	$\leftrightarrow$	$\eta + K^* + K^*$
2427	$\Xi + \bar{\mathrm{N}}$	$\leftrightarrow$	$K + K + \rho$
2428	$\Xi + \bar{\mathrm{N}}$	$\leftrightarrow$	$K + K + \omega$

Ch. No.	$B_1 + B_2$	$\leftrightarrow$	$M_1+M_2+M_3$
2429	$\Xi + \bar{\mathrm{N}}$	$\leftrightarrow$	$K + K + \phi$
2430	$\Xi + \bar{\mathrm{N}}$	$\leftrightarrow$	$K + K + \eta'$
2431	$\Xi + \bar{\mathrm{N}}$	$\leftrightarrow$	$K + K^* + \rho$
2432	$\Xi + \bar{\mathrm{N}}$	$\leftrightarrow$	$K + K^* + \omega$
2433	$\Xi + \bar{\mathrm{N}}$	$\leftrightarrow$	$K + K^* + \phi$
2434	$\Xi + \bar{\mathrm{N}}$	$\leftrightarrow$	$K + K^* + \eta'$
2435	$\Xi + \bar{\mathrm{N}}$	$\leftrightarrow$	$K^* + K^* + \rho$
2436	$\Xi + \bar{\mathrm{N}}$	$\leftrightarrow$	$K^* + K^* + \omega$
2437	$\Xi + \bar{\mathrm{N}}$	$\leftrightarrow$	$K^* + K^* + \phi$
2438	$\Xi + \bar{\mathrm{N}}$	$\leftrightarrow$	$K^* + K^* + \eta'$
2439	$\Xi + \bar{\Delta}(1232)$	$\leftrightarrow$	$\pi + K + K$
2440	$\Xi + \bar{\Delta}(1232)$	$\leftrightarrow$	$\pi + K + K^*$
2441	$\Xi + \bar{\Delta}(1232)$	$\leftrightarrow$	$\pi + K^* + K^*$
2442	$\Xi + \bar{\Delta}(1232)$	$\leftrightarrow$	$\eta + K + K$
2443	$\Xi + \bar{\Delta}(1232)$	$\leftrightarrow$	$\eta + K + K^*$
2444	$\Xi + \bar{\Delta}(1232)$	$\leftrightarrow$	$\eta + K^* + K^*$
2445	$\Xi + \bar{\Delta}(1232)$	$\leftrightarrow$	$K + K + \rho$
2446	$\Xi + \bar{\Delta}(1232)$	$\leftrightarrow$	$K + K + \omega$
2447	$\Xi + \bar{\Delta}(1232)$	$\leftrightarrow$	$K + K + \phi$
2448	$\Xi + \bar{\Delta}(1232)$	$\leftrightarrow$	$K + K + \eta'$
2449	$\Xi + \bar{\Delta}(1232)$	$\leftrightarrow$	$K + K^* + \rho$
2450	$\Xi + \bar{\Delta}(1232)$	$\leftrightarrow$	$K + K^* + \omega$
2451	$\Xi + \bar{\Delta}(1232)$	$\leftrightarrow$	$K + K^* + \phi$
2452	$\Xi + \bar{\Delta}(1232)$	$\leftrightarrow$	$K + K^* + \eta'$
2453	$\Xi + \bar{\Delta}(1232)$	$\leftrightarrow$	$K^* + K^* + \rho$
2454	$\Xi + \bar{\Delta}(1232)$	$\leftrightarrow$	$K^* + K^* + \omega$
2455	$\Xi + \bar{\Delta}(1232)$	$\leftrightarrow$	$K^* + K^* + \phi$
2456	$\Xi + \bar{\Delta}(1232)$	$\leftrightarrow$	$K^* + K^* + \eta'$
2457	$\Xi + \bar{\mathrm{N}}(1440)$	$\leftrightarrow$	$\pi + K + K$
2458	$\Xi + \bar{\mathrm{N}}(1440)$	$\leftrightarrow$	$\pi + K + K^*$
2459	$\Xi + \bar{\mathrm{N}}(1440)$	$\leftrightarrow$	$\pi + K^* + K^*$
2460	$\Xi + \bar{\mathrm{N}}(1440)$	$\leftrightarrow$	$\eta + K + K$
2461	$\Xi + \bar{\mathrm{N}}(1440)$	$\leftrightarrow$	$\eta + K + K^*$
2462	$\Xi + \bar{\mathrm{N}}(1440)$	$\leftrightarrow$	$\eta + K^* + K^*$
2463	$\Xi + \bar{\mathrm{N}}(1440)$	$\leftrightarrow$	$K + K + \rho$
2464	$\Xi + \bar{\mathrm{N}}(1440)$	$\leftrightarrow$	$K + K + \omega$
2465	$\Xi + \bar{\mathrm{N}}(1440)$	$\leftrightarrow$	$K + K + \phi$
2466	$\Xi + \bar{\mathrm{N}}(1440)$	$\leftrightarrow$	$K + K + \eta'$
2467	$\Xi + \bar{\mathrm{N}}(1440)$	$\leftrightarrow$	$K + K^* + \rho$
2468	$\Xi + \bar{\mathrm{N}}(1440)$	$\leftrightarrow$	$K + K^* + \omega$
2469	$\Xi + \bar{\mathrm{N}}(1440)$	$\leftrightarrow$	$K + K^* + \phi$
2470	$\Xi + \bar{\mathrm{N}}(1440)$	$\leftrightarrow$	$K + K^* + \eta'$
2471	$\Xi + \bar{\mathrm{N}}(1440)$	$\leftrightarrow$	$K^* + K^* + \rho$
2472	$\Xi + \bar{\mathrm{N}}(1440)$	$\leftrightarrow$	$K^* + K^* + \omega$
2473	$\Xi + \bar{\mathrm{N}}(1440)$	$\leftrightarrow$	$K^* + K^* + \phi$
2474	$\Xi + \bar{\mathrm{N}}(1440)$	$\leftrightarrow$	$K^* + K^* + \eta'$
2475	$\Xi + \bar{\mathrm{N}}(1535)$	$\leftrightarrow$	$K + K + a_1$
2476	$\Xi + \bar{\mathrm{N}}(1535)$	$\leftrightarrow$	$K + K^* + a_1$
2477	$\Xi + \bar{\mathrm{N}}(1535)$	$\leftrightarrow$	$K^* + K^* + a_1$
2478	$\Xi + \bar{\Lambda}$	$\leftrightarrow$	$\pi + \eta + K$
2479	$\Xi + \bar{\Lambda}$	$\leftrightarrow$	$\pi + \eta + K^*$
2480	$\Xi + \bar{\Lambda}$	$\leftrightarrow$	$\pi + K + \phi$
2481	$\Xi + \bar{\Lambda}$	$\leftrightarrow$	$\pi + K^* + \phi$
2482	$\Xi + \bar{\Lambda}$	$\leftrightarrow$	$\eta + \eta + K$
2483	$\Xi + \bar{\Lambda}$	$\leftrightarrow$	$\eta + \eta + K^*$
2484	$\Xi + \bar{\Lambda}$	$\leftrightarrow$	$\eta + K + \rho$
2485	$\Xi + \bar{\Lambda}$	$\leftrightarrow$	$\eta + K + \omega$
2486	$\Xi + \bar{\Lambda}$	$\leftrightarrow$	$\eta + K + \phi$
2487	$\Xi + \bar{\Lambda}$	$\leftrightarrow$	$\eta + K + \eta'$
2488	$\Xi + \bar{\Lambda}$	$\leftrightarrow$	$\eta + K^* + \rho$
2489	$\Xi + \bar{\Lambda}$	$\leftrightarrow$	$\eta + K^* + \omega$
2490	$\Xi + \bar{\Lambda}$	$\leftrightarrow$	$\eta + K^* + \phi$
2491	$\Xi + \bar{\Lambda}$	$\leftrightarrow$	$\eta + K^* + \eta'$
2492	$\Xi + \bar{\Lambda}$	$\leftrightarrow$	$K + K + K$
2493	$\Xi + \bar{\Lambda}$	$\leftrightarrow$	$K + K + K^*$
2494	$\Xi + \bar{\Lambda}$	$\leftrightarrow$	$K + K^* + K^*$
2495	$\Xi + \bar{\Lambda}$	$\leftrightarrow$	$K + \rho + \phi$
2496	$\Xi + \bar{\Lambda}$	$\leftrightarrow$	$K + \omega + \phi$
2497	$\Xi + \bar{\Lambda}$	$\leftrightarrow$	$K + \phi + \phi$
2498	$\Xi + \bar{\Lambda}$	$\leftrightarrow$	$K + \phi + \eta'$
2499	$\Xi + \bar{\Lambda}$	$\leftrightarrow$	$K^* + K^* + K^*$
2500	$\Xi + \bar{\Lambda}$	$\leftrightarrow$	$K^* + \rho + \phi$
2501	$\Xi + \bar{\Lambda}$	$\leftrightarrow$	$K^* + \omega + \phi$
2502	$\Xi + \bar{\Lambda}$	$\leftrightarrow$	$K^* + \phi + \phi$
2503	$\Xi + \bar{\Lambda}$	$\leftrightarrow$	$K^* + \phi + \eta'$
2504	$\Xi + \bar{\Sigma}$	$\leftrightarrow$	$\pi + \eta + K$
2505	$\Xi + \bar{\Sigma}$	$\leftrightarrow$	$\pi + \eta + K^*$
2506	$\Xi + \bar{\Sigma}$	$\leftrightarrow$	$\pi + K + \phi$
2507	$\Xi + \bar{\Sigma}$	$\leftrightarrow$	$\pi + K^* + \phi$
2508	$\Xi + \bar{\Sigma}$	$\leftrightarrow$	$\eta + \eta + K$
2509	$\Xi + \bar{\Sigma}$	$\leftrightarrow$	$\eta + \eta + K^*$
2510	$\Xi + \bar{\Sigma}$	$\leftrightarrow$	$\eta + K + \rho$
2511	$\Xi + \bar{\Sigma}$	$\leftrightarrow$	$\eta + K + \omega$
2512	$\Xi + \bar{\Sigma}$	$\leftrightarrow$	$\eta + K + \phi$
2513	$\Xi + \bar{\Sigma}$	$\leftrightarrow$	$\eta + K + \eta'$
2514	$\Xi + \bar{\Sigma}$	$\leftrightarrow$	$\eta + K^* + \rho$

Ch. No.	$B_1 + B_2$	$\leftrightarrow$	$M_1+M_2+M_3$
2515	$\bar{\Xi} + \Sigma$	$\leftrightarrow$	$\eta + K^* + \omega$
2516	$\Xi + \bar{\Sigma}$	$\leftrightarrow$	$\eta + K^* + \phi$
2517	$\Xi + \bar{\Sigma}$	$\leftrightarrow$	$\eta + K^* + \eta'$
2518	$\Xi + \bar{\Sigma}$	$\leftrightarrow$	$K + K + K$
2519	$\Xi + \bar{\Sigma}$	$\leftrightarrow$	$K + K + K^*$
2520	$\Xi + \bar{\Sigma}$	$\leftrightarrow$	$K + K^* + K^*$
2521	$\Xi + \bar{\Sigma}$	$\leftrightarrow$	$K + \rho + \phi$
2522	$\Xi + \bar{\Sigma}$	$\leftrightarrow$	$K + \omega + \phi$
2523	$\Xi + \bar{\Sigma}$	$\leftrightarrow$	$K + \phi + \phi$
2524	$\Xi + \bar{\Sigma}$	$\leftrightarrow$	$K + \phi + \eta'$
2525	$\Xi + \bar{\Sigma}$	$\leftrightarrow$	$K^* + K^* + K^*$
2526	$\Xi + \bar{\Sigma}$	$\leftrightarrow$	$K^* + \rho + \phi$
2527	$\Xi + \bar{\Sigma}$	$\leftrightarrow$	$K^* + \omega + \phi$
2528	$\Xi + \bar{\Sigma}$	$\leftrightarrow$	$K^* + \phi + \phi$
2529	$\Xi + \bar{\Sigma}$	$\leftrightarrow$	$K^* + \phi + \eta'$
2530	$\Xi + \bar{\Sigma}^*$	$\leftrightarrow$	$\pi + \eta + K$
2531	$\Xi + \bar{\Sigma}^*$	$\leftrightarrow$	$\pi + \eta + K^*$
2532	$\Xi + \bar{\Sigma}^*$	$\leftrightarrow$	$\pi + K + \phi$
2533	$\Xi + \bar{\Sigma}^*$	$\leftrightarrow$	$\pi + K^* + \phi$
2534	$\Xi + \bar{\Sigma}^*$	$\leftrightarrow$	$\eta + \eta + K$
2535	$\Xi + \bar{\Sigma}^*$	$\leftrightarrow$	$\eta + \eta + K^*$
2536	$\Xi + \bar{\Sigma}^*$	$\leftrightarrow$	$\eta + K + \rho$
2537	$\Xi + \bar{\Sigma}^*$	$\leftrightarrow$	$\eta + K + \omega$
2538	$\Xi + \bar{\Sigma}^*$	$\leftrightarrow$	$\eta + K + \phi$
2539	$\Xi + \bar{\Sigma}^*$	$\leftrightarrow$	$\eta + K + \eta'$
2540	$\Xi + \bar{\Sigma}^*$	$\leftrightarrow$	$\eta + K^* + \rho$
2541	$\Xi + \bar{\Sigma}^*$	$\leftrightarrow$	$\eta + K^* + \omega$
2542	$\Xi + \bar{\Sigma}^*$	$\leftrightarrow$	$\eta + K^* + \phi$
2543	$\Xi + \bar{\Sigma}^*$	$\leftrightarrow$	$\eta + K^* + \eta'$
2544	$\Xi + \bar{\Sigma}^*$	$\leftrightarrow$	$K + K + K$
2545	$\Xi + \bar{\Sigma}^*$	$\leftrightarrow$	$K + K + K^*$
2546	$\Xi + \bar{\Sigma}^*$	$\leftrightarrow$	$K + K^* + K^*$
2547	$\Xi + \bar{\Sigma}^*$	$\leftrightarrow$	$K + \rho + \phi$
2548	$\Xi + \bar{\Sigma}^*$	$\leftrightarrow$	$K + \omega + \phi$
2549	$\Xi + \bar{\Sigma}^*$	$\leftrightarrow$	$K + \phi + \phi$
2550	$\Xi + \bar{\Sigma}^*$	$\leftrightarrow$	$K + \phi + \eta'$
2551	$\Xi + \bar{\Sigma}^*$	$\leftrightarrow$	$K^* + K^* + K^*$
2552	$\Xi + \bar{\Sigma}^*$	$\leftrightarrow$	$K^* + \rho + \phi$
2553	$\Xi + \bar{\Sigma}^*$	$\leftrightarrow$	$K^* + \omega + \phi$
2554	$\Xi + \bar{\Sigma}^*$	$\leftrightarrow$	$K^* + \phi + \phi$
2555	$\Xi + \bar{\Sigma}^*$	$\leftrightarrow$	$K^* + \phi + \eta'$
2556	$\Xi + \bar{\Xi}$	$\leftrightarrow$	$\pi + \eta + \eta$
2557	$\Xi + \bar{\Xi}$	$\leftrightarrow$	$\pi + \eta + \phi$
2558	$\Xi + \bar{\Xi}$	$\leftrightarrow$	$\pi + \phi + \phi$
2559	$\Xi + \bar{\Xi}$	$\leftrightarrow$	$\eta + \eta + \eta$
2560	$\Xi + \bar{\Xi}$	$\leftrightarrow$	$\eta + \eta + \rho$
2561	$\Xi + \bar{\Xi}$	$\leftrightarrow$	$\eta + \eta + \omega$
2562	$\Xi + \bar{\Xi}$	$\leftrightarrow$	$\eta + \eta + \phi$
2563	$\Xi + \bar{\Xi}$	$\leftrightarrow$	$\eta + \eta + \eta'$
2564	$\Xi + \bar{\Xi}$	$\leftrightarrow$	$\eta + K + K$
2565	$\Xi + \bar{\Xi}$	$\leftrightarrow$	$\eta + K + K^*$
2566	$\Xi + \bar{\Xi}$	$\leftrightarrow$	$\eta + K^* + K^*$
2567	$\Xi + \bar{\Xi}$	$\leftrightarrow$	$\eta + \rho + \phi$
2568	$\Xi + \bar{\Xi}$	$\leftrightarrow$	$\eta + \omega + \phi$
2569	$\Xi + \bar{\Xi}$	$\leftrightarrow$	$\eta + \phi + \phi$
2570	$\Xi + \bar{\Xi}$	$\leftrightarrow$	$\eta + \phi + \eta'$
2571	$\Xi + \bar{\Xi}$	$\leftrightarrow$	$K + K + \phi$
2572	$\Xi + \bar{\Xi}$	$\leftrightarrow$	$K + K^* + \phi$
2573	$\Xi + \bar{\Xi}$	$\leftrightarrow$	$K^* + K^* + \phi$
2574	$\Xi + \bar{\Xi}$	$\leftrightarrow$	$\rho + \phi + \phi$
2575	$\Xi + \bar{\Xi}$	$\leftrightarrow$	$\omega + \phi + \phi$
2576	$\Xi + \bar{\Xi}$	$\leftrightarrow$	$\phi + \phi + \phi$
2577	$\Xi + \bar{\Xi}$	$\leftrightarrow$	$\phi + \phi + \eta'$
2578	$\Xi + \bar{\Xi}^*$	$\leftrightarrow$	$\pi + \eta + \eta$
2579	$\Xi + \bar{\Xi}^*$	$\leftrightarrow$	$\pi + \eta + \phi$
2580	$\Xi + \bar{\Xi}^*$	$\leftrightarrow$	$\pi + \phi + \phi$
2581	$\Xi + \bar{\Xi}^*$	$\leftrightarrow$	$\eta + \eta + \eta$
2582	$\Xi + \bar{\Xi}^*$	$\leftrightarrow$	$\eta + \eta + \rho$
2583	$\Xi + \bar{\Xi}^*$	$\leftrightarrow$	$\eta + \eta + \omega$
2584	$\Xi + \bar{\Xi}^*$	$\leftrightarrow$	$\eta + \eta + \phi$
2585	$\Xi + \bar{\Xi}^*$	$\leftrightarrow$	$\eta + \eta + \eta'$
2586	$\Xi + \bar{\Xi}^*$	$\leftrightarrow$	$\eta + K + K$
2587	$\Xi + \bar{\Xi}^*$	$\leftrightarrow$	$\eta + K + K^*$
2588	$\Xi + \bar{\Xi}^*$	$\leftrightarrow$	$\eta + K^* + K^*$
2589	$\Xi + \bar{\Xi}^*$	$\leftrightarrow$	$\eta + \rho + \phi$
2590	$\Xi + \bar{\Xi}^*$	$\leftrightarrow$	$\eta + \omega + \phi$
2591	$\Xi + \bar{\Xi}^*$	$\leftrightarrow$	$\eta + \phi + \phi$
2592	$\Xi + \bar{\Xi}^*$	$\leftrightarrow$	$\eta + \phi + \eta'$
2593	$\Xi + \bar{\Xi}^*$	$\leftrightarrow$	$K + K + \phi$
2594	$\Xi + \bar{\Xi}^*$	$\leftrightarrow$	$K + K^* + \phi$
2595	$\Xi + \bar{\Xi}^*$	$\leftrightarrow$	$K^* + K^* + \phi$
2596	$\Xi + \bar{\Xi}^*$	$\leftrightarrow$	$\rho + \phi + \phi$
2597	$\Xi + \bar{\Xi}^*$	$\leftrightarrow$	$\omega + \phi + \phi$
2598	$\Xi + \bar{\Xi}^*$	$\leftrightarrow$	$\phi + \phi + \phi$
2599	$\Xi + \bar{\Xi}^*$	$\leftrightarrow$	$\phi + \phi + \eta'$
2600	$\Xi + \bar{\Omega}$	$\leftrightarrow$	$\eta + \eta + K$

Ch. No.	$B_1 + B_2$	$\leftrightarrow$	$M_1+M_2+M_3$
2601	$\Xi + \bar{\Omega}$	$\leftrightarrow$	$\eta + \eta + K^*$
2602	$\Xi + \bar{\Omega}$	$\leftrightarrow$	$\eta + K + \phi$
2603	$\Xi + \bar{\Omega}$	$\leftrightarrow$	$\eta + K^* + \phi$
2604	$\Xi + \bar{\Omega}$	$\leftrightarrow$	$K + \phi + \phi$
2605	$\Xi + \bar{\Omega}$	$\leftrightarrow$	$K^* + \phi + \phi$
2606	$\Xi^* + \bar{N}$	$\leftrightarrow$	$\pi + K + K$
2607	$\Xi^* + \bar{N}$	$\leftrightarrow$	$\pi + K + K^*$
2608	$\Xi^* + \bar{N}$	$\leftrightarrow$	$\pi + K^* + K^*$
2609	$\Xi^* + \bar{N}$	$\leftrightarrow$	$\eta + K + K$
2610	$\Xi^* + \bar{N}$	$\leftrightarrow$	$\eta + K + K^*$
2611	$\Xi^* + \bar{N}$	$\leftrightarrow$	$\eta + K^* + K^*$
2612	$\Xi^* + \bar{N}$	$\leftrightarrow$	$K + K + \rho$
2613	$\Xi^* + \bar{N}$	$\leftrightarrow$	$K + K + \omega$
2614	$\Xi^* + \bar{N}$	$\leftrightarrow$	$K + K + \phi$
2615	$\Xi^* + \bar{N}$	$\leftrightarrow$	$K + K + \eta'$
2616	$\Xi^* + \bar{N}$	$\leftrightarrow$	$K + K^* + \rho$
2617	$\Xi^* + \bar{N}$	$\leftrightarrow$	$K + K^* + \omega$
2618	$\Xi^* + \bar{N}$	$\leftrightarrow$	$K + K^* + \phi$
2619	$\Xi^* + \bar{N}$	$\leftrightarrow$	$K + K^* + \eta'$
2620	$\Xi^* + \bar{N}$	$\leftrightarrow$	$K^* + K^* + \rho$
2621	$\Xi^* + \bar{N}$	$\leftrightarrow$	$K^* + K^* + \omega$
2622	$\Xi^* + \bar{N}$	$\leftrightarrow$	$K^* + K^* + \phi$
2623	$\Xi^* + \bar{N}$	$\leftrightarrow$	$K^* + K^* + \eta'$
2624	$\Xi^* + \bar{\Delta}(1232)$	$\leftrightarrow$	$\pi + K + K$
2625	$\Xi^* + \bar{\Delta}(1232)$	$\leftrightarrow$	$\pi + K + K^*$
2626	$\Xi^* + \bar{\Delta}(1232)$	$\leftrightarrow$	$\pi + K^* + K^*$
2627	$\Xi^* + \bar{\Delta}(1232)$	$\leftrightarrow$	$\eta + K + K$
2628	$\Xi^* + \bar{\Delta}(1232)$	$\leftrightarrow$	$\eta + K + K^*$
2629	$\Xi^* + \bar{\Delta}(1232)$	$\leftrightarrow$	$\eta + K^* + K^*$
2630	$\Xi^* + \bar{\Delta}(1232)$	$\leftrightarrow$	$K + K + \rho$
2631	$\Xi^* + \bar{\Delta}(1232)$	$\leftrightarrow$	$K + K + \omega$
2632	$\Xi^* + \bar{\Delta}(1232)$	$\leftrightarrow$	$K + K + \phi$
2633	$\Xi^* + \bar{\Delta}(1232)$	$\leftrightarrow$	$K + K + \eta'$
2634	$\Xi^* + \bar{\Delta}(1232)$	$\leftrightarrow$	$K + K^* + \rho$
2635	$\Xi^* + \bar{\Delta}(1232)$	$\leftrightarrow$	$K + K^* + \omega$
2636	$\Xi^* + \bar{\Delta}(1232)$	$\leftrightarrow$	$K + K^* + \phi$
2637	$\Xi^* + \bar{\Delta}(1232)$	$\leftrightarrow$	$K + K^* + \eta'$
2638	$\Xi^* + \bar{\Delta}(1232)$	$\leftrightarrow$	$K^* + K^* + \rho$
2639	$\Xi^* + \bar{\Delta}(1232)$	$\leftrightarrow$	$K^* + K^* + \omega$
2640	$\Xi^* + \bar{\Delta}(1232)$	$\leftrightarrow$	$K^* + K^* + \phi$
2641	$\Xi^* + \bar{\Delta}(1232)$	$\leftrightarrow$	$K^* + K^* + \eta'$
2642	$\Xi^* + \bar{N}(1440)$	$\leftrightarrow$	$\pi + K + K$
2643	$\Xi^* + \bar{N}(1440)$	$\leftrightarrow$	$\pi + K + K^*$
2644	$\Xi^* + \bar{N}(1440)$	$\leftrightarrow$	$\pi + K^* + K^*$
2645	$\Xi^* + \bar{N}(1440)$	$\leftrightarrow$	$\eta + K + K$
2646	$\Xi^* + \bar{N}(1440)$	$\leftrightarrow$	$\eta + K + K^*$
2647	$\Xi^* + \bar{N}(1440)$	$\leftrightarrow$	$\eta + K^* + K^*$
2648	$\Xi^* + \bar{N}(1440)$	$\leftrightarrow$	$K + K + \rho$
2649	$\Xi^* + \bar{N}(1440)$	$\leftrightarrow$	$K + K + \omega$
2650	$\Xi^* + \bar{N}(1440)$	$\leftrightarrow$	$K + K + \phi$
2651	$\Xi^* + \bar{N}(1440)$	$\leftrightarrow$	$K + K + \eta'$
2652	$\Xi^* + \bar{N}(1440)$	$\leftrightarrow$	$K + K^* + \rho$
2653	$\Xi^* + \bar{N}(1440)$	$\leftrightarrow$	$K + K^* + \omega$
2654	$\Xi^* + \bar{N}(1440)$	$\leftrightarrow$	$K + K^* + \phi$
2655	$\Xi^* + \bar{N}(1440)$	$\leftrightarrow$	$K + K^* + \eta'$
2656	$\Xi^* + \bar{N}(1440)$	$\leftrightarrow$	$K^* + K^* + \rho$
2657	$\Xi^* + \bar{N}(1440)$	$\leftrightarrow$	$K^* + K^* + \omega$
2658	$\Xi^* + \bar{N}(1440)$	$\leftrightarrow$	$K^* + K^* + \phi$
2659	$\Xi^* + \bar{N}(1440)$	$\leftrightarrow$	$K^* + K^* + \eta'$
2660	$\Xi^* + \bar{N}(1535)$	$\leftrightarrow$	$K + K + a_1$
2661	$\Xi^* + \bar{N}(1535)$	$\leftrightarrow$	$K + K^* + a_1$
2662	$\Xi^* + \bar{N}(1535)$	$\leftrightarrow$	$K^* + K^* + a_1$
2663	$\Xi^* + \bar{\Lambda}$	$\leftrightarrow$	$\pi + \eta + K$
2664	$\Xi^* + \bar{\Lambda}$	$\leftrightarrow$	$\pi + \eta + K^*$
2665	$\Xi^* + \bar{\Lambda}$	$\leftrightarrow$	$\pi + K + \phi$
2666	$\Xi^* + \bar{\Lambda}$	$\leftrightarrow$	$\pi + K^* + \phi$
2667	$\Xi^* + \bar{\Lambda}$	$\leftrightarrow$	$\eta + \eta + K$
2668	$\Xi^* + \bar{\Lambda}$	$\leftrightarrow$	$\eta + \eta + K^*$
2669	$\Xi^* + \bar{\Lambda}$	$\leftrightarrow$	$\eta + K + \rho$
2670	$\Xi^* + \bar{\Lambda}$	$\leftrightarrow$	$\eta + K + \omega$
2671	$\Xi^* + \bar{\Lambda}$	$\leftrightarrow$	$\eta + K + \phi$
2672	$\Xi^* + \bar{\Lambda}$	$\leftrightarrow$	$\eta + K + \eta'$
2673	$\Xi^* + \bar{\Lambda}$	$\leftrightarrow$	$\eta + K^* + \rho$
2674	$\Xi^* + \bar{\Lambda}$	$\leftrightarrow$	$\eta + K^* + \omega$
2675	$\Xi^* + \bar{\Lambda}$	$\leftrightarrow$	$\eta + K^* + \phi$
2676	$\Xi^* + \bar{\Lambda}$	$\leftrightarrow$	$\eta + K^* + \eta'$
2677	$\Xi^* + \bar{\Lambda}$	$\leftrightarrow$	$K + K + K$
2678	$\Xi^* + \bar{\Lambda}$	$\leftrightarrow$	$K + K + K^*$
2679	$\Xi^* + \bar{\Lambda}$	$\leftrightarrow$	$K + K^* + K^*$
2680	$\Xi^* + \bar{\Lambda}$	$\leftrightarrow$	$K + \rho + \phi$
2681	$\Xi^* + \bar{\Lambda}$	$\leftrightarrow$	$K + \omega + \phi$
2682	$\Xi^* + \bar{\Lambda}$	$\leftrightarrow$	$K + \phi + \phi$
2683	$\Xi^* + \bar{\Lambda}$	$\leftrightarrow$	$K + \phi + \eta'$
2684	$\Xi^* + \bar{\Lambda}$	$\leftrightarrow$	$K^* + K^* + K^*$
2685	$\Xi^* + \bar{\Lambda}$	$\leftrightarrow$	$K^* + \rho + \phi$
2686	$\Xi^* + \bar{\Lambda}$	$\leftrightarrow$	$K^* + \omega + \phi$

Ch. No.	$B_1 + B_2$	$\leftrightarrow$	$M_1+M_2+M_3$
2687	$\Xi^* + \bar{\Lambda}$	$\leftrightarrow$	$K^* + \phi + \phi$
2688	$\Xi^* + \bar{\Lambda}$	$\leftrightarrow$	$K^* + \phi + \eta'$
2689	$\Xi^* + \bar{\Sigma}$	$\leftrightarrow$	$\pi + \eta + K$
2690	$\Xi^* + \bar{\Sigma}$	$\leftrightarrow$	$\pi + \eta + K^*$
2691	$\Xi^* + \bar{\Sigma}$	$\leftrightarrow$	$\pi + K + \phi$
2692	$\Xi^* + \bar{\Sigma}$	$\leftrightarrow$	$\pi + K^* + \phi$
2693	$\Xi^* + \bar{\Sigma}$	$\leftrightarrow$	$\eta + \eta + K$
2694	$\Xi^* + \bar{\Sigma}$	$\leftrightarrow$	$\eta + \eta + K^*$
2695	$\Xi^* + \bar{\Sigma}$	$\leftrightarrow$	$\eta + K + \rho$
2696	$\Xi^* + \bar{\Sigma}$	$\leftrightarrow$	$\eta + K + \omega$
2697	$\Xi^* + \bar{\Sigma}$	$\leftrightarrow$	$\eta + K + \phi$
2698	$\Xi^* + \bar{\Sigma}$	$\leftrightarrow$	$\eta + K + \eta'$
2699	$\Xi^* + \bar{\Sigma}$	$\leftrightarrow$	$\eta + K^* + \rho$
2700	$\Xi^* + \bar{\Sigma}$	$\leftrightarrow$	$\eta + K^* + \omega$
2701	$\Xi^* + \bar{\Sigma}$	$\leftrightarrow$	$\eta + K^* + \phi$
2702	$\Xi^* + \bar{\Sigma}$	$\leftrightarrow$	$\eta + K^* + \eta'$
2703	$\Xi^* + \bar{\Sigma}$	$\leftrightarrow$	$K + K + K$
2704	$\Xi^* + \bar{\Sigma}$	$\leftrightarrow$	$K + K + K^*$
2705	$\Xi^* + \bar{\Sigma}$	$\leftrightarrow$	$K + K^* + K^*$
2706	$\Xi^* + \bar{\Sigma}$	$\leftrightarrow$	$K + \rho + \phi$
2707	$\Xi^* + \bar{\Sigma}$	$\leftrightarrow$	$K + \omega + \phi$
2708	$\Xi^* + \bar{\Sigma}$	$\leftrightarrow$	$K + \phi + \phi$
2709	$\Xi^* + \bar{\Sigma}$	$\leftrightarrow$	$K + \phi + \eta'$
2710	$\Xi^* + \bar{\Sigma}$	$\leftrightarrow$	$K^* + K^* + K^*$
2711	$\Xi^* + \bar{\Sigma}$	$\leftrightarrow$	$K^* + \rho + \phi$
2712	$\Xi^* + \bar{\Sigma}$	$\leftrightarrow$	$K^* + \omega + \phi$
2713	$\Xi^* + \bar{\Sigma}$	$\leftrightarrow$	$K^* + \phi + \phi$
2714	$\Xi^* + \bar{\Sigma}$	$\leftrightarrow$	$K^* + \phi + \eta'$
2715	$\Xi^* + \bar{\Sigma}^*$	$\leftrightarrow$	$\pi + \eta + K$
2716	$\Xi^* + \bar{\Sigma}^*$	$\leftrightarrow$	$\pi + \eta + K^*$
2717	$\Xi^* + \bar{\Sigma}^*$	$\leftrightarrow$	$\pi + K + \phi$
2718	$\Xi^* + \bar{\Sigma}^*$	$\leftrightarrow$	$\pi + K^* + \phi$
2719	$\Xi^* + \bar{\Sigma}^*$	$\leftrightarrow$	$\eta + \eta + K$
2720	$\Xi^* + \bar{\Sigma}^*$	$\leftrightarrow$	$\eta + \eta + K^*$
2721	$\Xi^* + \bar{\Sigma}^*$	$\leftrightarrow$	$\eta + K + \rho$
2722	$\Xi^* + \bar{\Sigma}^*$	$\leftrightarrow$	$\eta + K + \omega$
2723	$\Xi^* + \bar{\Sigma}^*$	$\leftrightarrow$	$\eta + K + \phi$
2724	$\Xi^* + \bar{\Sigma}^*$	$\leftrightarrow$	$\eta + K + \eta'$
2725	$\Xi^* + \bar{\Sigma}^*$	$\leftrightarrow$	$\eta + K^* + \rho$
2726	$\Xi^* + \bar{\Sigma}^*$	$\leftrightarrow$	$\eta + K^* + \omega$
2727	$\Xi^* + \bar{\Sigma}^*$	$\leftrightarrow$	$\eta + K^* + \phi$
2728	$\Xi^* + \bar{\Sigma}^*$	$\leftrightarrow$	$\eta + K^* + \eta'$
2729	$\Xi^* + \bar{\Sigma}^*$	$\leftrightarrow$	$K + K + K$
2730	$\Xi^* + \bar{\Sigma}^*$	$\leftrightarrow$	$K + K + K^*$
2731	$\Xi^* + \bar{\Sigma}^*$	$\leftrightarrow$	$K + K^* + K^*$
2732	$\Xi^* + \bar{\Sigma}^*$	$\leftrightarrow$	$K + \rho + \phi$
2733	$\Xi^* + \bar{\Sigma}^*$	$\leftrightarrow$	$K + \omega + \phi$
2734	$\Xi^* + \bar{\Sigma}^*$	$\leftrightarrow$	$K + \phi + \phi$
2735	$\Xi^* + \bar{\Sigma}^*$	$\leftrightarrow$	$K + \phi + \eta'$
2736	$\Xi^* + \bar{\Sigma}^*$	$\leftrightarrow$	$K^* + K^* + K^*$
2737	$\Xi^* + \bar{\Sigma}^*$	$\leftrightarrow$	$K^* + \rho + \phi$
2738	$\Xi^* + \bar{\Sigma}^*$	$\leftrightarrow$	$K^* + \omega + \phi$
2739	$\Xi^* + \bar{\Sigma}^*$	$\leftrightarrow$	$K^* + \phi + \phi$
2740	$\Xi^* + \bar{\Sigma}^*$	$\leftrightarrow$	$K^* + \phi + \eta'$
2741	$\Xi^* + \bar{\Xi}$	$\leftrightarrow$	$\pi + \eta + \eta$
2742	$\Xi^* + \bar{\Xi}$	$\leftrightarrow$	$\pi + \eta + \phi$
2743	$\Xi^* + \bar{\Xi}$	$\leftrightarrow$	$\pi + \phi + \phi$
2744	$\Xi^* + \bar{\Xi}$	$\leftrightarrow$	$\eta + \eta + \eta$
2745	$\Xi^* + \bar{\Xi}$	$\leftrightarrow$	$\eta + \eta + \rho$
2746	$\Xi^* + \bar{\Xi}$	$\leftrightarrow$	$\eta + \eta + \omega$
2747	$\Xi^* + \bar{\Xi}$	$\leftrightarrow$	$\eta + \eta + \phi$
2748	$\Xi^* + \bar{\Xi}$	$\leftrightarrow$	$\eta + \eta + \eta'$
2749	$\Xi^* + \bar{\Xi}$	$\leftrightarrow$	$\eta + K + K$
2750	$\Xi^* + \bar{\Xi}$	$\leftrightarrow$	$\eta + K + K^*$
2751	$\Xi^* + \bar{\Xi}$	$\leftrightarrow$	$\eta + K^* + K^*$
2752	$\Xi^* + \bar{\Xi}$	$\leftrightarrow$	$\eta + \rho + \phi$
2753	$\Xi^* + \bar{\Xi}$	$\leftrightarrow$	$\eta + \omega + \phi$
2754	$\Xi^* + \bar{\Xi}$	$\leftrightarrow$	$\eta + \phi + \phi$
2755	$\Xi^* + \bar{\Xi}$	$\leftrightarrow$	$\eta + \phi + \eta'$
2756	$\Xi^* + \bar{\Xi}$	$\leftrightarrow$	$K + K + \phi$
2757	$\Xi^* + \bar{\Xi}$	$\leftrightarrow$	$K + K^* + \phi$
2758	$\Xi^* + \Xi$	$\leftrightarrow$	$K^* + K^* + \phi$
2759	$\Xi^* + \bar{\Xi}$	$\leftrightarrow$	$\rho + \phi + \phi$
2760	$\Xi^* + \bar{\Xi}$	$\leftrightarrow$	$\omega + \phi + \phi$
2761	$\Xi^* + \Xi$	$\leftrightarrow$	$\phi + \phi + \phi$
2762	$\Xi^* + \bar{\Xi}$	$\leftrightarrow$	$\phi + \phi + \eta'$
2763	$\Xi^* + \bar{\Xi}^*$	$\leftrightarrow$	$\pi + \eta + \eta$
2764	$\Xi^* + \bar{\Xi}^*$	$\leftrightarrow$	$\pi + \eta + \phi$
2765	$\Xi^* + \bar{\Xi}^*$	$\leftrightarrow$	$\pi + \phi + \phi$
2766	$\Xi^* + \bar{\Xi}^*$	$\leftrightarrow$	$\eta + \eta + \eta$
2767	$\Xi^* + \bar{\Xi}^*$	$\leftrightarrow$	$\eta + \eta + \rho$
2768	$\Xi^* + \bar{\Xi}^*$	$\leftrightarrow$	$\eta + \eta + \omega$
2769	$\Xi^* + \bar{\Xi}^*$	$\leftrightarrow$	$\eta + \eta + \phi$
2770	$\Xi^* + \bar{\Xi}^*$	$\leftrightarrow$	$\eta + \eta + \eta'$
2771	$\Xi^* + \bar{\Xi}^*$	$\leftrightarrow$	$\eta + K + K$
2772	$\Xi^* + \bar{\Xi}^*$	$\leftrightarrow$	$\eta + K + K^*$

Ch. No.	$B_1 + B_2$	$\leftrightarrow$	$M_1+M_2+M_3$
2773	$\Xi^* + \bar{\Xi}^*$	$\leftrightarrow$	$\eta + K^* + K^*$
2774	$\Xi^* + \bar{\Xi}^*$	$\leftrightarrow$	$\eta + \rho + \phi$
2775	$\Xi^* + \bar{\Xi}^*$	$\leftrightarrow$	$\eta + \omega + \phi$
2776	$\Xi^* + \bar{\Xi}^*$	$\leftrightarrow$	$\eta + \phi + \phi$
2777	$\Xi^* + \bar{\Xi}^*$	$\leftrightarrow$	$\eta + \phi + \eta'$
2778	$\Xi^* + \bar{\Xi}^*$	$\leftrightarrow$	$K + K + \phi$
2779	$\Xi^* + \bar{\Xi}^*$	$\leftrightarrow$	$K + K^* + \phi$
2780	$\Xi^* + \bar{\Xi}^*$	$\leftrightarrow$	$K^* + K^* + \phi$
2781	$\Xi^* + \bar{\Xi}^*$	$\leftrightarrow$	$\rho + \phi + \phi$
2782	$\Xi^* + \bar{\Xi}^*$	$\leftrightarrow$	$\omega + \phi + \phi$
2783	$\Xi^* + \bar{\Xi}^*$	$\leftrightarrow$	$\phi + \phi + \phi$
2784	$\Xi^* + \bar{\Xi}^*$	$\leftrightarrow$	$\phi + \phi + \eta'$
2785	$\Xi^* + \bar{\Omega}$	$\leftrightarrow$	$\eta + \eta + K$
2786	$\Xi^* + \bar{\Omega}$	$\leftrightarrow$	$\eta + \eta + K^*$
2787	$\Xi^* + \bar{\Omega}$	$\leftrightarrow$	$\eta + K + \phi$
2788	$\Xi^* + \bar{\Omega}$	$\leftrightarrow$	$\eta + K^* + \phi$
2789	$\Xi^* + \bar{\Omega}$	$\leftrightarrow$	$K + \phi + \phi$
2790	$\Xi^* + \bar{\Omega}$	$\leftrightarrow$	$K^* + \phi + \phi$
2791	$\Omega + \bar{\mathrm{N}}$	$\leftrightarrow$	$K + K + K$
2792	$\Omega + \bar{\mathrm{N}}$	$\leftrightarrow$	$K + K + K^*$
2793	$\Omega + \bar{\mathrm{N}}$	$\leftrightarrow$	$K + K^* + K^*$
2794	$\Omega + \bar{\mathrm{N}}$	$\leftrightarrow$	$K^* + K^* + K^*$
2795	$\Omega + \bar{\Delta}(1232)$	$\leftrightarrow$	$K + K + K$
2796	$\Omega + \bar{\Delta}(1232)$	$\leftrightarrow$	$K + K + K^*$
2797	$\Omega + \bar{\Delta}(1232)$	$\leftrightarrow$	$K + K^* + K^*$
2798	$\Omega + \bar{\Delta}(1232)$	$\leftrightarrow$	$K^* + K^* + K^*$
2799	$\Omega + \bar{\mathrm{N}}(1440)$	$\leftrightarrow$	$K + K + K$
2800	$\Omega + \bar{\mathrm{N}}(1440)$	$\leftrightarrow$	$K + K + K^*$
2801	$\Omega + \bar{\mathrm{N}}(1440)$	$\leftrightarrow$	$K + K^* + K^*$
2802	$\Omega + \bar{\mathrm{N}}(1440)$	$\leftrightarrow$	$K^* + K^* + K^*$
2803	$\Omega + \bar{\Lambda}$	$\leftrightarrow$	$\eta + K + K$
2804	$\Omega + \bar{\Lambda}$	$\leftrightarrow$	$\eta + K + K^*$
2805	$\Omega + \bar{\Lambda}$	$\leftrightarrow$	$\eta + K^* + K^*$
2806	$\Omega + \bar{\Lambda}$	$\leftrightarrow$	$K + K + \phi$
2807	$\Omega + \bar{\Lambda}$	$\leftrightarrow$	$K + K^* + \phi$
2808	$\Omega + \bar{\Lambda}$	$\leftrightarrow$	$K^* + K^* + \phi$
2809	$\Omega + \bar{\Sigma}$	$\leftrightarrow$	$\eta + K + K$
2810	$\Omega + \bar{\Sigma}$	$\leftrightarrow$	$\eta + K + K^*$
2811	$\Omega + \bar{\Sigma}$	$\leftrightarrow$	$\eta + K^* + K^*$
2812	$\Omega + \bar{\Sigma}$	$\leftrightarrow$	$K + K + \phi$
2813	$\Omega + \bar{\Sigma}$	$\leftrightarrow$	$K + K^* + \phi$
2814	$\Omega + \bar{\Sigma}$	$\leftrightarrow$	$K^* + K^* + \phi$
2815	$\Omega + \bar{\Sigma}^*$	$\leftrightarrow$	$\eta + K + K$
2816	$\Omega + \bar{\Sigma}^*$	$\leftrightarrow$	$\eta + K + K^*$
2817	$\Omega + \bar{\Sigma}^*$	$\leftrightarrow$	$\eta + K^* + K^*$
2818	$\Omega + \bar{\Sigma}^*$	$\leftrightarrow$	$K + K + \phi$
2819	$\Omega + \bar{\Sigma}^*$	$\leftrightarrow$	$K + K^* + \phi$
2820	$\Omega + \bar{\Sigma}^*$	$\leftrightarrow$	$K^* + K^* + \phi$
2821	$\Omega + \bar{\Xi}$	$\leftrightarrow$	$\eta + \eta + K$
2822	$\Omega + \bar{\Xi}$	$\leftrightarrow$	$\eta + \eta + K^*$
2823	$\Omega + \bar{\Xi}$	$\leftrightarrow$	$\eta + K + \phi$
2824	$\Omega + \bar{\Xi}$	$\leftrightarrow$	$\eta + K^* + \phi$
2825	$\Omega + \bar{\Xi}$	$\leftrightarrow$	$K + \phi + \phi$
2826	$\Omega + \bar{\Xi}$	$\leftrightarrow$	$K^* + \phi + \phi$
2827	$\Omega + \bar{\Xi}^*$	$\leftrightarrow$	$\eta + \eta + K$
2828	$\Omega + \bar{\Xi}^*$	$\leftrightarrow$	$\eta + \eta + K^*$
2829	$\Omega + \bar{\Xi}^*$	$\leftrightarrow$	$\eta + K + \phi$
2830	$\Omega + \bar{\Xi}^*$	$\leftrightarrow$	$\eta + K^* + \phi$
2831	$\Omega + \bar{\Xi}^*$	$\leftrightarrow$	$K + \phi + \phi$
2832	$\Omega + \bar{\Xi}^*$	$\leftrightarrow$	$K^* + \phi + \phi$
2833	$\Omega + \bar{\Omega}$	$\leftrightarrow$	$\eta + \eta + \eta$
2834	$\Omega + \bar{\Omega}$	$\leftrightarrow$	$\eta + \eta + \phi$
2835	$\Omega + \bar{\Omega}$	$\leftrightarrow$	$\eta + \phi + \phi$
2836	$\Omega + \bar{\Omega}$	$\leftrightarrow$	$\phi + \phi + \phi$

Bibliography

[1] K. A. Olive *et al.* [Particle Data Group], Chin. Phys. C **38**, 090001 (2014).

[2] G. S. F. Stephans, Nucl. Phys. A **583**, 653C (1995).

[3] P. Romatschke and U. Romatschke, Phys. Rev. Lett. **99**, 172301 (2007).

[4] G. Aad *et al.* [ATLAS Collaboration], Phys. Lett. B **716**, 1 (2012).

[5] F. Zimmermann, arXiv:1801.03170 [physics.acc-ph].

[6] B. Friman, C. Höhne, J. Knoll, S. Leupold, J. Randrup, R. Rapp and P. Senger, Lect. Notes Phys. **814**, pp.1 (2011).

[7] Y. Aoki *et al.*, Phys. Lett. B **643**, 46 (2006).

[8] S. Borsanyi *et al.*, JHEP **1009**, 073 (2010); JHEP **1011**, 077 (2010); JHEP **1208**, 126 (2012).

[9] S. Borsanyi *et al.*, Phys. Lett B **730**, 99 (2014); Phys. Rev. D **92**, 014505 (2015).

[10] P. Petreczky [HotQCD Collaboration], PoS LATTICE **2012**, 069 (2012); AIP Conf. Proc. **1520**, 103 (2013).

[11] H.-T. Ding, F. Karsch, and S. Mukherjee, Int. J. Mod. Phys. E **24**, 1530007 (2015).

[12] A. Bazavov *et al.*, Phys. Rev. D **90**, 094503 (2014).

[13] K. Fukushima, Phys. Rev. D **77**, 114028 (2008) Erratum: [Phys. Rev. D **78**, 039902 (2008)].

[14] L. McLerran, Nucl. Phys. Proc. Suppl. **195**, 275 (2009).

[15] A. Palmese, W. Cassing, E. Seifert, T. Steinert, P. Moreau and E. L. Bratkovskaya, Phys. Rev. C **94**, 044912 (2016).

[16] T. K. Herbst, J. M. Pawlowski and B. J. Schaefer, Phys. Rev. D **88**, 014007 (2013).

[17] C. S. Fischer, J. Luecker and C. A. Welzbacher, Phys. Rev. D **90**, 034022 (2014).

[18] C. S. Fischer, L. Fister, J. Luecker and J. M. Pawlowski, Phys. Lett. B **732**, 273 (2014).

[19] G. Eichmann, H. Sanchis-Alepuz, R. Williams, R. Alkofer and C. S. Fischer, Prog. Part. Nucl. Phys. **91**, 1 (2016).

[20] G. Eichmann, C. S. Fischer and C. A. Welzbacher, Phys. Rev. D **93**, 034013 (2016).

[21] G. Eichmann, C. S. Fischer and W. Heupel, Phys. Lett. B **753**, 282 (2016).

[22] K. Adcox *et al.* [PHENIX Collaboration], Phys. Rev. Lett. **88**, 022301 (2002).

[23] C. Adler *et al.* [STAR Collaboration], Phys. Rev. Lett. **90**, 082302 (2003).

[24] K. G. R. Doss *et al.*, Phys. Rev. C **32**, 116 (1985).

[25] T. Matsui and H. Satz, Phys. Lett. B **178**, 416 (1986).

[26] O. Linnyk, E. L. Bratkovskaya, and W. Cassing, Prog. Part. Nucl. Phys. **87**, 50 (2016).

[27] Yu. B. Ivanov, V. N. Russkikh, and V. D. Toneev, Phys. Rev. C **73**, 044904 (2006); V. N. Russkikh, and Yu. B. Ivanov, Phys. Rev. C **74**, 034904 (2006); Yu. B. Ivanov, Phys. Rev. C **87**, 064904 (2013); Yu. B. Ivanov and D. Blaschke, Phys. Rev. C **92**, 024916 (2015).

[28] P. Huovinen and P. V. Ruuskanen, Ann. Rev. Nucl. Part. Sci. **56**, 163 (2006).

[29] K. H. Ackermann *et al.* [STAR Collaboration], Phys. Rev. Lett. **86**, 402 (2001).

[30] I. Karpenko, P. Huovinen and M. Bleicher, Comput. Phys. Commun. **185**, 3016 (2014).

[31] O. Socolowski, Jr., F. Grassi, Y. Hama and T. Kodama, Phys. Rev. Lett. **93**, 182301 (2004).

[32] S. A. Bass *et al.*, Prog. Part. Nucl. Phys. **41**, 255 (1998).

[33] M. Bleicher *et al.*, J. Phys. G **25**, 1859 (1999).

[34] H. Petersen, M. Bleicher, S. A. Bass and H. Stöcker, arXiv:0805.0567 [hep-ph].

[35] C. Hartnack, R. K. Puri, J. Aichelin, J. Konopka, S. A. Bass, H. Stöcker and W. Greiner, Eur. Phys. J. A **1**, 151 (1998)

[36] C. Hartnack and J. Aichelin, Phys. Lett. B **506**, 261 (2001)

[37] W. Cassing and S. Juchem, Nucl. Phys. A **665**, 377 (2000).

[38] W. Cassing and S. Juchem, Nucl. Phys. A **672**, 417 (2000).

[39] O. Linnyk, V. Konchakovski, T. Steinert, W. Cassing and E. L. Bratkovskaya, Phys. Rev. C **92**, 054914 (2015).

[40] V. P. Konchakovski, E. L. Bratkovskaya, W. Cassing, V. D. Toneev, S. A. Voloshin and V. Voronyuk, Phys. Rev. C **85**, 044922 (2012).

[41] B. Bäuchle and M. Bleicher, Phys. Lett. B **695**, 489 (2011).

[42] W. Cassing, Nucl. Phys. A **700**, 618 (2002).

[43] S. Pal, C. M. Ko, and Z.-W. Lin, Nucl. Phys. A **730**, 143 (2004).

[44] S. Pal, C. M. Ko, J. M. Alexander, P. Chung, and R. A. Lacey, Phys. Lett. B **595**, 158 (2004).

[45] L. P. Kadanoff and G. Baym, *Quantum Statistical Mechanics* (Benjamin, New York, 1962).

[46] J. S. Schwinger, J. Math. Phys. **2**, 407 (1961).

[47] L. V. Keldysh, Sov. Phys. JETP **20**, 1018 (1965).

[48] W. Botermans and R. Malfliet, Phys. Rept. **198**, 115 (1990).

[49] S. Juchem, W. Cassing and C. Greiner, Phys. Rev. D **69**, 025006 (2004).

[50] R. v. Leeuwen *et al.*, Lect. Notes Phys. **706**, 33 (2006).

[51] W. Cassing, Eur. Phys. J. ST **168**, 3 (2009).

[52] M. Bonitz, *Quantum kinetic theory* (B.G. Teubner Stuttgart, 1998).

[53] G. Baym, Phys. Rev. **127**, 1391 (1962).

[54] C. Greiner and S. Leupold, Annals Phys. **270**, 328 (1998).

[55] S. Leupold, Nucl. Phys. A **672**, 475 (2000); Nucl. Phys. A **695**, 377 (2001).

[56] Y. B. Ivanov, J. Knoll and D. N. Voskresensky, Nucl. Phys. A **672**, 313 (2000).

[57] Y. B. Ivanov, J. Knoll and D. N. Voskresensky, Phys. Atom. Nucl. **66**, 1902 (2003).

[58] E. L. Bratkovskaya, W. Cassing, V. P. Konchakovski and O. Linnyk, Nucl. Phys. A **856**, 162 (2011).

[59] V. Ozvenchuk, O. Linnyk, M. I. Gorenstein, E. L. Bratkovskaya and W. Cassing, Phys. Rev. C **87**, no. 2, 024901 (2013).

[60] A. Peshier, Phys. Rev. D **70**, 034016 (2004).

[61] A. Peshier, J. Phys. G **31**, S371 (2005).

[62] E. Riedel, Z. Phys. **210**, 403 (1968).

[63] B. Vanderheyden and G. Baym, J. Statist. Phys. **93**, 843 (1998).

[64] J.-P. Blaizot, E. Iancu, A. Rebhan, Phys. Rev. Lett. **83**, 2906 (1999); Phys. Rev. D **63**, 065003 (2001).

[65] Y. Aoki, S. Borsanyi, S. Durr, Z. Fodor, S. D. Katz, S. Krieg and K. K. Szabo, JHEP **0906**, 088 (2009).

[66] T. Song, H. Berrehrah, D. Cabrera, J. M. Torres-Rincon, L. Tolos, W. Cassing and E. Bratkovskaya, Phys. Rev. C **92**, 014910 (2015).

[67] T. Song, H. Berrehrah, D. Cabrera, W. Cassing and E. Bratkovskaya, Phys. Rev. C **93**, 034906 (2016).

[68] T. Song *et al.*, Phys. Rev. C **96**, 014905 (2017)

[69] K. Aamodt *et al.* [ALICE Collaboration], Phys. Rev. Lett. **106**, 032301 (2011).

[70] B. Andersson, G. Gustafson, G. Ingelman and T. Sjostrand, Phys. Rept. **97**, 31 (1983).

[71] B. Andersson, *The Lund Model* (Cambridge University Press, 1998).

[72] B. Nilsson-Almqvist and E. Stenlund, Comput. Phys. Commun. **43**, 387 (1987).

[73] E. Byckling and K. Kajantie, *Particle Kinematics* (John Wiley & Sons Ltd, 1973).

[74] T. Sjostrand, S. Mrenna, and P. Z. Skands, JHEP **0605**, 026 (2006).

[75] A. Lang, H. Babovsky, W. Cassing, U. Mosel, H.-G. Reusch and K. Weber, Journal of Computational Physics **106**, 391 (1993).

[76] Z. Xu and C. Greiner, Phys. Rev. C **71**, 064901 (2005).

[77] B. B. Back *et al.* [E917 Collaboration], Phys. Rev. Lett. **87**, 242301 (2001).

[78] T. Anticic *et al.* [NA49 Collaboration], Phys. Rev. C **83**, 014901 (2011).

[79] C. Alt *et al.* [NA49 Collaboration], Phys. Rev. C **78**, 034918 (2008).

[80] C. Alt *et al.* [NA49 Collaboration], Phys. Rev. Lett. **94**, 192301 (2005).

[81] C. Alt *et al.* [NA49 Collaboration], Phys. Rev. C **73**, 044910 (2006).

[82] C. Höhne *et al.* [NA49 Collaboration], Nucl. Phys. A **774**, 35 (2006).

[83] W. Cassing, A. Palmese, P. Moreau, and E. L. Bratkovskaya, Phys. Rev. C **93**, 014902 (2016).

[84] Y. B. Ivanov, Phys. Rev. C **87**, 064905 (2013).

[85] S. S. Adler *et al.* [PHENIX Collaboration], Phys. Rev. C **69**, 034909 (2004).

[86] B. Abelev *et al.* [ALICE Collaboration], Phys. Lett. B **720**, 52 (2013); Phys. Rev. Lett. **111**, 222301 (2013); Phys. Lett. B **728**, 216 (2014).

[87] ALICE Collaboration, B. Abelev *et al.*, Phys. Rev. C **88**, 044910 (2013).

[88] E. Abbas *et al.* [ALICE Collaboration], Phys. Lett. B **726**, 610 (2013).

[89] J. Adam *et al.* [ALICE Collaboration], Phys. Lett. B **754**, 373 (2016).

[90] V. P. Konchakovski, W. Cassing, and V.D. Toneev, J. Phys. G **42**, 055106 (2015).

[91] G. Agakishiev *et al.* [STAR Collaboration], Phys. Rev. Lett. **108**, 072301 (2012).

[92] J. Adams *et al.* [STAR Collaboration], Phys. Rev. Lett. **98**, 062301 (2007).

[93] K. Adcox *et al.* [PHENIX Collaboration], Phys. Rev. Lett. **89**, 092302 (2002); Phys. Rev. C **69**, 024904 (2004).

[94] C. Adler *et al.* [STAR Collaboration], Phys. Rev. Lett. **89**, 092301 (2002).

[95] J. Adams *et al.* [STAR Collaboration], Phys. Rev. Lett. **92**, 182301 (2004).

[96] L. Adamczyk *et al.* [STAR Collaboration], Phys. Rev. C **96**, 044904 (2017).

[97] L. Ahle *et al.* [E802 Collaboration], Phys. Rev. Lett. **81**, 2650 (1998).

[98] L. Ahle *et al.* [E866 and E917 Collaborations], Phys. Lett. B **476**, 1 (2000); Phys. Lett. B **490**, 53 (2000).

[99] J. L. Klay *et al.* [E-0895 Collaboration], Phys. Rev. C **68**, 054905 (2003).

[100] P. Chung *et al.* [E895 Collaboration], Phys. Rev. Lett. **91**, 202301 (2003).

[101] S. V. Afanasiev *et al.* [NA49 Collaboration], Phys. Rev. C **66**, 054902 (2002).

[102] C. Alt *et al.* [NA49 Collaboration], Phys. Rev. C **73**, 044910 (2006); Phys. Rev. C **77**, 024903 (2008).

[103] T. Anticic *et al.* [NA49 Collaboration], Phys. Rev. Lett. **93**, 022302 (2004); Phys. Rev. C **80**, 034906 (2009).

[104] M. K. Mitrovski *et al.* [NA49 Collaboration], J. Phys. G **32**, 43 (2006).

[105] F. Becattini *et al.*, Phys. Rev. C **85** (2013), 044921 (2012); Phys. Rev. Lett. **111**, 082302; Phys. Lett. B **764**, 241 (2017).

[106] Y. Pan and S. Pratt, Phys.Rev. C **89**, 044911 (2014).

[107] P. Huovinen and J. I. Kapusta, Phys. Rev. C **69**, 014902 (2004).

[108] E. Seifert and W. Cassing, Phys. Rev. C **97**, 024913 (2018).

[109] E. Seifert and W. Cassing, Phys. Rev. C, in print.

Selbstständigkeitserklärung

Ich erkläre: Ich habe die vorgelegte Dissertation selbstständig und ohne unerlaubte fremde Hilfe und nur mit den Hilfen angefertigt, die ich in der Dissertation angegeben habe. Alle Textstellen, die wörtlich oder sinngemäß aus veröffentlichten Schriften entnommen sind, und alle Angaben, die auf mündlichen Auskünften beruhen, sind als solche kenntlich gemacht. Ich stimme einer evtl. Überprüfung meiner Dissertation durch eine Antiplagiat-Software zu. Bei den von mir durchgeführten und in der Dissertation erwähnten Untersuchungen habe ich die Grundsätze guter wissenschaftlicher Praxis, wie sie in der "Satzung der Justus-Liebig-Universität Gießen zur Sicherung guter wissenschaftlicher Praxis" niedergelegt sind, eingehalten.

Datum	Unterschrift